The synthesis and evaluation of (*E*)-styrylisatin analogues as inhibitors of monoamine oxidase B

Elizna M. Van der Walt
B. Pharm.

Dissertation submitted in partial fulfillment of the requirements for the degree ***Magister Scientiae*** in Pharmaceutical Chemistry at the North-West University, Potchefstroom Campus

Supervisor:	Dr. J.P. Petzer
Co-supervisor:	Prof. J.J. Bergh
Assistant supervisor:	Prof. S.F. Malan

2008
Potchefstroom

UITTREKSEL

Monoamienoksidase B- (MAO-B-) inhibeerders word tans klinies gebruik vir die simptomatiese behandeling van Parkinson se siekte (PD) en mag moontlik ook neurobeskermende aktiwiteit besit. Die onomkeerbare MAO-B-inhibeerder, (R)-deprenyl, word algemeen gebruik in PD-terapie, gewoonlik in kombinasie met levodopa tydens dopamienvervangingsterapie. In teenstelling met omkeerbare inhibisie, behels ensiemherstel na onomkeerbare inhibisie *de novo* sintese. Relatief vinnige herstel van ensiemaktiwiteit veroorsaak dat potente omkeerbare MAO-B-inhibeerders veiliger en meer wenslik is.

Beide isatien en kaffeïen is klein molekules wat in staat is om MAO-B te inhibeer. Isatien is 'n relatief goeie endogene inhibeerder (K_i = 3 µM) maar kaffeïen is 'n swak inhibeerder (K_i = 650 µM). Daar is gevind dat die inhiberings potensie van kaffeïen verbeter kan word deur substitusie van 'n stirielsyketting op C-8 van die kaffeïenring. Addisie van 'n elektronontrekkende substituent op die C-3 posisie van die fenielsyketting het strukture gelewer wat MAO besonder kragtig geïnhibeer het, byvoorbeeld, (*E*)-8-(3-chlorostiriel)kaffeïen (CSC) (K_i = 0.1 µM). Tydens hierdie studie is ondersoek ingestel of stirielsubstitusie van die leidraadverbinding, isatien, op C-5 en C-6 soortgelyke verhoging in isatien se vermoë om MAO te inhibeer sal veroorsaak.

Rekenaarmodellering van die voorgestelde (E)-5-stirielisatien- en (E)-6-stirielisatienanaloë, asook isatien, in die aktiewe setel van rekombinante MAO-B het die hipotese van verbeterde MAO-B-inhiberings aktiwiteit vir hierdie stirielanaloë ondersteun. Modellering het aangetoon dat die stirielsyketting gestabiliseer word in die ingangsholte van die ensiem tydens binding, terwyl die isatiengedeelte in die substraat-bindingsholte geleë is en met waterstofbinding gestabiliseer word. Hierdie tweeledige bindingsmetode is soortgelyk aan die voorgestelde bindingsmetode vir die stirielkaffeïene en dit blyk dat dit die vermoë van die stirielkaffeïene om MAO-B te inhibeer, fasiliteer.

Na suksesvolle sintese van die (*E*)-5-stirielisatien- en (*E*)-6-stirielisatienanaloë, wat slegs verskil ten opsigte van die substituent op die C-3 posisie van die fenielring, is die verbindings *in vitro* geëvalueer as omkeerbare inhibeerders van bobbejaan-lewer MAO-B. Inhiberingsaktiwiteit van die stirielisatienanaloë is bepaal met 'n spektrofotometriese metode. Die inhibeerderpotensie vir al die stririelisatien analoë is uitgedruk in terme van die konsentrasie van die verbinding nodig vir 50% inhibisie van die ensiem *in vitro* (IC_{50} waarde). Die omkeerbaarheid van die inhibisie is bevestig deur 'n tyds-afhanklike inhibisiestudie uit te

voer waartydens daar aagetoon is dat die MAO-B-inhibisie deur die stirielisatienanaloë onafhanklik is van die tydperk waarmee dit saam met die ensiem geïnkubeer word.

Die resultate toon dat substitusie met 'n stirielsyketting op C-5 van die isatienring omkeerbare inhibeerders van MAO-B lewer wat uitsonderlik potent is. (*E*)-5-(3-Chlorostiriel)isatien (IC_{50} = 20.7 nM) is ongeveer 430 keer meer potent as die leidraadverbinding isatien (IC_{50} = 8.6 µM). (*E*)-5-stirielisatien is ook 'n baie goeie inhibeerder van MAO-B met 'n IC_{50} waarde van 41.7 nM, ongeveer 210 keer meer potent as die van isatien. Die (*E*)-6-stirielisatienanaloë het matige, omkeerbare MAO-B-inhibisie getoon. (*E*)-6-Stirielisatien het 'n IC_{50} waarde van 436.8 nM gehad. Die stirielsyketting sowel as elektroniese en lipofiliese eienskappe blyk belangrik te wees vir potente inhibisie van MAO-B deur hierdie verbindings.

In hierdie studie het die gesintetiseerde (*E*)-5-stirielisatienanaloë, veral (*E*)-5-(chlorostiriel)isatien, goeie potensiaal getoon as nuwe omkeerbare MAO-B-inhibeerders. Sintese en evaluering van 'n meer uitgebreide stirielisatienreeks sal 'n Hansch-tipe struktuuraktiwiteitsverwantskapstudie (SAV) moontlik maak wat die optimale fisieschemiese eienskappe vir die verbindings sal kan identifiseer.

ABSTRACT

Monoamine oxidase B (MAO-B) inhibitors are currently clinically used in the symptomatic treatment of Parkinson's disease (PD) and may also possess neuroprotective activity. The irreversible MAO-B inhibitor, (R)-deprenyl, is commonly used in PD treatment, usually in combination with levodopa during dopamine replacement therapy. In contrast with reversible inhibition, enzyme recovery after irreversible inhibition involves *de novo* synthesis. The relatively quick return of enzyme activity makes potent reversible MAO-B inhibitors safer and more desirable.

Both isatin and caffeine are small molecules that have been reported to inhibit MAO-B. Isatin is a relatively good endogenous inhibitor (K_i = 3 μM) whereas caffeine is a weak inhibitor (K_i = 650 μm). The inhibitory potency of caffeine have been improved by substitution at C-8 of the caffeine ring with a styryl side-chain. Addition of an electron withdrawing substituent at C-3 of the phenyl ring produced structures with exceptional reversible MAO-B inhibitory potency, for example (*E*)-8-(3-chlorostyryl)caffeine (CSC) (K_i = 0.1 μM). In this study we investigated whether styryl substitution of the lead compound, isatin, at C-5 and C-6 will similarly enhance isatin's MAO-B inhibitory potency.

Preliminary computer modelling of the proposed (*E*)-5-styrylisatin and (*E*)-6-styrylisatin analogues, as well as isatin, into the active site of recombinant MAO-B supported the hypothesis of increased MAO-B inhibitory activity for these styryl analogues. The styryl side-chain seems to be stabilised in the entrance cavity of the enzyme during binding, while the isatin moiety is located in the substrate-binding cavity where it is involved in hydrogen bonding. This duel binding mode is similar to that proposed for the styrylcaffeines and is thought to facilitate the potent MAO-B inhibition of styrylcaffeines.

After successful synthesis of the (*E*)-5-styrylisatin and (*E*)-6-styrylisatin analogues, the compounds were evaluated *in vitro* as reversible inhibitors of baboon liver MAO-B. Inhibitory activity of the styrylisatin analogues were determined with a spectrophotometric method. The inhibitory potencies for all the styrylisatin analogues were expressed in terms of the concentration of the compound necessary for 50% inhibition of the enzyme *in vitro* (IC_{50} value). Reversibility of inhibition was confirmed with a time-dependent inhibition study that showed that the potencies of inhibition of MAO-B by the (*E*)-styrylisatin analogues were independent of the time period for which the analogue was incubated with the enzyme.

The results confirmed that substitution with a styryl side-chain on C-5 of the isatin ring resulted in reversible inhibitors of MAO-B that are exceptionally potent. For example, (*E*)-5-

(3-chlorostyryl)isatin (IC_{50} = 20.7 nM) was found to be 430 times more potent than the lead compound isatin (IC_{50} = 8.6 μM). Also, (*E*)-5-styrylisatin was found to have a IC_{50} value of 41.7 nM, which is approximately 210 times more potent as a MAO-B inhibitor than isatin. The (*E*)-6-styrylisatin analogues showed moderate, reversible MAO-B inhibition. For example, (*E*)-6-styrylisatin has an IC_{50} value of 436.8 nM. The styryl side-chain as well as electronic and lipophilic properties seem to be important for potent inhibition of MAO-B by these compounds.

In this study, the synthesised *(E)*-5-styrylisatin analogues, in particular (*E*)-5-(3-chlorostyryl)isatin, showed potential as novel reversible MAO-B inhibitors. Synthesis and evaluatin of a more extensive series of styrylisatin analogues would enable a Hansch-type structure-activity relationship study that could identify the optimal physicochemical properties for the compounds.

TABLE OF CONTENT

Chapter 1

INTRODUCTION

1.1 Study aim

Parkinson's disease (PD) is the second most prevalent progressive neurodegenerative disorder after Alzheimer's disease, but treatment options available still provide only symptomatic relief. Treatment with monoamine oxidase B (MOA-B) inhibitors may not only provide symptomatic relief by restoring striatal dopamine activity (Bonuccelli & Del Dotto, 2006), but may also provide neuroprotection by reducing oxidative stress (Hubalek *et al.*, 2005). In order to further develop reversible MAO-B inhibitors, it is the aim of this study to firstly synthesise (*E*)-5-styrylisatin (**8a–c**; Fig. 1) and (*E*)-6-styrylisatin (**9a–b**; Fig. 1) analogues and secondly to evaluate these analogues as reversible competitive inhibitors of MAO-B.

1.2 Study hypothesis

The small endogenous molecule, isatin, is known to be a good inhibitor of MAO-B (Medvedev *et al.*, 1996), whereas caffeine, another small molecule, is a weak competitive inhibitor of MAO-B. The relatively larger (*E*)-8-styrylcaffeinyl analogues have been reported by our group to be moderate to very potent competitive MAO-B inhibitors (Petzer *et al.*, 2003; Vlok *et al.*, 2006; Van den Berg *et al.*, 2007). It was proposed that the relatively more potent inhibition observed with (*E*)-8-styrylcaffeines is dependent upon the styryl side-chain that is thought to bind in the entrance cavity of the enzyme while the caffeine ring binds within the substrate-binding cavity. This dual mode of binding is proposed to be responsible for the potent MAO-B inhibition observed with (*E*)-8-styrylcaffeines. It was further observed that C-3 substitution of the styryl ring with electron withdrawing substituents enhance inhibition potency to a great extent. In this study isatin, already a relatively good MAO-B inhibitor, will be substituted with a styryl side-chain at C-5 and C-6 of the isatin ring, respectively. The structures of the (*E*)-5-styrylisatin and (*E*)-6-styrylisatin analogues that will be investigated in this study is illustrated in Fig. 1. Preliminary modelling studies suggested that the (*E*)-5-styrylisatin and (*E*)-6-styrylisatin analogues will bind with the isatin ring in the substrate-binding cavity while the styryl side-chain is expected to project into the entrance cavity. This dual binding mode, as for (*E*)-8-styrylcaffeine, is expected to enhance the MAO-B inhibition potency of isatin to a large extent. The inclusion of analogues functionalised with electron withdrawing substituents at C-3 of the styryl ring may lead to compounds that are especially active.

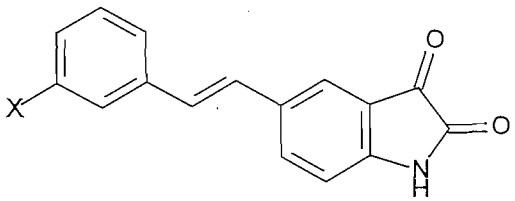

A: (*E*)-5-styrylisatin analogues

8a: X = H
8b: X = Cl
8c: X = F

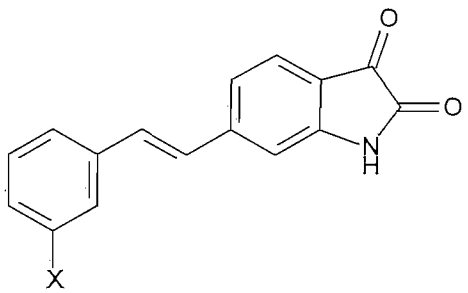

B: (*E*)-6-styrylisatin analogues

9a: X = H
9b: X = Cl

Figure 1: Structures of compounds investigated in this study.

LITERATURE OVERVIEW

2.1 Parkinson's disease

The physical characteristics of Parkinson's disease (PD) were first described by Dr. James Parkinson in 1817. Today, PD is the second most prevalent progressive neurodegenerative disorder after Alzheimer's disease. It affects about 1% of the population over 60 years of age and 0.3% of the entire population of industrialized countries (de Lau & Breteler, 2006). Dorsey *et al.* (2007) estimated the number of affected individuals in 10 of the world's most populous nations to be between 4.1 and 4.6 million in 2005 and predicted that this number would double by 2030. The risk of developing PD increases with increasing age (McDonald *et al.*, 2003), and as the average lifespan of individuals increases, the number of people affected by PD is also likely to increase (Smeyne & Jackson-Lewis, 2005).

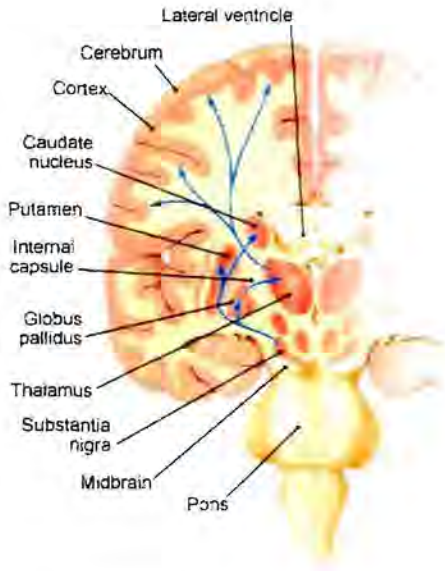

Figure 2: A coronal section of the brain showing dopaminergic neurons in the substantia nigra projecting to the striatum (caudate & putamen). Striatal neurons project to the globus pallidus. GABAergic pallidal neurons send inhibitory projections to the cerebral cortex and stimulatory glutamatergic projections project back to the striatum and down through the corticospinal tract (Young, 1999).

Clinical characteristics of PD include tremors at rest, slowness of movement, increased muscle tone, and postural instability (Blum *et al.*, 2001). The neuropathological and neurochemical characteristics of PD are well defined (Blum *et al.*, 2001). These are a decrease in neuromelanin containing dopaminergic neurons, specifically in the substantia nigra pars compacta (SNpc) region of the brain (Fig. 2), with an associated loss of striatal dopamine (DA) (Fig. 3) (Blum *et al.*, 2001). The cell bodies of these nigrostriatal neurons are located in the SNpc and project out primarily to the putamen (Dauer & Przedborski, 2003). Cell loss in SNpc is concentrated in the ventrolateral and caudal portions whereas the dorsomedial aspects are affected in normal aging (Dauer & Przedborski, 2003). PD symptoms start to manifest when about 80% of putamen and 60% of SNpc dopaminergic neurons have died off. It is thought that striatal dopaminergic nerve terminals are the primary target for initiation of neurodegeneration, and that neuronal death is a result of the "dying back" process (Dauer & Przedborski, 2003).

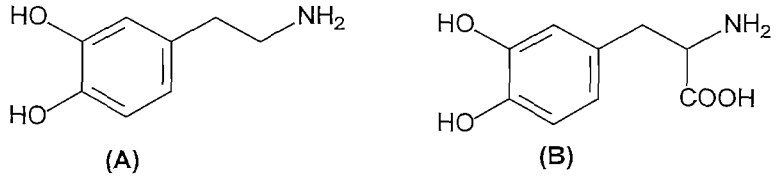

Figure 3: The structure of dopamine (**A**) and levodopa (**B**).

Eosinophilic intraneuronal inclusions, called Lewy bodies (LB), are histologically characteristic of the dopaminergic cell loss that are seen in, but that are not specific to PD (Dauer & Przedborski, 2003). Neurodegeneration and LB formation in other brain areas such as the noradrenergic locus coeruelus, serotonergic raphe, cholinergic Meynert basalis nucleus, cerebral cortex, olfactory bulb and autonomic nervous system are usually seen in more severe or late stages of PD (Dauer & Przedborski, 2003) and may be implicated in the non-motor symptoms of PD such as depression (Chaudhuri *et al.*, 2006).

The etiology of idiopathic PD is unknown. Several environmental and/or genetic factors have been suggested to contribute to PD pathogenesis (Blum *et al.*, 2001), yet no specific toxin has been proven to be a cause of PD. Environmental exposure or inherited differences may cause distorted metabolism leading to endogenous toxins (Dauer & Przedborski, 2003). Very few (5 to 10%) of PD cases are familial forms (Blum *et al.*, 2001) and older onset and sporadic cases of PD are not explained by genetic mutations (Jenner, 1999). Genetic mutations may cause misfolded proteins which can be neurotoxic and lead to activation of programmed cell death. Mutations may render cellular machinery, such as parkin, unable to detect and degrade misfolded proteins, causing accumulation and aggregation of these misfolded proteins, cell dysfunction and eventually cell death (Dauer & Przedborski, 2003). The first gene mutation (for the cytosolic protein α-synclein) to be associated with a familial form of PD were discovered in 1997 (Polymeropoulos & Lavendan, 1997). α-Synclein is

present in Lewy bodies which are characteristically seen in PD. More PD genes, such as for parkin and ubiquitin C-terminal hydrolase's L1 (UCH-L1), have since been identified (Dauer & Przedborski, 2003). The pathogenesis of PD may thus be seen as multifactorial cascade of deleterious factors (Bové *et al.*, 2005) that include the misfolding and aggregation of proteins and/or mitochondrial dysfunction with associated increased oxidative stress and toxic oxidised DA species (Dauer & Przedborski, 2003).

Current treatment options available for PD provide only symptomatic relief, and not a cure. Although neuroprotective strategies are believed to be possible (Blum *et al.*, 2001), none of the available treatments have yet conclusively proven to halt or retard PD progression (Dauer & Przedborski, 2003). The DA precursor drug, levodopa (3,4-dihydroxy-L-phenylalanine), is to date the main and most powerful symptomatic treatment option available (Fig. 3). The usefulness of levodopa is limited to 5 – 10 years because of complications such as diskinesia, motor fluctuations, and psychosis. DA agonists and monoamine oxidase inhibitors are other available symptomatic treatment options that may offer moderate improvement of levodopa associated complications (Lees, 2005). Drugs being researched for neuroprotective activity have properties such as MAO inhibition, mitochondrial enhancement (coenzyme Q10, creatine), anti-apoptotic activity, anti-inflammatory activity, protein aggregation inhibition, and neurotrophic activity. Some novel strategies for the effective control or reversal of motor complications include NMDA and AMPA antagonists or drugs acting on serotonin (5-HT) subtype 2_A, α_2-adrenergic and adenosine A_2 receptors (Bonucelli & Del Dotto, 2006).

New therapeutic approaches, which offer not only better symptomatic relief without complications, but also neuroprotection are important for overcoming the present shortcomings in the treatment of PD (Bonucelli & Del Dotto, 2006). Since a cascade of molecular events, involving several neurotransmitter systems, may lead to the complex etiology of PD involving multiple pathways, multifunctional drugs that act on multiple targets may be a better approach to the treatment of PD (Van der Schyf *et al.*, 2006). Among the multifunctional approaches suggested for the treatment of PD and other neuropsychiatric disorders are iron chelators with selective MAO inhibitory activity and adenosine antagonists with MAO inhibitory activity (Van der Schyf et al., 2006).

2.2 The role of MAO-B in Parkinsons's disease

The first successful use for MAO inhibitors was in depressive illness (Youdim *et al.*, 2006). Because of serious side effects such as the potentially fatal "cheese reaction", research efforts on MAO-A inhibitors for depressive illness ceased (Youdim & Bakhle, 2006). The "cheese reaction occurs when irreversible MAO inhibitors inhibit the usual "first past" metabolism of tyramine and other indirect acting sympathomimetic amines (common in certain cheeses), in the gut wall and liver. Tyramine and other indirect acting sympathomimetic amines are thus able to enter the systemic circulation and cause the release of noradrenaline from peripheral adrenergic neurons, leading to a severe and sometimes fatal

hypertensive response (Youdim & Bakhle, 2006). Research continued on an irreversible MAO-B inhibitor, (R)-deprenyl (also known as selegiline) (Fig. 4) (Knoll & Magyar, 1972). This compound, derived from propargylamine, inhibited oxidative deamination of dopamine, phenylethylamine, and benzylamine at low doses. Although devoided of the "cheese reaction", it did not show promising antidepressant effects. Further studies on this compound eventually led to the successful use of (R)-deprenyl in PD (Birkmeyer *et al.*, 1985; Youdim & Bakhle, 2006). (R)-deprenyl was found to delay the need for levodopa therapy with early PD, suggesting neuroprotective properties for (R)-deprenyl (Koller *et al.*, 1993; Shoulson, 1998). The value of longterm treatment with (R)-deprenyl, and whether it reduces mortality, remains uncertain (Birkmayer *et al.*, 1985; Youdim & Bakhle, 2006; Shoulson, 1998).

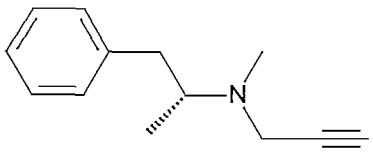

Figure 4: The structure of (R)-deprenyl.

There are a few theories about the etiology of PD. It shares some pathological features with other neurodegenerative disorders such as oxidative stress, iron accumulation, excitotoxicity, inflammatory processes, and the misfolding of toxic proteins that cannot be degraded after ubiquitination (Youdim *et al.*, 2006). An age-related increase in MAO-B has been seen in postmortem brains, and ontogenetic studies demonstrated a non-linear increase in MAO-B after the 60th life year. Since glial cells consist mainly of MAO-B, glial cell proliferation has been implicated in neuronal loss (Novaroli *et al.*, 2006). Increased MAO-B causes an increase in oxidative stress. Hydrogen peroxide, a normal product of MAO oxidation of substrates such as dopamine, is inactivated by glutathione peroxidase in the brain with glutathione (GSH) as the cofactor. An increase in MAO activity and insufficient brain levels of GSH can thus lead to the accumulation of hydrogen peroxide. This increases the availibility of hydrogen peroxide for usage in the Fenton reaction (Fig. 5) in which a ferrous ion (Fe^{2+}) generates a highly active hydroxyl free radical (Youdim & Bakhle, 2006). By damaging nucleic acids, proteins, and membrane lipids, these radicals may eventually cause neuronal degeneration. Iron levels are known to have an influence on the activity of MAO in both humans and animals and iron accumulation is seen at the same sites of neural death in degenerative diseases such as PD (Zecca *et al.*, 2004). Because brain MAO (Oreland & Gottfries, 1968), as well as iron (Youdim & Bakhle, 2006), increases with age, the risk of this reaction thus also increases with age.

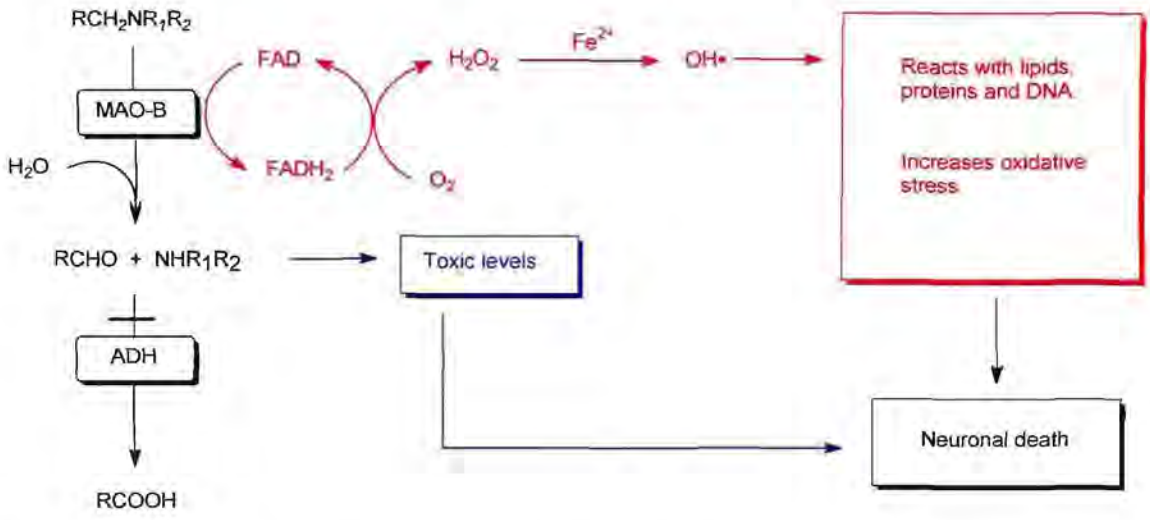

Figure 5: Proposed mechanisms of neurotoxicity via the Fenton reaction (represented in red) and via increased levels of aldehydes and ammonia (represented in blue). ADH is aldehyde dehydrogenase.

Other products of monoamine oxidative deamination are ammonia (as a primary amine product) or a substituted amine (as a secondary amine product) (Youdim *et al.*, 2006). It is known that ammonia can be neurotoxic at high levels (Yang *et al.*, 2004; Youdim *et al.*, 2006) and that the aldehyde derived from dopamine metabolism is cytotoxic, but does not seem to accumulate (Lamensdorf *et al.*, 2000). Midbrain dopaminergic neuronal lesions have however been discovered as a result of such aldehyde products. In PD, where levels of aldehyde dehydrogenase in the substantia nigra are greatly reduced (Galter *et al.*, 2003), the accumulation of aldehydes (Fig. 5) may become toxic, yielding compounds such as tetrahydropapaveroline (Shin *et al.*, 2004).

MAO inhibitors may be useful in PD in more than one way. By selectively inactivating the MAO-B enzyme, such inhibitors can increase the concentrations of both endogenous and exogeneously administered dopamine, restoring striatal dopamine activity (Bonuccelli & Del Dotto, 2006). By reducing MAO-B activity and consequently oxidative stress, the production of other reactive oxygen species and toxic products can also be avoided, thus providing neuroprotection. The further development of reversible MAO-B inhibitors will be clinically useful, not only for symptomatic treatment, but also as neuroprotection in PD (Hubalek *et al.*, 2005).

2.3 The neurotoxin MPTP

MPTP (1-methyl-4-phenyl-1,2,3,6-tetrahydropyridine) (Fig. 7) is a proneurotoxin that is metabolically activated by MAO-B. MPTP was discovered as a contaminant in the synthesis of the illegal narcotic meperidine analogue, MPPP (Fig. 6) (Langston *et al.*, 1983). It's neurotoxic properties came to light in the early 1980's when it caused parkinsonian symptoms in addicts (Dauer & Przedborski, 2003). These symptoms were irreversible and responsive to levodopa therapy. Post-mortem brain examinations of

these patients revealed substantia nigra lesions (Davis *et al.*, 1979; Blum *et al.*, 2001). MPTP administration also causes nigral degeneration in animal species such as the mouse and monkey. MPTP toxicity may not be restricted to DA-neurons (Blum *et al.*, 2001).

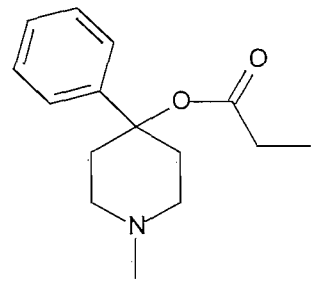

Figure 6: The structure of MPPP.

Important information about disease pathophysiology can be obtained from experimental animals treated with neurotoxins (Smeyne & Jackson-Lewis, 2005). MPTP animal models are able to induce oxidative stress, mitochondrial inhibition, and histological lesions which are also some of the main defects seen in PD (Blum *et al.*, 2001). Other aspects of PD, such as the precise anatomical lesions, the time-course of the disease, and long-term compensatory mechanisms are unfortunately not seen with MPTP animal models. The effects of MPTP on animal models depend on parameters such as administration mode, dosage, and animal age (Blum *et al.*, 2001).

A single administration of MPTP is thought to be able to start a self-sustained cascade of cellular and molecular events that have long-lasting detrimental effects (Bové *et al.*, 2005). The abolishment of oxidative phoshorylation have been suggested as a cause of MPTP-induced nigrostriatal cell death (Nicklas *et al.*, 1985; Blum *et al.*, 2001). Oxidative phosphorylation is dependent on a normal NADH oxidation pathway as well as coupled ATP synthesis (Singer *et al.*, 1988).

After intravenous administration, MPTP is peripherally (mainly in the liver) converted to MPP^+ which is unable to cross the blood-brain barrier for entry into the brain (Smeyne & Jackson-Lewis, 2005). Highly lipophilic MPTP does cross the blood-brain barrier (Dauer & Przedborski, 2003) before undergoing MAO-B catalysed 2-electron oxidation of the ring α-carbon to yield $MPDP^+$ (1-methyl-4-phenyl-2,3-dihydropyridinium) in astrocytes (Fig. 7). $MPDP^+$ spontaneously undergoes a second 2-electron oxidation to the corresponding active form, MPP^+ (Fig. 7). Pretreatment with non-selective MAO inhibitors pargyline, nialamide, and tranylcypromine, as well as the MAO-B selective inhibitor (R)-deprenyl, protects mice against MPTP-induced neurotoxicity by preventing MAO-B metabolism to the active neurotoxin, MPP^+ (Heikkila *et al.*, 1984).

Auto-oxidation of $MPDP^+$ may result in superoxide radical formation (Zang & Misra, 1992; Blum *et al.*, 2001) that may lead to protein damage (Smeyne & Jackson-Lewis, 2005). MPP^+ may cause the up-regulation of inducible nitric oxide synthase (iNOS) which produces nitric oxide (NO) that diffuses over membranes and react with a superoxide radical to form peroxynitrite ($OONO^-$), which is one of the most destructive oxidising molecules (Smeyne & Jackson-Lewis, 2005; Ischirapoulos & al-Mehdi, 1995). A potential target of $OONO^-$ nitration is the rate limiting enzyme of catecholamine synthesis, tyrosine hydroxylase (TH) that is found in the SNpc (Smeyne & Jackson-Lewis, 2005). Brains of PD patients have shown deficits in TH enzyme and its activity (Jan *et al.*, 2000).

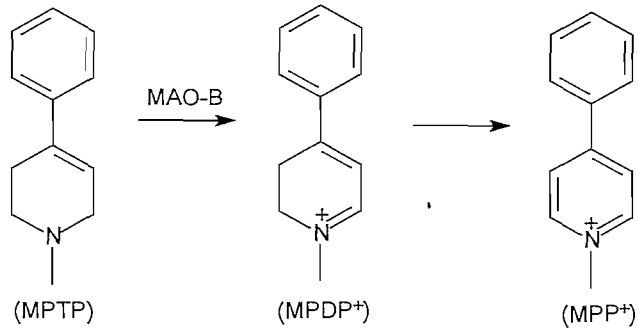

Figure 7: The MAO-B catalyzed oxidation of MPTP.

The mechanism by which MPP^+ is released from glial cells, where it is produced, is unknown (Smeyne & Jackson-Lewis, 2005), but after its extracellular release, MPP^+ accumulates in dopaminergic neuronal cells by means of dopamine transporters (DAT) (Smeyne & Jackson-Lewis, 2005) (Fig. 8). A hydrophobic and positively charged residue is required by the transporter, which explains why some more potent mitochondrial toxins, such as rotenone or MPTP, are not taken up by the transporter (Dauer & Przedborski, 2003, Heikkila *et al.*, 1984). Mice with null mutations of DAT were found to be protected against MPTP toxicity (Bezard *et al.*, 1999; Gainetdinov *et al.*, 1997; Smeyne & Jackson-Lewis, 2005). Intracytoplasmic accumulation has been suggested to be assisted by neuromelanin in neuronal cell bodies that form a complex with MPP^+ (D'Amato *et al.*, 1986). MPP^+ may also be confined to synaptic vesicles in DA neurons by means of vesicular monoamine transporters (VMAT2) (Takahashi *et al.*, 1997; Staal & Sonsalla, 2000), giving protection against MPP^+ toxicity (Staal & Sonsalla, 2000). Therefore, the ratio of DAT to VMAT2 expression may predict susceptibility towards neuronal degeneration in MPTP toxicity and even PD (Dauer & Przedborski, 2003).

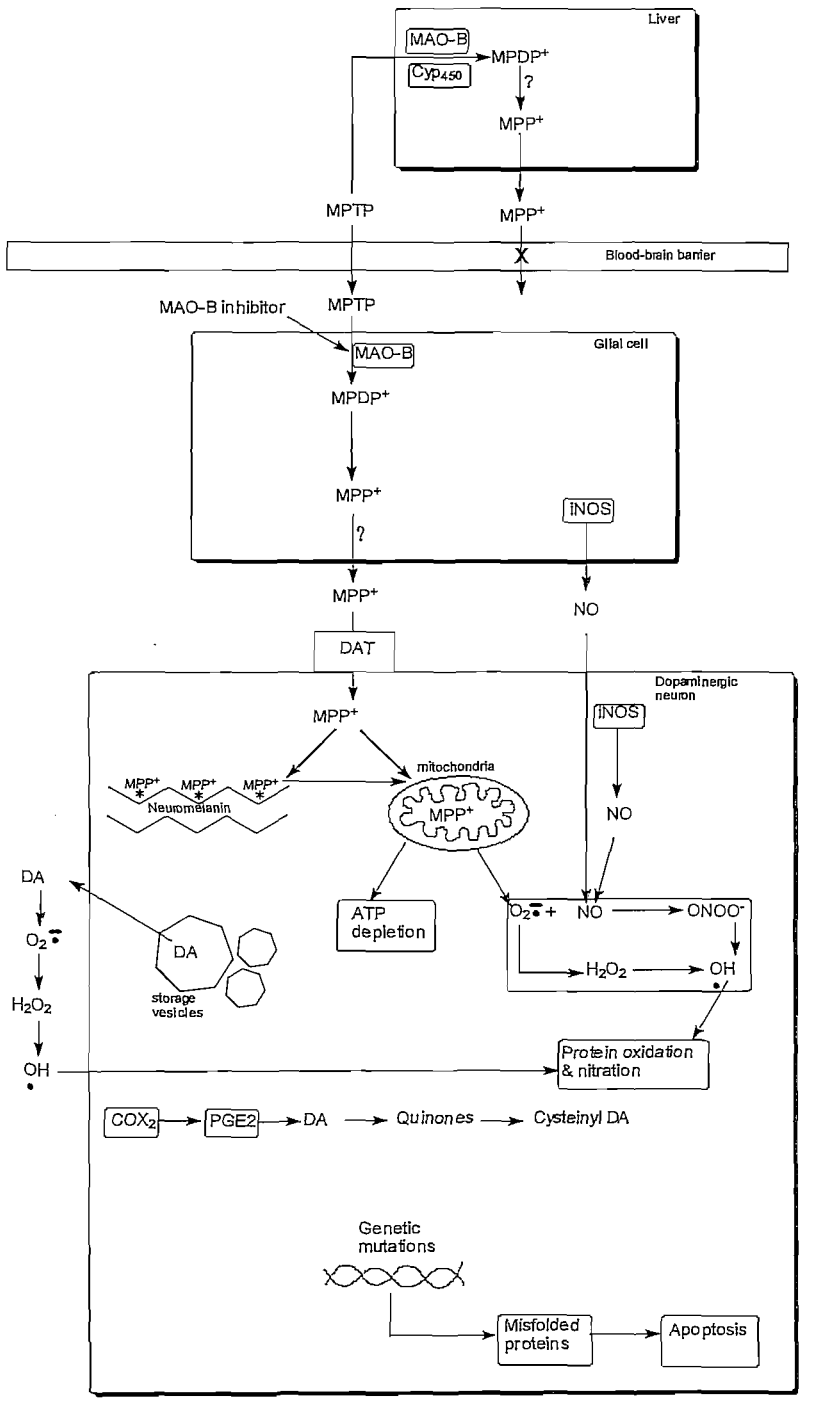

Figure 8: Proposed mechanisms of MPTP-induced neurotoxicity.

Free cytoplasmic MPP^+ is actively diffused across the mitochondrial membrane by a membrane electrical gradient (Smeyne & Jackson-Lewis, 2005). In the mitochondria, high concentrations of MPP^+ inhibit complex I (electron transport enzyme NADH:ubiquinone oxidoreductase), leading to downstream events such as the reduction of cellular ATP production (Nicklas *et al.*, 1985), oxidative stress and

eventually nigrostriatal dopaminergic neuron degeneration (Singer *et al.*, 1988). Although other pyridine derivatives have similar actions on NADH dehydrogenase, they are not concentrated by the MPP^+ transporter and are thus not acutely toxic. MPP^+-induced inhibition of NADH dehydrogenase is reversible but, because nigrostriatal cells do not regenerate, the damage done is permanent (Singer *et al.*, 1988). MPP^+ inhibition of complex III (uniquinol:ferrocytochrome c oxidoreductase) and complex IV (ferrocytochrome c:oxygen oxidoreductase) have also been suggested (Cardoso *et al.*, 1999). The reduction in cellular energy (ATP) leads to the generation of superoxide radicals, hydrogen peroxide, and hydroxyl radicals that can oxidise and nitrate proteins, leading to neurotoxicity (Smeyne & Jackson-Lewis, 2005).

Accumulation and nitration of α-synclein was also observed in mouse midbrain and striatum 4 hours after MPTP administration (Smeyne & Jackson-Lewis, 2005). α-Synclein may promote apoptosis (Xu *et al.*, 2002; Dauer & Przedborski, 2003), that is believed to be under control of p53 protein, Bcl-2 family genes, and caspase activity (Blum *et al.*, 2001). Bax (a member of the Bcl-2 family) is upregulated in SNpc dopaminergic neurons of mice after prolonged administration of low to moderate doses of MPTP (Vila *et al.*, 2001; Dauer & Przedborski, 2003). Together with Bax upregulation and its translocation to the mitochondria, cytochrome c is released from mitochondria and caspase 9 and 3 are activated (Viswanath *et al.*, 2001; Dauer & Przedborski, 2003). DNA damage may be involved in Bax induction via p53 activation (Dauer & Przedborski, 2003). Activation of the JNK (c-jun N-terminal kinase) pathway is seen after MPTP administration (Saporito *et al.*, 2000; Xia *et al.*, 2001; Dauer & Przedborski, 2003) and is required for Bax mitochondrial translocation (Dauer & Przedborski, 2003).

Studies of MPTP toxicity may help to better understand PD and may lead to novel targets for therapeutic interventions (Smeyne & Jackson-Lewis, 2005).

2.4 Known inhibitors of MAO-B

There are many known inhibitors of MAO-B (Youdim & Bakhle, 2006) of which only a few will be discussed. MAO-B inhibitors can be classified as irreversible or reversible inhibitors, and as selective or non selective inhibitors (Riederer *et al.*, 2004; Petzer *et al.*, 2003). Some MAO-B inhibitors are used as monotherapy or adjunctive therapy when motor fluctuations occur with levodopa treatment. Other MAO-B inhibitors are under investigation as alternatives to (R)-deprenyl therapy and for neuroprotection (Vlok *et al.*, 2006; Lees, 2005).

2.4.1 Irreversible MAO-B inhibitors

Irreversible inhibitors act as substrates for the target enzyme and cause the irreversible inactivation of the enzyme (Gerlach *et al.*, 1992). The return of enzyme activity after irreversible inhibition requires *de novo* synthesis of the MAO-B protein (Vlok *et al.*, 2006) which may last for weeks (Thebault et al., 2004). Depending on the individual catalytic mechanism of inhibition, different irreversible inhibitors will

form either N(5) or C(4a) flavin adducts with MAO-B. The twisted conformation of the flavin ring is conserved with both C(4a) and N(5) flavin adducts (Binda *et al.*, 2003; Edmondson *et al.*, 2004)

Nonselective irreversible MAO inhibitors, such as tranylcypromine (**A**, Fig. 9), inhibit both MAO-A and B. Tranylcypromine (*trans*-2-phenylcyclopropylamine) binds covalently to the flavin ring of MAO-B to form a C(4a) flavin adduct (Binda *et al.*, 2003). Nonselective inhibition can lead to the "cheese reaction" and to potentially fatal hypertensive crises. Tranylcypromine is registered in South Africa for use in atypical depression, depression not responding to other therapies, and phobic or panic disorders (Gibbon, 2003). Pargyline (**B**), a propargylamine (**D**) derivative, is another nonselective irreversible MAO inhibitor but it forms a covalent N(5) adduct with the flavin. Ladostigil (**C**), a propargylamine derivative with combined cholinesterase and nonselective irreversible MAO inhibitory properties, is in phase II clinical studies for diffuse Lewy body disease and PD among others (Sagi *et al.*, 2005; Youdim *et al.*, 2006).

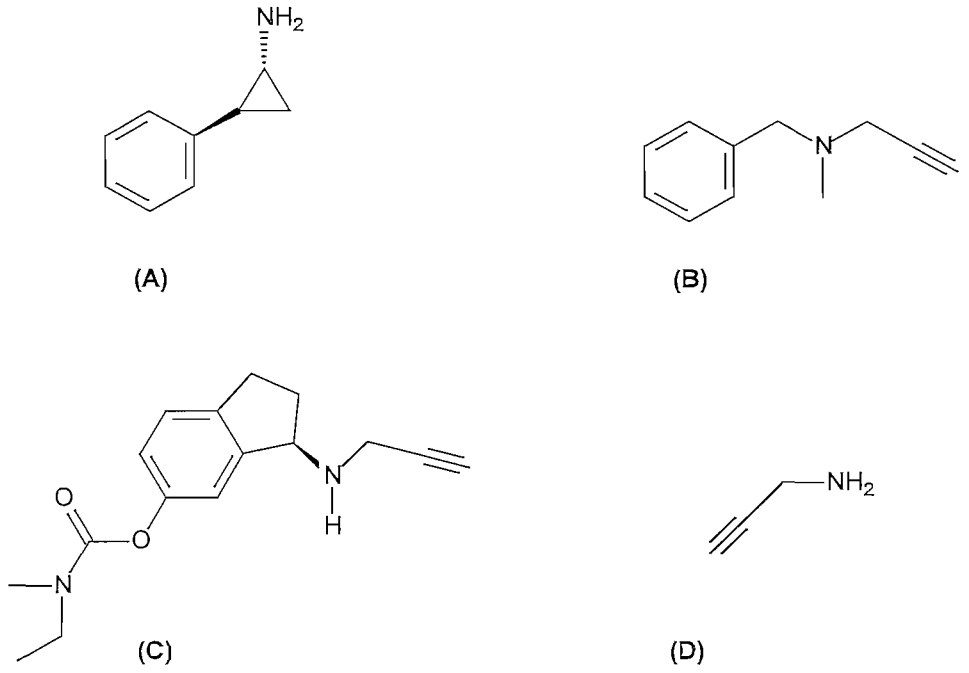

Figure 9: The structures of tranylcypromine (A), pargyline (B), ladostigil (C) and propargylamine (D).

The propargylamines (**D**) are an important class of compounds used for the symptomatic treatment of PD and is suspected of having neuroprotective properties. The propargylamine derivative, (*R*)-deprenyl (Fig. 4), was one of the first selective irreversible inhibitors of MAO-B (Casero & Woster, 2001). During MAO-B inhibition, (*R*)-deprenyl first forms a noncovalent complex with the enzyme, followed by reduction of the enzyme-bound FAD (flavin adenine dinucleotide) and concomitant oxidation of (*R*)-deprenyl. Oxidised (*R*)-deprenyl is then able to react covalently with the N(5) position of the flavin moiety, forming an irreversible adduct (Gerlach *et al.*, 1992). The long term safety of (*R*)-deprenyl has

been studied (Marras *et al.*, 2005), and it is registered in South Africa as adjunctive management of early and late phase PD, and for the control of some forms of response fluctuations (Gibbon, 2003), but can also be used as monotherapy (Lees, 2005). (*R*)-Deprenyl also seems to slow disease progression during the first years of treatment (Riederer *et al.*, 2004). Questions remain over the contribution of l-amphetamine, an (*R*)-deprenyl metabolite, towards the beneficial effects on PD symptoms (Youdim *et al.*, 2006).

Rasagiline (Fig. 10) is another selective irreversible MAO-B inhibitor and is more potent than (*R*)-deprenyl. It is the R(+)-enantiomer of a N-demethylated aminoidan propargylamine derivative, originallly developed as an anti-hypertensive (Finberg *et al.*, 1981; Youdim & Bakhle, 2006). Clinical use has shown rasagiline to be efficient as monotherapy in early PD (Parkinson study group, 2004), or as adjunct to levodopa therapy in the advanced disease (Parkinson study group, 2005; Rascol *et al.*, 2005; Lees, 2005), or where motor fluctuations, as a result of levodopa therapy, exists (Parkinson study group, 2003; Lees, 2005). Rasagiline also showed neuroprotective and anti-apoptotic properties in animal models (Am *et al.*, 2004; Maruyama *et al.*, 2002; Lees, 2005) and its use is already approved in some countries (Youdim & Bakhle, 2006). N-(2-Heptyl)-N-methylpropargylamine is another irreversible selective MAO-B inhibitor that has been studied (Youdim *et al.*, 2006).

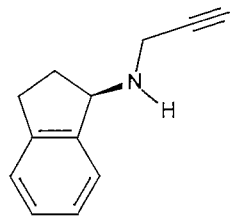

Figure 10: The structure of rasagiline.

Other *non*-propargylamine derivates which are under investigation as irreversible selective MAO-B inhibitors, are CGP3466, that is currently undergoing clinical trials (Sagot *et al.*, 2000; Youdim *et al*, 2006), and N-(2-aminoethyl)-p-chlorobenzamide (Fig. 11). N-(2-Aminoethyl)-p-chlorobenzamide has been shown to form an N(5) adduct with the flavin co-factor (Binda *et al.*, 2003; Edmondson *et al.*, 2004).

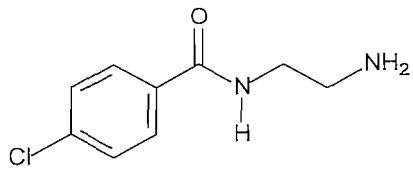

Figure 11: The structure of N-(2-aminoethyl)-p-chlorobenzamide.

2.4.2 Reversible MAO-B inhibitors

Because irreversible selective inhibitors, such as (R)-deprenyl, will also inhibit MAO-A at high levels, the best way to avoid the potentially fatal "cheese reaction" is by using reversible inhibitors. Reversible inhibitors compete for the binding to the active site of the MAO enzyme (Youdim & Bakhle, 2006).

The lead compound of this study, isatin (Fig. 12), was first identified as the selective MAO-B inhibitory component of tribulin, found in human urine (Glover *et al.*, 1998). It has been found in mammalian brain and peripheral tissues (Medvedev *et al.*, 1996, 2005) and in high concentrations in the human striatum (Hamaue *et al.*, 1999). Levels of this inhibitor have been found to increase following physiological stress in animal models (Igosheva *et al.*, 2004; Tozawa *et al.*, 1998) and also to increase in urinary excretion in patients with PD according to the severity of the disease (Li *et al.*, 2004; Hamaue *et al.*, 1999, 2000). It has therefore been suggested as an endogenous diagnostic marker in PD (Hamaue *et al.*, 1999). A range of biological activities (Hamaue *et al.*, 1999; Medvedev *et al.*, 1996, 2005), but only a few targets (MAO, natriuretic peptide receptor type A and soluble NO-stimulated guanylate cyclase) have been identified for isatin (Glover *et al.*, 1998; Buneeva *et al.*, 2003, Medvedev *et al.*, 2006). Isatin binds reversibly in the substate-binding cavity of MAO-B, as shown by the crystal structure of isatin bound MAO-B (Edmondson *et al.*, 2004; Hubalek *et al.*, 2004; 2005). The potential pharmacological actions of isatin itself and its analogues, have led to the use of the isatin moiety in diverse compounds which act for example as antineoplastic, antihypotensive, analgesic, anti-inflammatory, anticonvulsant, antiviral, anti-bacterial and anti-fungal drugs (Varma & Kahn, 1978; Medvedev *et al.*, 2005).

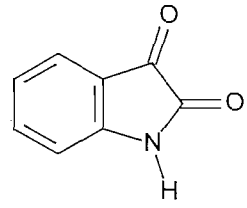

Figure 12: The structure of isatin (indole-2,3-dione).

The reversible styrylxanthinyl and styrylbenzimidazole derived MAO-B inhibitors have been investigated by our group (Petzer *et al.*, 2003; Vlok *et al.*, 2006; Van den Berg et al., 2007). The nonselective A_1/A_{2A} antagonist, caffeine (**A** in Fig. 13) (Chen *et al.*, 2001) and the potent selective A_{2A} antagonist, CSC [(*E*)-8-(3-chlorostyryl)caffeine] (**B**) (Petzer *et al.*, 2003; Jacobson *et al.*, 1993) were also studied as possible MAO-B inhibitors after neuroprotective properties were observed with certain A_{2A} antagonists. While caffeine was found to be a very weak MAO-B inhibitor, CSC proved to be an exceptionally potent selective reversible MAO-B inhibitor (Chen *et al.*, 2002). Subsequently other (*E*)-8-styrylxanthinyl (**C**) and (*E*)-2-styrylbenzimidazolyl (**D**) analogues of CSC were also found to be reversible competitive

inhibitors of MAO-B with moderate to potent activities (Petzer *et al.*, 2003; Vlok *et al.*, 2006; Van den Berg, 2007). The (*E*)-8-styrylcaffeinyl analogue, KW-6002 [(*E*)-1,3-diethyl-8-(3,4-dimethoxystyryl)-7-methylxanthine] (**E**), is currently in clinical trial as a possible therapeutic agent (Youdim & Riederer, 2004; Vlok *et al.*, 2006). The anti-parkinsonian action of KW-6002 appears to rely upon its antagonism of the A_{2A} receptor rather than inhibition of MAO-B since this compound inhibited MAO-B with moderate potency (Petzer *et al.*, 2003).

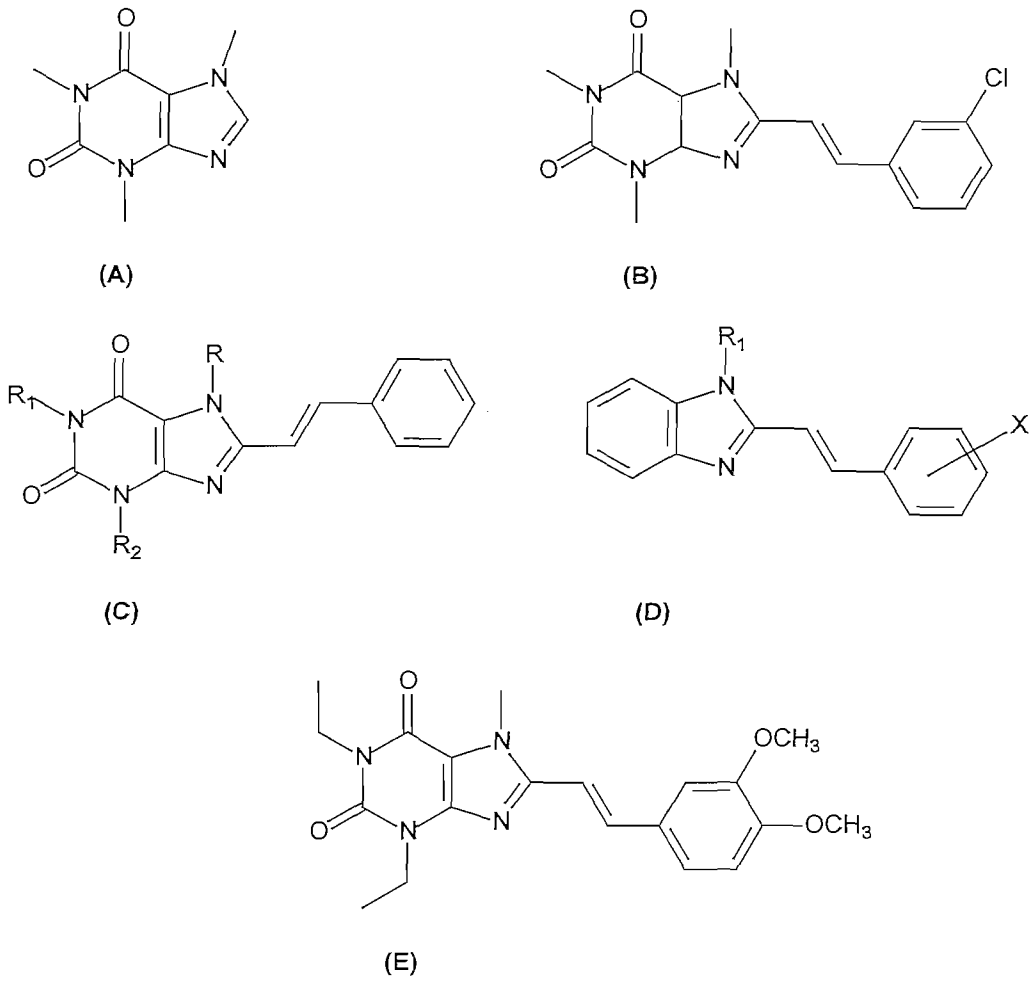

Figure 13: The structures of caffeine (**A**), (*E*)-8-(3-chlorostyryl)caffeine (CSC) (**B**), the (*E*)-8-styrylxanthinyl analogues (**C**), the (*E*)-2-styrylbenzimidazole analogues (**D**) and (*E*)-1,3-diethyl-8-(3,4-dimethoxystyryl)-7-methylxanthine (KW-6002) (**E**).

CSC and analogues thereof, is believed to extend into both the entrance and substrate-binding cavities of MAO-B when bound. Rotation of the Ile199 side-chain may facilitate fusion of the two cavities in order to accomodate these large inhibitors. It is expected that the phenyl ring of these compounds projects into the entrance cavity, while the polar functional groups of the caffeine ring are in close proximity to the flavin in the substrate-binding cavity (Vlok *et al.*, 2006). It seems that the extention and

binding of the styryl moiety into the entrance cavity may be responsible for the potent inhibition of these large MAO-B inhibitors (Petzer *et al.*, 2003; Vlok *et al.*, 2006; Van den Berg, 2007).

Ooms *et al.* (2003) developed and then used a general MAO-B pharmacophore model to design potent, 5H-indeno[1,2-c]pyridazin-5-one derived, reversible selective MAO-B inhibitors (**A** in Fig. 14). This led to the design of an exceptionally potent and selective MAO-B inhibitor, 3-methyl-8-(4,4,4,-trifluorobutoxy)indeno[1,2-c]pyridazin-5-one (**B**). The study confirmed the importance of specific hydrogen bonds in the substrate cavity as well as hydrophobic interactions for potent and selective MAO-B inhibition (Ooms *et al.*, 2003).

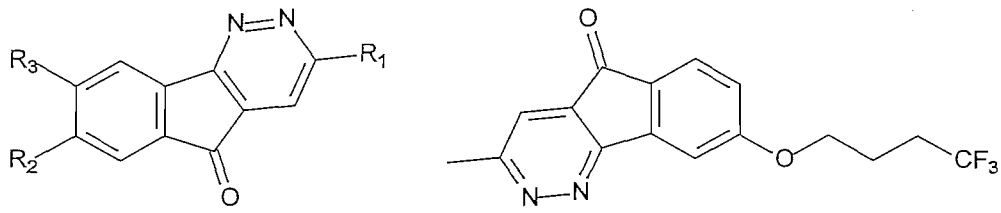

Figure 14: The structures of the 5*H*-indeno[1,2-c]pyridazin-5-one derivatives (**A**) and 3-methyl-8-(4,4,4,-trifluorobutoxy)indeno[1,2-c]pyridazin-5-one (**B**).

Other reversible selective MAO-B inhibitors that have been reported include: 1,4-diphenyl-2-butene (**A** in Fig. 15), *trans,trans*-farnesol (**B**), lazabemide (**C**), and safinamide (**D**) (Youdim *et al.*, 2006) and its coumarin analogues (Binda et al., 2007).

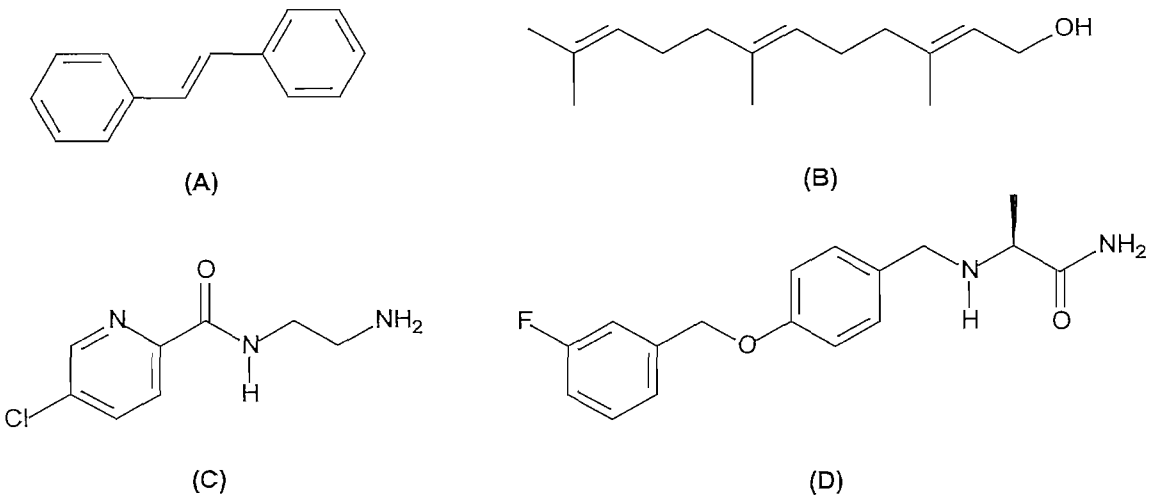

Figure 15: The structures of 1,4-diphenyl-2-butene (**A**), *trans,trans*-farnesol (**B**), lazabemide (C) and safinamide (D).

2.5 Copper containing amine oxidases

Amine oxidases can be divided into two main groups according to their attached cofactor (Fig. 16). MAO and polyamine oxidases fall into one group because of their shared FAD cofactor, whereas diamine oxidases, lysyl oxidases, plasma membrane and soluble MAOs fall into another group, the semicarbazide-sensitive amine oxidases (SSAOs). SSAOs all have a topaquinone (TPQ) cofactor. Three human SSAOs have been identified by the sequencing of the human genome and are known as kidney diamine oxidase, retinal amine oxidase, and human placental amine oxidase (Jalkanen & Salmi, 2001).

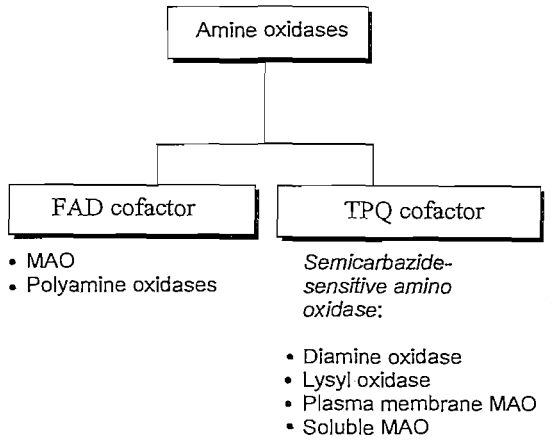

Figure 16: Diagrammatic classification of amine oxidases.

There are wide species and tissue differences in the activities of SSAOs (Tipton *et al.*, 2004). SSAO is widely expressed in mammals (Lyles, 1996), but is restricted to microvessels in the human brain (Jalkanen & Salmi, 2001), where it may contribute to the function of the blood-brain barrier (Tipton *et al.*, 2004). Except for diamine oxidase, SSAOs are extra cellular enzymes that are mainly found on outer membranes of vascular smooth muscle and endothelia, but are also found in soluble form (Yu, 2001; Jalkanen & Salmi, 2001). The plasma SSAOs may arise from proteolytic cleavage of membrane-bound SSAO (Tipton *et al.*, 2004). They are mostly dimeric glycoproteins with molecular masses ranging from 140 to 200 kDA (Jalkanen & Salmi, 2001; Lyles, 1996). Each dimer contains a TPQ cofactor and a copper atom that is always coordinated with three histidine residues (Jalkanen & Salmi, 2001) (Fig. 17).

The SSAOs catalyze the oxidative deamination of primary amines such as benzylamine (Jalkanen & Salmi, 2001), and there is evidence for its oxidative deamination of secondary arylamines (Lee *et al.*, 2002). Some of the physiological substrates believed to be metabolized by SSAO and not by MAO include aminoacetone and methylamine (Tipton *et al.*, 2004). The deamination reaction of SSAOs consists of two half reactions (Fig. 18). The substrate first reduces the enzyme by forming a transient

covalent schiff base and an aldehyde is concomitantly released. An oxygen molecule then re-oxidizes the enzyme and hydrogen peroxide and ammonia are released (Jalkanen & Salmi, 2001).

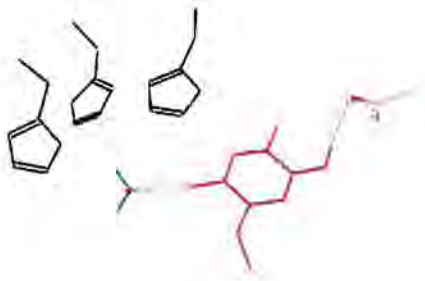

Figure 17: Representation of the SSAO active site. TPQ cofactor (in red) is involved in hydrogen bonds with a water molecule (WAT90) (in blue) and the Asp389 (carbon atoms in grey and oxygens in red) residue. The copper atom (in yellow) is coordinated via Van der Waals interactions with three histidines (HIS684, HIS520 and HIS522) (in black).

Unlike MAO, SSAO is inhibited by semicarbazides (hence the name semicarbazide-sensitive amine oxidase) (Tipton *et al.*, 2004). SSAOs are either insensitive or weakly sensitive to the classical MAO inhibitors [clogyline and (R)-deprenyl]. They are very sensitive to hydroxylamine inhibition and non-specifically sensitive to propargylamine, aminoguanidine, carbidopa, and procarbazine inhibition (Jalkanen & Salmi, 2001).

The physiological function of SSAO is not clear, although a few functions have been suggested. It is reported to be involved in the catabolism of xenobiotic and biogenic amines, histamine degradation, leukocyte adhesion and up-regulation during inflammation, glucose uptake and formation of extracellular matrix (Jalkanen & Salmi, 2001; Yu, 2001).

The products of SSAO mediated biogenic amine metabolism, such as formaldehyde and hydrogen peroxide, are known to be toxic. Formaldehyde forms cross-linked complexes with proteins and single stranded DNA (Heck *et al.*, 1990; Yu, 2001) and has an inflammatory effect (Wilmot *et al.*, 2004), whereas hydrogen peroxide leads to oxidative stress (Wilmot *et al.*, 2004).

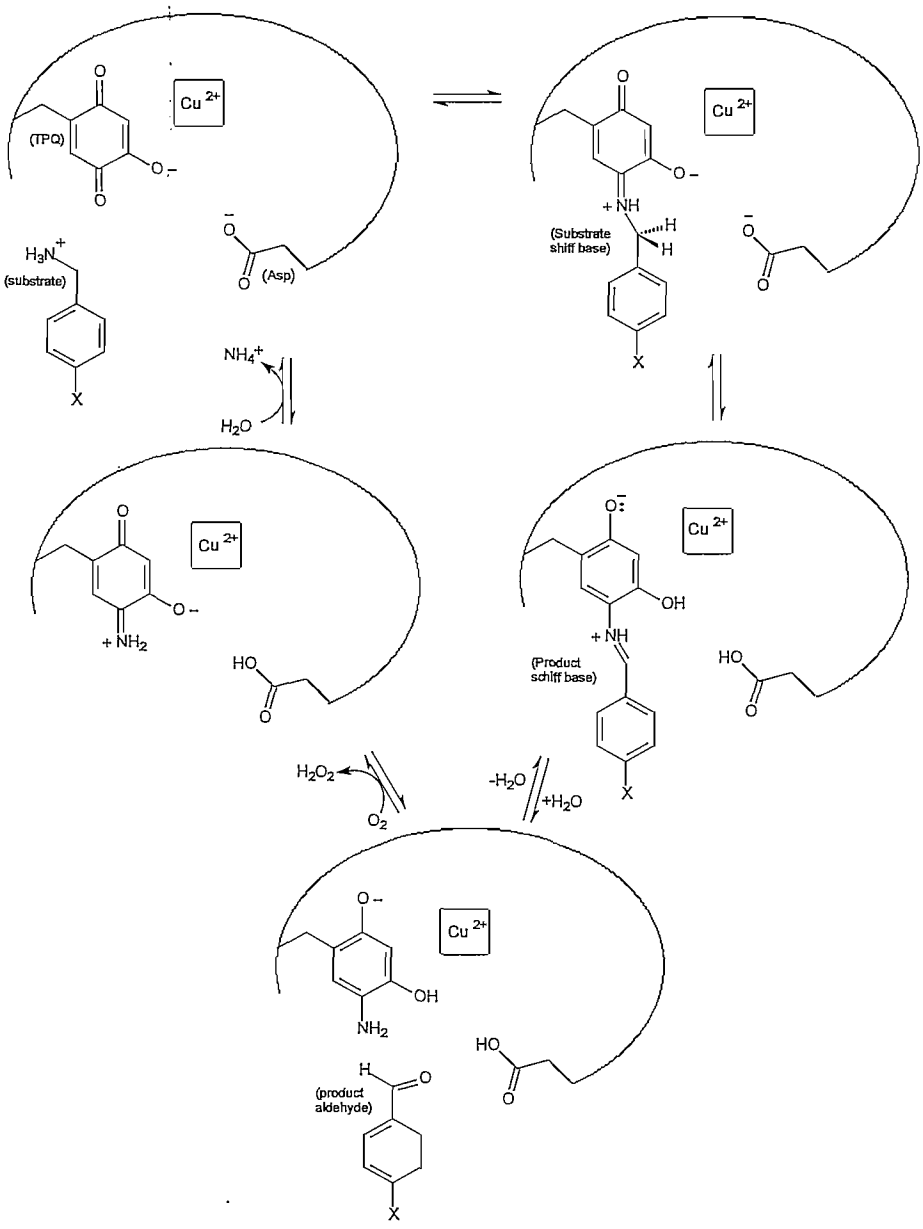

Figure 18: A possible catalytic reaction of SSAO. The reductive half-reaction starts with the reaction of a primary amine with the TPQ of the enzyme. A proton is removed by the active-site base, aspartate (Asp), and a schiff base is formed. The product aldehyde is released after hydrolysis and the reduced cofactor is left attached to the anzyme. In the oxidative half-reaction the reduced enzyme is recycled with accompanied release of hydrogen peroxide and ammonia.

2.6 Enzymology

2.6.1 General background of MAO-B

The mammalian monoamine oxidase enzyme is classified by the Enzyme Commission (2007) as EC 1.4.3.4 and named amine oxidase (flavin-containing). Alternative names for this enzyme are adrenaline oxidase, tyraminease, and tyramine oxidase.

MAO enzymes exist as two isoforms, MAO-A and MAO-B. The proteins of these isoforms are encoded by different genes on the X chromosome but have about 70% similarity (Youdim *et al.*, 2006). MAO-A consists of 527 amino acids whereas MAO-B consists of 520 amino acids (Shih *et al.*, 1999). Both isoforms are situated on the outer mitochondrial membrane of cells, such as neurons and glia, and contain a FAD molecule as cofactor (Ooms *et al.*, 2003). A small portion of MAO is associated with the microsomal fraction (Youdim *et al.*, 2006).

MAO is responsible for the regulation of neurotransmitter levels as well as for protection against xenobiotic amines by catalysing its oxidative deamination (Holt *et al.*, 1997) and has been shown to be important in brain development and function (Youdim *et al.*, 2006). These enzymes metabolise primary, secondary, and tertiary amines to the corresponding aldehydes. The resulting aldehydes are subsequently metabolised by aldehyde dehydrogenase to acid metabolites (Youdim & Bakhle, 2006).

The two MAO isoforms have differences in substrates and inhibitor selectivities that can be used to distinguish between them. MAO-A shows a preference for serotonin (5-HT) as substrate and its activity is inhibited by clorgyline whereas MAO-B shows a preference for benzylamine and 2-phenylethylamine as substrates and is inhibited by (R)-deprenyl (Youdim & Bakhle, 2006). Both isoforms metabolise tyramine and dopamine (Youdim *et al.*, 2005; Youdim & Bakhle, 2006).

Both MAO isoforms can be found in most mammalian tissues in different amounts (Shih *et al.*, 1999; Tipton *et al.*, 2004). Peripheral MAO is found in tissue such as the intestine, liver, lungs and placenta, where it may prevent amines from entering circulation. MAO-B in blood microvessels and the blood-brain barrier also seems to have a protective function (Youdim *et al.*, 2006). The highest brain activity level for MAO-B is in the basal ganglia where amines are oxidised extraneural in glial cells (Youdim *et al.*, 2006). Immunohistochemical studies showed that serotonergic neurons (for example in the dorsal raphe nucleus) mainly contain MAO-B, whereas catecholaminergic neurons (for example in the substantia nigra, locus coeruleus and periventricular region of hypothalamus) contain mainly MAO-A (Westlund *et al.*, 1985).

The primary source of purified MAO-B for use in studies has been the bovine liver mitochondrial fraction because of its availability and absence in MAO-A activity (Hubalek *et al.*, 2005; Newton-Vison *et al.*, 2000). Bovine MAO-B however, is larger than human MAO-B (Salach & Weyler, 1987) and has different

kinetic properties (Inoue *et al.*, 1999). Baboon liver mitochondrial MAO-B seems to be a better source because of its inhibitory specificities being similar to that of human liver MAO-B, and since it is devoid of MAO-A activity (Vlok *et al.*, 2006; Inoue *et al.*, 1999). Inoue *et al.* (1999) found a greater similarity in MAO activity profile between humans and rodents (particularly rats) than between humans and subhuman primates, but rat liver preparations have high MAO-A activity. Brain tissue and blood platelets can also be used as sources to screen MAO-B inhibitors. Human blood platelets contain prevalently the MAO-B isoform but may be difficult to obtain because of practical and ethical reasons (Novaroli *et al.*, 2006). Several species-dependent differences in substrate and inhibitor specificities for MAO have been reported (Novaroli *et al.*, 2006; Inoue *et al.*, 1999; Hubalek *et al.*, 2005) and extrapolating conclusions to the human should thus be done with caution.

Recombinant MAO-B has been validated as a convenient enzyme source (Novaroli *et al.*, 2005) that enables the direct determination of the kinetic and inhibitory properties of MAO-B, with a variety of substrates and inhibitors, without interference of MAO-A. The availability of large quantities of the enzyme permit detailed rapid reaction kinetic studies as well as detailed potential and redox studies on wild-type and mutated forms of the enzyme (Newton-Vinson *et al.*, 2000). High-levels of human recombinant MAO-B have been obtained from the methylotrophic yeast *Pichia pastoris* (Newton-Vinson *et al.*, 2000; Hubalek *et al.*, 2005) and from a *Baculovirus* (Novaroli *et al.*, 2005). Improvements in mass spectrometric techniques have also aided in the characterisation of recombinant MAO (Newton-Vinson *et al.*, 2000).

2.6.2 The three-dimensional structure of MAO-B

The 3 Å crystal structure of human flavin-dependent MAO-B was first determined by Binda *et al.* (2001). MAO-B is a dimer (Fig. 19), with each monomer composed out of 520 amino acids. A C-terminal transmembrane helix, formed by amino acids 461-520, connects each MAO-B monomer to the outer mitochondrial membrane. The helixes protrude from the basal face of the dimer, approximately parallel to the molecular two-fold axis. Other protein regions, such as apolar loops, may also be involved in membrane binding of MAO-B (Binda *et al.*, 2001).

The enzyme monomeric unit is divided into two domains: the substrate domain and the FAD-binding domain (Fig. 20). An anionic enzyme membrane surface facilitates the entry of a positively charged amine into the entrance cavity (Binda *et al.*, 2002). The outside of the protein is connected to the entrance cavity via a small pocket (Fig. 21) that is surrounded by polar residues and amino acids that are available for hydrogen bonding (Navaroli *et al.*, 2006). The entrance cavity has a volume of 290 $Å^3$ and is lined with hydrophobic residues; Phe103, Pro104, Trp119, Leu164, Leu167, Phe168, Leu171, Ile199, Ile316 and Tyr326, creating a highly lipophilic enviroment (Binda *et al.*, 2001). Movement of a substrate through the entrance cavity into the substrate-binding cavity involves negotiating a protein loop (Binda *et al.*, 2002). The two cavities are separated by the residues, Tyr326, Ile199, Leu171 and

Phe168. A momentary movement of these residues are necessary to allow substrates to enter the substrate-binding cavity. Ile199 is described as a "gate" for entrance into the substrate-binding cavity (Fig. 21) (Binda *et al.*, 2001). The cavities can be separated or fused as one large cavity depending on the position of Ile199. This Ile199 chain is found in all known MAO-B enzymes, except for bovine (and possibly sheep), where it is substituted with Phe199. This Phe199 substitution is also found in human MAO-A (Hubalek *et al.*, 2005). The substrate-binding cavity is a flat space with a volume of 420 $Å^3$ (Binda *et al.*, 2001). The character of the substrate cavity is mostly hydrophilic for recognition and directionality of the amine, with a hydrophobic patch near the flavin ring (Tyr60, Phe343 and Tyr398) to fasilitate the tight binding of apolar substrates and inhibitors (Novaroli *et al.*, 2006; Binda *et al.*, 2003).

Figure 19: A ribbon representation of the MAO-B dimer. Monomer A is in red and monomer B in blue. The membrane-binding C-terminal helixes of each monomer is in yellow. The N-terminals of both monomers are shown.

The substrate-binding cavity is directly in front of the flavin adenine dinucleotide (FAD) cofactor (Binda *et al.*, 2002) that is covalently bound to the protein via an 8α-thioether linkage to a cysteinyl residue (Cys397) (Kearney *et al.*, 1971 in Edmondson *et al.*, 2004). The FAD coenzyme is stretched out at full length (Edmondson *et al.*, 2004) with the aromatic isoalloxazine ring of the flavin (Fig. 22) bent aproximately 30° about the N(5)-N(10) axis into a twisted nonplanar conformation (Binda *et al.*, 2002; Binda *et al.*, 2003). This twisted conformation is retained when N(5) and C(4a) adducts are formed (Binda *et al.*, 2003). The ribityl side of the flavin ring that includes the N(5) and C(4a) reactive centres, is pointed towards the substrate binding site (Edmondson *et al.*, 2004). An ordered water molecule, hydrogen-bonded to the N(5) of the flavin, together with the ε-amino group of Lys296, forms a triad [Lys-H(2)-flavin N(5)], that participates in catalysis (Binda *et al.*, 2002). Other water molecules, that may participate in hydrogen bonds, are also present in the substrate-binding cavity (Binda *et al.*, 2003). The flavin, together with the aromatic side chains of Tyr398 and Tyr435, forms an aromatic cage (Fig. 21) for amine recognition (Binda *et al.*, 2001; Binda *et al*, 2002). The aromatic side chains are about 8 Å

apart, face each other, and are perpendicular to the flavin re-side (Binda *et al.*, 2002). . The broad substrate specificity of MAO-B may be because an aromatic ring is allowed to bind at many positions, farther or closer to the flavin in the substrate-binding cavity (Binda *et al.*, 2001).

Figure 20: The three-dimensional structure of the human MAO-B monomeric unit with three functionally distinct domains. The substrate domain is in green and contains the two fused cavities in gray semitransparent surface. The FAD-binding domain is in blue with the FAD molecule in black. The helical C-terminal region which anchors the protein to the outer mitochondrial membrane is in yellow.

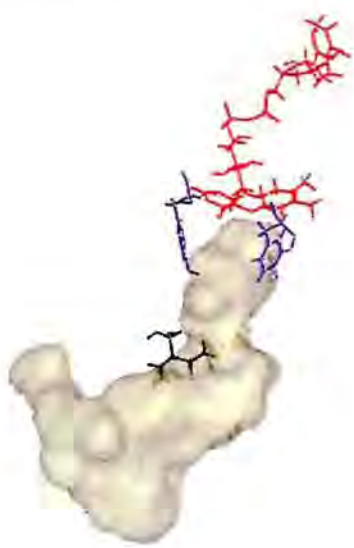

Figure 21: Representation of the entrance cavity and substrate-binding cavity (in grey) of MAO-B that are seperated by Ile199 (in black). The FAD molecule (in red), together with Tyr398 and Tyr435 (in blue) form the aromatic cage at the end of the substrate-binding cavity. The small pocket preceding the entrance cavity is also shown.

MAO-B inhibitors, such as the irreversible inhibitor pargyline, have been used to model the binding of substrates in the active site (Binda *et al.*, 2001), and the crystal structures of these inhibitor-MAO-B complexes have helped our understanding of the mode of binding and inhibition of reversible and irreversible inhibitors. Irreversible inhibitors bind covalently to the flavin ring whereas reversible inhibitors bind noncovalently in the substrate cavity (Binda *et al.*, 2003).

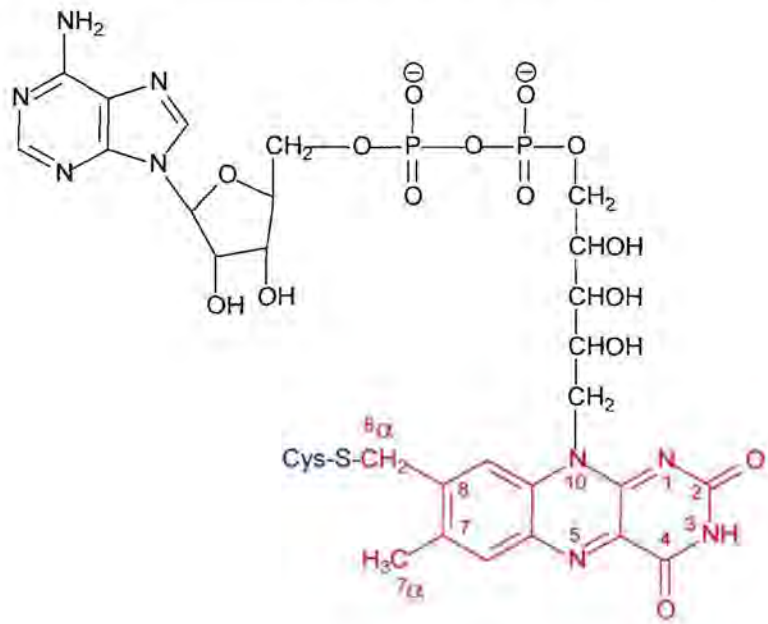

Figure 22: The structure of 8α-S-cysteinyl flavin-adenine dinucleotide (FAD). The 8α-S-cysteinyl linkage is represented in blue, the aromatic isoalloxazine ring of the flavin in red and the rest of the FAD molecule in black.

The dioxoindole ring of the reversible inhibitor, isatin (Fig. 12), is perpendicular to the flavin ring with the *oxo groups on the pyrrole ring pointing toward the flavin*. The 2-oxo group and the pyrrole NH are involved in hydrogen bonds with water molecules in the active site. Many van der Waals contacts are also found between the isatin ring and amino acid residues in the hydrophobic substrate-binding cavity. The Ile199 side chain separates the two cavities when isatin is bound. Another reversible inhibitor, 1,4-diphenyl-2-butene (**A** in Fig. 15), has a phenyl ring in the substrate-binding cavity in the same position as seen with isatin, but in contrast with isatin it also has a phenyl ring extending into the entrance cavity (Binda *et al.*, 2003). Other large reversible selective MAO-B inhibitors, such as *trans,trans*-farnesol (**B** in Fig. 15), also span both cavities of the MAO when bound. The Ile199 side chain is in the 'open' position when these large inhibitors are bound (Hubalek *et al.*, 2005) and is in a position that enables the two cavities to fuse together into one larger cavity (Binda *et al.*, 2003). The ability of isatin and the inability of the above selective reversible MAO-B inhibitors to bind to the human mutant MAO-B I199F, that has a bulky Phe199 side-chain, show that the Ile199 'gate' is a determinant for MAO-B specificity

(Hubalek *et al.*, 2005). New reversible MAO-B inhibitors can be developed to use both cavities as potential binding targets (Binda *et al.*, 2003).

The Irreversible inhibitors, pargyline (**B** in Fig. 9) and N-(2-aminoethyl)-p-chlorobenzamide (Fig. 11) bind covalently to the *re*-side of the flavin to form N(5) adducts (Binda *et al.*, 2001; Binda *et al.*, 2003). N-(2-Aminoethyl)-p-chlorobenzamide has an aromatic ring in the same orientation and position in the substrate-binding cavity as isatin (Binda *et al.*, 2003), and its p-chloro substituent on the benzamide ring necessitates the Ile199 side chain to be in the "open" position. *Trans*-2-phenylcyclopropargylamine (Tranylcypromine) (**A** in Fig. 9) also inhibits MAO-B covalently but binds to a different area on the flavin ring than N-(2-aminoethyl)-p-chlorobenzamide, to form a C(4a) adduct. The *trans*-2-phenylcyclopropargylamine adduct is parallel to the flavin ring whereas N-(2-aminoethyl)-p-chlorobenzamide is perpendicular. Because the phenyl ring of *trans*-2-phenylcyclopropargylamine does not extend far enough into the entrance cavity, the Ile199 side chain is in the "closed" position as seen with isatin (Binda *et al.*, 2003).

2.6.3 The catalytic cycle of MAO-B

As described previously, the catalytic area of MAO-B is situated in the substrate binding cavity and contains an FAD molecule that acts as cofactor (Kearney *et al.*, 1971). Upon entering this catalytic area, amine substrates are believed to be deprotonated to the free base (Binda *et al.*, 2002).

Several mechanisms have been proposed for the chemical events involved in flavin-dependent amino oxidation (Binda *et al.*, 2002). A popular description is the single electron transfer mechanism (Silverman *et al.*, 1995; Ottoboni *et al.*, 1990) where the flavin serves as a one-electron oxidant of the amine, leading to the formation of the aminium cation radical which is the initial reversible step in catalysis. This would render the α-proton sufficiently acidic to allow a basic amino acid residue at the active site to abstract the proton, thus leading to radical recombination to form the imine product and reduced flavin. Current structural data on MAO-B doesn't show an amino acid residue at the catalytic site which could function as an active site base (Binda *et al.*, 2002).

There is evidence for α-CH bond cleavage by an initial proton abstraction. In this suggested concerted reaction the amine functionality adds to the C(4a)-position of the flavin in a nucleophilic manner (Fig. 23). This addition activates the N(5)-position, which then functions as a strong active site base, leading to the reduction of the flavin and the formation of imine (Binda *et al.*, 2002). The Lys296 residue of MAO-B is bridged to the N(5)-atom of the flavin through a water molecule and seems to participate in catalysis by compensating for the change in the flavin protonation state during cofactor reduction (Binda *et al.*, 2001; Binda *et al.*, 2002). The imine product is hydrolysed to the corresponding aldehyde and ammonia (or amine if the substrate is a secondary or tertiary amine). Molecular oxygen subsequently

acts as an electron acceptor, oxidising the reduced flavin, and forming hydrogen peroxide. The catalytic cycle is thereby completed (Binda *et al.*, 2002).

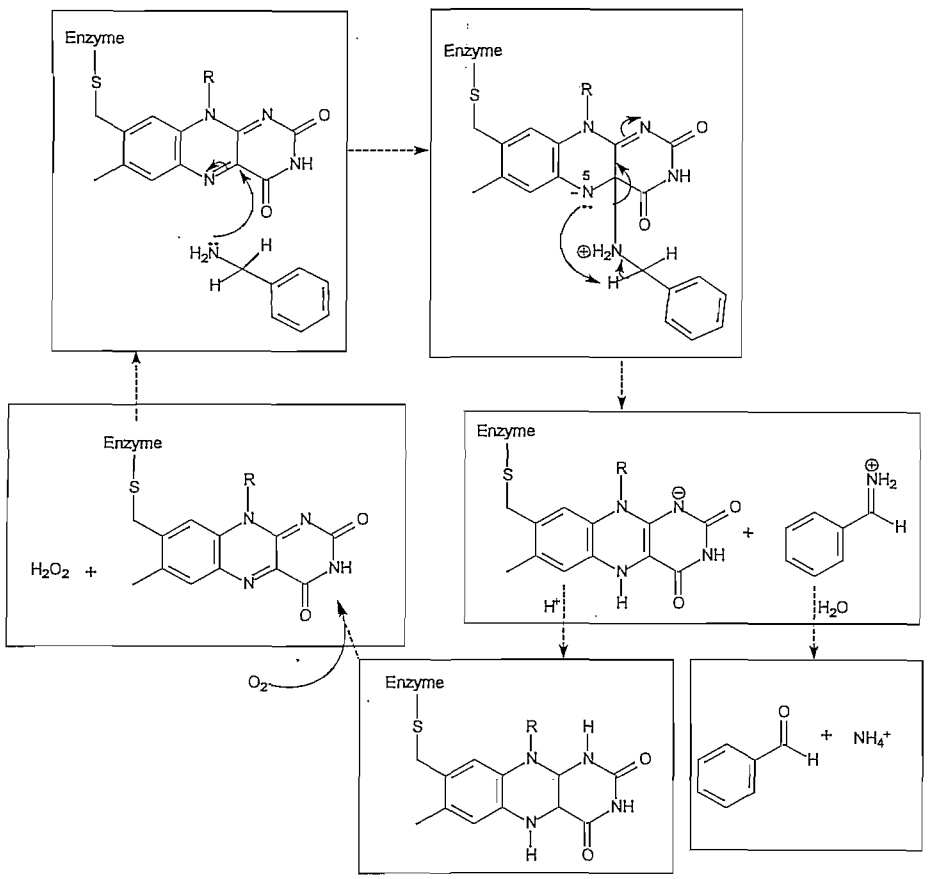

Figure 23: *Proposed concerted covalent catalysis mechanism for MAO catalysis.*

2.6.4 The measurement of MAO-B catalytic activity *in vitro*

The MAO-B catalysed oxidation of amines can be described by the following (Holt *et al.*, 1997):

$$RCH_2NR_1R_2 + H_2O + O_2 \rightarrow RCHO + NHR_1R_2 + H_2O_2.$$

There are a variety of approaches to assaying MAO-B activity. These are based on the disappearance of substrates (Zhou *et al.*, 1996), oxygen consumption (Meyerson *et al.*, 1978), aldehyde formation (Holt *et al.*,1997), ammonia formation (Meyerson *et al.*, 1978; Zhou *et al.*, 1996; Holt *et al.*, 1997), hydrogen peroxide formation (Holt *et al.*, 1997) and acid formation following oxidation of the amine to the aldehyde (Southgate & Collins, 1969; Meyerson *et al.*, 1978). These assay protocols can be either continuous or discontinuous (Holt *et al.*, 1997), but since discontinuous procedures are prone to errors, continuous systems are usually preferred.

Some of the techniques used for measuring MAO-B activity include spectrophotometry, radiometry, fluorometry, luminometry (Zhou *et al.*, 1996), colorimetry (Udenfriend *et al.*, 1954; Meyerson *et al.*, 1978), chromatography (Vlok *et al.*, 2006) and the use of an oxygen electrode (Tipton, 1971; Weetman & Sweetman, 1971; Meyerson *et al.*, 1978). In general, MAO-B activity is measured by adding a substrate to MAO-B and measuring the concentration of the product formed after a specified time (Vlok *et al.*, 2006).

The disappearence of a MAO-B substrate, such as (*E*)-2,5-dimethoxycinnamylamine (Zhou *et al.*, 1996), can be determined by measuring its fluorescence where the corresponding product does not fluoresce. A fluorometric analysis is more sensitive than normal spectrophotometric methods (Zhou *et al.*, 1996; Guilbault, 1968), but sample manipulations are necessary and are subject to error (Meyerson *et al.*, 1978). MMTP [1-methyl-4-(1-methylpyrrol-2-yl)-1,2,3,6-tetrahydropyridine] (Fig. 24) is known to be an excellent substrate for MAO-B (low K_m) (Inoue *et al.*, 1999). Its corresponding MAO-B catalyzed product ($MMDP^+$) is stable, soluble in an aqueous buffer solution, and is a good chromophore. It absorbs radiation at 420 nm whereas MMTP only absorbs at much lower wavelengths. This enables one to spectrophotometrically measure the rate of the MAO-B catalysed oxidation of MMTP to $MMDP^+$ [1-methyl-4-(1-methylpyrrol-2-yl)-2,3-dihydropyridinium] (Vlok *et al.*, 2006). In assays where benzylamine is used as substrate, the corresponding benzaldehyde product may be measured by HPLC analysis (Vlok *et al.*, 2006). Another frequently reported MAO-B activity assay is measuring the MAO-B catalysed disappearance of the MAO-B substrate, kynuramine, or the formation of its fluorescent product (Weissbach *et al.*, 1960).

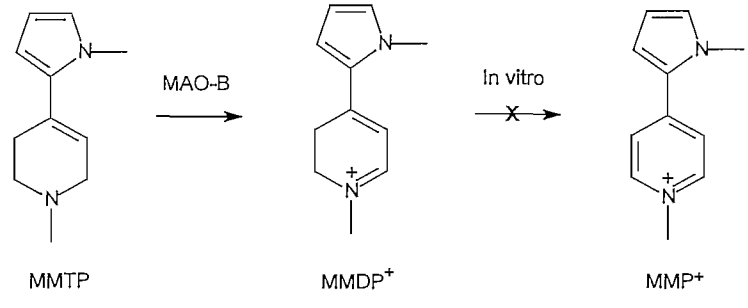

Figure 24: MAO-B catalyzed oxidation of MMTP [1-methyl-4-(1-methylpyrrol-2-yl)-1,2,3,6-tetrahydropyridine].

Oxygen consumption by MAO-B can be measured with a polarographic oxygen electrode, but this method is reported to lack sensitivity and specificity (Meyerson *et al.*, 1978).

By using labelled amine MAO-B substrates, a radiochemical assay method can be used to detect radiolabelled aldehydes formed during the incubation (Lyles & Callingham, 1982; Holt *et al.*,1997). The deaminated metabolites of the radioactive substrates, ^{3}H-tyramine or ^{14}C-serotonin, may be measured

by means of liquid scintillation counting (Fuller *et al.*, 1970). Nonspecific binding of these radioactive metabolites can be problematic and the availability of labeled compounds, as well as safety hazards, may limit the use of radiometry (Meyerson *et al.*, 1978). Radiometric MAO-B assays are frequently used to measure MAO-B activity when aldehydes are difficult to detect by spectrophotometry (Tabor *et al.*, 1954; Holt *et al.*, 1997). Light absorption by proteins and other material in the ultraviolet spectral range during spectrophotometric methods often make the spectrophotometric quantification of aldehyde products difficult (Meyerson *et al.*, 1978).

The amount of ammonia formed during oxidative deamination of amine substrates is equal to substrate consumed (Meyerson *et al.*, 1978). Assays for measuring ammonia are not very sensitive (Zhou *et al.*, 1996) and can not be used for secondary monoamine substrates since alkylamine and not ammonia is produced during oxidative deamination (Meyerson *et al.*, 1978). Ammonia production can be measured with a continuous coupled colorimetric assay (Holt *et al.*, 1997) or potentiometrically with the use of an ammonia-selective electrode (Meyerson *et al.*, 1978).

Hydrogen peroxide (H_2O_2) is the only product of MAO oxidation that remains constant, independent of the substrate used (Holt *et al.*, 1997) and can be detected by a discontinuous coupled fluorometric assay (Yu, 1986; Holt *et al.*, 1997). Although fluorometric assays involving the measurement of H_2O_2 with a coupled fluorogenic reaction are continuous, the method is not direct since a second enzyme is still required (Zhou *et al.*, 1996). A peroxidase-linked spectrophotometric assay (Holt *et al.*, 1997), and a peroxidase-linked colorimetric assay, have been reported (Yamada *et al.*, 1979; Holt *et al.*, 1997).

2.6.5 Enzyme kinetics

2.6.5.1 General background

In the field of enzyme kinetics, enzyme-catalyzed reaction rates are quantitatively measured and effects (such as the presence of inhibitors) on these rates are systematically studied (Rodwell & Kennelly, 2003).

The direction of a chemical reaction, as well as the concentrations of reactants and products present at equilibrium, are determined by the changes in free energy as described by the Gibbs free energy change (ΔG). The term ΔG is equal to the sum of the free energies of formation of the products (ΔG_p) minus the sum of the free energies of the formation of substrates (ΔG_s). A negative sign for $\Delta G°$ shows that the energy of the products is lower than that of the substrates and the reaction proceeds spontaneously from substrates to products, leading to a greater concentration of the products at equilibrium. Both the sign and the magnitude of free energy change thus give information concerning the direction and equilibrium state of a reaction, but not of the rate of reaction. Equation 1 can be used to determine $\Delta G°$, where K_{eq} is the equilibrium constant, R is the gas constant (1.98 cal/K.mol or 8.31 J/K.mol) and T is the absolute temperature in degrees Kelvin (Rodwell & Kennelly, 2003).

$$\Delta G^{\circ} = -RT \ln K_{eg}$$ **Equation 1**

Transition states are an important concept in understanding catalysis, and imply a situation where neither the free substrate nor the product exists. During such a state, "partial bonds" exist that are undergoing formation and rupture with characteristic changes in free energy. If the sum of these energy changes is positive, energy barriers need to be surmounted. Such energy is often termed the activation energy (E_{act}) and is inversely related to the rate of reaction (Equation 2) (Rodwell & Kennelly, 2003).

$$Rate \propto e^{\frac{-E_{act}}{RT}}$$ **Equation 2**

Enzymes help to accelerate reaction rates by providing transition states with lowered activation energy. Such transition states can be stabilised by the suitable positioning of acid-base groups to transfer protons between transition state intermediates, by the suitable positioning of charged groups or metal ions to stabilise the developing charges, or by imposing steric strain on substrates to insure that their geometry approaches that of the transition state. A unique catalysis mechanism occurs when the transition state intermediate forms a covalent bond with the enzyme. Enzymes have no effect on ΔG° for the overall reaction or on K_{eq}, and emerge unchanged at the completion of the reaction (Rodwell & Kennelly, 2003).

2.6.5.2 Michaelis-Menten kinetics

In an enzyme-catalyzed reaction assay the initial velocity (V_i) can be seen as the rate of the forward reaction. Under the conditions of large molar excess (10^3-10^7) of substrate over enzyme, initial velocity is proportional to the concentration of enzyme. As the substrate concentration increases, initial velocity usually increases to a maximum value (V_{max}) where the enzyme is "saturated" with substrate and a further increase in substrate concentration does not increase initial velocity. The Michaelis-Menten equation (Equation 3) is used to illustrate the relationship between the initial velocity and the concentration of the substrate in a hyperbolic curve (Fig. 25). The Michaelis constant (K_m) is the concentration of substrate at which half of the maximal velocity ($V_{max}/2$) is attainable at a particular enzyme concentration (Rodwell & Kennelly, 2003; Shargel & Yu, 1999). When the concentration of the substrate is much less than K_m, the initial velocity is directly proportional to the concentration of the substrate. When the concentration of the substrate is much greater than K_m, initial velocity is maximal (V_{max}) and unaffected by further increases in the concentration of the substrate (Rodwell & Kennelly, 2003).

$$V_i = \frac{V_{max} \times [S]}{K_m + [S]}$$ Equation 3

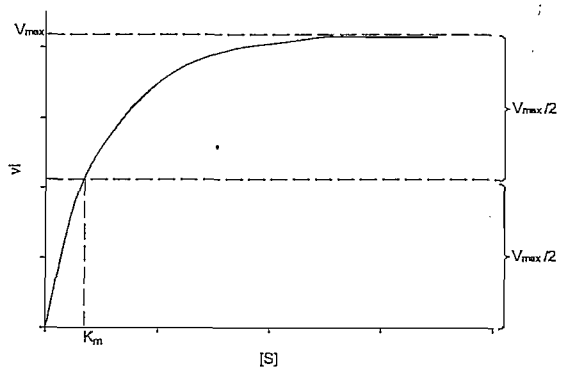

Figure 25: A hyperbolic curve demonstrating the effect of substrate concentration on the initial velocity of an enzyme-catalysed reaction.

As seen in the above equation, K_m can be determined by direct measurement of V_{max} and may require impractically high concentrations of substrate. In order to avoid this, the linear form of Michaelis-Menten (Equation 4) is used to determine K_m and V_{max}. A plot using this equation is called a double reciprocal or Lineweaver-Burk plot (Fig. 26). By setting y ($1/V_i$) equal to zero, K_m can be calculated from the x intercept ($-1/K_m$) (Rodwell & Kennelly, 2003; Shargel & Yu, 1999).

$$\frac{1}{V_i} = \left(\frac{K_m}{V_{max}}\right)\frac{1}{[S]} + \frac{1}{V_{max}}$$ Equation 4

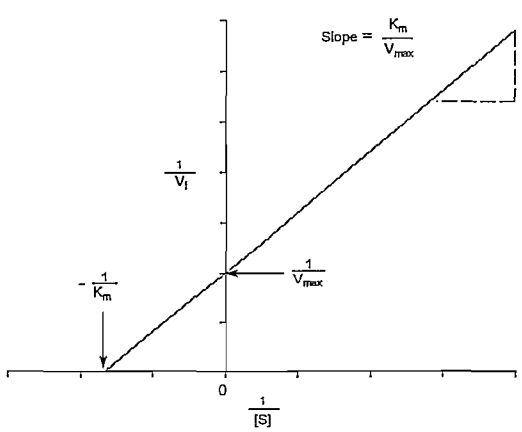

Figure 26: Double reciprocal plot.

2.6.5.3 Competitive inhibition of enzyme function

The structure of a competitive enzyme inhibitor is similar to the substrate (**S** in Fig. 27) or product (**P**) of the target enzyme. Such an inhibitor (**I**) binds to the substrate-binding site of the enzyme to form a complex (**EI**) with the enzyme (**E**), blocking the binding and catalytic conversion of substrates. Blocking of the active site of an enzyme by a competitive inhibitor can be overcome by raising the concentration of the substrate (Silverman, 2004; Shargel & Yu, 1999). The formation and dissociation of the enzyme-inhibitor complex is a dynamic process with equilibrium constant (K_i) (Equation 5). The amount by which the concentration of substrate needs to be increased in order to overcome inhibition depends on the concentration of the inhibitor, the K_i value and K_m (Rodwell & Kennelly, 2003).

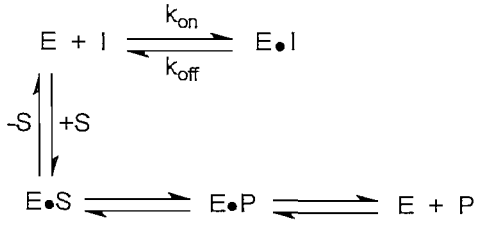

Figure 27: Kinetic scheme for competitive enzyme inhibition.

$$K_i = \frac{[Enz][I]}{[Enz]} \qquad \textbf{Equation 5}$$

Double reciprocal plots are used to evaluate K_i as well as to determine the mode of inhibition. The initial velocity is determined at different concentrations of substrate, in both the presence and absence of an inhibitor, using Equation 6. For competitive inhibitors, the Lineweaver-Burk plots are constructed (*Fig. 28*) from the experimental data. The lines of the Lineweaver-Burk plots meet at the y-axis, showing that when 1/[S] approaches 0, the initial velocity is independent of the presence of an inhibitor. A competitive inhibitor has no effect on V_{max} but raises K'_m (the apparent K_m for the substrate) as seen with the varying intercepts on the x-axis at different inhibitor concentrations (Rodwell & Kennelly, 2003; Shargel & Yu, 1999). K_i values of different inhibitors of the same enzyme can be calculated from the x-axis intercept as shown in Equation 7. K_i values may also be calculated from a plot of the slopes of Lineweaver-Burk plots (constructed in the absence and presence of various inhibitor concentrations) versus inhibitor concentration (Fig. 29). The most effective inhibitor has the lowest K_i (Rodwell & Kennelly, 2003).

$$\frac{1}{V_i} = \frac{K_m}{V_{\max}}\left(1 + \frac{[I]}{K_i}\right)\frac{1}{[S]} + \frac{1}{V_{\max}} \qquad \textbf{Equation 6}$$

$$x = \frac{-1}{K_m}\left(1 + \frac{[I]}{K_i}\right)$$ Equation 7

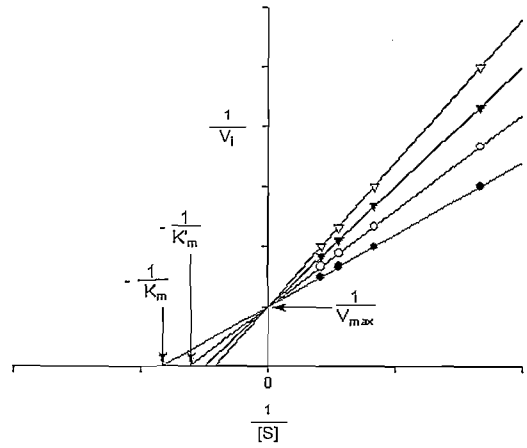

Figure 28: A double reciprocal plot is used to evaluate the potencies of competitive inhibitors. Filled circles indicate the absence of an inhibitor. Open circles, filled triangles and open triangles indicate inhibitor present at increasing concentrations.

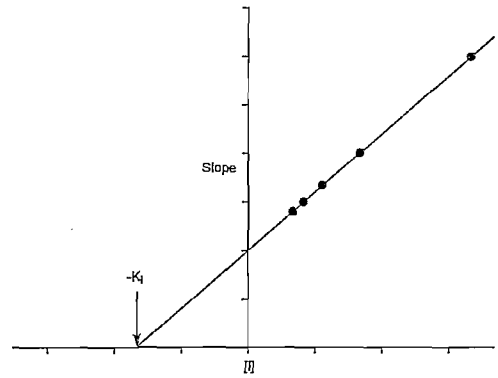

Figure 29: Plot of the slopes of Lineweaver-Burk plots versus inhibitor concentrations is used to calculate K_i values.

2.7 Hansch-type structure-activity relationship study

A structure-activity relationship study can be used to identify compounds with optimal physiochemical properties. A Hansch-type structure-activity relationship study is based on physical organic chemistry concepts and was initiated by L.P. Hammett (Hansch & Leo, 1995). Parameters are used to determine the effect on biological activity for a series of compounds with different substituents at the *meta* or *para* position of a phenyl ring. These parameters are experimentally determined and derived from models. The main effects of different substituents are electronic, steric, and lipophilic in nature

(Hansch & Leo, 1995). Because the effect of a substituent is usually the result of a combination of factors (Carey & Sundberg, 2000), more than one parameter is usually used to describe each substituent. The classical Hammet constant (σ_m and σ_p) and Swain-Lupton constant (F) are used as electronic parameters (Swain *et al.*, 1968; Vlok *et al.*, 2006), the van der Waals volume (V_w) (Van de Waterbeemb & Testa, 1987) and the Taft steric parameter (E_s) (Hansch & Leo, 1995) as steric parameters and the Hansch constant (π) as a parameter of lipophilicity (Fujita *et al.*, 1964; Vlok *et al.*, 2006). All the above physicochemical parameters for substituents can be found in published standard compilations (Hansch & Leo, 1995; Van de Waterbeemb & Testa, 1987).

The Hammet constant (σ_m and σ_p) takes into account both the resonance and inductive effects (Fig. 30 and 31) caused by a substituent on the *meta* or *para* position of a phenyl ring. The resonance effect occurs when electrons are donated or withdrawn through overlapping orbitals of neighbouring π bonds, whereas the inductive effect is the withdrawing of electrons through σ bonds (McMurry, 2000). When σ is positive, the substituent is electron-withdrawing and when σ is negative, the substituent is electron-donating (Carey & Sundberg, 2000). A substituent that is more electronegative (electron-withdrawing) than aromatic carbons, will induce a net positive charge on an aromatic carbon atom, whereas a substituent that is more electropositive (electron-donating) will induce a net negative charge. The Swain-Lupton constant (F) takes only the inductive effect into account. The higher the value of F is, the greater the electronegative inductive effect of the substituent.

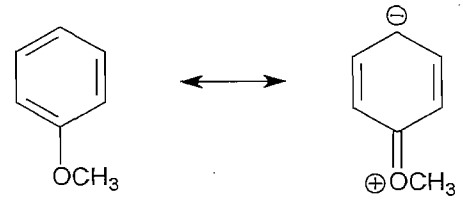

Figure 30: An example of the resonance effect.

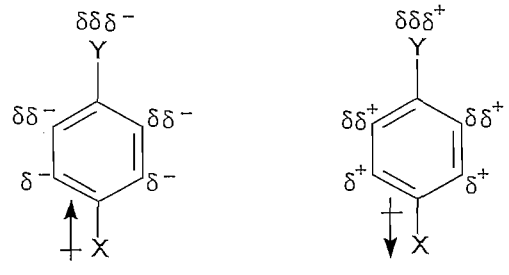

Figure 31: The inductive effect.

The van der Waals volume (V_w) as well as the Taft steric parameter (E_s) describes the volume or size of a substituent. The higher the value of V_w for a substituent, the bigger the size of the subtituent. Higher negative E_s values indicate bigger substituents.

Lipophilic changes are modeled with the octane-water partition coefficients (π or logP) (Hansch & Leo, 1995). The higher the value of π, the greater the lipophilicity of the substituent (Vlok *et al.*, 2006).

Regression analysis can be used to establish the relationship between two or more variables (Fuller *et al.*, 1968). The regression analysis of $\log K_i$ can be carried out with one substituent parameter using the equation $y = ax_1 + c$, where y equals $\log K_i$, a equals the slope, x_1 equals the substituent parameter and c equals the y-intercept. It can also be carried out with multiple substituent parameters (multiple linear regressions) using the equation $y = ax_1 + bx_2 + c$. Here x_1 equals one substituent parameter and x_2 equals another substituent parameter (Vlok *et al.*, 2006). The quality of regression models can be judged by statistical tests, such as the F-test and the correlation coefficient (R^2) (Fuller *et al.*, 1968). A large F value means a great significance can be attached to the correlation achieved. A perfect correlation is achieved when $R^2 = 1$. Correlation may improve when multiple parameters are used (Vlok *et al.*, 2006).

2.8 Summary

From literature it is clear that MAO-B is an attractive target for the development of antiparkinson drugs. Novel MAO-B inhibitors may provide improved symptomatic treatment without complications as well as neuroprotection. The relatively quick return of enzyme activity after inhibition, make potent, reversible MAO-B inhibitors more safe and desirable. The recently reported potent styrylcaffeine analogues (Petzer *et al.*, 2003; Vlok *et al.*, 2006; Van den Berg, 2007) has prompted us to prepare and evaluate styrylisatin analogues as MAO-B inhibitors. This study is thus part of the effort to develop potent reversible MAO-B inhibitors.

Chapter 3

MOLECULAR MODELLING

3.1 Introduction

Molecular modelling increases the efficiency of identifying and screening drug candidates and includes a wide range of molecular graphics and computational chemistry techniques used to build, display, manipulate, simulate and analyse molecular structures and to calculate properties of these structures (Vlok et al., 2006). A molecular modeling study was carried out with a variety of (*E*)-5-styrylisatin and (*E*)-6-styrylisatin analogues, prior to synthesis, in order to test the hypothesis of increased MAO-B inhibitory activity. These structures, docked into the active site of a recently published human MAO-B crystal structure (Binda et al., 2003), gave insight into specific interactions between the analogues and the active site of MAO-B. The resulting binding modes and affinities were compared in order to predict the potential of these styrylisatin analogues as lead candidates and to determine structural properties necessary for potent MAO-B inhibition. The docking scores for the successfully synthesised (*E*)-5-styrylisatin and (*E*)-6-styrylisatin analogues were compared with the calculated IC_{50} values for these analogues (Tables 2–5).

3.2 Method

The molecular docking study was carried out in Windows-based Discovery Studio (DS) 1.7 modelling and simulation environment (Accelrys Software Inc.). All the ligands used were first constructed and optimised in DS Visualizer Pro and then prepared with the Prepare Ligands application within DS before docking simulations. The Brookhaven Protein Data Bank (www.rcsb.org/pdb) was used to retrieve the crystallographic structures of farnesol in complex with MAO-B (2BK3.pdb) (Hubálek *et al.*, 2005). The cocrystallised farnesol was manually deleted, leaving only the crystallographic structure of MAO-B. The MAO-B receptor model was typed with the CHARMm forcefield, whereafter the binding site was identified by means of the Ligandfit floodfilling algorithm. All the prepared ligands were then docked into the A subunit of the enzyme, using the LigandFit module in DS that employs total ligand flexibility, and whereby the final ligand conformations are determined by the Monte Carlo conformation search method set to a variable number of trial runs. All applications in DS were set to their default values. *In situ* ligand minimisation with the Smart Minimizer algorithm were used to refine the docked ligands. Docking solutions were scored, using Dock_Score, and compared. The docking procedure efficiency was evaluated by redocking of the cocrystallised ligand.

3.3 Results and discussion

A variety of (*E*)-5-styrylisatin (**8a–g** in Table 2) and (*E*)-6-styrylisatin analogues (**9a–b** in Table 3), as well as isatin (**10** in Table 1), were successfully docked in the MAO-B active site and the docking modes were compared. None of the (*E*)-5-styrylisatin or (*E*)-6-styrylisatin analogues are co-planar molecules when docked and all extended through both the entrance and substrate-binding cavities. The styryl side-chain extends into the entrance cavity where it is stabilized by hydrophobic interaction with entrance cavity residues such as Leu164 and Leu167. The styryl moiety of all the styrylisatin analogues force the side-chain of Ile199 into the "open" position (Fig. 33–41), whereas the Ile199 side-chain is in a "closed" position when the smaller molecule, isatin, is bound in only the substrate-binding cavity (Fig.32). The dioxoindole rings of compounds **8a–g** are perpendicular to the flavin ring in the substrate-binding cavity, with the carbonyl oxygens directed toward the flavin, similar to the binding mode of isatin described by Binda *et al.* (2003). The dioxoindole rings of compounds **8f** and **8g** differ somewhat from the other (*E*)-5-styrylisatin analogues in their position relative to the flavin ring (Fig. 38-39). The isatin moiety of compounds **9a** and **9b** is also perpendicular to the flavin ring but the carbonyl oxygens are turned further away from the flavin (Fig. 40–41).

The amine proton of isatin is involved in a hydrogen bond with the oxygen of water 318 (Fig. 32) that stabilises isatin in the substrate-binding cavity. A carbonyl oxygen of compounds **8a–e** are also involved in hydrogen bonding with a proton of water 166 (Fig. 33–37). Compounds **8f** and **8g** are docked deeper into the substrate-binding cavity (Fig.38–39). Steric interactions between the methoxy and trifluoromethyl functional groups of compounds **8f** and **8g** and the entrance cavity amino acid residues may be responsible for these binding modes. The carbonyl groups of compound **8f** are orientated in such a way as to prevent hydrogen bonding in the substrate-binding cavity (Fig. 38). Compound **8g** is stabilised by two hydrogen bonds, between the 2-oxo group of the compound and the phenolic proton of Tyr398 and between the amine proton of the isatin ring and the phenolic oxygen of Tyr435 (Fig. 39). The isatin ring of compound **8g** is thus stabilised in the aromatic cage (Tyr435, Tyr398 and the flavin ring) of the substrate-binding cavity. The carbonyl oxygen of compound **9a** is involved in hydrogen bonding with a water (103) molecule (Fig. 40) in a different area than seen with the (*E*)-5-styrylisatin analogues (Fig. 33–37). Compound **9b** does not show stabilisation by means of hydrogen bonding (Fig. 41).

Several scoring functions can be used to find the best binding modes for compounds docked into a receptor model. All compounds were scored according to the available scoring functions and the consensus score according to Dock_Score were used for comparison of the compounds. The docking score for each compound is presented in Tables 1 to 3. The docking scores of both the (*E*)-5-styrylisatin and (*E*)-6-styrylisatin analogues are considerably higher than that of isatin (**10**) (Table 1). Compound **8b** has the highest docking score. The docking score of compound **8d,** slightly lower than

that of compound **8b**, indicated that their affinities for the MAO-B active site may be equal. The lowest scores for the (*E*)-5-styrylisatin analogues were obtained with compounds **8a**, **8f** and **8g**.

The halogenated (*E*)-5-styrylisatin analogues **8b–c** thus showed higher docking scores than that of the unsubstituted (*E*)-5-styrylisatin analogue **8a**. Similarly, compound **9a**, the unsubstituted (*E*)-6-styrylisatin analogue, has the lowest docking score of the 6-series. The low scores of the (*E*)-6-styrylisatin analogues **9a–b** may be explained by the different orientation of their dioxoindole rings towards the flavin ring that leads to less favourable hydrogen bond formation as seen with compound **9a** or a lack of hydrogen bond formation as seen with compound **9b**. Comparison of docking scores with IC_{50} values for the synthesised styrylisatin analogues (Tables 4–6) showed that there is a correlation between higher docking score values and the potency of MAO-B inhibition.

Table 1: Docking score of isatin.

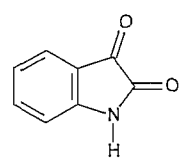

Compound	*Compound Name*	*Dock_Score*
10	Isatin	27.33

Table 2: Docking scores of the (*E*)-5-styrylisatin analogues.

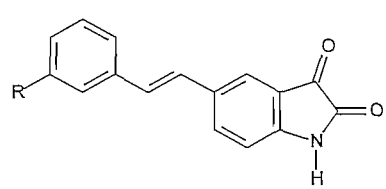

Compound	*Compound Name*	*R =*	*Dock_Score*
8a	(E)-5-Styrylisatin	H	59.15
8b	(E)-5-(3-Chlorostyryl)isatin	Cl	62.56
8c	(E)-5-(3-Fluorostyryl)isatin	F	60.30
8d	(E)-5-(3-Bromostyryl)isatin	Br	62.39
8e	(E)-5-(3-Methylstyryl)isatin	CH_3	60.87
8f	(E)-5-(3-Methoxystyryl)isatin	OCH_3	57.89
8g	(E)-5-(3-Trifluoromethylstyryl)isatin	CF_3	54.49

Table 3: Docking scores of the (E)-6-styrylisatin analogues.

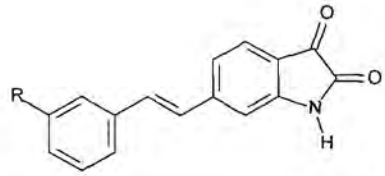

Compound	*Compound Name*	*R =*	*Dock_Score*
9a	(E)-6-Styrylisatin	H	50.24
9b	(E)-6-(3-Chlorostyryl)isatin	Cl	54.63

Figure 32: Isatin (**10**) (carbons are yellow, hydrogens white, oxygens red and nitrogen blue) docked in MAO-B. The Ile199 side chain is orange, Tyr60 green. Phe343 light blue, Tyr398 purple, Tyr435 brown, water blue, FAD red and hydrogen bonds black dotted lines.

Figure 33: (*E*)-5-Styrylisatin (**8a**) (carbons are yellow, hydrogens white, oxygens red and nitrogen blue) docked in MAO-B. Colour representations of other structures are the same as for Fig. 32.

Figure 34: (*E*)-5-(3-Chlorostyryl)isatin (**8b**) (carbons are yellow, hydrogens white, oxygens red, chlorine green and nitrogen blue) docked in MAO-B. Colour representations of other structures are the same as for Fig. 32.

Figure 35: (*E*)-5-(3-Fluorostyryl)isatin (**8c**) (carbons are yellow, hydrogens white, oxygens red, fluorine light blue and nitrogen blue) docked in MAO-B. Colour representations of other structures are the same as for Fig. 32.

Figure 36: (*E*)-5-(3-Bromostyryl)isatin (**8d**) (carbons are yellow, hydrogens white, oxygens red, bromine brown and nitrogen blue) docked in MAO-B. Colour representations of other structures are the same as for Fig. 32.

Figure 37: (*E*)-5-(3-Methylstyryl)isatin (**8e**) (carbons are yellow, hydrogens white, oxygens red and nitrogen blue) docked in MAO-B. Colour representations of other structures are the same as for Fig. 32.

Figure 38: (*E*)-5-(3-Methoxystyryl)isatin (**8f**) (carbons are yellow, hydrogens white, oxygens red and nitrogen blue) docked in MAO-B. Colour representations of other structures are the same as for Fig. 32.

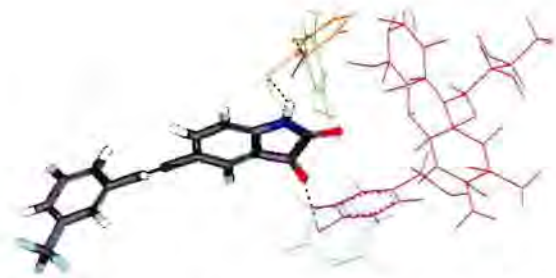

Figure 39: (*E*)-5-(3-Triflouromethylstyryl)isatin (**8g**) (carbons are yellow, hydrogens white, oxygens red, fluorine light blue and nitrogen blue) docked in MAO-B. Colour representations of other structures are the same as for Fig. 32.

Figure 40: (*E*)-6-Styrylisatin (**9a**) (carbons are yellow, hydrogens white, oxygens red and nitrogen blue) docked in MAO-B. Colour representations of other structures are the same as for Fig. 32.

Figure 41: (*E*)-6-(3-Chlorostyryl)isatin (**9b**) (carbons are yellow, hydrogens white, oxygens red, chlorine green and nitrogen blue) docked in MAO-B. Colour representations of other structures are the same as for Fig. 32.

3.4 Summary

Molecular docking of both the (*E*)-5-styrylisatin (**8a–g**) and (*E*)-6-stryrylisatin (**9a–b**) analogues suggests improved affinity over isatin, for the MAO-B enzyme. This modelling study supported the hypothesis of increased reversible MAO-B inhibitory activity for the styrylisatin analogues compared to isatin.

Hydrogen bonding of the isatin moiety in the substrate-binding cavity and properties, such as lipophilicity and size of the extended styryl moiety in the entrance cavity, seem to be important factors that affect the binding affinity of these compounds. The estimated docking scores proved to be relatively accurate in predicting the trend of affinity for these series of analogues (See chapter 5).

SYNTHESIS

4.1 Overview

Three (*E*)-5-styrylisatin analogues **8a–c** (Fig. 42), as well as two (*E*)-6-styrylisatin analogues **9a–b** were successfully synthesised in this study. Insolubility problems for the rest of the proposed (*E*)-5-styrylisatin analogues (**8d–g** in Table 2) prevented purification of the final products and led to the exclusion of these compounds from biological evaluation. The synthesis of all analogues followed the same four step synthetic pathway (Fig. 42). Diethyl(4-nitrobenzyl) (**3a**) and diethyl(3-nitrobenzyl)phosphonate (**3b**), prepared from 4-nitrobenzyl (**1a**) and 3-nitrobenzyl bromide (**1b**) respectively and triethyl phosphite (**2**) (Kuo *et al*, 2002), were used in a modified Wittig reaction with appropriately substituted benzaldehydes (**4**) to produce the required 4-nitrostilbenes (**5a–c**) and 3-nitrostilbenes (**5d–e**). Subsequent reduction of these nitrostilbenes produced the corresponding 4-aminostilbenes (**6a–c**) and 3-aminostilbenes (**6d–e**) (Hanna *et al.*, 1980).

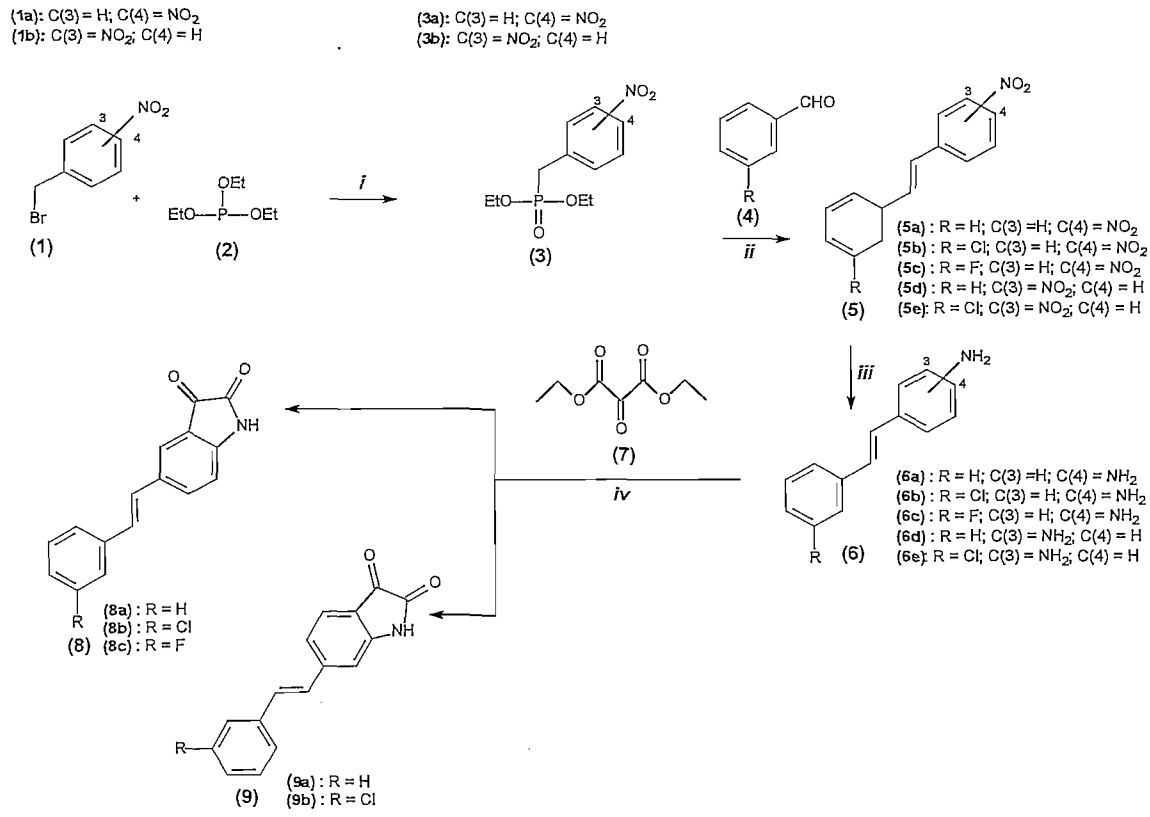

Figure 42: Synthetic pathway to (*E*)-5-styrylisatin (**8a–c**) and (*E*)-6-styrylisatin (**9a–b**) analogues. (*i*) 130 °C, 3 hrs. (*ii*) NaOEt (*iii*) $SnCl_2/CH_3COOH$, HCl/H_2O (*iv*) CH_3COOH, O_2.

Various methods were considered for the synthesis of the isatin moiety. A good overview of methods available is given in a review by da Silva *et al.* (2001). The Sandmeyer method seems to be the most frequently used method for the synthesis of isatin from anilines (da Silva *et al.*, 2001; Bramson *et al.*, 2001; DeMarinis *et al.*, 1986; Baker *et al.*, 1951; Marvel & Hiers, 1941). It involves the reaction of aniline [**a** in Fig. 43] with chloral hydrate and hydroxylamine hydrochloride in order to form an isonitrosoacetanilide intermediate (**b**) which is cyclised to isatin (**c**) in concentrated sulfuric acid. Insolubility problems with the 4- and 3-aminostilbene analogues prevented the use of this method. A modification of the Sandmeyer method, that involved the incorporation of ethanol (da Silva *et al.*, 2001; Garden *et al.*, 1997), was subsequently tried but the same insolubility problems were encountered.

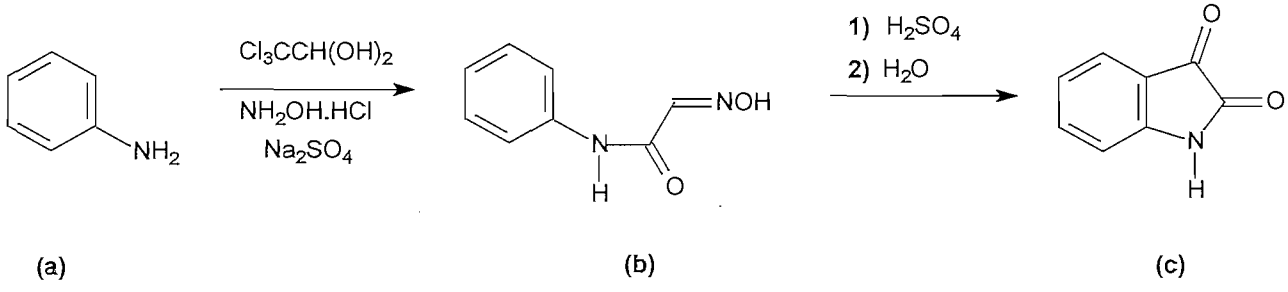

Figure 43: The Sandmeyer isatin synthesis

Another frequently used alternative for the synthesis of isatin from aniline is the Stolle method (da Silva *et al.*, 2001; Fukuda *et al.*, 1994; Lopes & da Silva, 1993; Welstead *et al.*, 1979). It involves the reaction of anilines [**a** in Fig. 44] with oxalyl chloride to produce a chloro-oxalylanilide intermediate (**b**) which is cyclised to isatin (**c**) with the use of a Lewis acid. This method was tried, using $SnCl_4$ as the Lewis acid, but failed to produce the desired styrylisatin analogues.

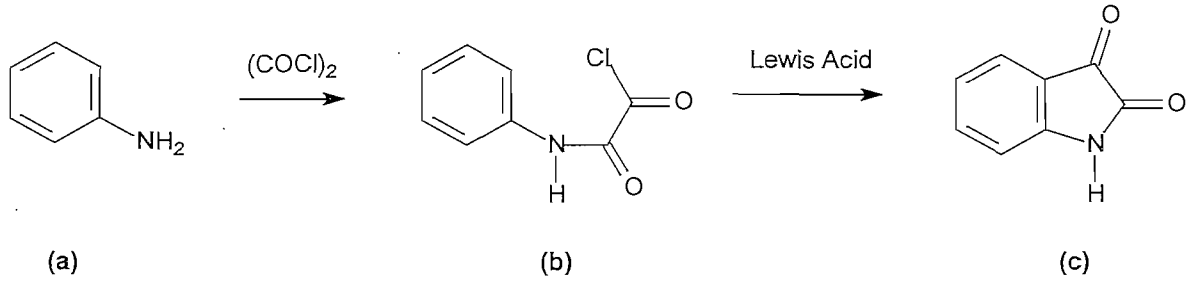

Figure 44: The Stolle isatin synthesis

The Martinet isatin synthesis (da Silva *et al.*, 2001), in accordance with the method of Langenbeck *et al.* (1956), finally produced the desired (*E*)-5-styrylisatin as well as (*E*)-6-styrylisatin analogues. This method involves the reaction of an aromatic amine [**a** in Fig. 45] with mesoxalic acid diethyl ester [**7** in Fig. 42] in the presence of an acid to yield a 3-(3-hydroxy-2-oxindole)carboxylic acid intermediate (**b**) which yielded the isatin product after oxidative decarboxylation (**c**) (da Silva *et al.*, 2001).

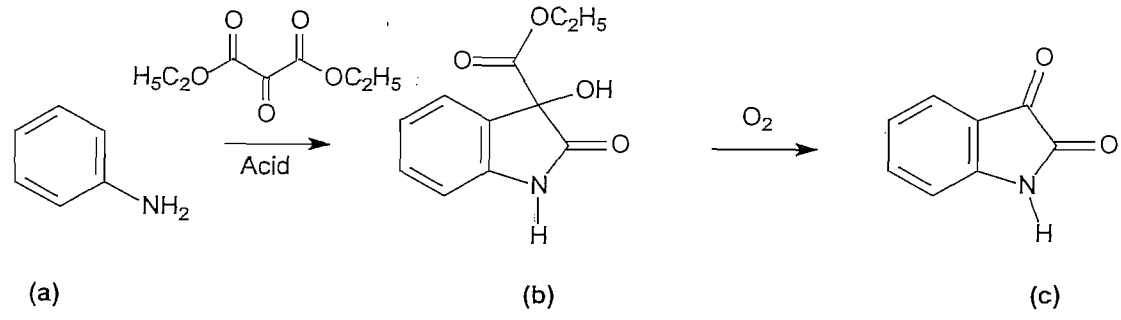

Figure 45: The Martinet isatin synthesis

4.2 Materials and instrumentation

All starting materials not prepared and described elsewhere were obtained form Sigma-Aldrich and used without further purification. Proton and carbon NMR spectra were recorded on a Varian Gemini 300 spectrometer. Proton (^{1}H) spectra were recorded in DMSO and $CDCl_3$ at a frequency of 300 MHz and carbon spectra at 75 MHz. Chemical shifts are reported in parts per million (δ) downfield from the signal of tetramethylsilane added to the deuterated solvent. Spin multiplicities are given as s (singlet), d (doublet), t (triplet), q (quartet) or m (multiplet) and the coupling constants (J) are given in hertz (Hz). Direct insertion impact ionization (EIMS) and high resolution mass spectra (HRMS) were obtained on a VG 7070E mass spectrometer. Melting points (mp) were determined on a Stuart SMP1 melting point apparatus and are uncorrected.

4.3 General procedures

4.3.1 Diethyl (4-nitrobenzyl)phosphonate (3a)

The synthesis of compound **3a** was based on the procedure described by Kuo *et al.* (2002). Triethyl phosphite (69.4 mmol) (**2**) was combined with 4-nitrobenzyl bromide (**1a**) (43.6 mmol) and the resulting yellow/orange solution was refluxed (130 °C) for 4 hours, which resulted in the formation of a dark orange solution. Excess triethyl phosphite was removed under reduced pressure while stirring, first at 0 °C for an hour and then at 100 °C for another hour. The resulting product was an oily orange-brown solution that was used subsequently without further purification.

4.3.2 Diethyl (3-nitrobenzyl)phosphonate (3b)

The synthesis of compound **3b** was based on the procedure described by Kuo *et al.* (2002). Triethyl phosphite (35.8 mmol) (**2**) was combined with 3-nitrobenzyl bromide (**1b**) (22.5 mmol) and the resulting yellow/orange orange solution was refluxed (130 °C) for 4 hours, which resulted in the formation of a brown solution. Excess triethyl phosphite was removed under reduced pressure while stirring, first at 0 °C for an hour and then at 100 °C for another hour. The resulting product was an oily orange-brown solution that was used subsequently without further purification.

4.3.3 (*E*)-4-Nitrostilbene analogues (5a–c)

Compounds **5a-c** were synthesised using the procedure described by Kuo *et al.* (1996). A sodium ethoxide solution was prepared by dissolving sodium (99.3 mmol) in ethanol (104 ml). This solution was added dropwise to a solution of previously prepared diethyl (4-nitrobenzyl)phosphonate (**3a**) (94.9 mmol) and the appropriate benzaldehyde (94.9 mmol) in ethanol (150 ml) (Kuo *et al.*, 1996). The mixture changed form a red solution to a yellow-orange suspension that was stirred for 13 hours. The resulting suspension was filtered and washed with cold petroleum ether. The yellow precipitate obtained as residue was dried *in vacuo* and the product was used without further purification.

4.3.4 (*E*)-3-Nitrostilbene analogues (5d–e)

Compounds **5d–e** were synthesised using the procedure described by Kuo *et al.* (1996). A sodium ethoxide solution was prepared by dissolving sodium (35.9 mmol) in ethanol (38 ml). This solution was added dropwise to a solution of previously prepared diethyl (3-nitrobenzyl)phosphonate (**3b**) (34.3 mmol) and the appropriate benzaldehyde (34.3 mmol) in ethanol (57 ml) (Kuo *et al.*, 1996). The mixture changed form an orange solution to a dark orange suspension that was stirred for 13 hours. The resulting orange suspension was filtered and washed with cold petroleum ether. The yellow precipitate obtained as residue was dried *in vacuo* and the product was used without further purification.

4.3.5 (*E*)-4-Aminostilbene (6a–c)

Compounds **6a–c** were synthesised using the procedure described by Hanna *et al.* (1980). A solution of hydrochloric acid (70 ml) and $SnCl_2$ (0.3 mol) was prepared and added to the refluxing yellow-orange solution of a previously prepared (*E*)-4-nitrostilbene (**5a–c**) (35.0 mmol) in glacial acetic acid (220 ml) and tetrahydrofuran (100 ml). After 4 hours of refluxing in an argon atmosphere, the tetrahydrofuran was removed from the yellow suspension with a rotary evaporator. The resulting suspension was cooled to room temperature and basified to pH 10 using a 40% aqueous sodium hydroxide solution. Extraction with $CHCl_3$ (2 x 200 ml) followed. The combined organic phases were filtered several times in order to obtain a clear yellow solution. A yellow solid was isolated from the final filtrates after rotary evaporation. Recrystallisation of the solid with ethanol yielded a yellow crystalline product.

4.3.6 (*E*)-3-Aminostilbene analogues (6d–e)

Compounds **6d–e** were synthesised using the procedure described by Hanna *et al.* (1980). A solution of hydrochloric acid (35 ml) and $SnCl_2$ (0.15 mol) was prepared and added to the refluxing yellow-orange solution of a previously prepared (*E*)-3-nitrostilbene analogue (**5d–e**) (18.0 mmol) in glacial acetic acid (113 ml) and tetrahydrofuran (50 ml). After 4 hours of refluxing in argon atmosphere, the tetrahydrofuran was removed from the yellow suspension with a rotary evaporator. The resulting suspension was cooled to room temperature and basified to pH 10 using a 30% aqueous sodium

hydroxide solution. Extraction with $CHCl_3$ (2 x 200 ml) followed. The combined organic phases were filtered several times in order to obtain a clear yellow solution. A yellow solid was isolated from the final filtrates after rotary evaporation. Recrystallisation of the solid from ethanol yielded a yellow crystalline product.

4.3.7 (*E*)-5-styrylisatin analogues (8a–c)

Compounds **8a–c** were synthesised using the procedure described by Langenbeck *et al.* (1956). A mixture of a previously prepared (*E*)-4-aminostilbene analogue (**6a–c**) (5.1 mmol), mesoxalic acid diethyl ester hydrate (**7**) (5.1 mmol) and glacial acetic acid (8 ml) was heated (120 °C) and stirred under reflux for 4 hours, resulting in a dark yellow-green suspension. Excess acetic acid and ethylacetate was removed from the mixture by means of steam distillation before basifying the mixture (pH 11) with a 10% KOH solution to form a yellow suspension. Oxidation was achieved by passing air through the refluxing (120 °C) basic mixture for 4 hours, whereafter the cooled mixture was filtered in order to obtain a yellow solution as filtrate. A red precipitate was produced by acidifying (pH 2) the filtrate with a 32% HCl solution. This precipitate was washed with distilled water and isolated by filtration before being dried. A brick-red solid was obtained as product.

4.3.8 (*E*)-6-styrylisatin (9a–b) analogues

Compounds **9a–b** were synthesised using the procedure described by Langenbeck *et al.* (1956). A mixture of a previously prepared (*E*)-3-aminostilbene analogue (**6d–e**) (5.1 mmol), mesoxalic acid diethyl ester hydrate (**7**) (5.1 mmol) and glacial acetic acid (8 ml) were heated (120°C) and stirred under reflux for 4 hours, resulting in a dark brown suspension. Excess acetic acid and ethylacetate was removed from the mixture by means of steam distillation before basifying the mixture (pH 11) with a 10% KOH solution to form a yellow suspension. Oxidation was achieved by passing air through the refluxing (120 °C) basic mixture for 4 hours, whereafter the cooled mixture was filtered in order to obtain a yellow solution as filtrate. A red precipitate was produced by acidifying (pH 2) the filtrate with a 32% HCl solution. This precipitate was washed with distilled water and isolated by filtration before being dried. Recrystallisation of the brick-red solid product from ethanol yielded a brick-red crystalline product.

4.4 Synthesis of compounds

4.4.1 (*E*)-4-Nitrostilbene

Compound **5a** was synthesised from diethyl (4-nitrobenzyl)phosphonate (**3a**) and benzaldehyde in a yield of 90%: mp 157-158 °C (capillary method); literature mp 157 °C (Bergman & Schapiro, 1947). ^{1}H-NMR (DMSO-d6) δ 7.15 (m, 1H), 7.27 (m, 1H), 7.47 (m, 1H), 7.56 (m, 4H); ^{13}C-NMR (DMSO-d6) δ

124.07, 126.24, 126.80, 126.98, 128.79, 128.85, 133.27, 136.16, 143.80, 146.75; EIMS m/z 225 ($M^{\cdot+}$); HR-EIMS m/z calc. 225.078979, found 225.078564.

4.4.2 (*E*)-3'-Chloro-4-nitrostilbene

Compound **5b** was synthesised from diethyl (4-nitrobenzyl)phosphonate (**3a**) and 3-chlorobenzaldehyde in a yield of 77%: mp 120–121 °C (capillary method). ^{1}H-NMR ($CDCl_3$) δ 7.13 (m, 2H), 7.32 (m, 2H), 7.52 (m, 1H), 7.58 (s, 1H), 7.61 (m,2H), 8.19 (m, 2H); ^{13}C-NMR ($CDCl_3$) δ 124.09, 124.11, 125.22, 126.72, 127.00, 127.66, 128.63, 130.05, 131.67, 134.86, 138.03, 143.20, 147.04; EIMS m/z 259 ($M^{\cdot+}$).

4.4.3 (*E*)-3'-Fluoro-4-nitrostilbene

Compound **5c** was synthesised from diethyl (4-nitrobenzyl)phosphonate (**3a**) and 3-fluorobenzaldehyde in a yield of 79%: mp 133–135 °C (capillary method). ^{1}H-NMR ($CDCl_3$) δ 7.01 (m, 1H), 7.08 (s, 1H), 7.15 (d, 1H, J = 12.2 Hz), 7.29 (m, 3H), 7.61 (m, 2H), 8.21 (m, 2H); ^{13}C-NMR ($CDCl_3$) δ 122.99, 124.13, 127.12, 127.59, 130.35, 131.96, 138.46, 138.56, 143.26, 147.04, 161.53, 164.79; EIMS m/z 243 ($M^{\cdot+}$); HR-EIMS m/z calc. 243.069557, found 243.069610.

4.4.4 (*E*)-3-Nitrostilbene

Compound **5d** was synthesised from diethyl (3-nitrobenzyl)phosphonate (**3b**) and benzaldehyde in a yield of 53%: 112 °C (capillary method); literature mp 112 °C (Bergman & Schapiro, 1947). ^{1}H-NMR (DMSO-d6) δ 7.32 (m, 1H), 7.41 (m, 2H), 7.47 (s, 1H), 7.50 (s, 1H), 7.66 (t, 2H, J = 8.1 Hz), 8.06 (d, 1H, J = 7.7 Hz), 8.10 (m, 1H); ^{13}C-NMR (DMSO-d6) δ 121.99, 123.17, 127.49, 128.25, 129.57, 130.05, 131.42, 132.65, 133.82, 137.74, 140.39, 149.76; EIMS m/z 225 ($M^{\cdot+}$); HR-EIMS m/z calc. 225.078979, found 225.077501.

4.4.5 (*E*)-3'-Chloro-3-nitrostilbene

Compound **5e** was synthesised from diethyl (3-nitrobenzyl)phosphonate (**3b**) and 3-chlorobenzaldehyde in a yield of 78%; mp 152 °C (capillary method). ^{1}H-NMR (DMSO-d6) δ 7.35 (d, 1H, J = 8.0 Hz), 7.43 (t, 1H, J = 7.7 Hz), 7.50 (d, 2H, J = 3.3 Hz), 7.59 (m, 1H), 7.67 (t, 1H, J = 7.9 Hz), 7.74 (s, 1H), 8.04–8.13 (dd, 2H, J = 8.0), 8.43 (s, 1H); ^{13}C-NMR (DMSO-d6) δ 122.17, 123.55, 126.84, 127.50, 129.15, 131.01, 131.50, 131.87, 134.00, 134.91, 139.96, 140.08, 149.69; EIMS m/z 259 ($M^{\cdot+}$); HR-EIMS m/z calc. 259.040006, found 259.040260.

4.4.6 (E)-4-Aminostilbene

Compound **6a** was synthesised from (*E*)-4-nitrostilbene (**5a**) in a yield of 67%: mp 150-151 °C (capillary method); literature mp 151 °C (Bergman & Schapiro, 1947). ^{1}H-NMR ($CDCl_3$) δ 6.67 (m, 2H), 6.91–7.08 (q, 2H, J = 16.21, 34.72 Hz), 7.23 (m, 1H), 7.35 (m, 2H), 7.49 (m, 1H); ^{13}C-NMR ($CDCl_3$) δ 115.14, 125.05, 126.05, 126.83, 127.70, 127.95, 128.54, 128.67, 137.92, 146.12; EIMS m/z 195 ($M^{\cdot+}$); HR-EIMS m/z calc. 195.104799, found 195.104154.

4.4.7 (*E*)-4-Amino-3'-chlorostilbene

Compound **6b** was synthesised from (*E*)-3'-chloro-4-nitrostilbene (**5b**) in a yield of 66%: mp 140–141 °C (capillary method). ^{1}H-NMR ($CDCl_3$) δ 6.66 (m, 2H), 6.80–7.04 (q, 2H, J = 16.3, 56.0 Hz), 7.24 (m, 4H), 7.45 (m, 1H); ^{13}C-NMR ($CDCl_3$) δ 115.13, 123.50, 124.27, 125.83, 126.65, 127.41, 127.92, 129.72, 130.11, 134.49, 139.91, 146.51; EIMS m/z 229 ($M^{\cdot+}$). HR-EIMS m/z calc. 229.065827, found 229.064762.

4.4.8 (*E*)-4-Amino-3'-fluorostilbene

Compound **6c** was synthesised from (*E*)-3'-fluoro-4-nitrostilbene (**5c**) in a yield of 63%. ^{1}H-NMR ($CDCl_3$) δ 6.66 (m, 2H), 6.88 (m, 2H), 7.01 (d, 1H, J = 16.4 Hz), 7.17 (m, 1H), 7.26 (m, 1H), 7.32 (m, 2H) ^{13}C-NMR ($CDCl_3$) δ 121.97, 123.77, 123.81, 127.42, 127.91, 129.85, 129.96, 130.01, 140.42, 146.49, 161.57, 164.82 ; EIMS m/z 213 ($M^{\cdot+}$).

4.4.9 (*E*)-3-Aminostilbene

Compound **6d** was synthesised from (*E*)-3-nitrostilbene (**5d**) in a yield of 57%: mp 119–120 °C (capillary method); literature mp 120 °C (Bergman & Schapiro, 1947). ^{1}H-NMR (DMSO-d6) δ 6.51 (m, 1H), 6.78 (m, 2H), 7.03 (m, 1H), 7.10 (m, 1H), 7.25 (m, 1H), 7.36 (t, 2H, J = 7.6 Hz), 7.57 (m, 2H) ^{13}C-NMR (DMSO-d6) δ 112.85, 114.98, 115.83, 127.61, 128.55, 128.68, 129.96, 130.42, 130.57, 138.49, 138.75, 150.27; EIMS m/z 195 ($M^{\cdot+}$); HR-EIMS m/z calc. 195.104799, found 195.104799.

4.4.10 (*E*)-3-Amino-3'-chlorostilbene

Compound **6e** was synthesised from (*E*)-3'-chloro-3-nitrostilbene (**5e**) in a yield of 40%: mp 62-64 °C (capillary method): ^{1}H-NMR (DMSO-d6) δ 7.12 (s, 1H), 7.24 (m, 1H), 7.38 (m, 3H), 7.53 (d, 1H, J = 7.8 Hz), 7.61 (dd, 2H, J = 3.4, 7.7 Hz), 7.71 (m, 1H), 7.79 (s, 1H), 11.20 (s, 1H); ^{13}C-NMR (DMSO-d6) δ 110.79, 114.12, 116.30, 127.47, 127.84, 128.90, 129.54, 130.13, 130.60, 139.98, 140.39, 152.67; EIMS m/z ($M^{\cdot+}$); HR-EIMS m/z calc. 229.065827, found 229.064762.

4.4.11 (*E*)-5-Styrylisatin

Compound **9a** was synthesised from (*E*)-4-aminostilbene (**6a**) and mesoxalic acid diethyl ester in a yield of 77%: mp 254-255 °C (capillary method); literature mp 264-266 °C (Langenbeck *et al.*, 1956): ^{1}H-NMR (DMSO-d6) δ 6.90–6.96 (dd, 1H, J = 11.7, 19.9 Hz), 7.20 (m, 3H), 7.35 (m, 2H), 7.57 (m, 2H), 7.78 (m, 1H), 7.80–7.82 (dd, 1H, J = 1.8, 8.1 Hz), 11.2 (s, 1H); ^{13}C-NMR (DMSO-d6) δ112.38, 118.22, 122.03, 126.34, 126.96, 127.51, 127.75, 128.61, 132.12, 136.16, 136.90, 149.69, 159.49, 184.35; EIMS m/z 249 ($M^{\cdot+}$); HR-EIMS m/z calc. 249.078979, found 249.080332.

4.4.12 (*E*)-5-(3-Chlorostyryl)isatin

Compound **9b** was synthesised from (*E*)-4-Amino-3-chlorostilbene (**6b**) and mesoxalic acid diethyl ester in a yield of 28%: mp 252 °C (capillary method). ^{1}H-NMR (DMSO-d6) δ 6.94 (d, 1H, J = 8.1 Hz), 7.22 (m, 1H), 7.30 (m, 2H), 7.34 (s, 1H), 7.39 (t, 1H, J= 7.9 Hz), 7.52 (d, 1H, J = 7.8 Hz), 7.65 (s, 1H), 7.78 (m, 1H), 7.80 (dd, 1H, J = 1.7, 8.2 Hz); ^{13}C-NMR (DMSO-d6) δ 113.83, 119.41, 123.46, 126.35, 127.05, 127.46, 128.19, 130.03, 131.77, 132.87, 134.88, 137.78, 140.91, 151.28, 161.18, 185.92; EIMS m/z 283 ($M^{\cdot+}$); HR-EIMS m/z calc. 283.040001, found 283.03829.

4.4.13 (*E*)-5-(3-Fluorostyryl)isatin

Compound **8c** was synthesised from (*E*)-4-Amino-3'-fluorostilbene (**6c**) and mesoxalic acid diethyl ester (**9**) in a yield of 5%: mp 230-235 °C (capillary method). ^{1}H-NMR (DMSO-d6) δ 6.94 (d, 1H, J = 8.1 Hz), 7.09 (m, 1H), 7.23-7.33 (q, 2H, J = 16.5, 42.7 Hz), 7.41 (m, 3H), 7.77 (m, 1H), 7.80 (dd, 1H, J = 8.2, 1.7 Hz); ^{13}C-NMR (DMSO-d6) δ 113.58, 115.35, 119.54, 123.44, 124.06, 127,.79, 129.91, 131.85, 133.05, 137.75, 141.07, 151.39, 161.04, 163.28, 164.90, 185.99; EIMS m/z 267 ($M^{\cdot+}$); HR-EIMS m/z calc. 267.069557, found 267.069991.

4.4.14 (*E*)-6-Styrylisatin

Compound **9a** was synthesised from (*E*)-3-aminostilbene (**6d**) and mesoxalic acid diethyl ester in a yield of 66%: mp 257-258 °C (capillary method); literature mp 261-265 °C (Langenbecket al., 1956). ^{1}H-NMR (DMSO-d6) δ 7.08 (m, 1H), 7.36 (m, 5H), 7.50 (m, 1H), 7.60 (m, 1H), 11.10 (s, 1H); ^{13}C-NMR (DMSO-d6) δ 109.34, 116.77, 121.03, 125.14, 127.15, 127.61, 128.66, 128.74, 133.05, 136.22, 147.05, 151.19, 159.95, 183.20; EIMS m/z 249 ($M^{\cdot+}$); HR-EIMS m/z calc. 249.078979, found 249.082581.

4.4.15 (*E*)-6-(3-Chloro)styrylisatin

Compound **9b** was synthesised from (*E*)-3-Amino-3'-chlorostilbene (**6e**) and mesoxalic acid diethyl ester in a yield of 61%: mp 167-170 °C (capillary method). ^{1}H-NMR (DMSO-d6) δ 6.56 (m, 1H), 6.81 (d, 2H, J + 6.8 Hz), 7.06 (m, 2H), 7.20 (d, 1H, J = 16.4 Hz), 7.30 (d, 1H, J = 7.9 Hz), 7.38 (t, 1H, J = 7.8

Hz), 7.53 (d, 1H, J = 7.8 Hz), 7.67 (s, 1H); ^{13}C-NMR (DMSO-d6) δ 63.96, 113.49, 115.68, 116.45, 126.29, 127.10, 127.19, 128.28, 130.47, 131.71, 132.27, 134.88, 138.49, 140.91, 149.58, 171.89; EIMS m/z 283 ($M^{\cdot+}$); HR-EIMS m/z calc. 283.040006, found 283.040436.

4.5 Summary

Three (*E*)-5-styrylisatin (**8a–c**) and two (*E*)-6-styrylisatin analogues (**9a–b**) were synthesised successfully according to literature as described above and the identity and purity of these compounds were verified by mass spectrometry, ^{1}H-NMR and ^{13}C-NMR. It was decided to exclude some of the proposed (*E*)-5-styrylisatin analogues (**8d–g** in Table 2) from biological evaluation because of insolubility, which prevented purification.

BIOLOGICAL EVALUATION

5.1 Introduction

A discontinuous spectrophotometric assay was used for the determination of MAO-B catalytic activity. The IC_{50} values (Tables 4 & 5) for the styrylisatin analogues (**8a–c** and **9a–b**) and the K_i value for compound **8b** were estimated by measuring the extent to which different concentrations of the analogues slowed the rate of the MAO-B catalyzed oxidation of the substrate, MMTP [1-methyl-4-(1-methylpyrrol-2-yl)-1,2,3,6-tetrahydropyridine] (Inoue *et al.*, 1999). MMTP (K_m = 60.9 μM) is oxidised to the product, $MMDP^+$ [1-methyl-4-(1-methylpyrrol-2-yl)-2,3-dihydropyridinium] (Fig. 24). $MMDP^+$ does not undergo further *in vitro* oxidation to MMP^+ [1-methyl-4-(1-methylpyrrol-2-yl)pyridinium] (Petzer *et al.*, 2003).

MMTP was chosen as substrate for several reasons. It is a good substrate (low K_m value) and is oxidised to a stable product ($MMDP^+$). Both MMTP and its product are soluble in an aqueous buffer solution. $MMDP^+$ is a good chromophore that absorbs radiation at 420 nm, a wavelength where MMTP does not absorb radiation. The lack of interference in light absorption from other components of the assay makes it ideal for spectrophotometry (Inoue *et al.*, 1999; Vlok *et al.*, 2006). Since MMTP is a structural analogue of the nigrostriatal neurotoxin MPTP and should be used with caution, disposable gloves and protective eyewear were worn and safe handling procedures were followed (Pitts *et al.*, 1986; Vlok *et al.*, 2006).

MMTP is a substrate for both MAO-A and B. In order to exclude oxidation of MMTP by MAO-A, baboon liver mitochondrial fractions, which are devoid of MAO-A activity, were used as enzyme source. Another benefit of baboon liver MAO-B is its similarity to human MAO-B in inhibitory specificities.

5.2 Material and instrumentation

Prof. Neal Castagnoli Jr., Virginia Tech, Blacksburg, USA, generously supplied us with the oxalate salt of MMTP. UV-Vis spectra were recorded on a Shimadzu 2100 UV-visible spectrophotometer.

5.3 Binding affinity assay

We have measured the K_i value (inhibition constant) for only one inhibitor, (*E*)-5-(3-chlorostyryl)isatin (**8b** in Fig. 42), in order to determine whether the mode of inhibition is competative. A set of Lineweaver-Burk plots that intersects at the y-axis will be indicative of competative inhibition.

Mitochondrial fractions isolated from baboon liver tissue according to the methods of Salach and Weyler (1987) and stored at -70 °C were used. These fractions were suspended in sodium phosphate buffer (100 mM, pH 7.4, containing 50% glycerol, w/v) before determining the protein concentration according to the method of Bradford (1976). Incubations (500 µl) contained the mitochondrial fractions [3 mg/ml] suspended in sodium phosphate buffer (100 mM sodium phosphate buffer, pH 7.4), MMTP (30 – 120 µM), the mitochondrial isolate (0.15 mg protein/ml), and various concentrations of the test inhibitor. Final mixtures were incubated at 37 °C for 10 minutes in order to ensure that the initial velocity in the linear phase of metabolite production is measured (Vlok *et al.*, 2006; Inoue *et al.*, 1999). The reactions were terminated by adding 10 µl of 70% perchloric acid. The supernatant fractions were removed from the centrifuged (16,000 g for 10 minutes) samples and the concentrations of the product, $MMDP^+$, in these fractions were measured spectrophotometrically at a wavelength of 420 nm. The initial velocity [V_i in mol/(mg protein.min) of the dihydropyridinium formed] of MAO-B catalytic oxidation was calculated using equation 8 as given by Vlok *et al.* (2006). In equation 8, Abs is the measured absorbance of the dihydropyridinium metabolite $MMDP^+$, ε is the reported molecular absorptivity for $MMDP^+$ (24,000 M^{-1}), [E] is the enzyme concentration (0.15 mg protein/ml) and Time is the incubation time (10 minutes).

$$V_i = \frac{Abs}{\varepsilon} \times \frac{1}{[E]} \times \frac{1}{Time} \qquad \textbf{Equation 8}$$

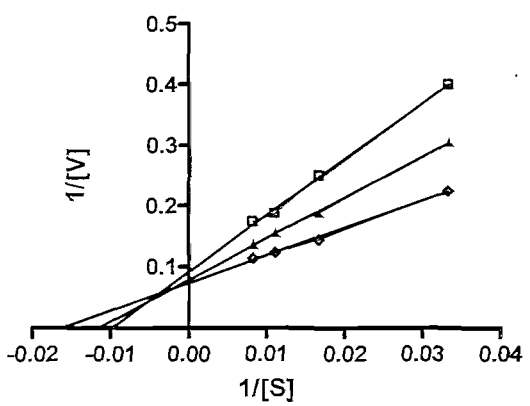

Figure 46: Lineweaver-Burke plots of the oxidation MMTP by baboon liver MAO-B in the absence (open diamond) and presence of various concentrations of **8b** (filled triangle, 10 nM; open square, 20 nM;). The concentration of the baboon liver mitochondrial preparation was 0.15 mg/ml and the rates are expressed as nmoles.mg protein $^{-1}$. min^{-1} of $MMDP^+$ formed.

For each inhibitor concentration, a Lineweaver-Burk plot was constructed by plotting the inverse of the measured initial rates of oxidation (expressed as nmoles of $MMDP^+$ formed per mg mitochondrial protein per minute) as a function of the inverse of the substrate concentration (Vlok *et al.*, 2006) (Fig. 46). The slope of each Lineweaver-Burk plot was plotted as a function of the inhibitor concentration (Fig. 47) and the K_i value was determined from the abscissa intercept (Vlok *et al.*, 2006).

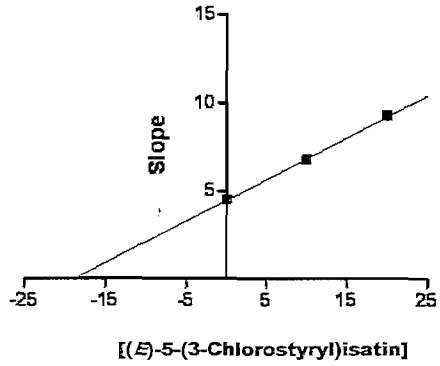

Figure 47 : Plot of slopes of Lineweaver-Burk plots versus (E)-5-(3-chlorostyryl)isatin (**8b**) concentration. The K_i value was calculated from the x-axis intercept (y=0) which is equal to $-K_i$

5.4 Time-dependent inhibition assay

A time-dependent inhibition assay was performed for the representative (*E*)-5-(3-chlorostyryl)isatin analogue (**8b**) in order to test reversibility of inhibition. Mitochondrial fractions isolated from baboon liver tissue according to the methods of Salach and Weyler (1987) and stored at -70 °C were used. The fractions [0.3 mg/ml] were incubated at 37 °C with test inhibitor (40 nM) and these incubation mixtures were added to the substrate MMTP (90 µM) after 0, 15, 30 and 60 minutes respectively to yield an enzyme concentration of 0.15 mg/ml. The resulting incubation mixtures were incubated for a further 15 minutes at 37 °C before terminating the reactions by adding 10 µl of 70% perchloric acid. The supernatant fractions were removed from the centrifuged (16,000 g for 10 minutes) samples and the concentrations of the product, $MMDP^+$, in these fractions were measured spectrophotometrically at a wavelength of 420 nm. Reversibility was determined by plotting a histogram (Fig. 48) of the measured initial rates of oxidation (Eq. 8) (nmoles of $MMDP^+$ formed per mg mitochondrial protein per minute) at different pre-incubation times (min) with the inhibitor (*E*)-5-(3-chlorostyryl)isatin (**8b**).

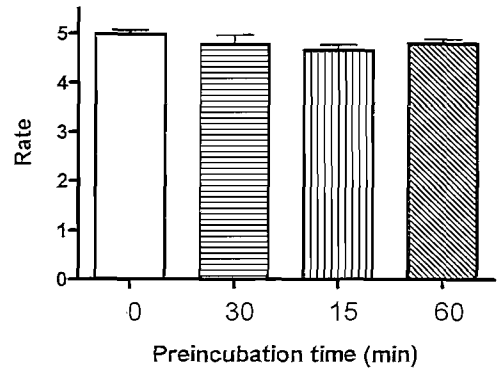

Figure 48 : *Histogram of initial rates of oxidation* (nmol/min.mg) against different preincubation times (min) with the inhibitor (*E*)-5-(3-chlorostyryl)isatin (**8b**).

5.5 Functional inhibition assay

To compare the MAO-B inhibition potency of the styrylisatin analogues investigated here, IC_{50} values were determined for all. An IC_{50} value represents the concentration of a drug that is required for 50% inhibition *in vitro* of an enzyme or antagonism of a receptor (Silverman, 2004) and describes the functional strength of the inhibitor (Jozwaik *et al.*, 2005). IC_{50} values were determined in duplicate for all styrylisatin analogues (**8a–c**, **9a–b**) as well as for isatin (**10**). Mitochondrial fractions were isolated from baboon liver tissue according to the methods of Salach and Weyler (1987) and were stored at -70 °C. These fractions were suspended in sodium phosphate buffer (100 mM, pH 7.4, containing 50% glycerol, w/v) before determining the protein concentration according to the method of Bradford (1976). A typical incubation (500 µl final volume in 100 mM sodium phosphate buffer, pH 7.4) contained MMTP (50 µM) as substrate, the mitochondrial isolate (0.15 mg protein/ml), and various concentrations of the test inhibitors in DMSO. Final mixtures were incubated at 37 ° C for 10 minutes in order to ensure that the initial velocity in the linear phase of metabolite production is measured (Vlok *et al.*, 2006; Inoue *et al.*, 1999). The reactions were terminated by adding 10 µl of 70% perchloric acid. The supernatant fractions were removed from the centrifuged (16,000 g for 10 minutes) samples and the concentrations of the product, $MMDP^+$, in these fractions were measured spectrophotometrically at a wavelength of 420 nm. As demonstrated in Fig. 49–54, the initial velocity (V_i) of MAO-B catalytic oxidation was calculated using equation 8, and plotted as a function of the test inhibitor concentration in order to determine the IC_{50} value. Nonlinear regression analysis was carried out with the Prism software package (GraphPad Software Inc.).

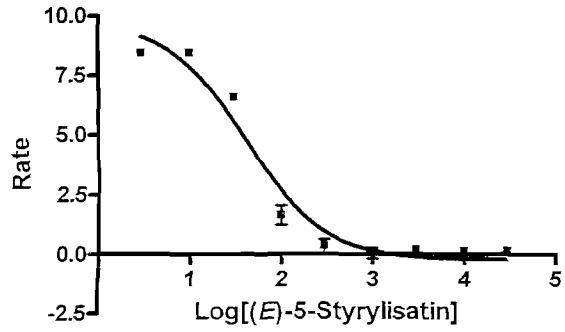

Figure 49: Plot of rate (nmol/min.mg) versus log of (*E*)-5-styrylisatin (**8a**) concentrations. All measurements were in duplicate

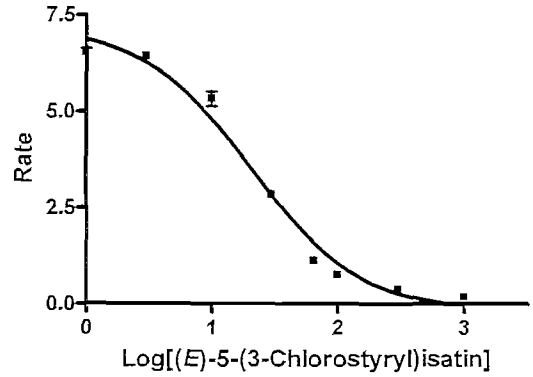

Figure 50: Plot of rate (nmol/min.mg) versus log of (*E*)-5-(3-chlorostyryl)isatin (**8b**) concentrations. All measurements were in duplicate.

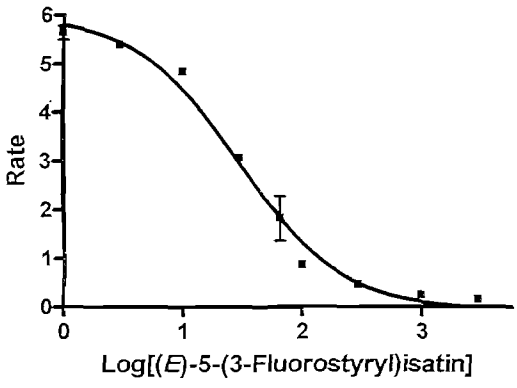

Figure 51: Plot of rate (nmol/min.mg) versus log of (*E*)-5-(3-flourostyryl)isatin (**8c**) concentrations. All measurements were in duplicate.

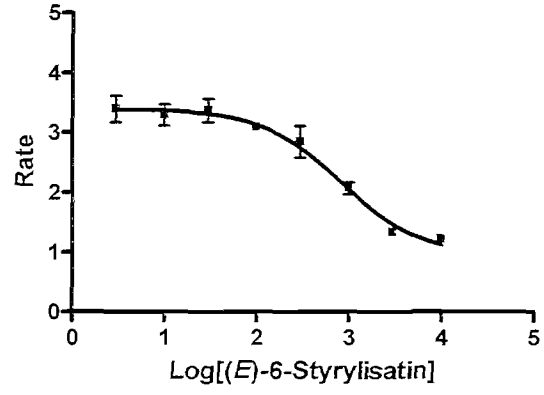

Figure 52: Plot of rate (nmol/min.mg) versus log of (*E*)-6-styrylisatin (**9a**) concentrations. All measurements were in duplicate.

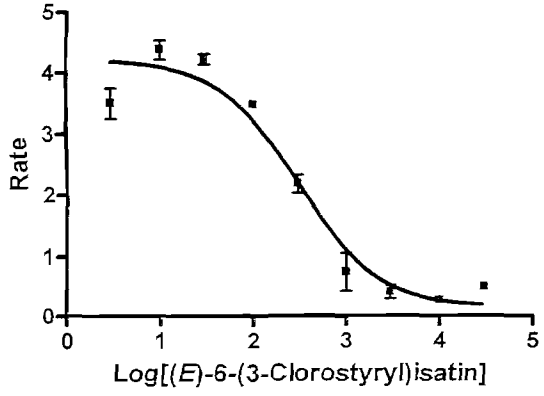

Figure 53: Plot of rate (nmol/min.mg) versus log of (*E*)-6-(3-chlorostyryl)isatin (**9b**) concentrations. All measurements were in duplicate.

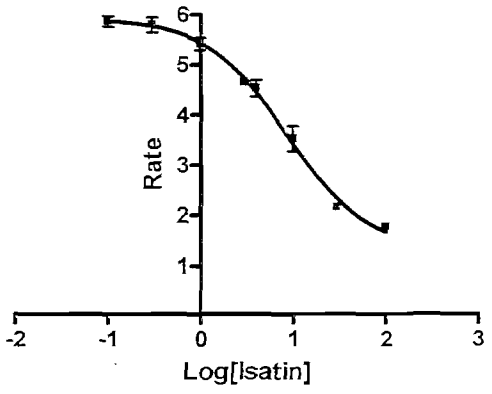

Figure 54: Plot of rate (nmol/min.mg) versus log of isatin (**10**) concentrations. All measurements were in duplicate.

5.6 Results and discussion

The K_i value obtained for the selected representative compound, (*E*)-5-(3-chlorostyryl)isatin (**8b**), was calculated as 18.8 nM. Compound **8b** is therefore approximately 160 times more potent as a MAO-B inhibitor than the lead compound isatin (K_i = 3 μM) (Hubálek et al., 2005). As demonstrated in Fig. 46, the lines of the Lineweaver-Burke plots for **8b** intersected, indicating that the mode of inhibition was competitive (Rodwell & Kennelly, 2003).

Reversibility of inhibition for the chosen representative compound, (*E*)-5-(3-chlorostyryl)isatin (**8b**), was confirmed in the time-dependent inihibition study. As seen in Figure 48, the measured initial rates of oxidation were not affected by preincubation of the enzyme with the test inhibitor for different time periods. This is in contrast to irreversible inhibition that would have led to a reduction in rate of oxidation with increased pre-incubation time.

Table 4: IC_{50} values for the (E)-5-styrylisatin analogues tested.

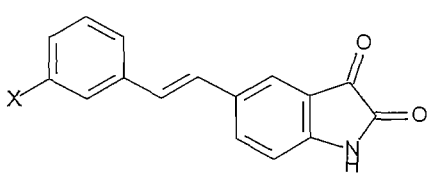

Compound	*X*	*IC_{50} value (nM)*
8a	H	41.7 ± 1.86
8b	Cl	20.7 ± 0.63
8c	F	30.1 ± 4.63

The MAO-B inhibitory potency of all the styrylisatin analogues synthesised were confirmed with IC_{50} values in the low nM range (Table 4) for the (*E*)-5-styrylisatin analogues (**8a–c**) and in the low μM range (Table 5) for the (*E*)-6-styrylisatin analogues (**9a–b**). The most potent inhibitor was found to be (*E*)-5-(3-chlorostyryl)isatin (**8b**) with an IC_{50} value of 20.7 nM. Compound **8b** is approximately twice more potent than the unsubstituted (*E*)-5-styrylisatin analogue (**8a**) and approximately 415 times that of the lead compound, isatin (Table 6). The second most potent inhibitor was (*E*)-5-(3'-fluorostyryl)isatin (**8c**) with an IC_{50} value of 30.1 nM. The series of (*E*)-6-styrylisatin analogues (**9a–b**) were found to be about ten times less potent than the (*E*)-5-styrylisatin analogue series (**8a–c**), with (*E*)-6-(3'-chlorostyryl)isatin (**9b**) having the lowest IC_{50} value (313.2 nM) for the series.

Qualitative inspection of the results in Tables 4 to 6 show that substitution with a styryl side-chain at C-5 and C-6 of the isatin ring produced inhibitors of MAO-B that are more potent than the lead compound, isatin. The potency of MAO-B inhibition may be further enhanced by substitution of the styryl phenyl ring with halogens at C-3 of the styryl ring. For example both **8b** and **8c**, bearing chlorine and fluorine respectively at C-3 of the styryl ring were found to be more potent MAO-B inhibitors than the corresponding unsubstituted **8a**.

Table 5: IC_{50} values for the (E)-6-styrylisatin analogues tested.

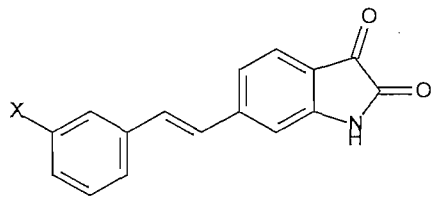

Compound	*X*	*IC_{50} value (nM)*
9a	H	436.8 ± 4.85
9b	Cl	313.2 ± 56.20

Table 6: IC_{50} value for isatin.

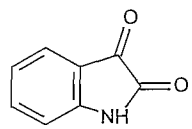

Compound	*IC_{50} value (μM)*
10	8.6 ± 0.52

5.7 Summary

The K_i value was determined for one chosen representative compound, (*E*)-5-(3-chlorostyryl)isatin (**8b**). The results confirmed competitive inhibition of MAO-B. Reversibility of inhibition was confirmed for the representative compound (**8b**) with a time-dependent inhibition assay. The IC_{50} values for the inhibition of MAO-B by the (*E*)-styrylisatin analogues (**8a–c**, **9a–b**) and isatin (**10**) were determined. The results

indicated that substitution with a styryl side-chain at C-5 of the isatin ring produced inhibitors of MAO-B that are considerably more potent than the lead compound, isatin.

CONCLUSION

Monoamine oxidase B (MAO-B) inhibitors are currently clinically used in the symptomatic treatment of Parkinson's disease (PD) and may also protect against further neurodegeneration. The irreversible MAO-B inhibitor, (*R*)-deprenyl, is most often used in PD treatment, usually in combination with levodopa as part of dopamine replacement therapy. In contrast with reversible inhibition, enzyme recovery after irreversible inhibition involves *de novo* synthesis of the enzyme, which may require several weeks. This makes reversible MAO-B inhibitors safer and more desirable.

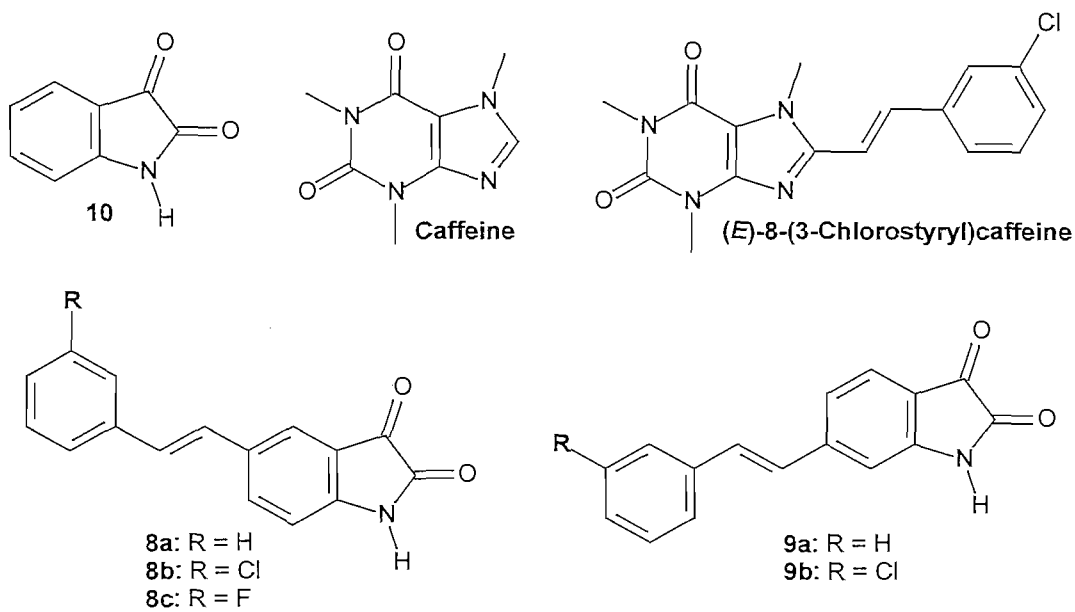

Figure 55. The structures of the compounds discussed in the text.

Both isatin (**10**) and caffeine (Fig. 55) are small molecules that have been reported to inhibit MAO-B. Isatin is a relatively good endogenous inhibitor (K_i = 3 μM) whereas caffeine is a weak inhibitor (K_i = 650 μM). The inhibitory potency of caffeine has reportedly been improved by substitution at C-8 of the caffeine ring with a styryl side-chain (Petzer *et al.*, 2003). Addition of an electron withdrawing substituent at C-3 of the phenyl ring produced structures with exceptional reversible MAO-B inhibitory potency, for example (*E*)-8-(3-chlorostyryl)caffeine (K_i = 0.1 μM). In this study we investigated whether

styryl substitution of the lead compound, isatin, at C-5 and C-6 will similarly enhance isatin's MAO-B inhibitory potency.

Molecular docking of the proposed (*E*)-5-styrylisatin (**8a–c**) and (*E*)-6-styrylisatin (**9a–b**) analogues into the active site of recombinant human MAO-B supported the hypothesis of increased MAO-B inhibitory activity compared to isatin. The styryl side-chain seems to be stabilised in the entrance cavity of the enzyme, while the isatin moiety is involved in hydrogen bonding in the substrate-binding cavity. This *dual binding mode is similar* to that proposed for the styrylcaffeines and *is thought* to facilitate the potent MAO-B inhibition of styrylcaffeines.

Two (*E*)-6-Styrylisatin (**9a–b**) as well as three (*E*)-5-styrylisatin (**8a**–c) analogues were synthesized from the appropriately substituted aminostilbene derivatives and diethyl ketomalonate (Langenbeck *et al.*, 1956). The compounds were evaluated *in vitro* as inhibitors of baboon liver MAO-B. The inhibitory activity of the styrylisatin analogues were determined with a spectrophotometric method wherein the extent by which different concentrations of the analogues slowed the rate of oxidation of a MAO-B substrate was measured. The inhibitory potencies for all the styrylisatin analogues were expressed in terms of the concentration of the compound necessary for 50% inhibition of the enzyme (IC_{50} value). The inhibitory potency was also expressed as the enzyme-inhibitor dissociation constant (K_i value) for one chosen representative compound, (*E*)-5-(3-chlorostyryl)isatin (**8b**). Reversibility of inhibition was confirmed with a time-dependent inhibition study that documented that the potencies of inhibition of MAO-B by the *(E)*-styrylisatin analogues are independent of the time period for which the analogues were incubated with the enzyme.

The results showed that substitution with a styryl side-chain at C-5 of the isatin ring resulted in exceptionally potent reversible inhibitors of MAO-B. For example, (*E*)-5-(3-chlorostyryl)isatin (**8b**) was found to be 415 times more potent (IC_{50} = 20.7 nM) than the lead compound isatin (IC_{50} = 8566 nM). Also, (*E*)-5-styrylisatin (**8a**) was found to have an IC_{50} value of 41.69 nM, which is approximately 206 times more potent than the lead compound, isatin. (*E*)-6-Styrylisatin (**9a**) was found to be a moderately potent, reversible inhibitor of MAO-B with an IC_{50} value of 851 nM.

In this study (*E*)-5-styrylisatin analogues have been identified as promising new reversible inhibitors of MAO-B. This study provides evidence that potent MAO-B inhibitors may be obtained by designing structures that bind to both the entrance and substrate cavities of the enzyme.

REFERENCES

AM, O.B., AMIT, T. & YOUDIM, M.B. 2004. Contrasting neuroprotective and neurotoxic actions of respective metabolites of anti-Parkinson drugs rasagiline and selegiline. *Neuroscience letters*, 355:169-172.

BAKER, B.R., SCHAUB, R.E., JOSEPH, J.P., MCEVOY, F.J. & WILLIAMS, J.H. 1952. An antimalarial alkaloid from hydrangea: synthesis of 5-, 6-, 7- and 8-derivatives with two identical substituents. *Journal of organic chemistry*, 17:52-57.

BERGMAN, F. & SCHAPIRO, D. 1947. Applications of the meerwein reaction. Part IV. The synthesis of new mono- and di-substituted stilbenes. *Journal of organic chemistry*, 12:57-66.

BEZARD, E., GROSS, C.E., FOURNIER, M.C., DOVERO, S., BLOCH, B. & JABER, M. 1999. Absence of MPTP-induced neuronal death in mice lacking the dopamine transporter. *Experimental neurology*, 155:268-273.

BINDA, C., LI, M., HUBALEK, F., RESTELLI, N., EDMONDSON, D.E. & MATTEVI, A. 2003. Insights into the mode of inhibition of human mitochondrial monoamine oxidase B form high-resolution crystal structures. *Proceedings of the national academy of sciences of the United States of America*, 100:9750-9755.

BINDA, C., MATTEVI, A. & EDMONDSON, D.E. 2002. Structure-function relationships in flavoenzyme-dependent amine oxidations. *The journal of biological chemistry*, 277:23973-23976.

BINDA, C., NEWTON-VINSON, P., HUBALEK, F., EDMONDSON, D.E. & MATTEVI, A. 2001. Structure of human monoamine oxidase B, a drug target for the treatment of neurological disorders. *Nature structural biology*, 9:22-26.

BINDA, C., WANG, J., PISANI, L., CACCIA, C., CAROTTI, A., SALVATI, P., EDMONDSON, D.E. & MATTEVI, A. 2007. Structures of human monoamine oxidase B complexes with selective noncovalent inhibitors: safinamide and coumarin analogues. *Journal of medicinal chemistry*, 50:5848-5852.

BIRKMAYER, W., KNOLL, J., RIEDERER, P., YOUDIM, M.B., HARS, V. & MARTON, J. 1985. Increased life expectancy resulting from addition of l-deprenyl to Madopar treatment in Parkinson's disease: a longterm study. *Journal of neural transmission*, 64:113-127.

BLUM, D., TORCH, S., LAMBENG, N., NISSOU, M., BENABID, A., SADOUL, R. & VERNA, J. 2001. Molecular pathways involved in the neurotoxicity of 6-OHDA, dopamine and MPTP: contribution to the apoptotic theory in Parkinson's disease. *Progress in neurobiology,* 65:135-172.

BONUCELLI, U. & DEL DOTTO, P. 2006. New pharmacologic horizons in the treatment of Parkinson disease. *Neurology*, 67(Suppl 2):S30-S38.

BOVé, J., PROU, D., PERIER, C. & PRZEDBORSKI, S. 2005. Toxin-induced models of Parkinson's disease. *The journal of the American society for experimental neurotherapeutics*, 2:484-494.

BRADFORD, M.M. 1976. Rapid and sensitive method for quantitation of microgram quantities of protein utilizing principle of protein-dye binding. *Analytical biochemistry*, 72:248-254.

BRAMSON, H.N., CORONA, J., DAVIS, S.T., DICKERSON, S.H., EDELSTEIN, M., FRYE, S.V., GAMPE, R.T., HARRIS, P.A., HASSELL, A., HOLMES, W.D., HUNTER, R.N., LACKEY, K.E., VEAL, J.M., WALKER, D.H. & KUYPER, L.F. 2001. Oxindole-based inhibitors of cyclin-dependent kinase 2 (CDK2): design, synthesis, enzymatic activities, and x-ray crystallographic analysis. *Journal of medicinal chemistry*, 44:4339-4358.

BUNEEVA, O.A., GNEDENKO, O.V., PANOVA, N.G., MEDVEDEVA, M.V., IVANOV, YU.D. & MEDVEDEV, A.E. 2003. Glycerol-3-phosphate dehydrogenase is a cytosolic isatin-binding protein. *Biomeditsinskaya Khimiya,* 49:627-631.

CARDOSO, S.M., PEREIRA, C. & OLIVEIRA, C.R. 1999. Mitochondrial function is differentially affected upon oxidative stress. *Free radical biology & medicine,* 26:3-13.

CAREY, F.A. & SUNDBERG, R.J. 2000. Advanced organic chemistry. 4th ed. New York : Kluwer Academic/Plenum Publishers. 823 p.

CASERO, R.A. & WORSTER, P.M. 2001. Terminally alkylated polyamine analogues as chemotherapeutic agents. *Journal of medicinal chemistry*, 44:1-26.

CHAUDHURI, K.R., HEALY, D.G. & SCHAPIRA, A.H.V. 2006. Non-motor symptoms of Parkinson's disease: diagnosis and management. *Lancet neurology*, 5:235-245.

CHEN, J., STEYN, S., STAAL, R., PETZER, J.P., XU, K., VAN DER SCHYF, C.J., CASTAGNOLI, K., SONSALLA, P.K., CASTAGNOLI, N. & SCHWARZSCHILD, M.A. 2002. 8-(3-Chlorostyryl)caffeine may attenuate MPTP neurotoxicity through dual actions of monoamine oxidase inhibition and A_{2A} receptor antagonism. *Journal of biological chemistry*, 277:36040-36044.

CHEN, J., XU, K., PETZER, J.P., STAAL, R., XU, Y., BEILSTEIN, M., SONSALLA, P.K., CASTAGNOLI, K., CASTAGNOLI, N. & SCHWARZSCHILD, M.A. 2001. Neuroprotection by caffeine and A_{2A} adenosine receptor inactivation in a model of Parkinson's disease. *The journal of neuroscience*, 21:1-6.

D'AMATO, R.J., LIPMAN, Z.P. & SNYDER, S.H. 1986. Selectivity of the parkinsonian neurotoxin MPTP: toxic metabolite MPP^+ binds to neuromelanin. *Science*, 231:987-989.

DA SILVA, J.F.M., GARDEN, S.J. & PINTO, A.C. 2001. The Chemistry of Isatins: a review from 1975 to 1999. *Journal of Brazilian chemical society*, 12:273-324.

DAUER, W. & PRZEDBORSKI, S. 2003. Parkinson's disease: mechanisms and models. *Neuron*, 39:889-909.

DAVIS, G.C., WILLIAMS, A.C., MARKEY, S.P., EBERT, M.H., CAINE, E.D., REICHERT, C.M. & KOPIN, I.J. 1979. Chronic Parkinsonism secondary to intravenous injection of meperidine analogues. *Psychiatry research*, 1:249-254.

DE LAU, L.M.L. & BRETELER, M.M.B. 2006. Epidemiology of Parkinson's disease. *Lancet Neurology*, 5:525-535.

DEMARINIS, R.M., GALLAGHER, G., HALL, R.F., FRANZ, R.G., WEBSTER, C., HUFFMAN, W.F., SCHWARTZ, M.S., KAISER, C., ROSS, S.T., WILSON, J.W. & HIEBLE, P. 1986. Syntheses and in vitro evaluation of 4-(2-aminoethyl)-2(3H)-indolones and related compounds as peripheral prejunctional dopamine receptor agonists. *Journal of medicinal chemistry*, 29:939-947.

DORSEY, E.R., THOMPSON, J.P., HOLLOWAY, R.G., MARSHALL, F.J., SCHIFITTO, G. & TANNER, C.M. 2007. Projected number of people with Parkinson disease in the most populous nations, 2005 through 2030. *Neurology*, 68:384-386.

EDMONDSON, D.E., MATTEVI, A., BINDA, C., LI, M. & HUBALEK, F. 2004. Structure and mechanism of monoamine oxidase. *Current medicinal chemistry*, 11:1983-1993.

ENZYME COMMISION. 2007. Nicezyme view of enzyme: EC 1.4.3.4. [Web:] http://au.expasy.org/enzyme/1.4.3.4 [Date of access: 17 May. 2007].

FINBERG, J.P., TENNE, M. & YOUDIM, M.B. 1981. Tyramine antagonistic properties of AGN 1135, an irreversible inhibitor of monoamine oxidase type B. *British journal of pharmacology*, 73:65-74.

FUJITA, T., IWASA, J. & HANSCH, C. 1964. A new substituent constant, π, derived from partition coefficients. *Journal of the American chemical society*, 86:5175-5180.

FUKUDA, Y., ITOH, Y., NAKATANI, K. & TERASHIMA, S. 1994. *Tetrahedron*, 50:2793-2808.

FULLER, R.W., WARREN, B.J. & MOLLOY, B.B. 1970. Selective inhibition of monoamine oxidase in rat brain mitochondria. *Biochemical pharmacology,* 19:2934-2936.

FULLER, R.W., MARSH, M.M. & MILLS, J. 1968. Inhibition of monoamine oxidase by N-(Phenoxyethy1)cyclopropylamines. Correlation of inhibition with Hammett constants and partition coefficients. *Journal of medicinal chemistry*, 11:397-398.

GAINETDINOV, R.R, FUMAGALLI, F., JONES, S.R. & CARON, M.G. 1997. Dopamine transporter is required for *in vivo* MPTP neurotoxicity: evidence from mice lacking the transporter. *Journal of neurochemistry*, 69:1322-1325.

GALTER, D., BUERVENICH, S., CARMINE, A., ANVRET, M. & OLSON, L. 2003. ALDH1 mRNA: presence in human dopamine neurons and decreases in substantia nigra in Parkinson's disease and in the ventral tegmental area in schizophrenia. *Neurobiology of disease*, 14:637-647.

GARDEN, S.J., TORRES, J.C., FERREIRA, A.A., SILVA, R.B. & PINTO, A.C. 1997. A modified sandmeyer methodology and the synthesis of (±)-convolutamydine A. Tetrahedron *letters*, 38:1501-1504.

GERLACH, M., RIEDERER, P. & YOUDIM, M.B.H. 1992. The molecular pharmacology of L-deprenyl. *European journal of pharmacology: molecular pharmacology,* 226:97-108.

GIBBON, C.J. ed. 2003. South African medicine formulary. 6th ed. Pinelands : Health and medical publishing group. 568 p.

GLOVER, V., BHATTACHARYA, S.K., CHAKRABARTP, A. & SANDLER, M. 1998. The psychopharmacology of isatin: a brief review. *Stress medicine*. 14:225-229.

GUILBAULT, G.G., BRIGNAC, P.J. & JUNEAU, M. 1968. New substrates for the fluorometric determination of oxidative enzymes. *Analytical chemistry*, 40:1256-1263.

HAMAUE, N., MINAMI, M., HIRAFUJI, M., TERADO, M., MACHIDA, M., YAMAZAKI, N., YOSHIOKA, M. & TASHIRO, K. 1999. Isatin, an endogenous MAO inhibitor, as a new biological modulator. *CNS drug reviews*, 5:331-346.

HAMAUE, N. 2000. Pharmacological role of isatin, an endogenous MAO inhibitor. *Yakugaku zasshi,* 120:352-362.

HAMAUE, N., YAMAZAKI, N., TERADO, M., MINAMI, M., OHNO, K., IDE, H., OGATA, A. & TASHIRO, K. 2000. Urinary isatin concentrations in patients with Parkinson's disease determined by a newly developed HPLC-UV method. *Research communications in molecular pathology and pharmacology,* 108:63-73.

HANNA, P.E., GAMMANS, R.E., SEHON, R.D. & LEE, M. 1980. *Journal of medicinal chemistry,* 23:1038-1044.

HANSCH, C. & LEO, A. 1995. Exploring QSAR. Fundamentals and applications in chemistry and biology. Washington DC : American chemical society. 1-124 p.

HECK, H., CASANOVA, M. & STARR, T.B. 1990. Formaldehyde toxicity – new understanding. *Toxicology*, 20:397-426.

HEIKKILA, R.E., HESS, A. & DUVOISIN, R.C. 1984. Dopaminergic neurotoxicity of 1-methyl-4-phenyl-1,2,5,6-tetrahydropyridine in mice. *Science*, 224:1451-1453.

HOLT, A., SHARMAN, D.F., BAKER, G.B. & PALCIC, M.M. 1997. A continuous spectrophotometric assay for monoamine oxidase and related enzymes in tissue homogenates. *Analytical biochemistry*, 244:384-392.

HUBALEK, F., BINDA, C., LI, M., HERZIG, Y., STERLING, J., YOUDIM, M.B.H., MATTEVI, A. & EDMONDSON, D.E. 2004. Inactivation of purified human recombinant monoamine oxidases A and B by rasagiline and its analogues. *Journal of medicinal chemistry*, 47:1760-1766.

HUBALEK, F., BINDA, C., KHALIL, A., LI, M., MATTEVI, A., CASTAGNOLI, N. & EDMONDSON, D.E. 2005. Demonstration of isoleucine 199 as a structural determinant for the selective inhibition of human monoamine oxidase B by specific reversible inhibitors. *Journal of biological chemistry*, 280:15761-15766.

IGOSHEVA, N., MATTA, S. & GLOVER, V. 2004. Effect of acute stress and gender on isatin in rat tissues and serum. *Physiology & behavior*, 80:665–668.

INOUE, H., CASTAGNOLI, K., VAN DER SCHYF, C., MABIC, S., IGARASHI, K. & CASTAGNOLI, N. 1999. Species-dependent differences in monoamine oxidase A and B-catalyzed oxidation of various C4 substituted 1-methyl-4-phenyl-1,2,3,6-tetrahydropyridinyl derivatives. *The journal of pharmacology and experimental therapeutics*, 291:856-864.

ISCHIROPOULOS, H. & AL-MEHDI, A.B. 1995. Peroxynitrite-mediated oxidative protein modifications. *FEBS letters*, 364:279-282.

JACOBSON, K.A., NIKODIJEVIC, O., PADGETT, W.L., GALLO-RODRIGUEZ, C., MAILLARD, M. & DALY, J.W. 1993. 8-(3-Chlorostyryl)caffeine (CSC) is a selective A-adenosine antagonist *in vitro* and *in vivo*. *FEBS letters*, 323:141-144.

JALKANEN, S. & SALMI, M. 2001. Cell surface monoamine oxidases: enzymes in search of a function. New EMBO member's review. *The EMBO journal*, 20:3893-3901.

JAN, C., FRANCOIS, C., TANDE, D., YELNIK, J., TREMBLAY, L., AGID, Y. & HIRSCH, E. 2000. Dopaminergic innervation of the pallidum in the normal state, in MPTP-treated monkeys and in parkinsonian patients. *European journal of neuroscience*, 12:4525-4535.

JENNER, P. 1999. Genetic susceptibility and the occurrence of Parkinson's disease. *Parkinsonism and related disorders*, 5:173-177.

JOZWAIK, K., MOADDEL, R., YAMAGUCHI, R., RAVICHANDRAN, S., COLLINS, J.R., WAINER, I.W. 2005. Qualitative assessment of IC_{50} values of inhibitors of the neuronal nicotinic acetylcholine receptor using a single chromatographic experiment and multivariate cluster analysis. *Journal of chromatography b*, 819: 169-174.

KEARNEY, E.B., SALACH, J.I., WALKER, W.H., SENG, R.I., KENNEY, W. & ZESZOTEK, E. 1971. The covalently bound flavin of hepatic monoamine oxidase. *European journal of biochemistry*, 24:321-327.

KNOLL, J. & MAGYAR, K. 1972. Some puzzling pharmacological effects of monoamine oxidase inhibitors. *Advances in biochemical psychopharmacology*, 5:393-408.

KOLLER, W., OLANOW, C.W., RODNITZKY, R., FINK, J.S., GROWDON, J.H., PAULSON, G., KURLAN, R., FRIEDMAN, J.H., GANCHER, S., NUTT, J., RAJPUT, A.H., BENNETT, J.B., WOOTEN, G.F., LEWITT, P., GOETZ, C., TANNER, C., SHANNON, K., SUCHOWERSKY, O. & BRIN, M.F. 1993. Effects of tocopherol and deprenyl on the progression of disability in early Parkinson's disease. *New England journal of medicine*, 328:176-183.

KUO, E.A., HAMBLETON, P.T., KAY, D.P., EVANS, P.L., MATHARU, S.S., LITTLE, E., MCDOWALL, N., JONES, C.B., HEDGECOCK, C.J.R., YEA, C.M., CHAN, A.W.E., HAIRSINE, P.W., AGER, I.R., TULLY, W.R., WILLIAMSON, R.A. & WESTWOOD, R. 1996. Synthesis, structure-activity relationships, and pharmacokinetic properties of dihydroorotate dehydrogenase inhibitors: 2-cyano-3-

cyclopropyl-3-hydroxy-N-[3'-methyl-4'-(trifluoromethyl)phenyl]propenamide and related compounds. *Journal of medicinal chemistry*, 39:4608-4621.

KUO, W., HSIUE, G. & JENG, R. 2002. Synthesis and macroscopic second-order nonlinear optical properties of poly(ether imide)s containing a novel two-dimensional carbazole chromophore with nitro acceptors. *Journal of materials chemistry*, 12:868-878.

LAMENSDORF, I., EISENHOFER, G., HARVEY-WHIT, J., NECHUSTAN, A., KIRK, K. & KOPIN, I.J. 2000. 3,4-Dihydroxyphenylacetaldehyde potentiates the toxic effects of metabolic stress in PC12 cells. *Brain research*, 868:191-201.

LANGENBECK, V.W., RUHLMANN, K., REIF, H.H. & STOLZE, F. 1956. Künstliche dehydrasen VII. *Journal für praktische chemie*, 4:136-146.

LANGSTON, J.W., BALLARD, P., TETRUD, J.W. & IRWIN, I. 1983. Chronic Parkinsonism in humans due to a product of meperidine-analog synthesis. *Science*, 219:979-980.

LEE, Y., KE-QING, L., LU, X., SILVERMAN, R.B., SHEPARD, E.M., DOOLEY, D.M., SAYRE, L.M. 2002. 3-Pyrrolines are mechanism-based inactivators of the quinone-dependent amine oxidases but only substrates of flavin-dependent amine oxidases. *Journal of the American chemical society,* 124:12155-12143.

LEES, A. 2005. Alternatives to levodopa in the initial treatment of early Parkinson's disease. *Drugs & aging*, 22:731-70.

LI, J., SUN, W., LI, Y., LIU, X., LIU, Y. & YUE, W. 2004. Study on isatin in urine as the maker of Parkinson's disease. *Chinese pharmaceutical journal,* 39:776-778.

LOPES, W.A. & SILVA, G.A. 1993. Synthesis of new tetracyclic derivatives of 10H-phenoxazine, 10,11-dibenzo{b,f}azepine and (9)10H-acridinone through isatinic intermediates. *Journal of the brazilian chemical society*, 4:34-39.

LYLES, G.A. & CALLINGHAM, B.A. 1982. *In vitro* and *in vivo* inhibition by benserazide of clorgyline-resistant amine oxidases in rat cardiovascular tissues. *Biochemical pharmacology*, 31:1417-1424.

MARRAS, C., MCDERMOTT, M.P., ROCHON, P.A., TANNER, C.M., NAGLIE, G., RUDOLPH, A., LANG, A.E. & THE PARKINSON STUDY GROUP. 2005. Survival in Parkinson disease: thirteen-year follow-up of the DATATOP cohort. *Neurology*, 64:87-93.

MARUYAMA, W., TAKAHASHI, T., YOUDIM, M.B. & NAOI, M. 2002. The anti-Parkinson drug, rasagiline, prevents apoptotic DNA damage induced by peroxynitrite in human dopaminergic neuroblastoma SH-SY5Y cells. *Journal of neural transmission*, 109:467-481.

MARVEL, C.S. & HIERS, G.S. 1941. Isatin. *Organic syntheses*, 1:327.

McDONALD, W.M., RICHARD, T.H. & DE LANG, M.R. 2003. Prevalence, etiology and treatment of depression in Parkinson's disease. *Biological psychiatry*, 54:363-375.

McMURRY, J. 2000. Organic chemistry. 5th ed. USA : Brooks/Cole. 1284 p.

MEDVEDEV, A.E., CLOW, A., SANDLER, M. & GLOVER, V. 1996. Isatin: a link between natriuretic peptides and monoamines? *Biochemical pharmacology*, 52:385-391.

MEDVEDEV, A., IGOSHEVA, N., CRUMEYROLLE-ARIAS, M. & GLOVER, V. 2005. Isatin: role in stress and anxiety. *Stress*, 8: 175-183.

MEDVEDEV, A., BUNEEVA, O., GNEDENKO, O., FEDCHENKO, V., MEDVEDEVA, M., IVANOV, Y., GLOVER, V. & SANDLER, M. 2006. Isatin interaction with glyceraldehyde-3-phosphate dehydrogenase, a putative target of neuroprotective drugs: partial agonism with deprenyl. *Journal of Neural Transmission, supplement*, 71:97-103.

MEYERSON, L.R., McMURTREY, K.D. & DAVIS, V.E. 1978. A rapid and sensitive potentiometric assay for monoamine oxidase using an ammonia-selective electrode. *Analytical biochemistry*, 86:287-297.

NEWTON-VINSON, P., HUBALEK, F. & EDMONDSON, D.E. 2000. High-level expression of human liver monoamine oxidase B in Pichia pastoris. *Protein expression and purification*, 20:334-345.

NICKLAS, W.J., VYAS, I. & HEIKKILA, R.E. 1985. Inhibition of NADH-linked oxidation in brain mitochondria by 1-methyl-4-phenylpyridine, a metabolite of the neurotoxin 1-methyl-4-phenyl-1,2,5,6-tetrahydropyridine. *Life sciences*, 36:2503-2508.

NOVAROLI, L., REIST, M., FAVRE, E., CAROTTI, A., CATTO, M. & CARRUPT, P. 2005. Human recombinant monoamine oxidase B as reliable and efficient source for inhibitor screening. *Bioorganic & medicinal chemistry*, 13:6212-6217.

NOVAROLI, L., DAINA, A., FAVRE, E., BRAVO, J., CAROTTI, A., LEONETTI, F., CATTO, M., CARRUPT, P. & REIST, M. 2006. Impact of species-dependent differences on screening, design, and development of MAO B inhibitors. *Journal of medicinal chemistry*, 49:6264-6272.

OOMS, F., FRÉDÉRICK, R., DURANT, F., PETZER, J.P., CASTAGNOLI, N., VAN DER SCHYF, C.J. & WOUTERS, J. 2003. Rational approaches towards reversible inhibition of type B monoamine oxidase. Design and evaluation of a novel 5H-indeno[1,2-c]pyridazin-5-one derivative. *Bioorganic & medicinal chemistry letters*, 13:69-73.

ORELAND, L. & GOTTFRIES, C. 1986. Brain monoamine oxidase in aging and in dementia of Alzheimer's type. *Progress in neuro-psychopharmacology and biological psychiatry*, 10:533-540.

OTTOBONI, S., CARLSON, T.J., TRAGER, W.F., CASTAGNOLI, K. & CASTAGNOLI, N. 1990. Studies on the cytochrome P-450 catalyzed ring α-carbon oxidation of the nigrostriatal toxin 1-methyl-4-phenyl-1,2,3,6-tetrahydropyridine (MPTP). Chemical *research in toxicology*, 3:423-427.

PARKINSON STUDY GROUP. 2005. A randomized placebo-controlled trial of rasagiline in levodopa-treated patients with Parkinson's disease and motor fluctuations: the PRESTO study. *Archives of neurology*, 62:241-248.

PARKINSON STUDY GROUP. 2004. A controlled, randomized, delayed-start study of rasagiline in early Parkinson disease. *Archives of neurology,* 61:561-566.

PARKINSON STUDY GROUP. 2003. A controlled trial of rasagiline in Parkinson's disease patients with levodopa-related motor fluctuations (PRESTO study). *Annals of neurology*, 54:S27.

PETZER, J.P., STEYN, S., CASTAGNOLI, K.P., CHEN, J.F., SCHWARZSCHILD, M.A.M., VAN DER SCHYF, C.J. 2003. Inhibition of monoamine oxidase B by selective adenosine A_{2A} receptor antagonists. *Bioorganic & medicinal chemistry*, 11:1299-1310.

PITTS, S.M., MARKEY, S.P., MURPHY, D.L. & WEISZ, A. 1986. Recommended practices for the safe handling of MPTP. (*In* Markey, S.P., Castagnoli, N., Trevor, A.J. & Kopin, I.J., eds. MPTP: a neurotoxin producting a parkinsonian syndrome. Orlando : Academic press. p. 703-716.)

POLYMEROPOULOS, M.H. & LAVENDAN, C. 1997. Mutation in the alpha-synclein gene identified in families with Parkinson's disease. *Science*, 276:2045-2047.

RASCOL, O., BROOKS, D.J. & MELAMED, E. 2005. Rasagiline as an adjunct to levodopa in patients with Parkinson's disease and motor fluctuations: a randomized, double-blind, parallel-group trial. *Lancet*, 365:947-954.

RIEDERER, P., LACHENMAYER, L. & LAUX, G. 2004. Clinical applications of MAO-inhibitors. *Current medicinal chemistry*, 11:2033-2043.

RODWELL, V.W. & KENNELLY, P.J. 2003. Enzymes: kinetics. (In Robert, K. et al., eds. *Harper's illustrated biochemistry*. Stamford, Conn. : Appleton & Lange. p. 60-71.)

SAGI, Y., DRIGUES, N. & YOUDIM, M.B.H. 2005. The neurochemical and behavioral effects of the novel cholinesterase-monoamine oxidase inhibitor, ladostigil, in response to L-dopa and L-tryptophan, in rats. *British journal of pharmacology*, 146:553-560.

SAGOT, Y., TONI, N., PERRELET, D., LUROT, S., KING, B., RIXNER, H., MATTENBERGER, L., WALDMEIER, P.C. & KATO, A.C. 2000. An orally active anti-apoptotic molecule (CGP 3466B) preserves mitochondria and enhances survival in an animal model of motorneuron disease. *British journal of pharmacology*, 131:721-728.

SALACH, J.I. & WEYLER, W. 1987. Preparation of the flavin-containing aromatic amine oxidases of human placenta and beef liver. *Methods in enzymology*, 142:627-637.

SAPORITO, M.S., THOMAS, B.A., & SCOTT, R.W. 2000. MPTP activates c-Jun NH(2)-terminal kinase (JNK) and its upstream regulatory kinase MKK4 in nigrostriatal neurons in vivo. *Journal of neurochemistry*, 75:1200-1208.

SHIH, J.C., CHEN, K. & RIDD, M.J. 1999. Monoamine oxidase: from genes to behavior. *Annual review of neuroscience*, 22:197-217.

SHIN, M., JANG, J. & SURH, Y. 2004. Potential roles of NF-kB and ERK1/2 in cytoprotection against oxidative cell death induced by tetrahydropapaveroline. *Free radical biology & medicine*, 36:1185-1194.

SILVERMAN, R.B. 2004. The organic chemistry of drug design and drug action. 2nd ed. New York : Elsevier academic press. 617 p.

SILVERMAN, R.B. 1995. Radical ideas about monoamine oxidase. *Accounts of chemical research*, 28:335-342.

SINGER, T.P., RAMSAY, R.R., MCKEOWN, K., TREVOR, A. & CASTAGNOLI, N., JR. 1988. Mechanism of the neurotoxicity of 1-methyl-4-phenylpyridinium (MPP^+), the toxic bioactivation product of 1-methyl-4-phenyl-1,2,3,6-tetrahydropyridine (MPTP). *Toxicology*, 49:17-23.

SHARGEL, L. & YU, A.B.C. 1999. Applied biopharmaceutics and pharmacokinetics. 4th ed. New York : McGraw-Hill. 768 p.

SHOULSON, I. 1998. Mortality in DATATOP: a multicenter trial in early Parkinson's disease. *Annals of neurology*, 43:318-325.

SMEYNE, R.J. & JACKSON-LEWIS, V. 2005. The MPTP model of Parkinson's disease. *Molecular brain research*, 134:57-66.

SOUTHGATE, J. & COLLINS, G.G.S. 1969. The estimation of monoamine oxidase using ^{14}C-labelled substrates. *Biochemical pharmacology*, 18:2285-2287.

STAAL, R.G.W. & SONSALLA, P.K. 2000. Inhibition of brain vesicular monoamine transporter (VMAT2) enhances 1-methyl-4-phenylpyridinium neurotoxicity *in vivo* I rat striata. *The Journal of pharmacology and experimental therapeutics*, 293:336-342.

SWAIN, C.G. LUPTON, E.C. 1968. Field and resonance components of substituent effects. *Journal of the American chemical society*, 90:4328-4337.

TABOR, C.W., TABOR, H. & ROSENTHAL, S.M. 1954. Purification of amine oxidase from beef plasma. *The journal of biological chemistry*, 208:645-661.

TAKAHASHI, N., MINER, L.L., SORA, I., UJIKE, H., REVAY, R.S., KOSTIC, V., JACKSON-LEWIS, V., PRZEDBORSKI, S. & UHL, G.R. 1997. VMAT2 knockout mice: heterozygotes display reduced amphetamine-conditioned reward, enhanced amphetamine locomotion, and enhanced MPTP toxicity. *Proceedings of the national academy of sciences of the United States of America*, 94:9938-9943.

THEBAULT, J.J., GUILLAUME, M. & LEVY, R. 2004. Tolerability, safety, pharmacodynamics, and pharmacokinetics of rasagiline: a potent, selective, and irreversible monoamine oxidase type B inhibitor. *Pharmacotherapy*, 24:1295-1305.

TIPTON, K.F., BOYCE, S., O'SULLIVAN, J., DAVEY, G.P. & HEALY, J. 2004. Monoamine oxidases: certainties and uncertainties. *Current medicinal chemistry*, 11:1965-1982.

TIPTON, K.F. 1971. Monoamine oxidase (pig brain mitochondria). *Methods in enzymology*, 17:717-722.

TOZAWA, Y., UEKI, A., MANABE, S. & MATSUSHIMA, K. 1998. Stress-induced increase in urinary isatin excretion in rats. *Biochemical pharmacology*, 56:1041–1046.

UDENFRIEND, S., WEISSBACH, H. & CLARK, C.T. 1954. The estimation of 5-hydroxytryptamine (serotonin) in biological tissues. *Journal of biological chemistry*, 215:337-344.

VAN DER SCHYF, C.F., GELDENHUYS, W.J. & YOUDIM, M.B. 2006. Multifunctional drugs with different CNS targets for neuropsychiatric disorders. *Journal of neurochemistry*, 99:1033-1048.

VAN DER BERG, D., ZOELLNER, K.R., OGUNROMBI, M.O., MALAN, S.F., TERRE'BLANCHE, G., CASTAGNOLI, N., BERGH, J.J., PETZER, J.P. 2007. Inhibition of monoamine oxidase B by selected benzimidazole and caffeine analogues. *Bioorganic & medicinal chemistry*, 15:3692-3702.

VAN DE WATERBEEMB, H. & TESTA, B. 1987. Advances in drug research. London : Academic Press. 85-225 p.

VARMA, R.S., KHAN, I.A. 1978. Isatins as potential biologically active agents. *Defence science journal*, 28: 191-202

VILA, M., JACKSON-LEWIS, V., VUKOSAVIC, S., DJALDETTI, R., LIBERATORE, G., OFFEN, D., KORSMEYER, S.J. & PRZEDBORSKI, S. 2001. Baxableation prevents dopaminergic neurodegeneration in the 1-methyl-4-phenyl-1,2,3,6-tetrahydropyridine mouse model of Parkinson's disease. *Proceedings of the national academy of sciences of the United States of America*, 98:2837-2842.

VISWANATH, V., WU, Y., BOONPLUENG, R., CHEN, S., STEVENSON, F.F., YANTIRI, F., YANG, L., BEAL, M.F. & ANDERSEN J.K. 2001. Caspase-9 activation results in downstream caspase-8 activation and bid cleavage in 1-methyl-4-phenyl-1,2,3,6-tetrahydropyridine-induced Parkinson's disease. *Journal of neuroscience*, 21:9519-9528.

VLOK, N., MALAN, S.F., CASTAGNOLI, N., BERGH, J.J. & PETZER, J.P. 2006. Inhibition of monoamine oxidase B by analogues of the adenosine A_{2A} receptor antagonist (E)-8-(3-chlorosyryl)caffeine (CSC). *Bioorganic & medicinal chemistry*, 14:3512-3521.

WEETMAN, D.F. & SWEETMAN, A.J. 1971. Realistic estimations of kinetic constants for the oxidation of naturally occurring monoamines by monoamine oxidase. *Analytical biochemistry,* 41:517-521.

WEISSBACH, H., SMITH, T.E., DALY, J.W., WITKOP, B. & UDENFRIEND, S. 1960. Rapid spectrophotometric assay of monoamine oxidase based on the rate of disappearance of kynuramine. *The journal of biological chemistry*, 235:1160-1163.

WELSTEAD, W.J., MORAN, H.W., STAUFFER, H.F., TURNBULL, L.B. & SANCILIO, L.F. 1979. Antiinflammatory agents: synthesis and anti-inflammatory activity of 2-amino-3-benzoylphenylacetic acid. *Journal of medicinal chemistry*, 22:1074-1079.

WESTLUND, K.N., DENNEY, R.M., KOCHERSPERGER, L.M., ROSE, R.M. & ABELL, C.W. 1985. Distinct monoamine oxidase A and B populations in primate brain. *Science*, 230:181-183.

WILMOT, C.M., SAYSELL, C.G., BLESSINGTON, A., CONN, D.A., KURTIS, C.R., MCPHERSON, M.J., KNOWLES, P.F., PHILLIPS, S.E.V. 2004. Medical implications form the crystal structure of a copper-containing amine oxidase complexed with the antidepressant drug tranylcypromine. *FEBS letters*, 576:301-305.

XIA, X.G., HARDING, T., WELLER, M., BIENEMAN, A., UNEY, J.B. & SCHULZ, J.B. 2001. Gene transfer of the JNK interacting protein-1 protects dopaminergic neurons in the MPTP model of Parkinson's disease. *Proceedings of the national academy of sciences of the United States of America,* 98:10433-10438.

XU, J., KAO, S.Y., LEE, F.J., SONG, W., JIN, L.W. & YANKNER, B.A. 2002. Dopamine-dependent neurotoxicity of alpha-synuclein: a mechanism for selective neurodegeneration in Parkinson disease. *Nature medicine*, 8:600-606.

YAMADA, H., ISOBE, K., TANI, Y. & HIROMI, K. 1979. A differential determination procedure for spermine and spermidine with beef plasma amine oxidase. *Agricultural and biological chemistry*, 42:2487-2491.

YANG, L., OMORI, K., SUZUKAWA, J. & INAGAKI, C. 2004. Calcineurin-mediated BAD Ser155 dephosphorylation in ammonia-induced apoptosis of cultured rat hippocampal neurons. *Neuroscience Letters*, 357:73-75.

YOUDIM, M.B. & BAKHLE, Y.S. 2006. Monoamine oxidase: isoforms and inhibitors in Parkinson's disease and depressive illness. *British journal of pharmacology*. 147(Suppl1):S287-296.

YOUDIM, M.B. & RIEDERER, P.F. 2004. A review of the mechanisms and role of monoamine oxidase inhibitors in Parkinson's disease. *Neurology*, 63: S32-S35.

YOUDIM, M.B.. EDMONDSON, D. & TIPTON, K.F. 2006. The therapeutic potential of monoamine oxidase inhibitors. *Nature reviews, neuroscience*, 7:295-309.

YOUDIM, M.B., MARUYAMA, W. & NAOI, M. 2005. Neuropharmacological, neuroprotective and amyloid precursor processing properties of selective MAO-B inhibitor anti-Parkinsonian drug, rasagiline. *Drugs today*, 41:369-391.

YOUNG, R. 1999. Update on Parkinson's disease. *American family physician*, 59:2155-2168.

YU, P.H. 2001. Involvement of cerebrovascular semicarbazide-sensitive amine oxidase in the pathogenesis of Alzheimer's disease and vascular dementia. *Medical hypotheses*, 57:175-179.

YU, P.H. 1986. Monoamine oxidase. *Neuromethods, neurotransmitter enzymes, 5*:235-272.

ZANG, L.Y. & MISRA, H.P. 1992. Superoxide radical production during the autoxidation of 1-metyl-4-phenyl-2,3-dihydropyridinium perchlorate. *Journal of biological chemistry*, 267:17547-17552.

ZECCA, L., YOUDIM, M.B., RIEDERER, P., CONNOR, J.R. & CRICHTON, R.R. 2004. Iron, brain ageing and neurodegenerative disorders. *Nature reviews, neuroscience*, 5:863-873.

ZHOU, J.J.P., ZHONG, B. & SILVERMAN, R.B. 1996. Direct continuous fluorometric assay for monoamine oxidase B. *Analytical biochemistry*. 234:9-12.

APPENDIX A

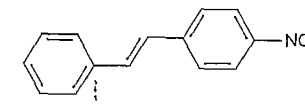

MS, ^{1}H-NMR, ^{13}C-NMR spectra

(5a) (*E*)-4-Nitrostilbene:

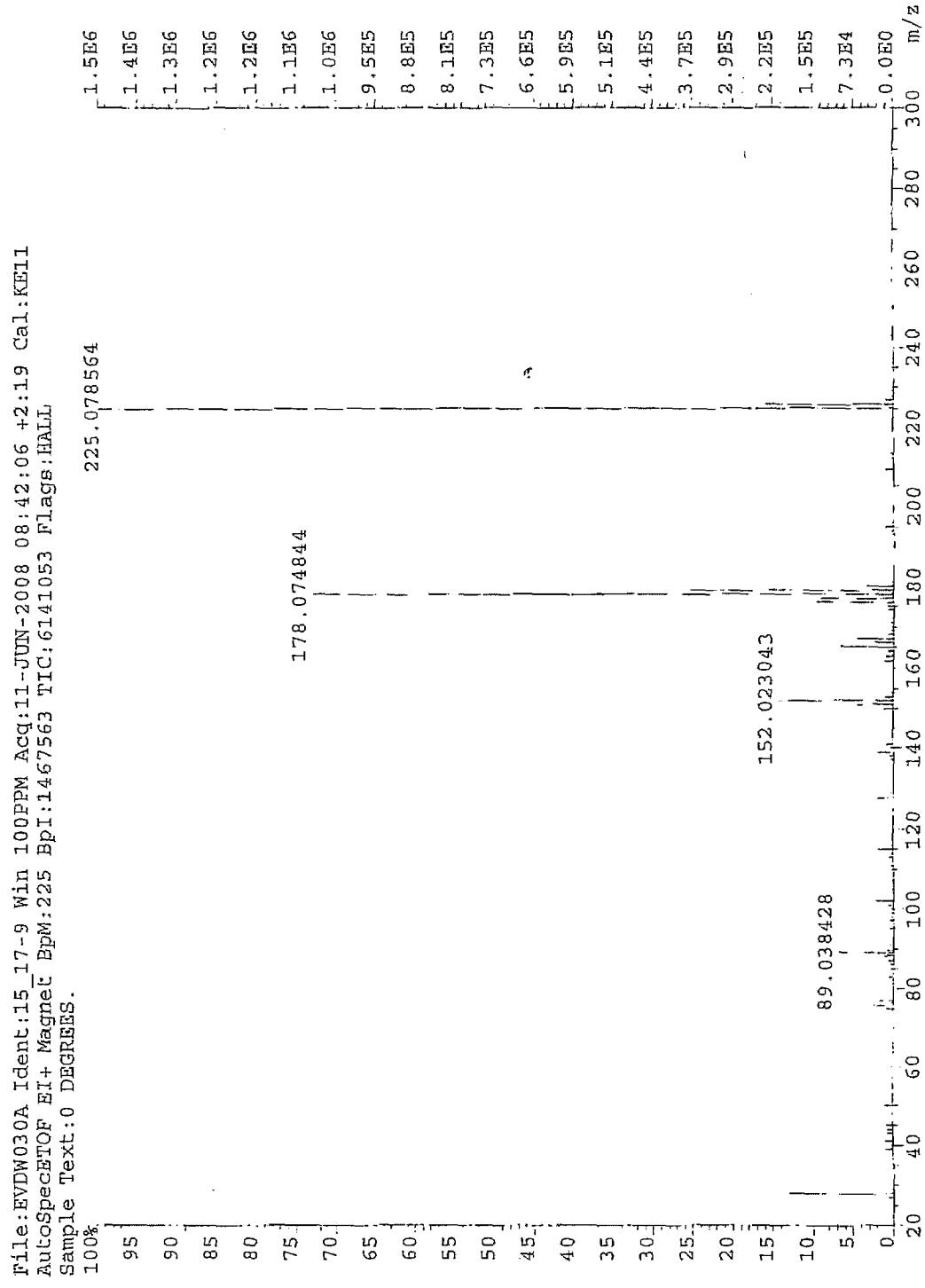

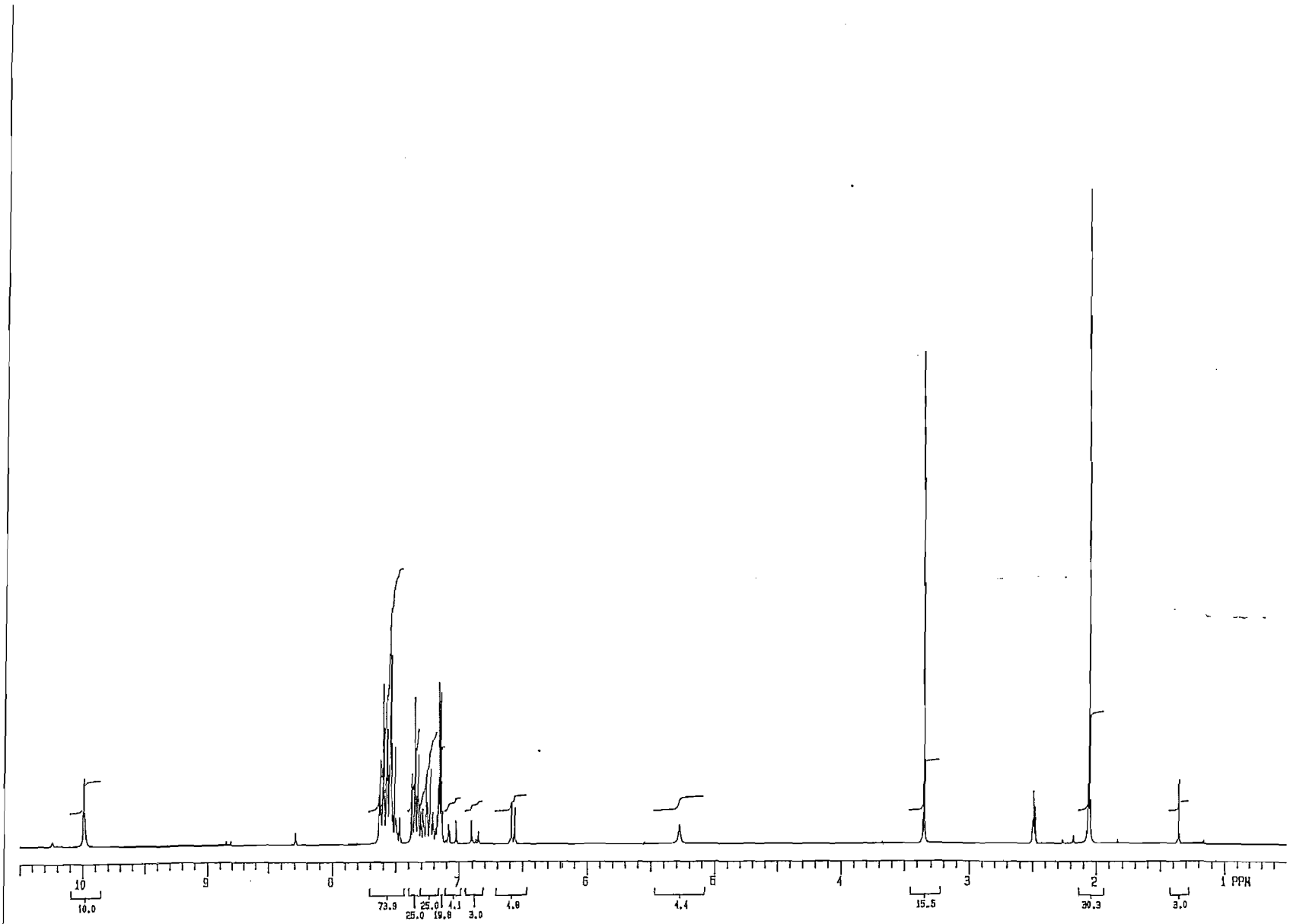
10
9
8
7
6
5
4
3
2
1 PPM
10.0
73.9
25.0
25.0
19.8
4.1
3.0
4.8
4.4
15.5
30.3
3.0
1.000
300
1.000
-450.0
64
SAMPL
4500.5
0
1023.0
1.998
2.000
C
10000
3000.8
150.0
30.0
08-27-07
12:46:08
DMSO
36.0
H

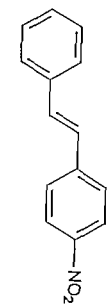
NO2

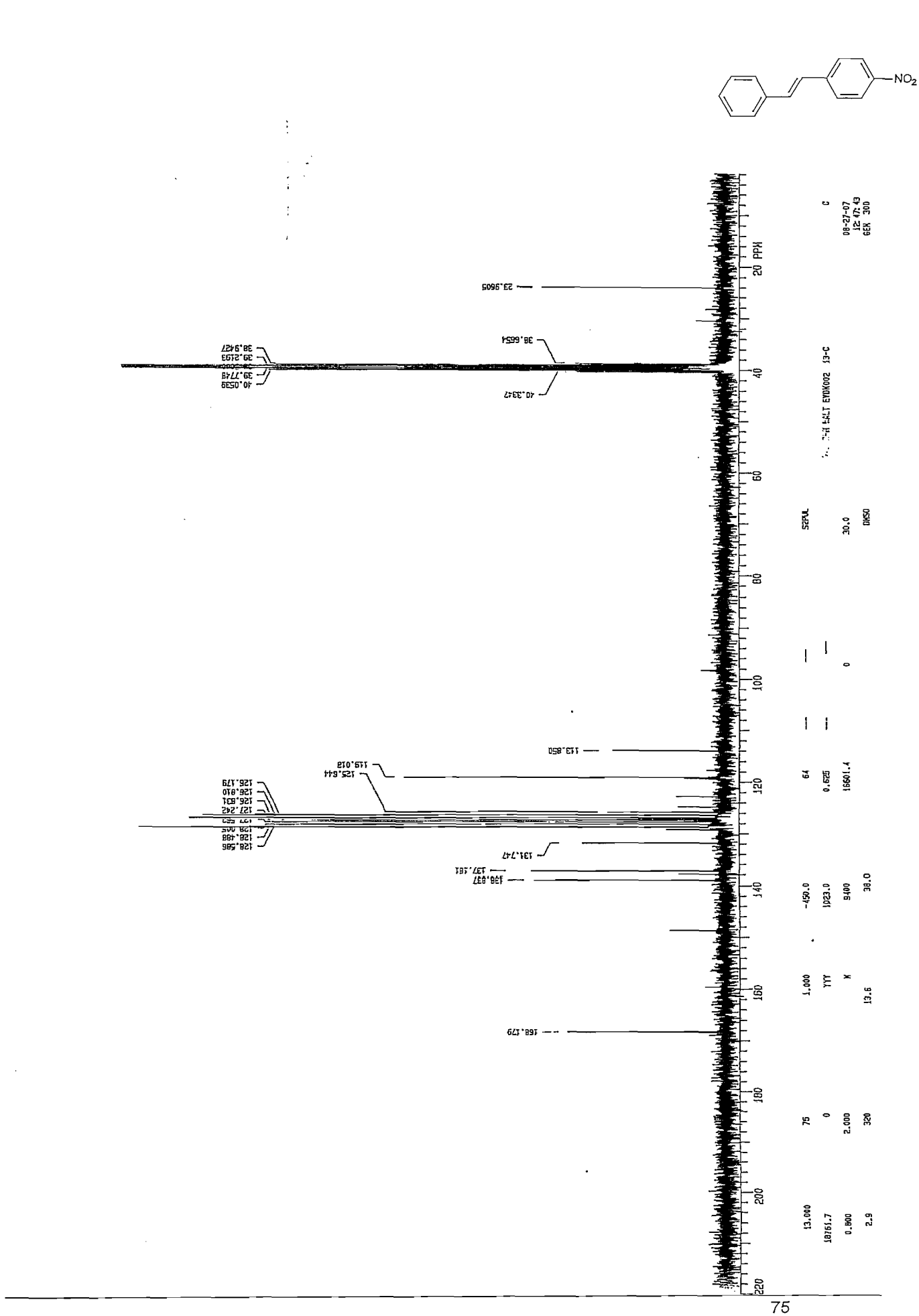
NO2
23.9603
38.6654
40.3342
38.9427
39.2193
39.7748
40.0539
113.850
119.018
125.644
126.179
126.810
126.831
127.242
128.586
128.488
131.747
137.161
138.937
168.179
20 PPH
40
60
80
100
120
140
160
180
200
220
08-27-07
12:47:43
GER 300
C
13-C
SEPUL
30.0
DMSO
0
64
0.625
15601.4
-450.0
1023.0
9400
38.0
1.000
YYY
K
13.6
75
0
2.000
320
13.000
18761.7
0.800
2.9

(5b) (*E*)-3'-Chloro-4-nitrostilbene:

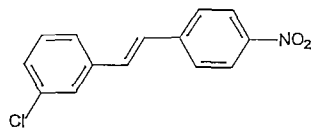

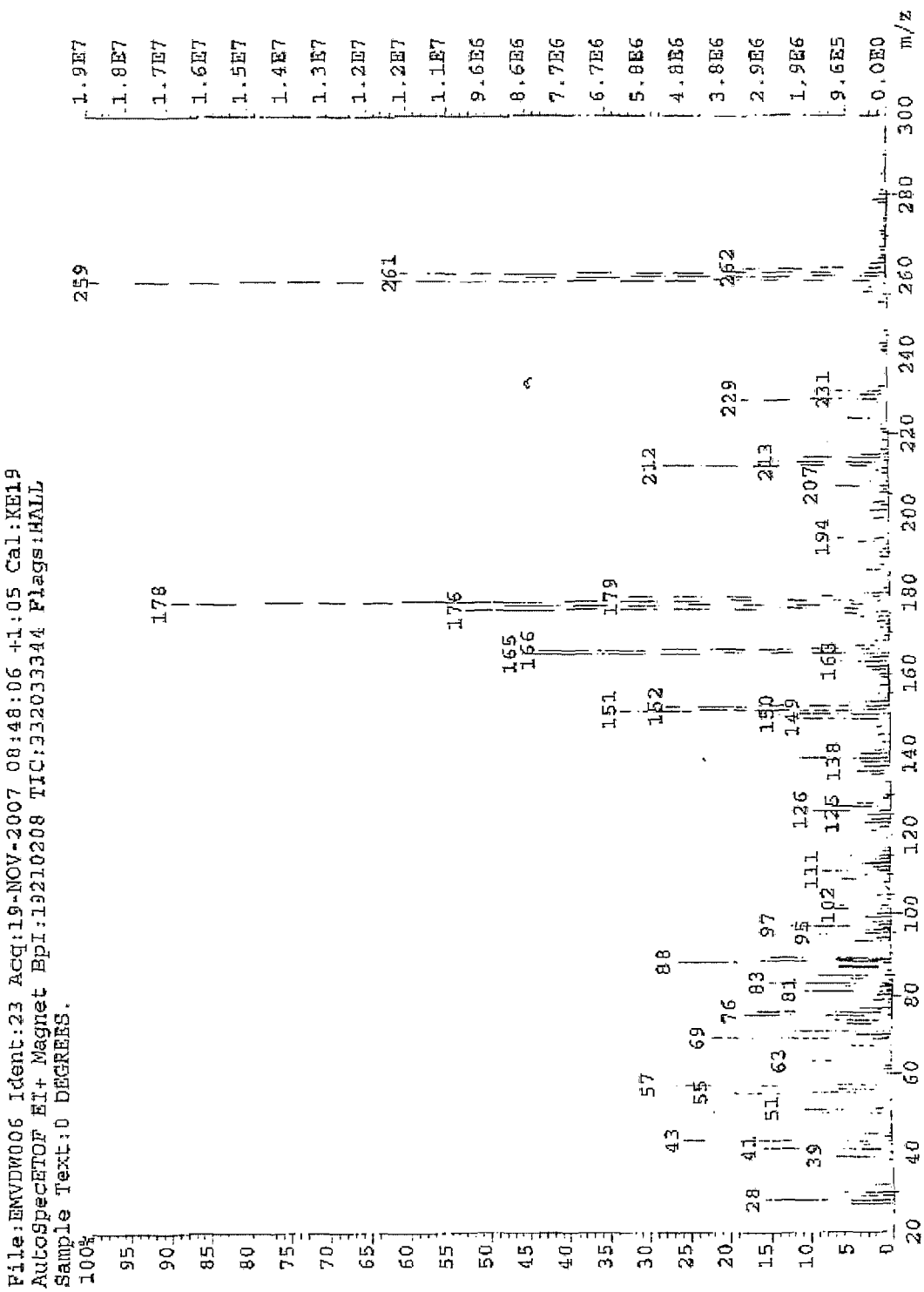

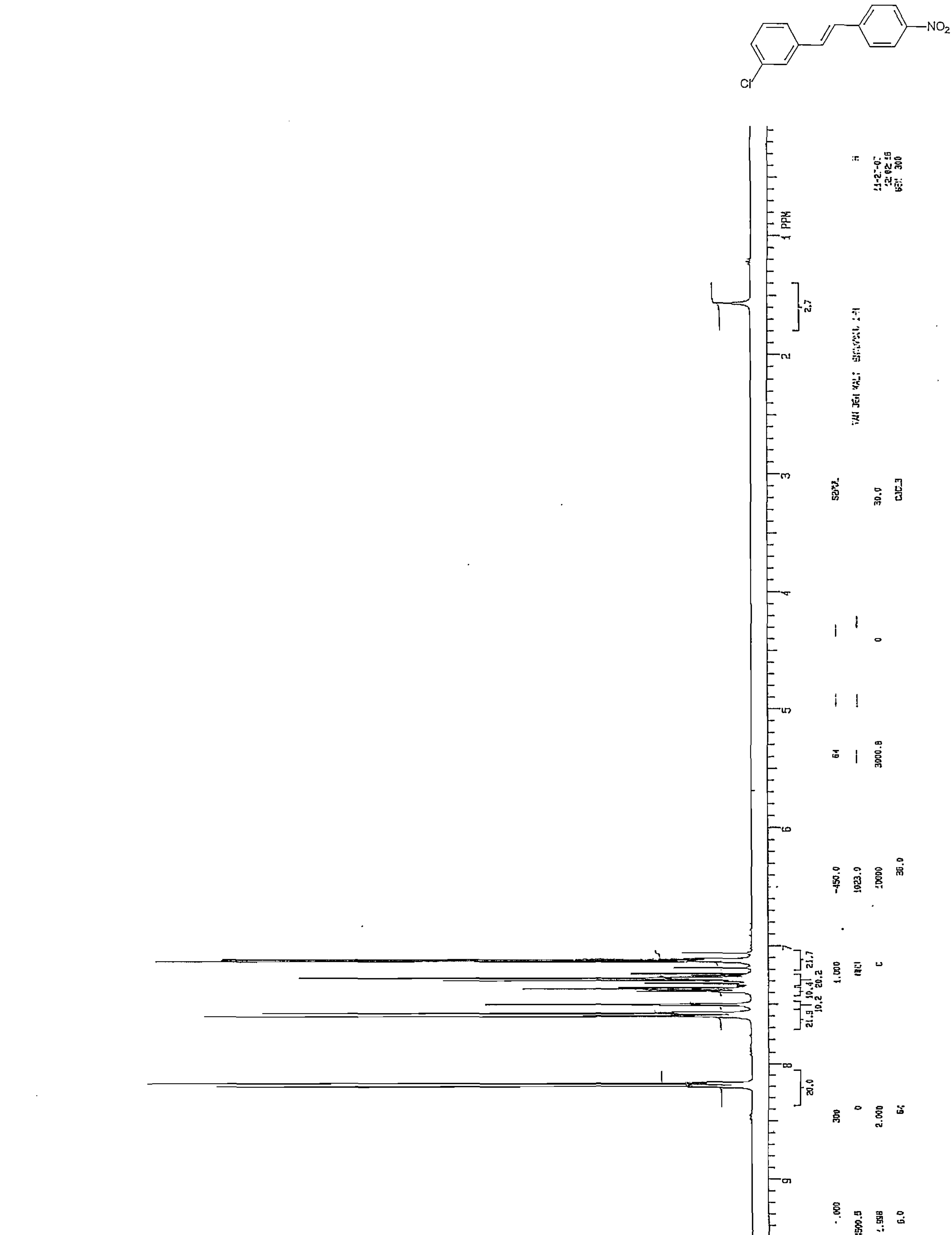

147.027
143.201
136.024
134.824
131.672
130.023
129.822
127.855
127.004
125.222
124.068
77.4266
77.0024
76.5799
220
200
180
160
140
120
100
80
60
40
20 PPM

Cl
NO2

File:EVDW029A Ident:14+16-8 Win 100PPM Acq:11-JUN-2008 08:31:39 +2:11 Cal:KE11
AutoSpecETOF EI+ Magnet BpM:243 BpI:1371904 TIC:6781700 Flags:HALL
Sample Text:0 DEGREES.

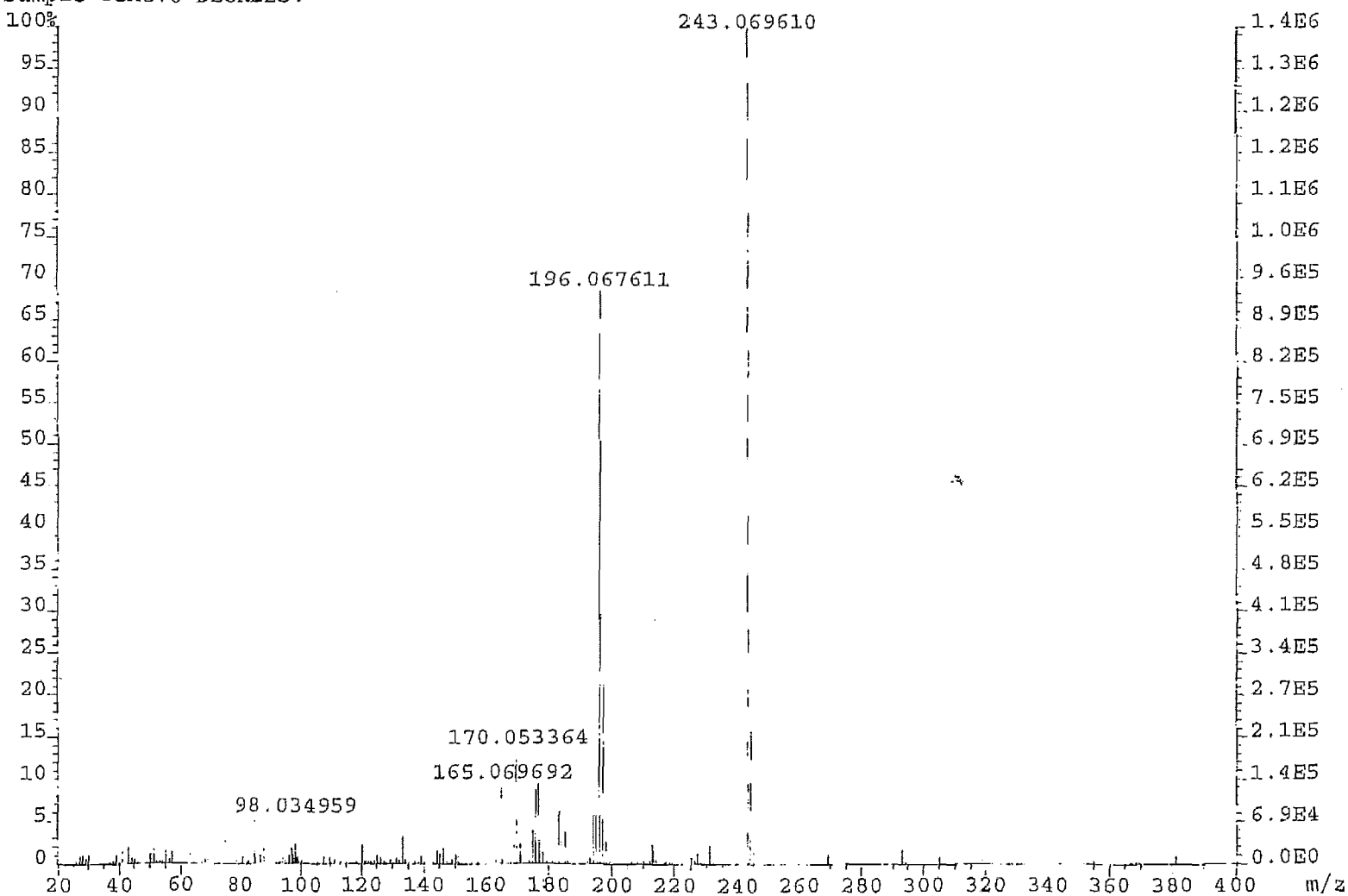

(5c) (*E*)-3'-Fluoro-4-nitrostilbene:

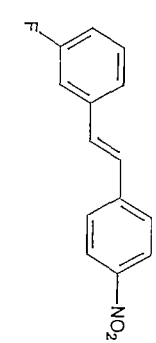

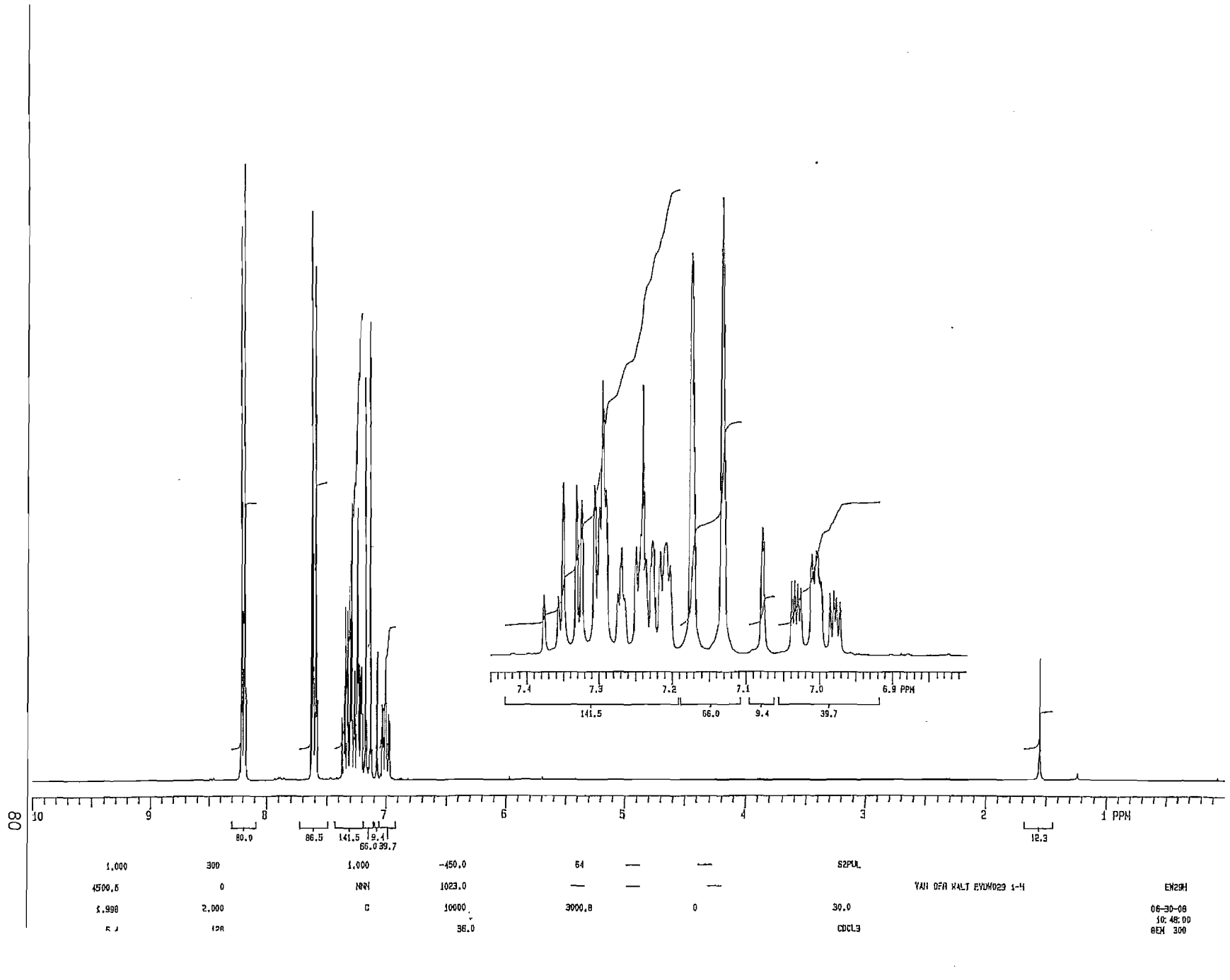
80
10
9
8
7
6
5
4
3
2
1 PPM
80.0
86.5
141.5
9.4
66.0
39.7
12.3
7.4
7.3
7.2
7.1
7.0
6.9 PPM
141.5
66.0
9.4
39.7
1.000 300 1.000 -450.0 64 S2PUL
4500.6 0 NNN 1023.0 YAN DER WALT EYDM029 1-H EM29H
1.998 2.000 C 10000 3000.8 0 30.0 06-30-08
10:48:00
CDCL3 8EM 300
Cl
NO2

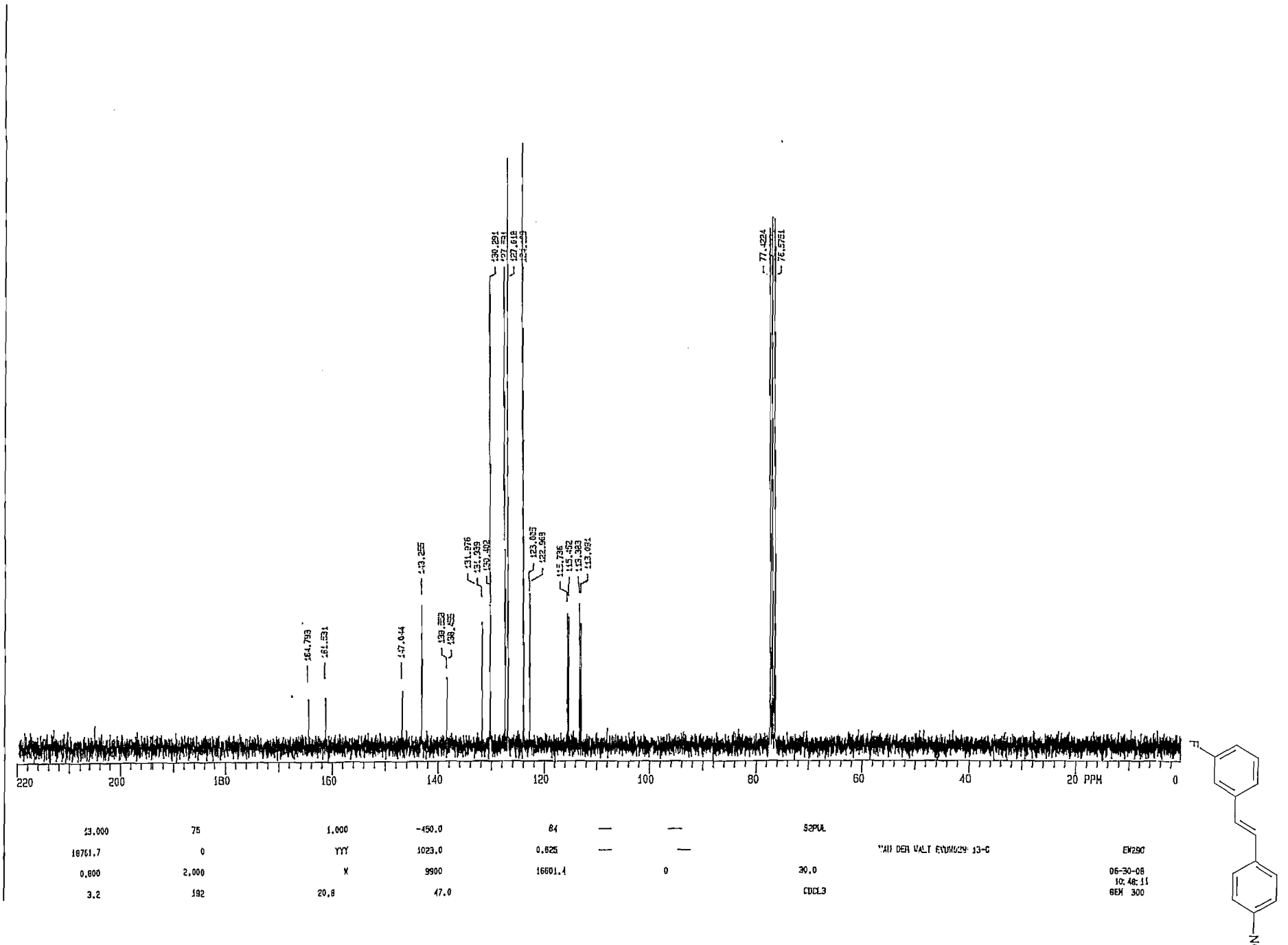

13.000	75	1.000	-450.0	84	—	—	S2PUL	
18761.7	0	YYY	1023.0	0.825	—	—	"AU DER WALT EXUM629 13-C	EM29C
0.800	2.000	N	9900	16601.4		0	30.0	06-30-08 10:46:11
3.2	192	20.8	47.0				CDCL3	GEM 300

81

File:EVDW021_A Ident:12_13-6_7 Win 100PPM Acq: 8-APR-2008 12:35:30 +1:52 Cal:KE8
AutoSpecETOF EI+ Magnet BpM:178 BpI:7205703 TIC:78385880 Flags:HALL
Sample Text:0 DEGREES.

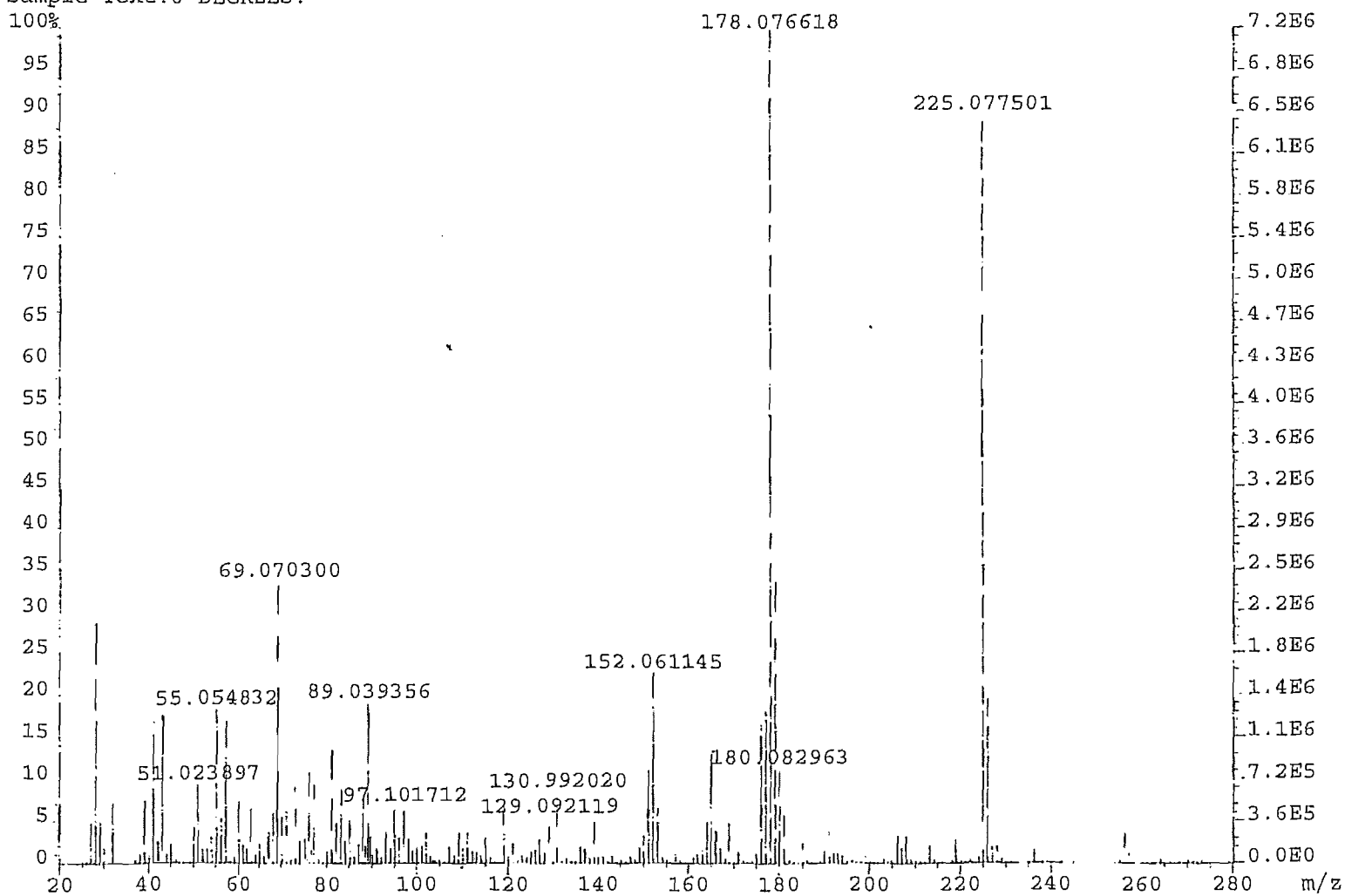

(5d) (*E*)-3-Nitrostilbene:

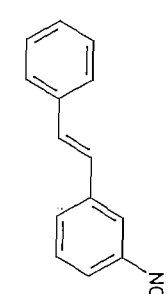

EMVDW021 20.3 mg DMSO 1H

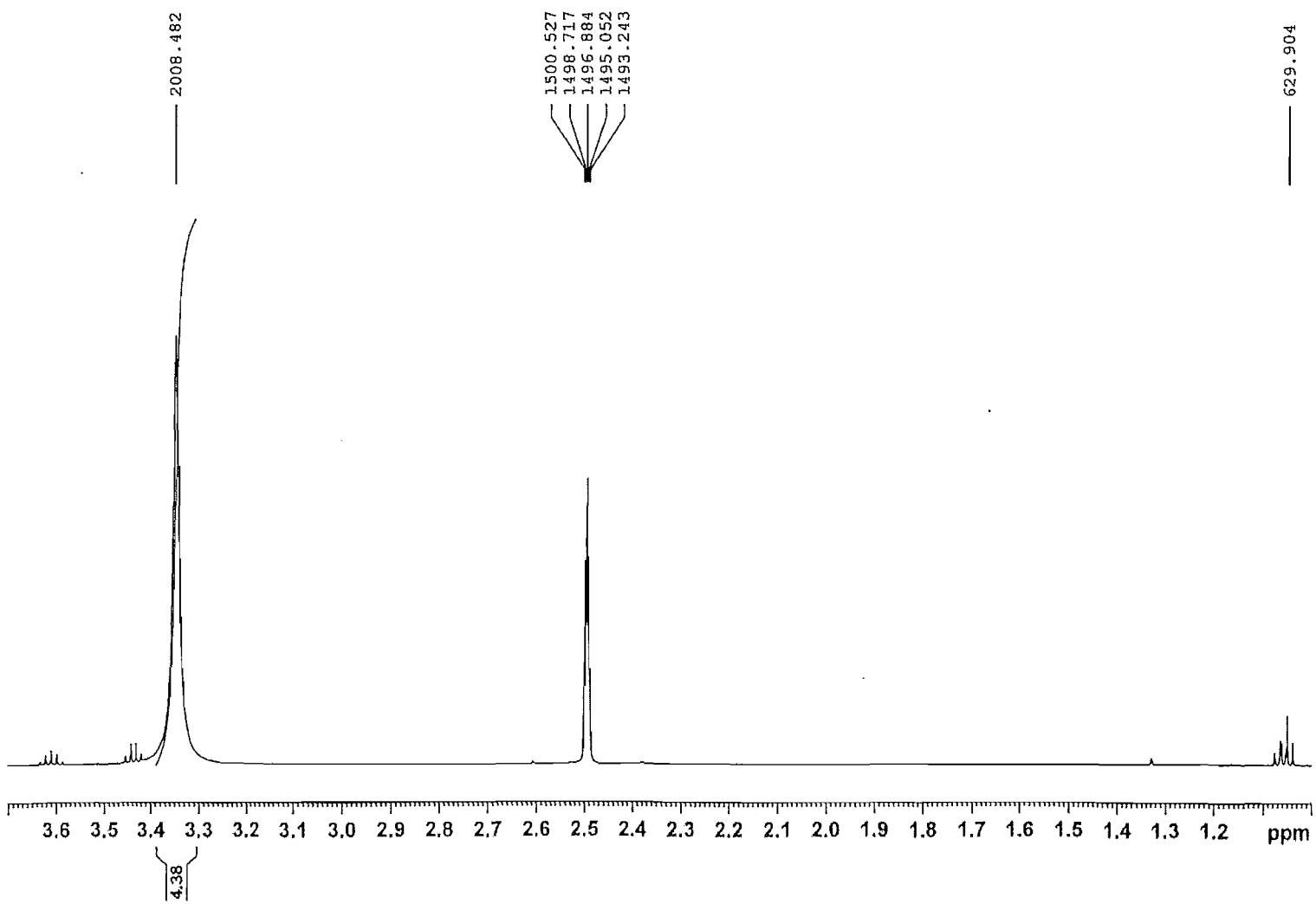

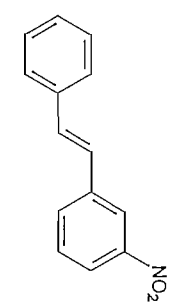

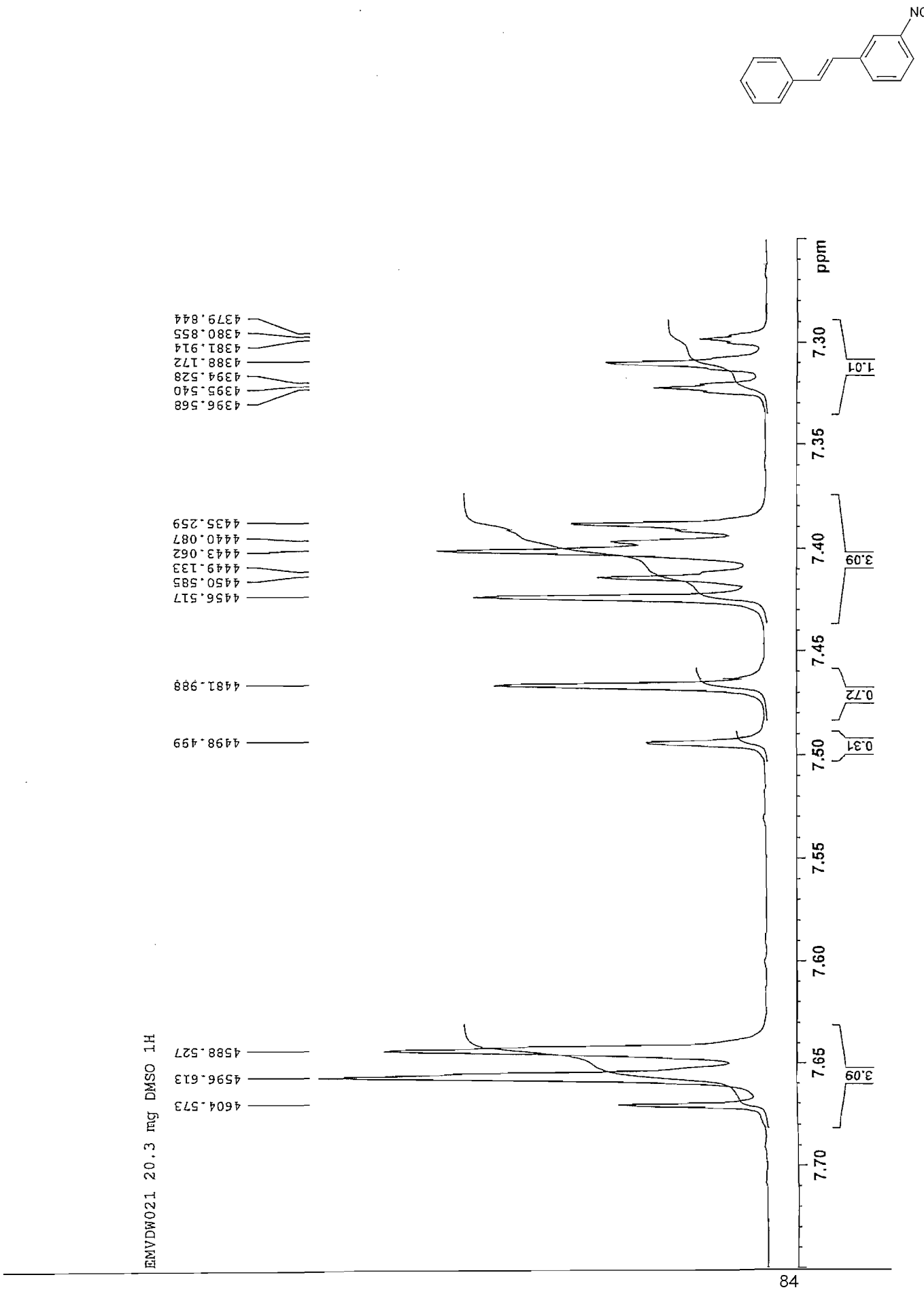
NO2
EMVDW021 20.3 mg DMSO 1H
4604.573
4596.613
4588.527
4481.989
4498.499
4456.517
4450.585
4449.133
4443.062
4440.087
4435.259
4396.568
4395.540
4394.528
4388.172
4381.914
4380.855
4379.844
ppm
7.70
7.65
7.60
7.55
7.50
7.45
7.40
7.35
7.30
3.09
0.31
0.72
3.09
1.01

EMVDW021 20.3 mg DMSO 1H
5056.086
5054.143
5052.226
4863.339
4862.521
4861.094
4860.250
4855.105
4854.445
4852.902
4852.213
4842.493
4834.776
1.00
0.96
1.00
8.45
8.40
8.35
8.30
8.25
8.20
8.15
8.10
8.05
ppm

NO2

EMVDW021 20.3 mg DMSO 13C

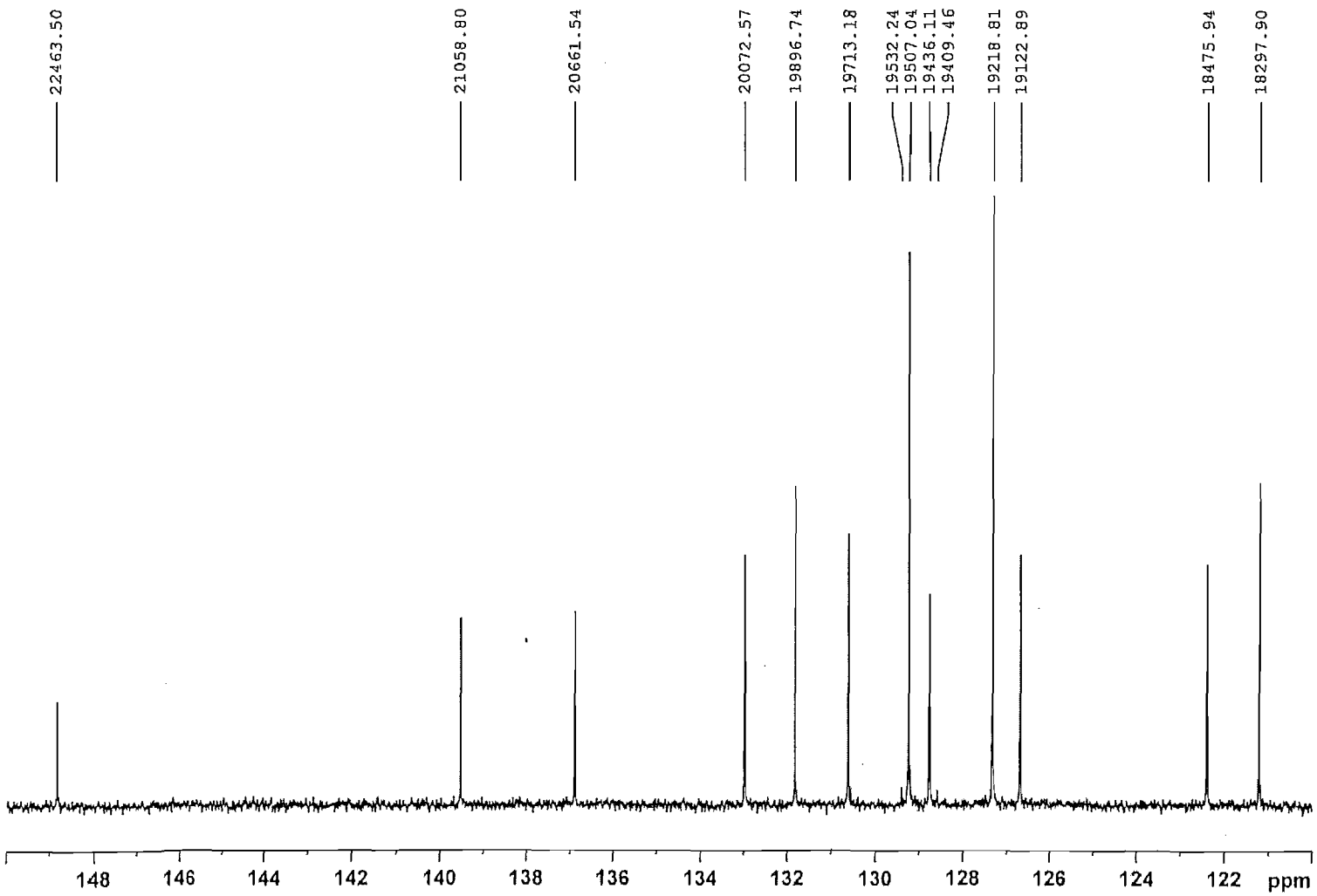

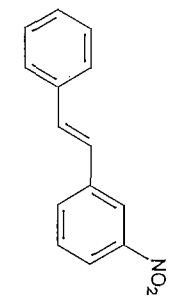

EMVDW021 20.3 mg DMSO 13C
22463.50
21058.80
20661.54
20072.57
19896.74
19713.18
19532.24
19507.04
19436.11
19409.46
19218.81
19122.89
18475.94
18297.90
160
140
130
120
110
100
90
80
70
60
50
40
ppm

NO2

File:EVDW024A Ident:14 Acq:28-MAY-2008 12:26:34 +2:03 Cal:KE28
AutoSpecETOF EI+ Magnet BpM:259 BpI:1700352 TIC:9416530 Flags:ACC
Sample Text:0 DEGREES.

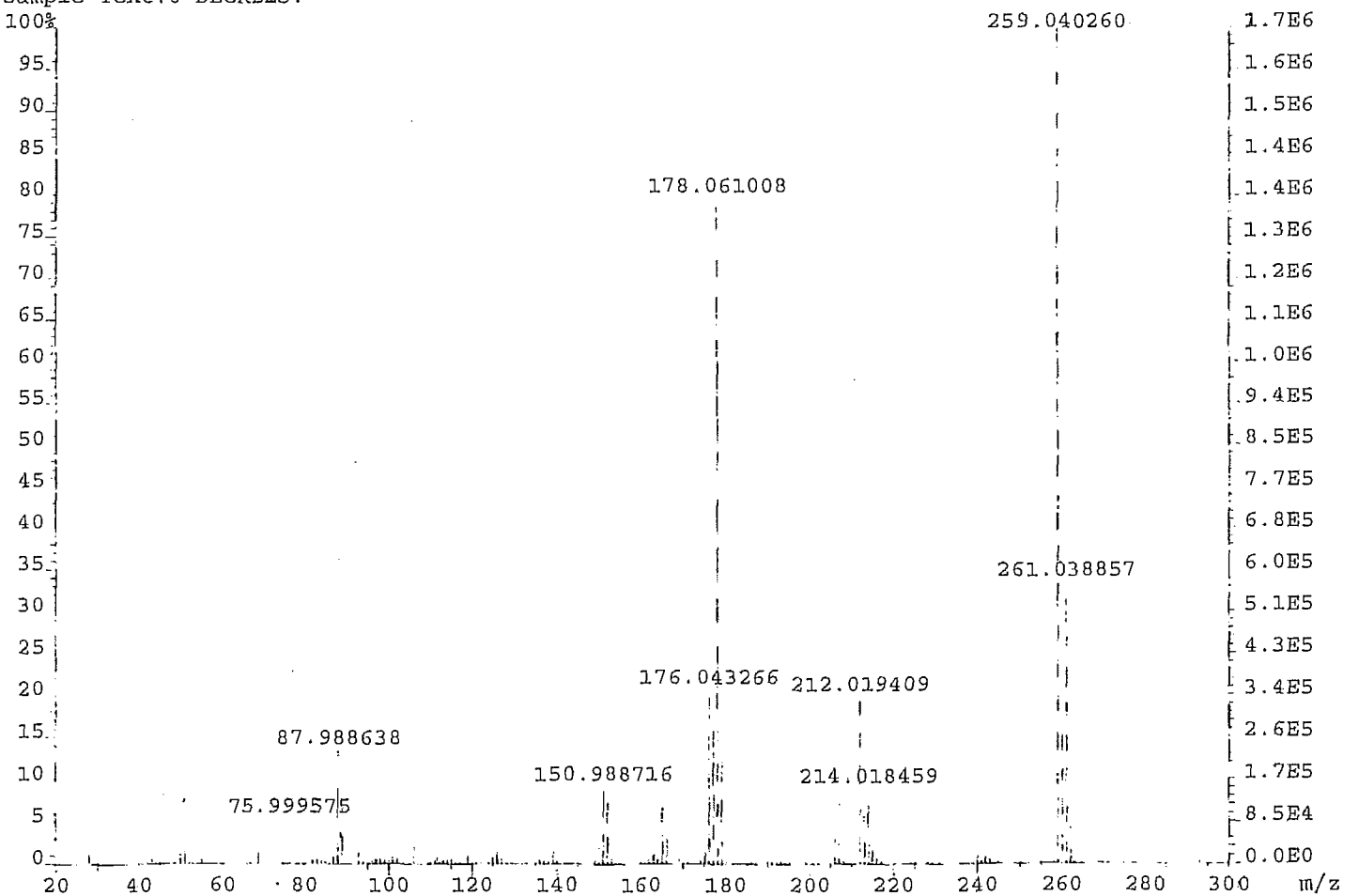

(5e) (*E*)-3'-Chloro-3-nitrostilbene:

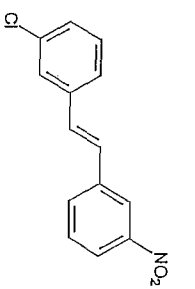

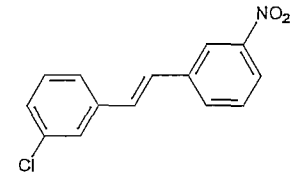
NO2
Cl

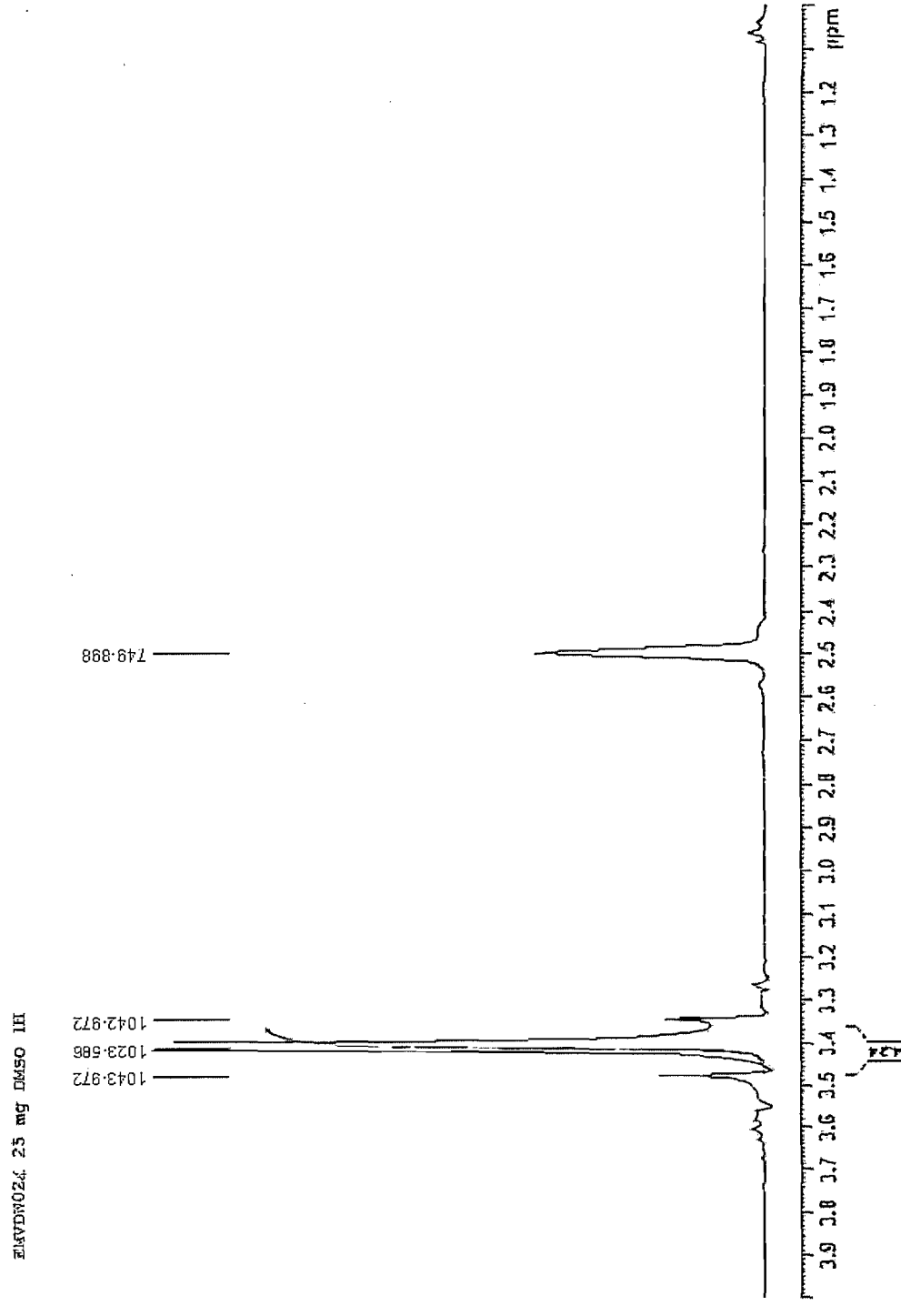
EMVDM024. 25 mg DMSO 1H
1043.972
1023.586
1042.972
749.898
ppm

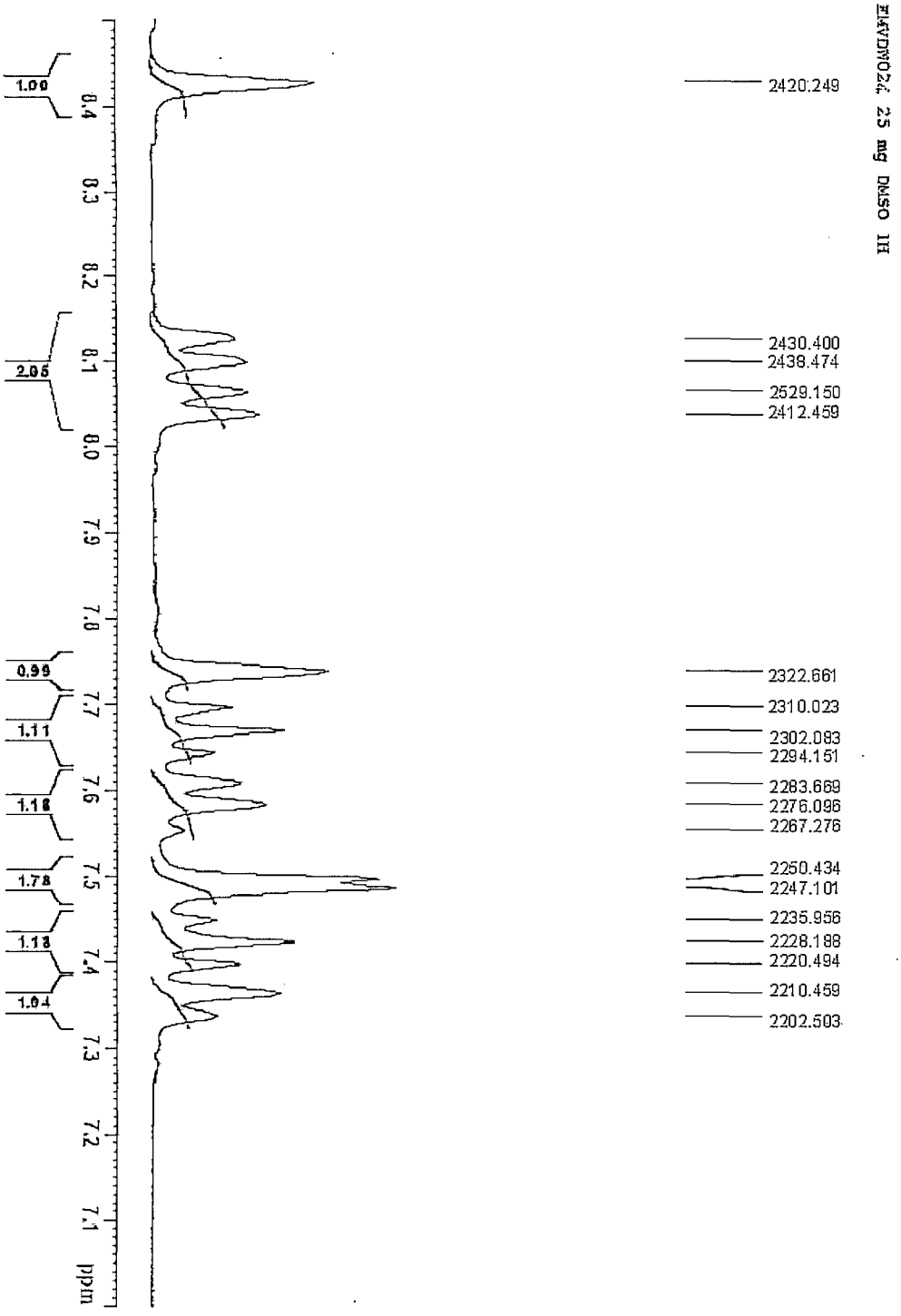
EIAVD0024, 25 mg DMSO 1H
2420.249
2430.400
2438.474
2529.150
2412.459
2322.661
2310.023
2302.083
2294.151
2283.669
2276.096
2267.276
2250.434
2247.101
2235.956
2228.188
2220.494
2210.459
2202.503
1.00
2.05
0.99
1.11
1.18
1.78
1.13
1.04
8.4
8.3
8.2
8.1
8.0
7.9
7.8
7.7
7.6
7.5
7.4
7.3
7.2
7.1
ppm

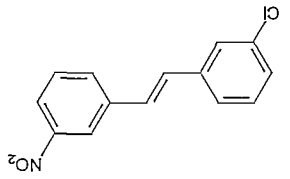
Cl
NO2

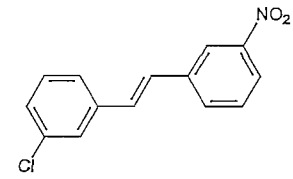
NO2
Cl

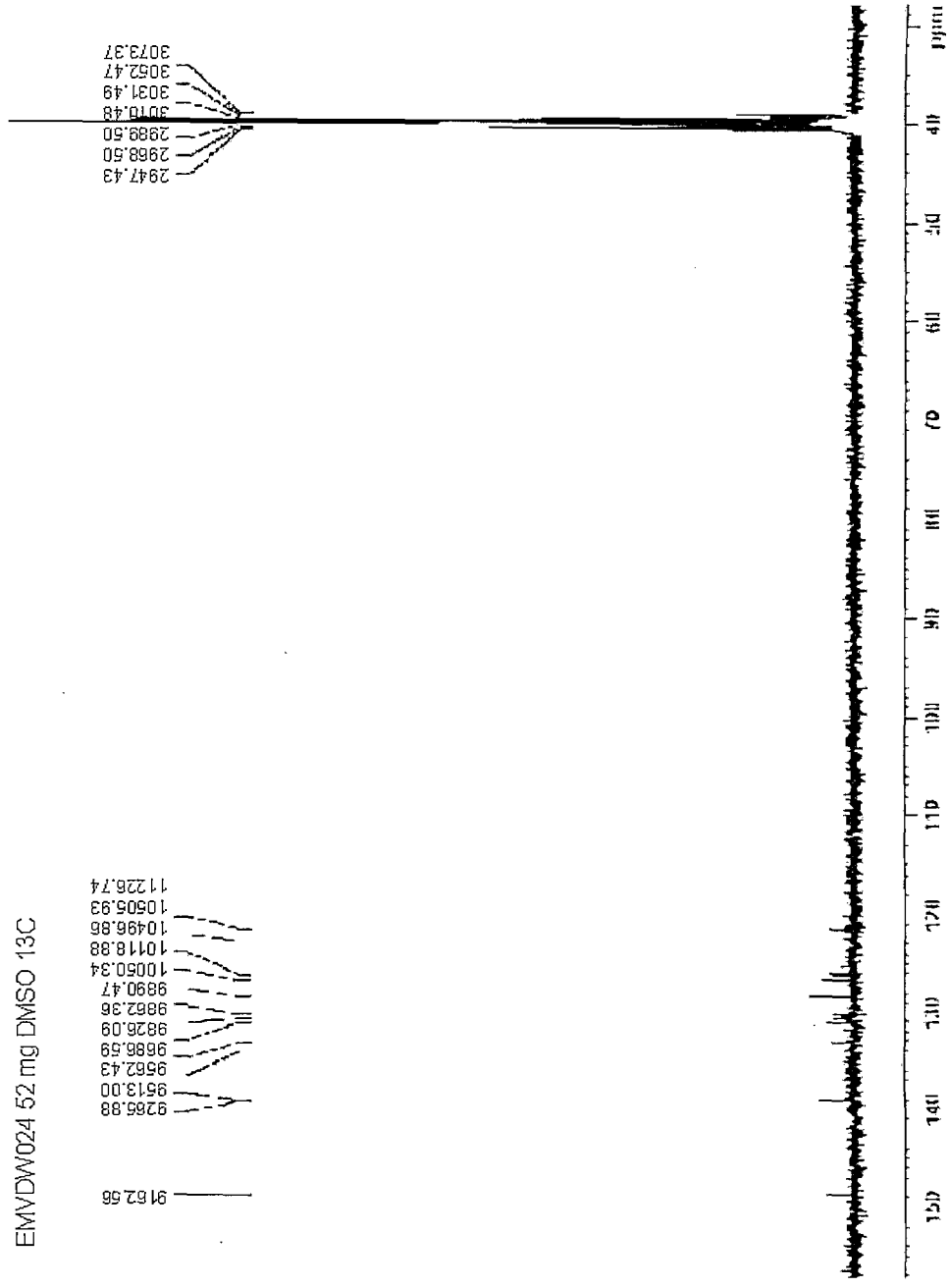
EMVDW024 52 mg DMSO 13C
3073.37
3052.47
3031.49
3010.48
2989.50
2968.50
2947.43
11226.74
10506.93
10496.86
10118.88
10050.34
9890.47
9862.36
9826.09
9686.59
9562.43
9513.00
9265.88
9162.66

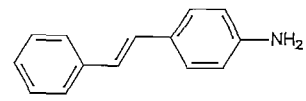

(6a) (*E*)-4-Aminostilbene:

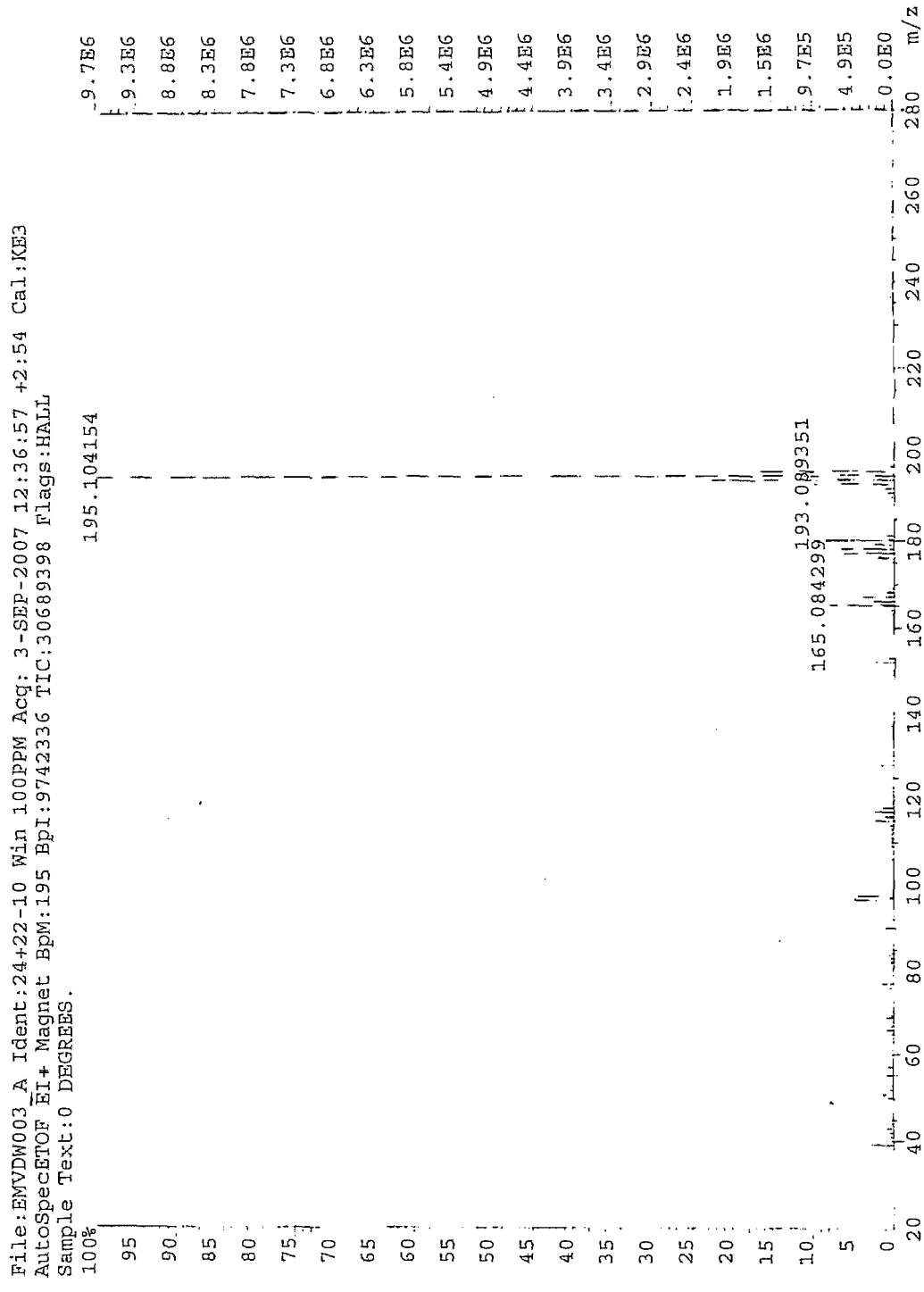

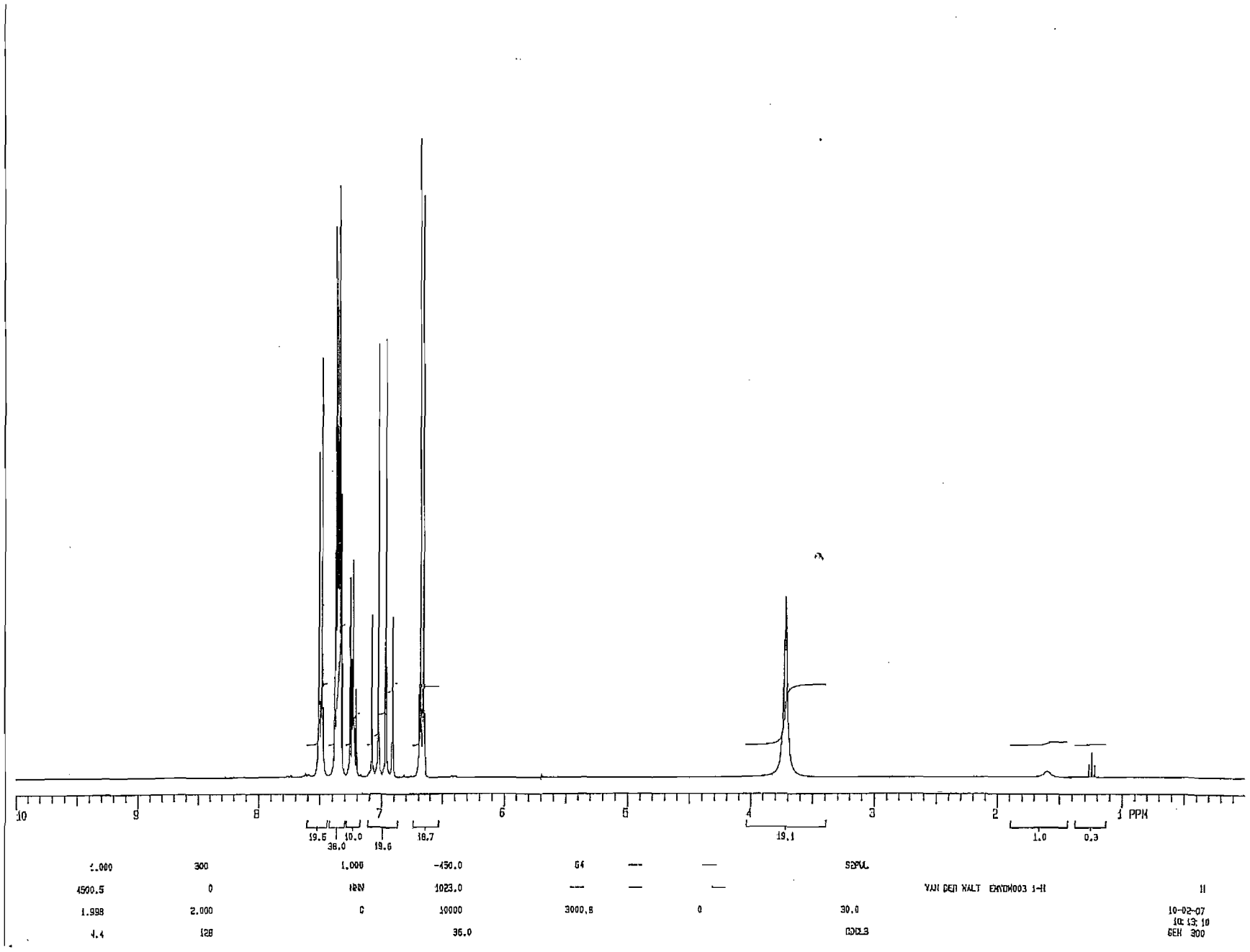
10
9
8
7
6
5
4
3
2
1 PPM
19.5
38.0
10.0
19.6
18.7
19.1
1.0
0.3
1.000
300
1.000
-450.0
64
SGPUL
4500.5
0
1823.0
YAN DER WALT EKYDW003 1-H
1.998
2.000
C
10000
3000.8
0
30.0
10-02-07
4.4
128
36.0
CDCL3
GEM 300

NH2

File:EMVDW007 Ident:21 Acq:19-NOV-2007 08:50:35 +1:01 Cal:KE19
AutoSpecETOF EI+ Magnet BpI:13448893 TIC:185062720 Flags:HALL
Sample Text:0 DEGREES.

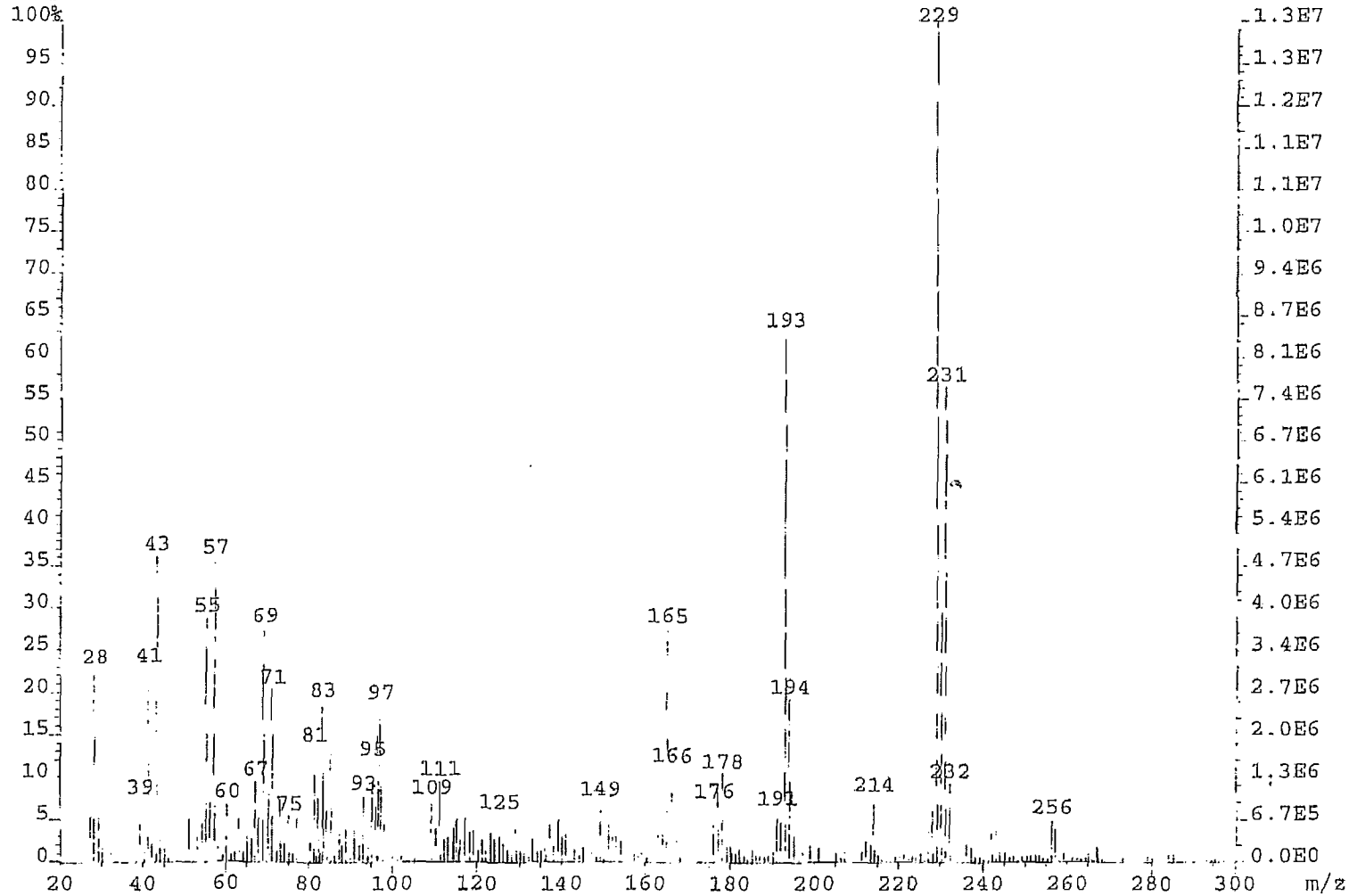

(6b) (*E*)-4-Amino-3'-chlorostilbene:

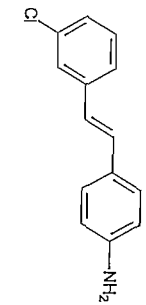

NH2
Cl
1 PPN
2.1
10.1
38.9
20.0
98.4
21.1
20.5
38.3

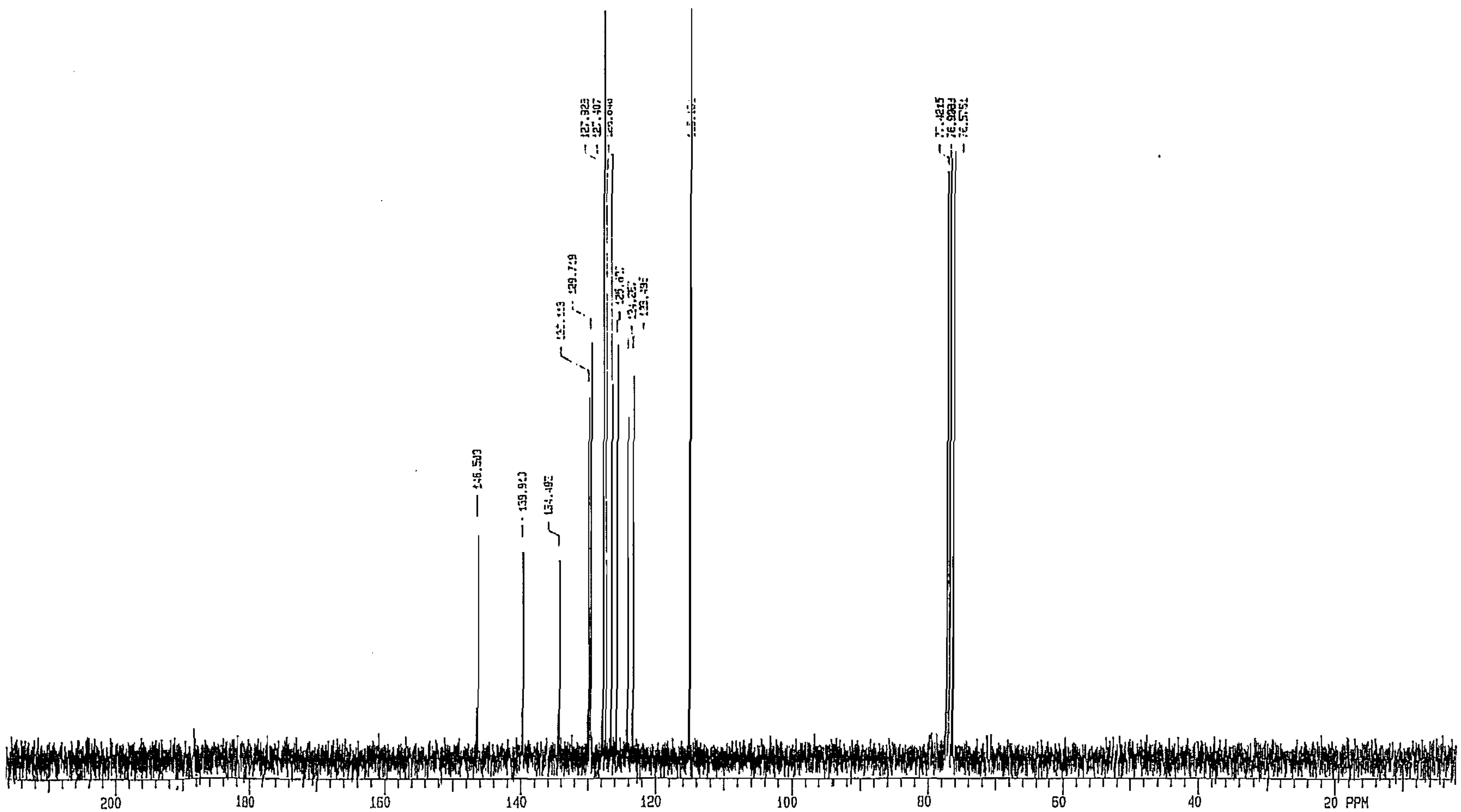

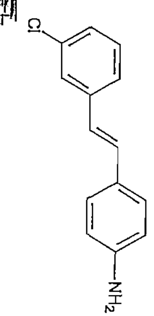

3.000	75	1.000	-450.0	64	---	—	S2PUL		
18761.7	0	YYY	1023.0	0.625	---	---		VAN DER KALT ENVJM007 13-C	ENZC
0.800	2.000	N	9900	16601.4		0	30.0		11-27-07 13:23:53
3.9	128	22.4	47.0				CDCL3		6E4 300

File:EMVDW009 Ident:20 Acq:26-NOV-2007 10:21:27 +0:57 Cal:KE26
AutoSpecETOF EI+ Magnet BpI:17529950 TIC:296978400 Flags:HALL
Sample Text:0 DEGREES.

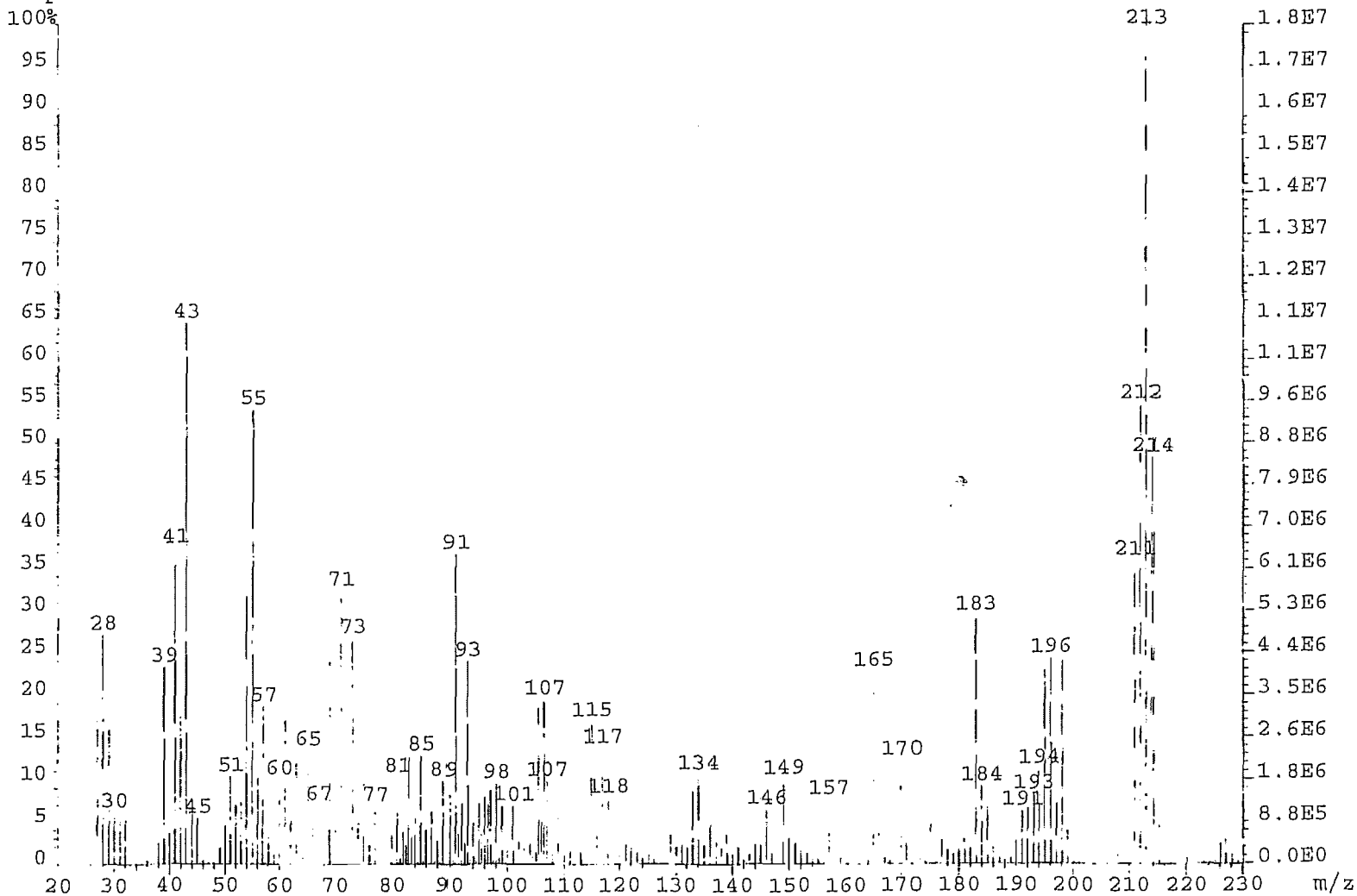

(6c) (*E*)-4-Amino-3'-fluorostilbene:

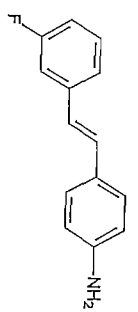

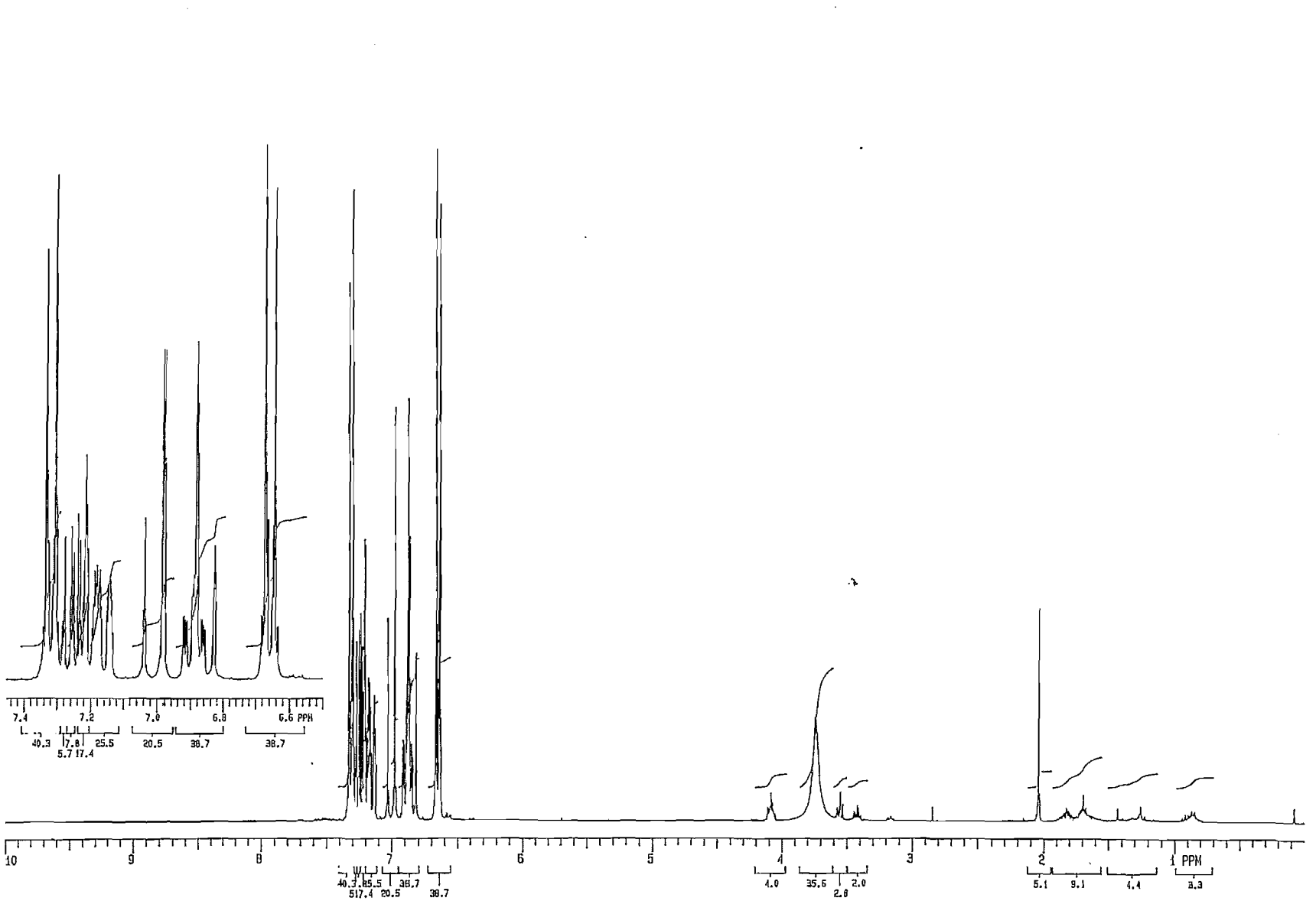

1.000	300	1.000	-450.0	64	—	—	S2PUL	
4500.5	0	NNN	1023.0	—	—	—	VAN DER WALT EVAN032 1-H	H
1.998	2.000	C	10000	3000.8	0	30.0		06-30-08 12:04:56
5.4	128		36.0			CDCL3		GEM 300

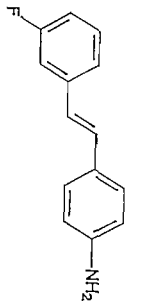

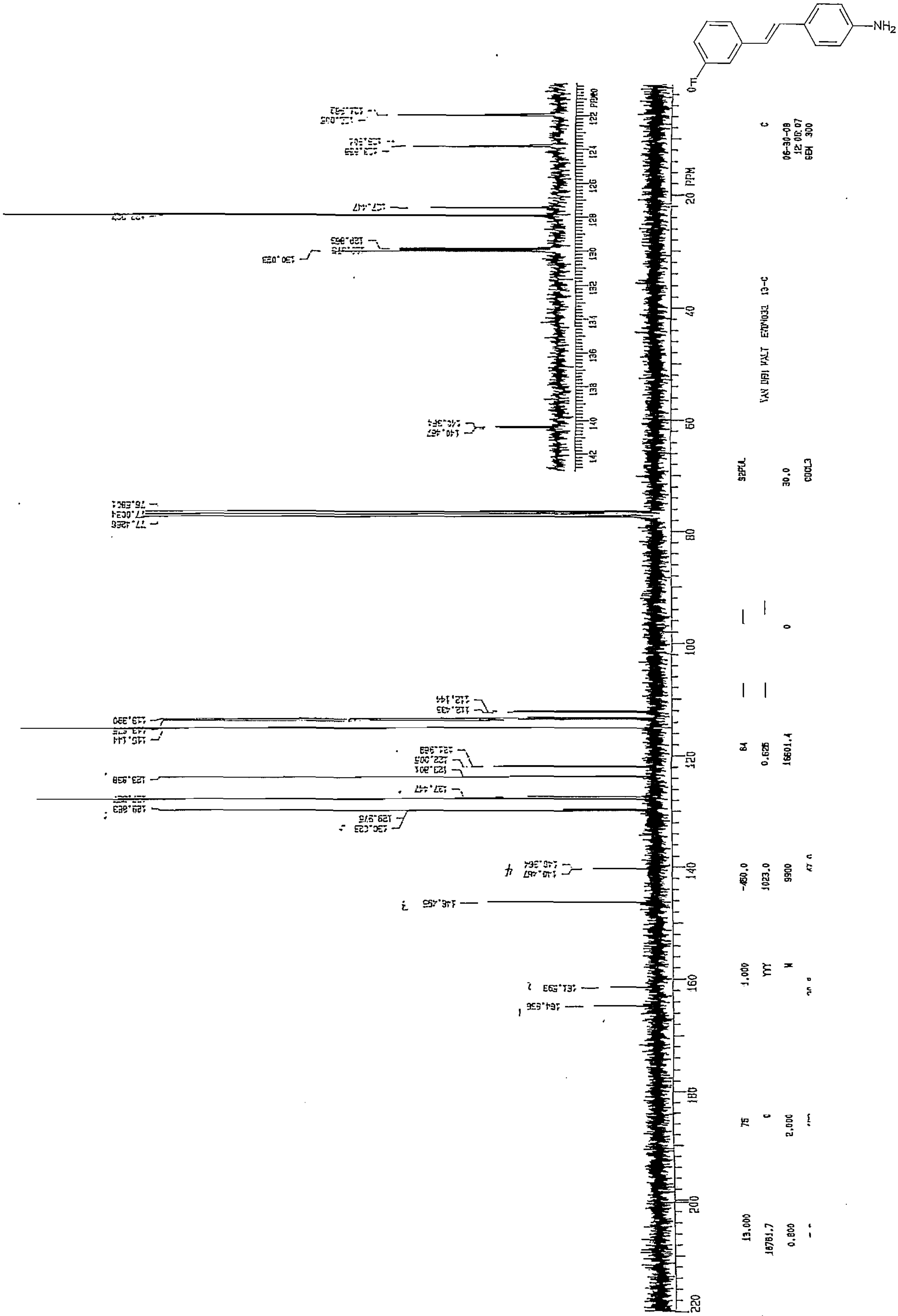

File:EVDW022_A Ident:13-7 Win 100PPM Acq: 8-APR-2008 12:41:05 Cal:KE8
AutoSpecETOF EI+ Magnet BpM:195 BpI:11186176 TIC:106142760 Flags:HALL
Sample Text:0 DEGREES.

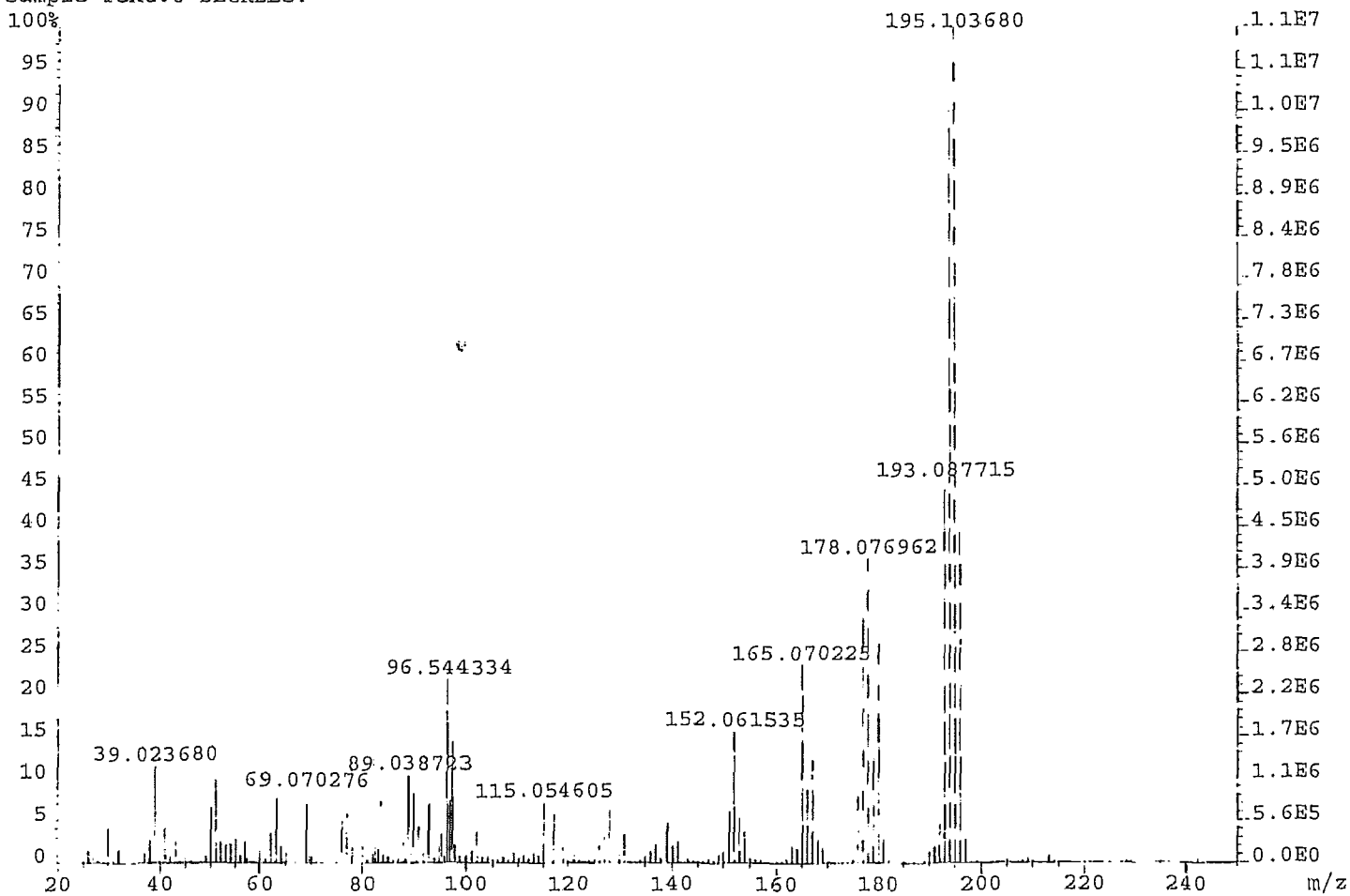

(6d) (*E*)-3-Aminostilbene:

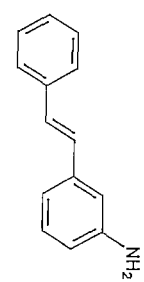

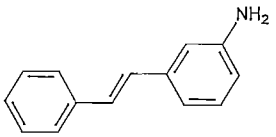
NH2

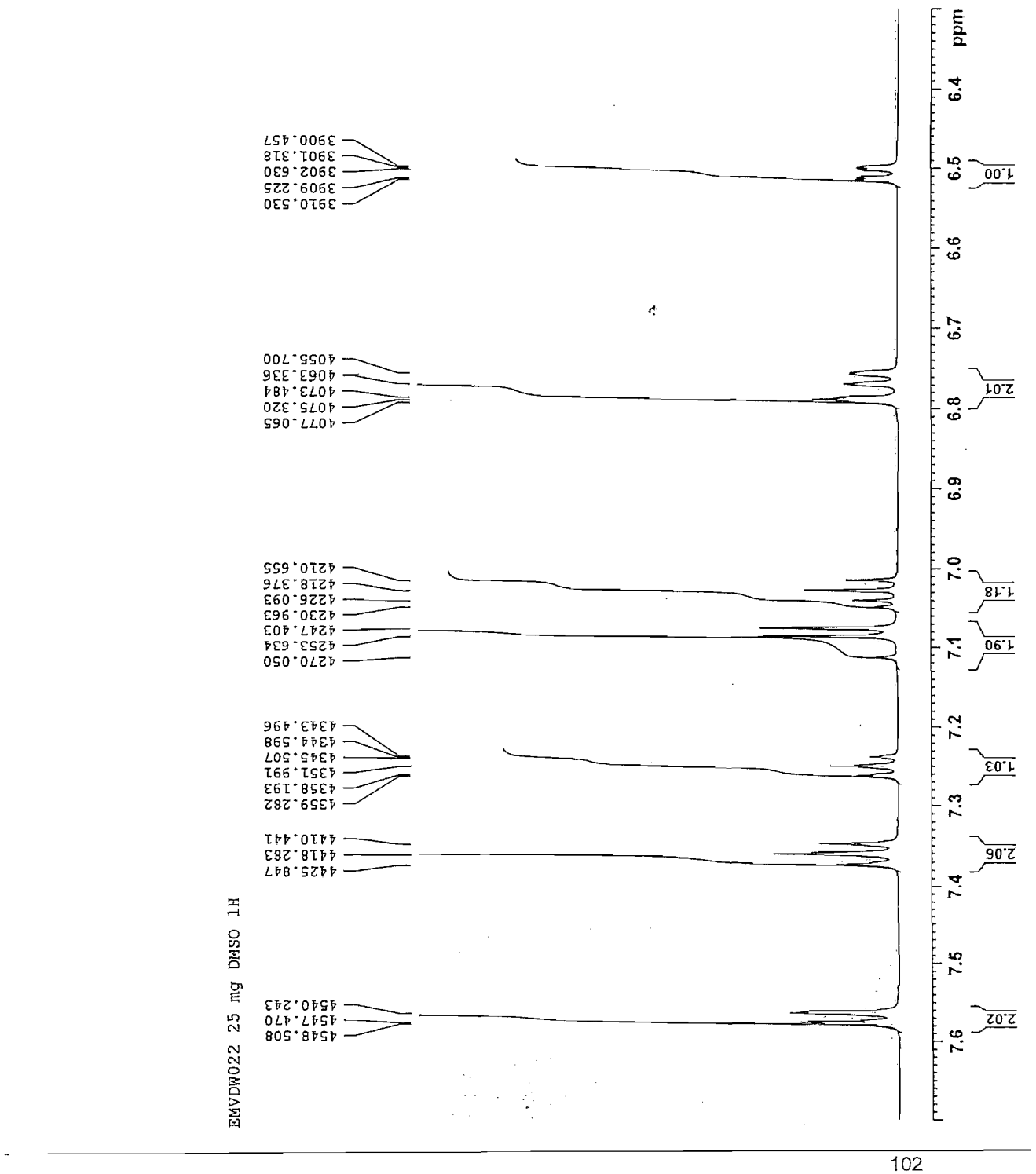
EMVDW022 25 mg DMSO 1H
4548.508
4547.470
4540.243
4425.847
4418.283
4410.441
4359.282
4358.193
4351.991
4345.507
4344.598
4343.496
4270.050
4253.634
4247.403
4230.963
4226.093
4218.376
4210.655
4077.065
4075.320
4073.484
4063.336
4055.700
3910.530
3909.225
3902.630
3901.318
3900.457
7.6
7.5
7.4
7.3
7.2
7.1
7.0
6.9
6.8
6.7
6.6
6.5
6.4
ppm
2.02
2.06
1.03
1.90
1.18
2.01
1.00

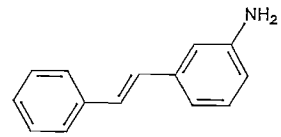
NH2

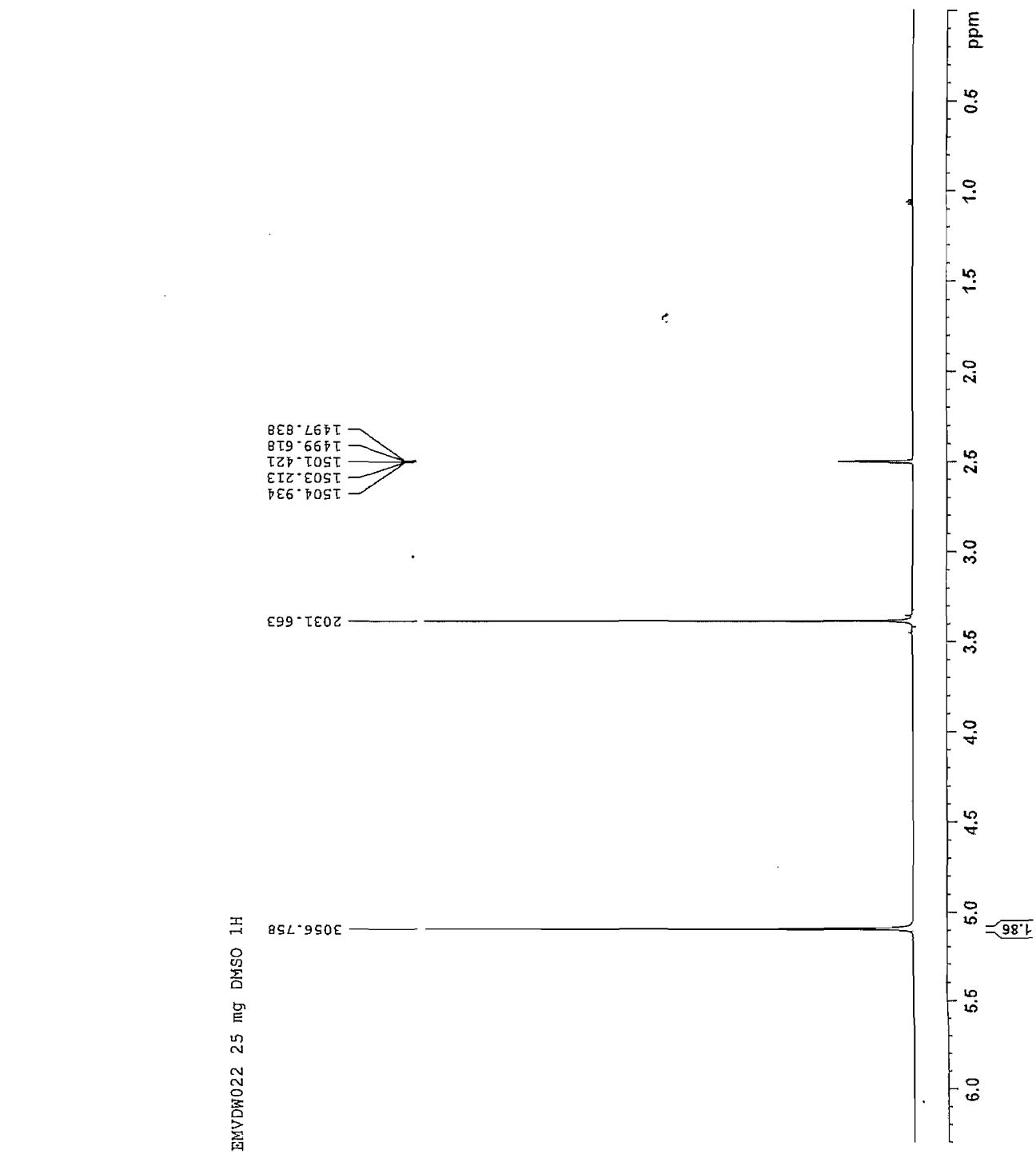
EMVDW022 25 mg DMSO 1H
3056.758
2031.663
1504.934
1503.213
1501.421
1499.618
1497.838
1.86
ppm
6.0
5.5
5.0
4.5
4.0
3.5
3.0
2.5
2.0
1.5
1.0
0.5

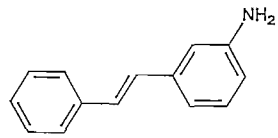
NH2

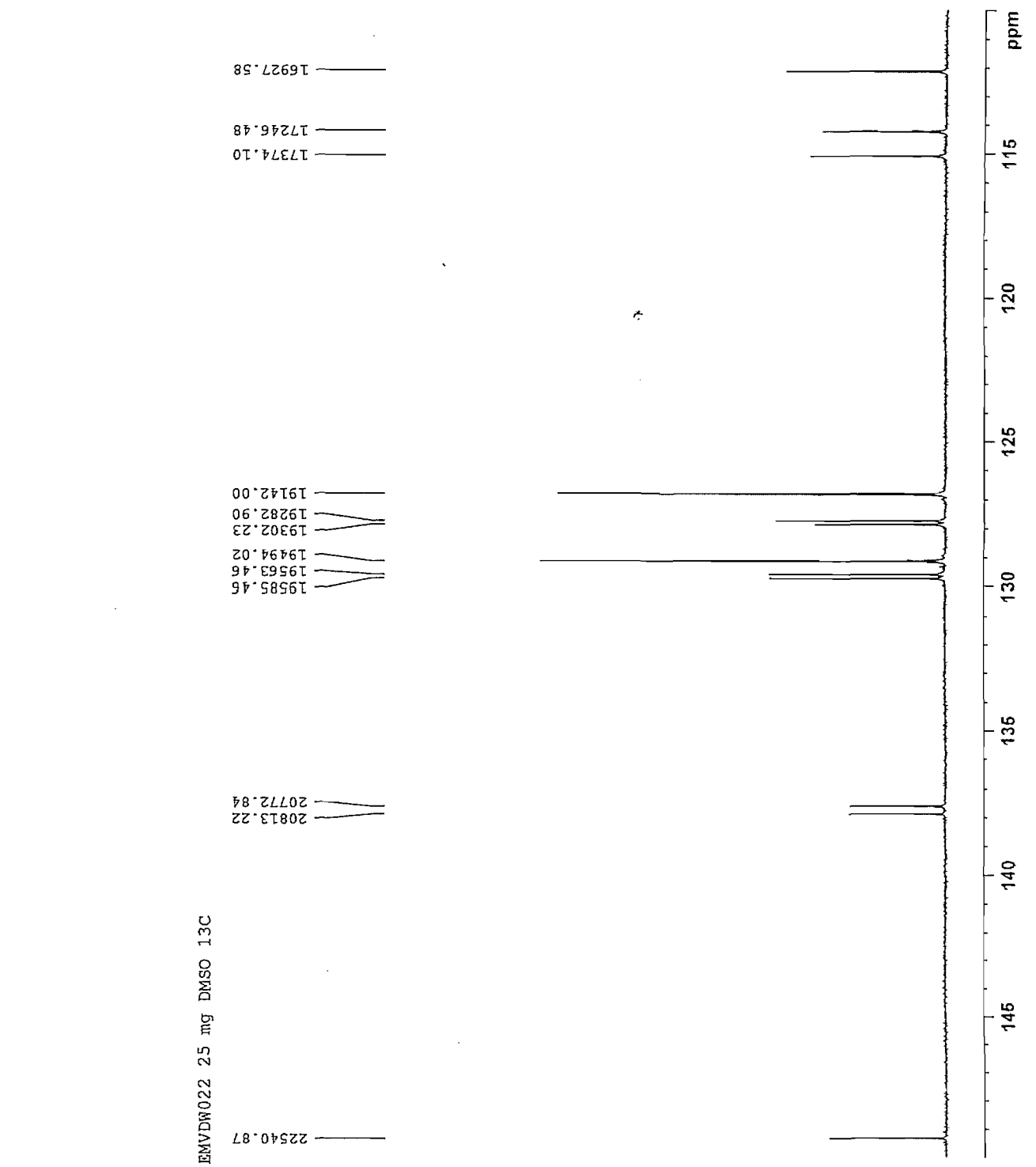
EMVDW022 25 mg DMSO 13C
22540.87
20813.22
20772.84
19585.46
19563.46
19494.02
19302.23
19282.90
19142.00
17374.10
17246.48
16927.58
ppm
145
140
135
130
125
120
115

File:EVDW025A Ident:16_19-7_8 Win 100PPM Acq:28-MAY-2008 12:14:34 +2:32 Cal:KE28
AutoSpecETOF EI+ Magnet BpM:229 BpI:1117888 TIC:6462529 Flags:HALL
Sample Text:0 DEGREES.

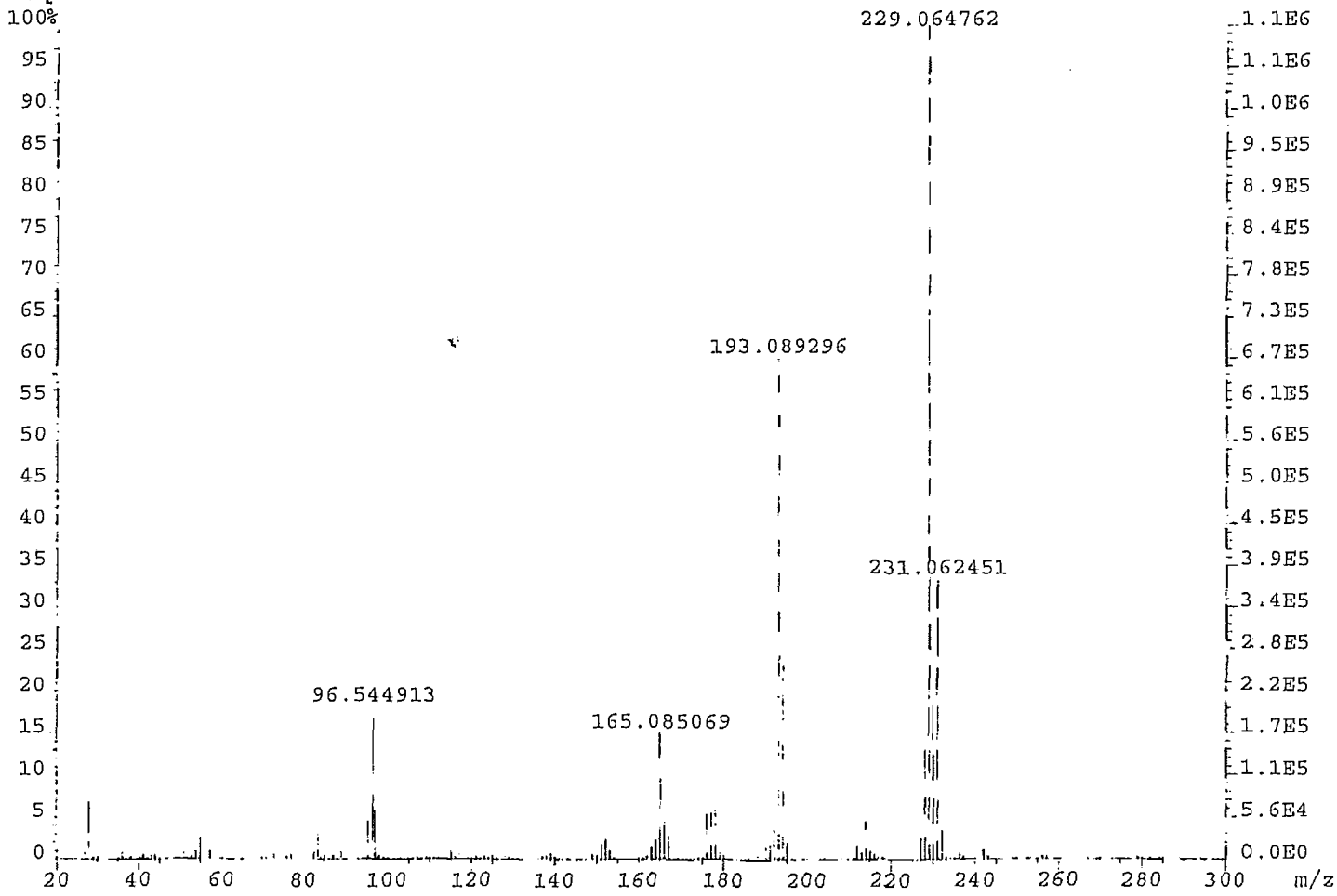

(6e) (*E*)-3-Amino-3'-chlorostilbene:

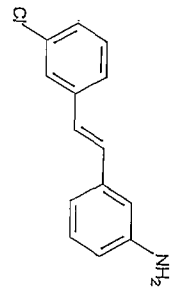

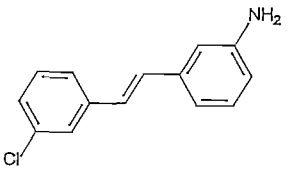
NH2
Cl

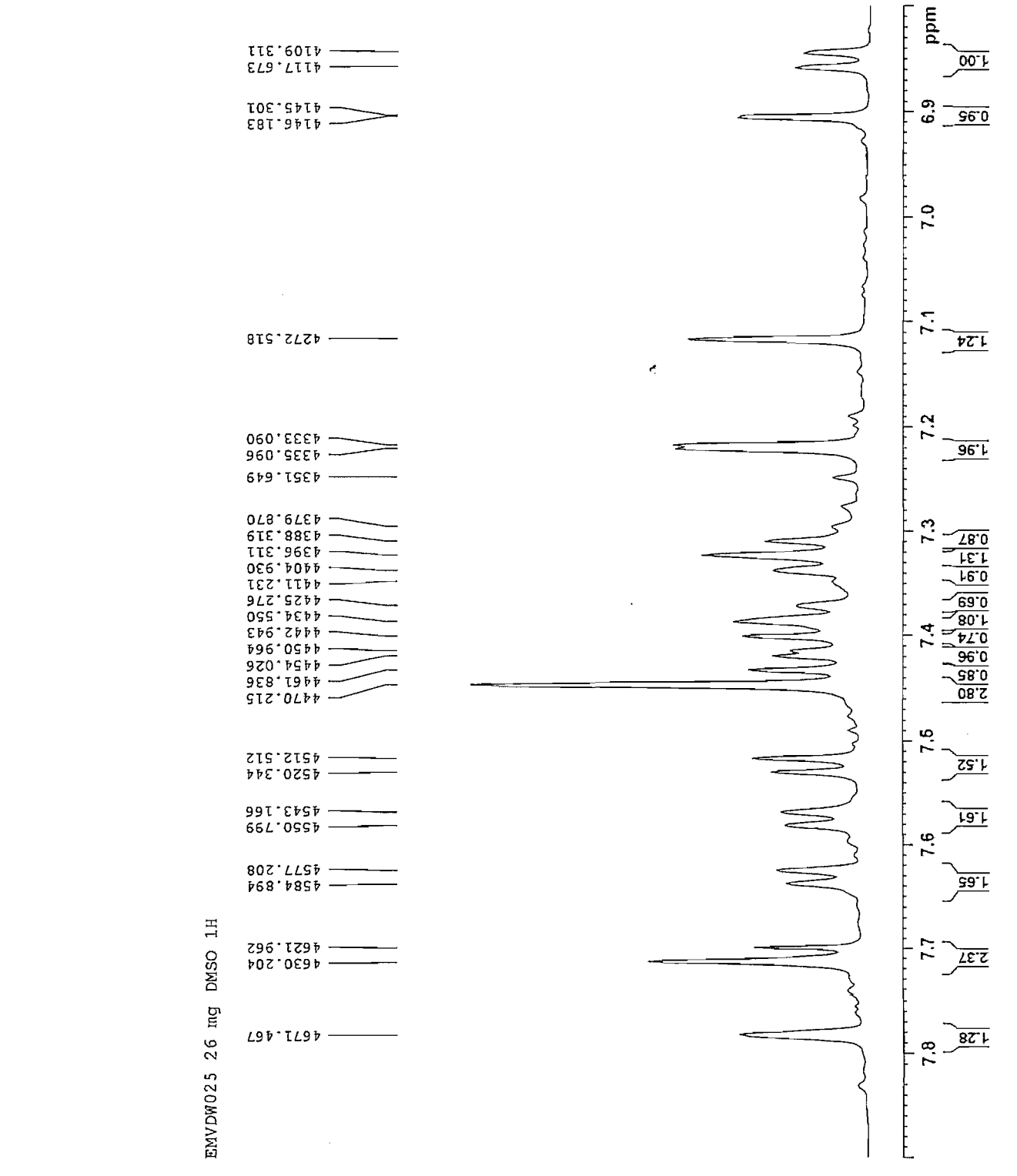
EMVDW025 26 mg DMSO 1H
ppm
7.8
7.7
7.6
7.5
7.4
7.3
7.2
7.1
7.0
6.9
1.28
2.37
1.65
1.61
1.52
2.80
0.85
0.96
0.74
1.08
0.69
0.91
1.31
0.87
1.96
1.24
0.95
1.00
4671.467
4630.204
4621.962
4584.894
4577.208
4550.799
4543.166
4520.344
4512.512
4470.215
4461.836
4454.026
4450.964
4442.943
4434.550
4425.276
4411.231
4404.930
4396.311
4388.319
4379.870
4351.649
4335.096
4333.090
4272.518
4146.183
4145.301
4117.673
4109.311

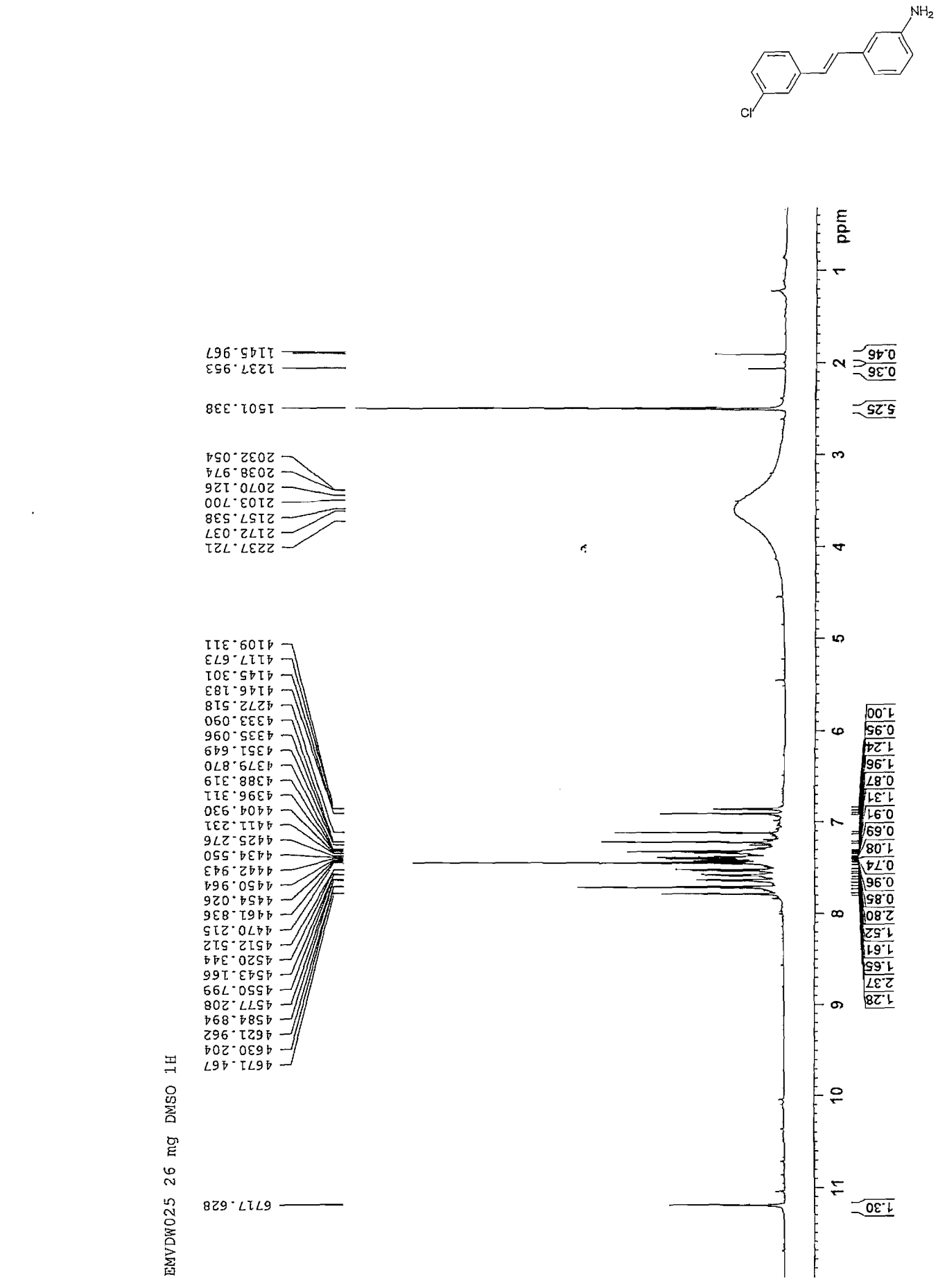
NH2
Cl
EMVDW025 26 mg DMSO 1H
ppm
1.30
5.25
1.28
2.37
1.65
1.61
1.52
2.80
0.85
2.80
0.96
0.74
1.08
0.69
0.91
1.31
0.87
1.96
1.24
0.95
1.00
0.36
0.46
6717.628
4671.467
4630.204
4621.962
4584.894
4577.208
4550.799
4543.166
4520.344
4512.512
4470.215
4461.836
4454.026
4450.964
4442.943
4434.550
4425.276
4411.231
4404.930
4396.311
4388.319
4379.870
4351.649
4335.096
4333.090
4272.518
4146.183
4145.301
4117.673
4109.311
2237.721
2172.037
2157.538
2103.700
2070.126
2038.974
2032.054
1501.338
1237.953
1145.967

NH2
Cl

EMVDW025 26 mg DMSO 13C
20249.47
20238.70
19931.14
19907.94
19783.48
19769.97
19649.72
19590.39
19518.82
19430.97
19334.66
19175.70
19120.05
19078.67
19006.48
18969.14
18375.50
17746.21
17444.89
17118.05
16618.82
16580.85
ppm
134
132
130
128
126
124
122
120
118
116
114
112
110
108

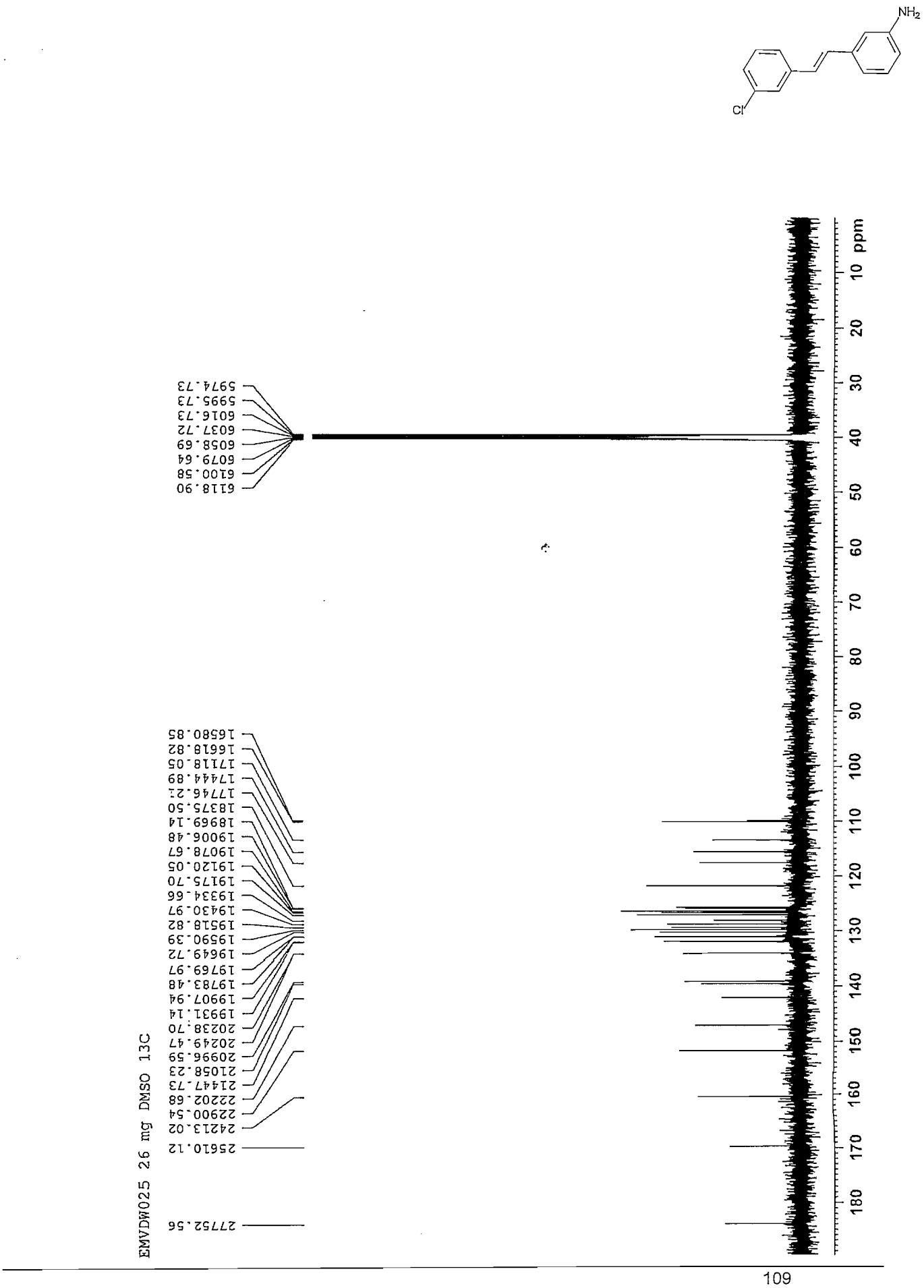
NH2
Cl
EMVDW025 26 mg DMSO 13C
27752.56
25610.12
24213.02
22900.54
22202.68
21447.73
21058.23
20996.59
20249.47
20238.70
19931.14
19907.94
19783.48
19769.97
19649.72
19590.39
19518.82
19430.97
19334.66
19175.70
19120.05
19078.67
19006.48
18969.14
18375.50
17746.21
17444.89
17118.05
16618.82
16580.85
6118.90
6100.58
6079.64
6058.69
6037.72
6016.73
5995.73
5974.73
10 ppm

File:EVDW019_A Ident:18_23-8_9 Win 100PPM Acq:20-MAR-2008 12:00:42 +2:56 Cal:KE20
AutoSpecETOF EI+ Magnet BpM:221 BpI:2298203 TIC:31058728 Flags:HALL
Sample Text:0 DEGREES.

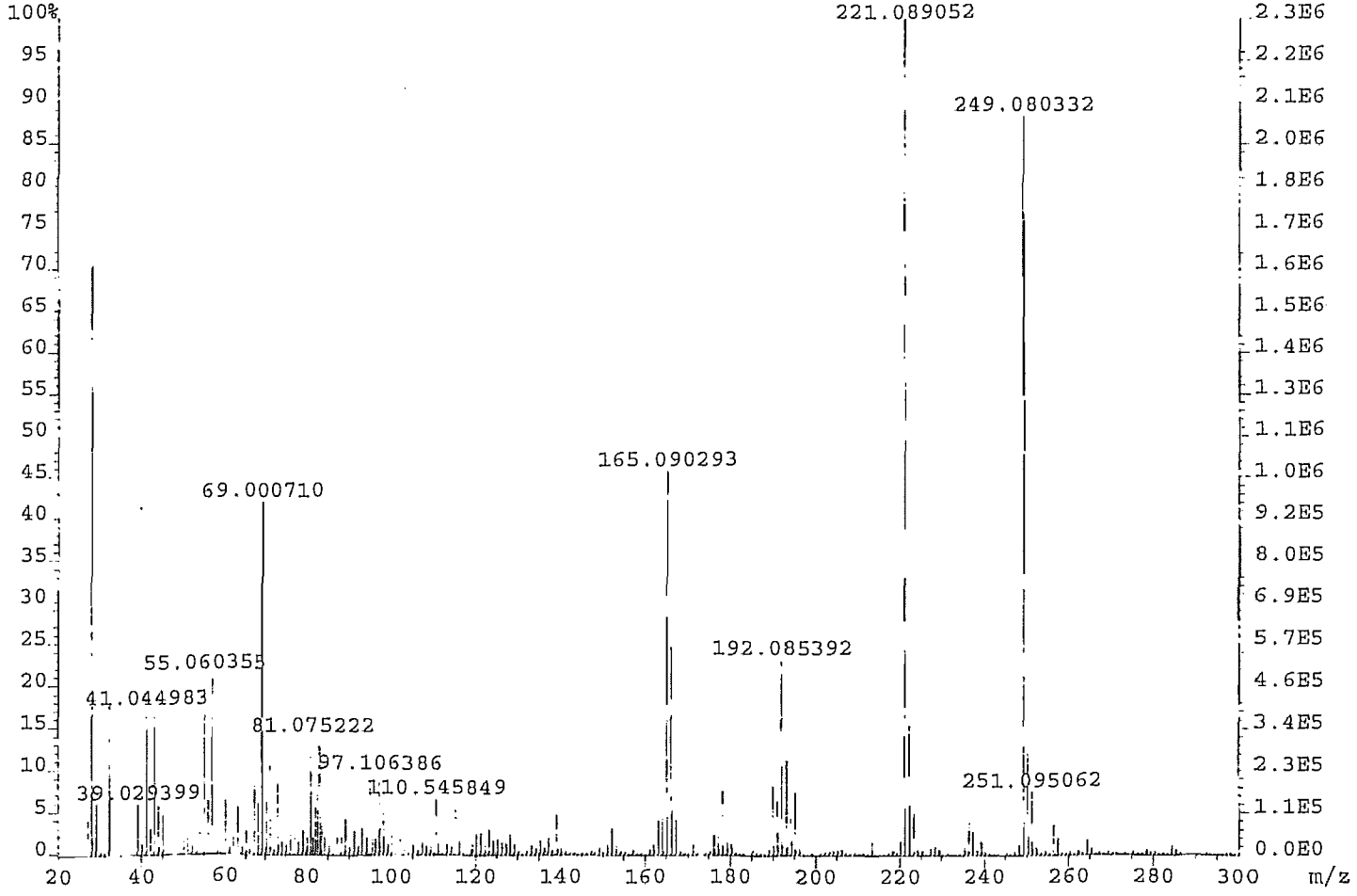

(8a) (*E*)-5-Styrylisatin:

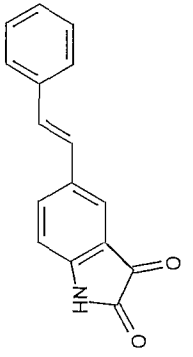

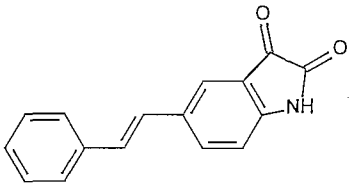
O
O
NH

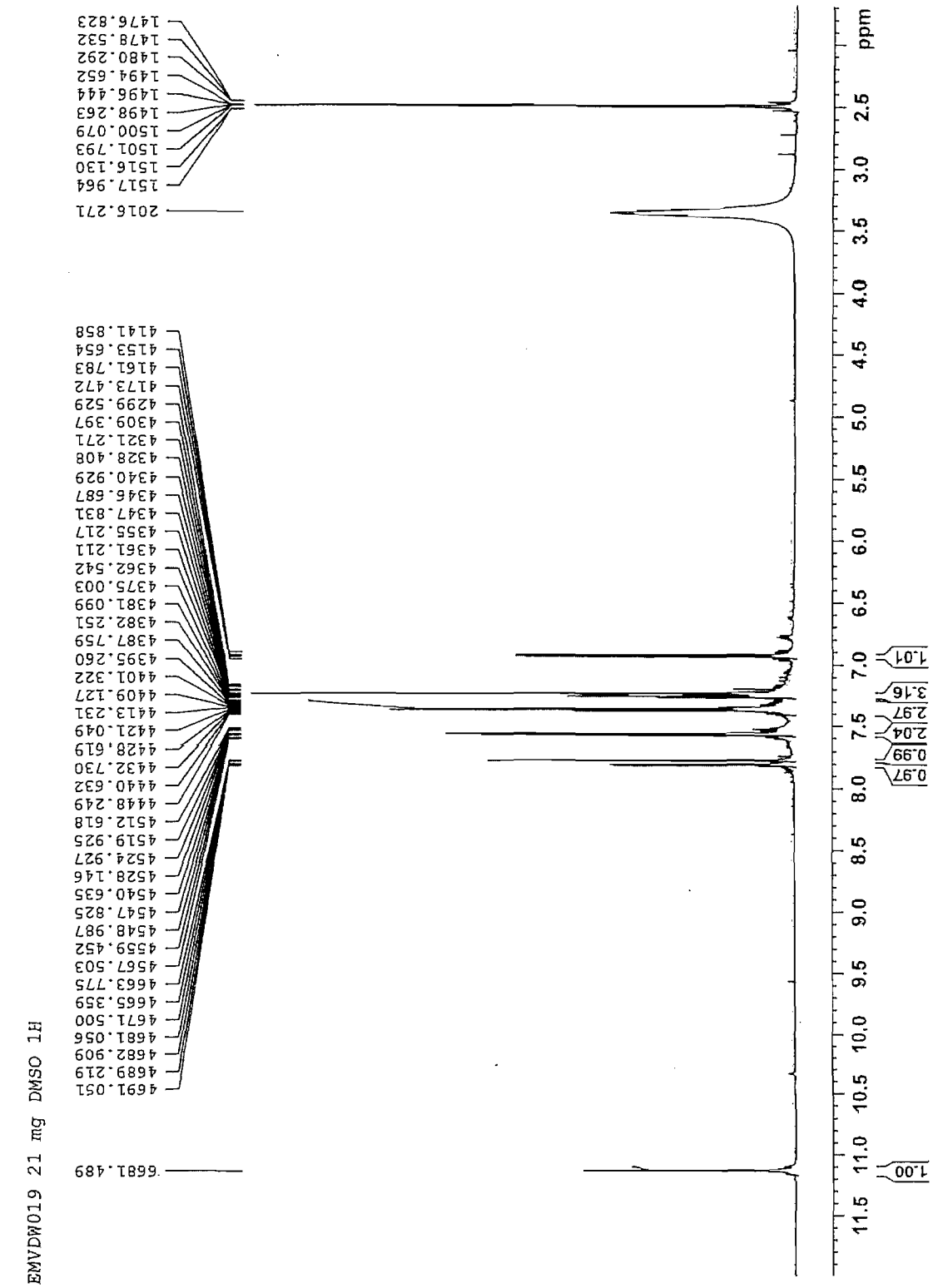
EMVDW019 21 mg DMSO 1H
ppm
1.00
1.01
3.16
2.97
2.04
0.99
0.97

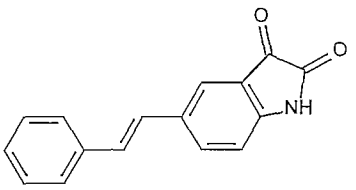
O
O
NH

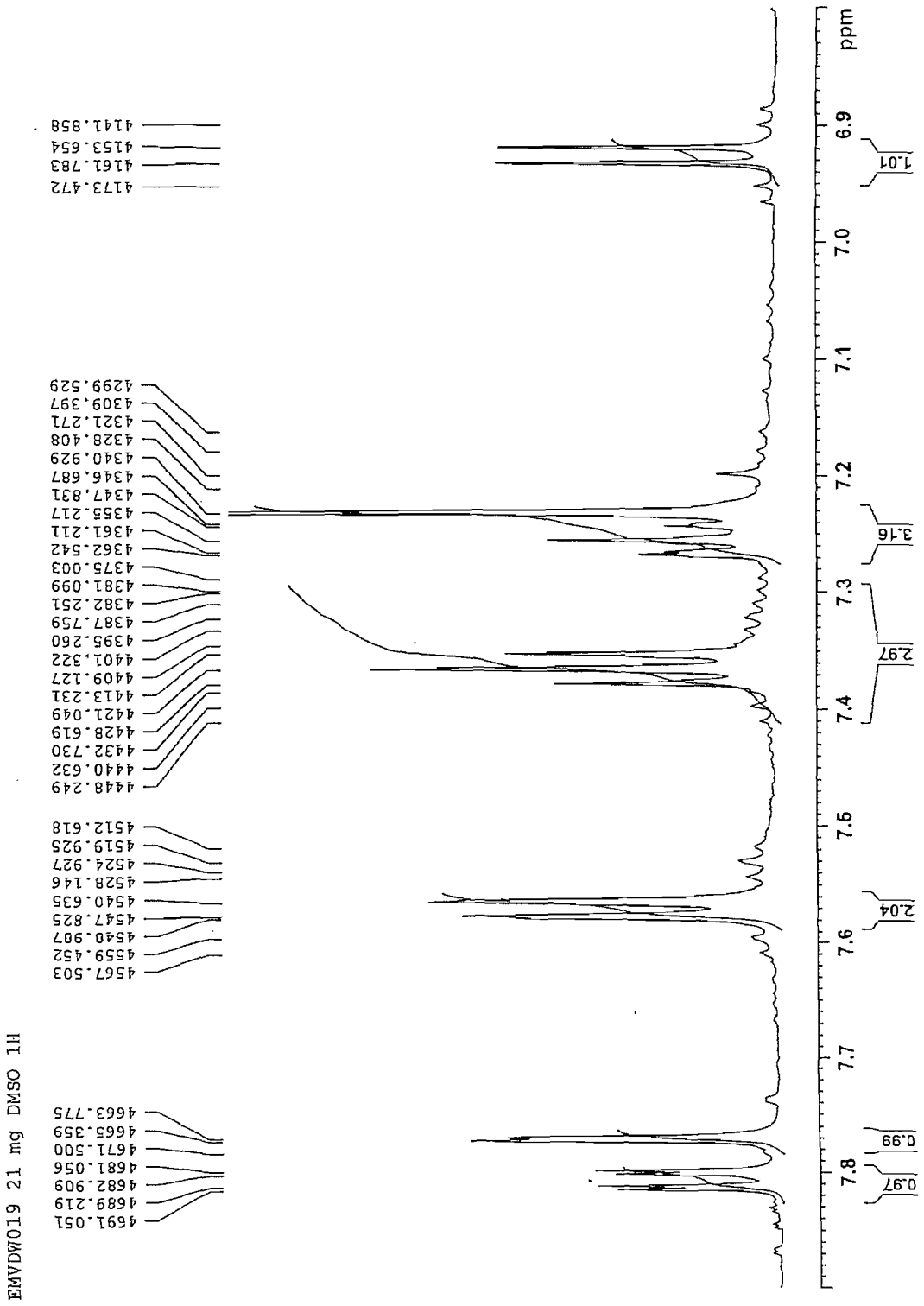
EMVDW019 21 mg DMSO 1H
4691.051
4689.219
4682.909
4681.056
4671.500
4665.359
4663.775
4567.503
4559.452
4548.907
4547.825
4540.635
4528.146
4524.927
4519.925
4512.618
4448.249
4440.632
4432.730
4428.619
4421.049
4413.231
4409.127
4401.322
4395.260
4387.759
4382.251
4381.099
4375.003
4362.542
4361.211
4355.217
4347.831
4346.687
4340.929
4328.408
4321.271
4309.397
4299.529
4173.472
4161.783
4153.654
4141.858
ppm
6.9
7.0
7.1
7.2
7.3
7.4
7.5
7.6
7.7
7.8
1.01
3.16
2.97
2.04
0.99
0.97

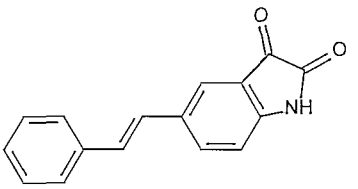
O
O
NH

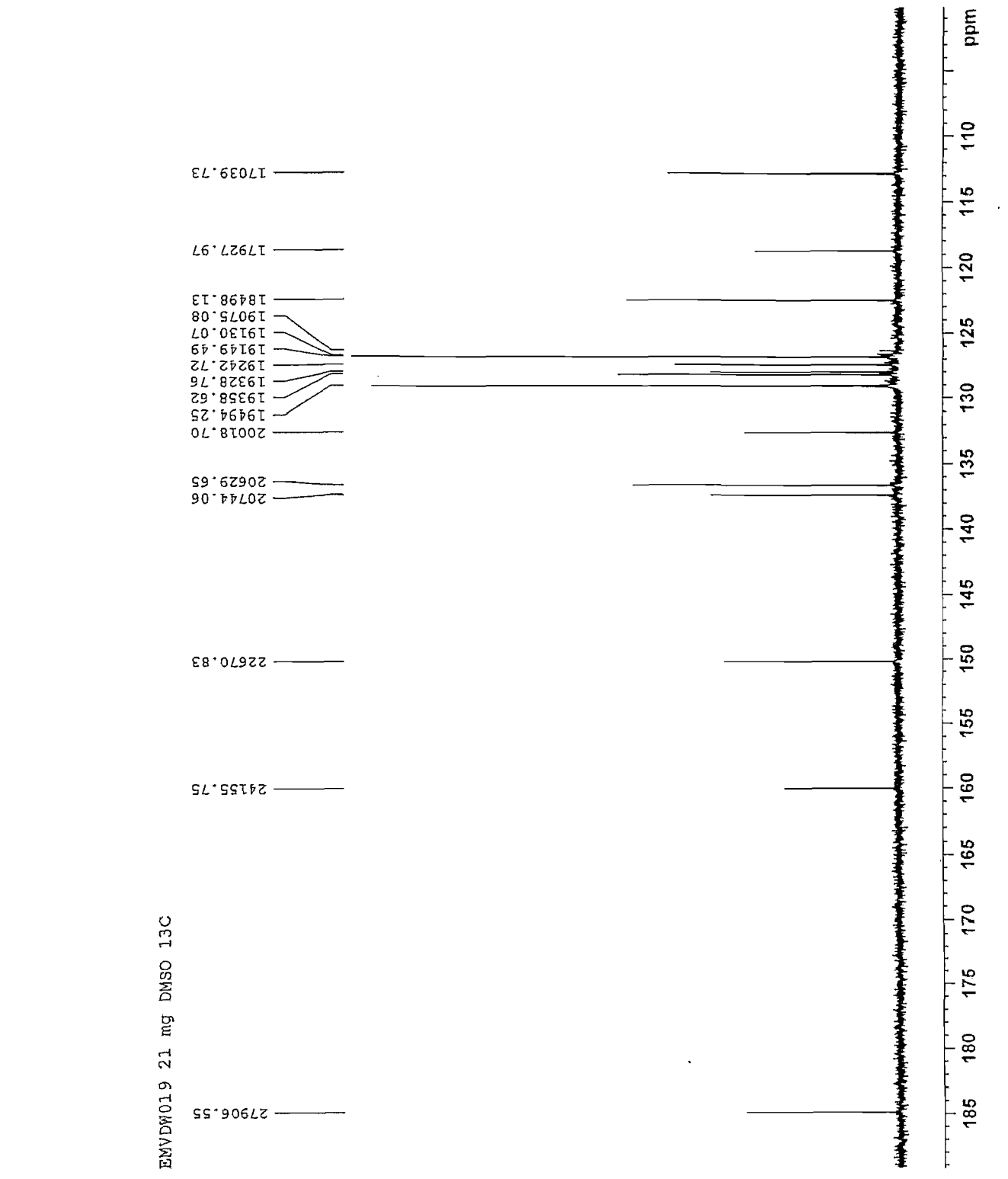
EMVDW019 21 mg DMSO 13C
27906.55
24155.75
22670.83
20744.06
20629.65
20018.70
19494.25
19358.62
19328.76
19242.72
19149.49
19130.07
19075.08
18498.13
17927.97
17039.73
ppm
185
180
175
170
165
160
155
150
145
140
135
130
125
120
115
110

(8b) (*E*)-5-(3-Chlorostyryl)isatin:

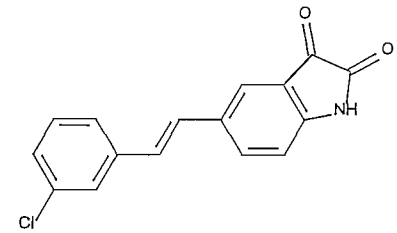

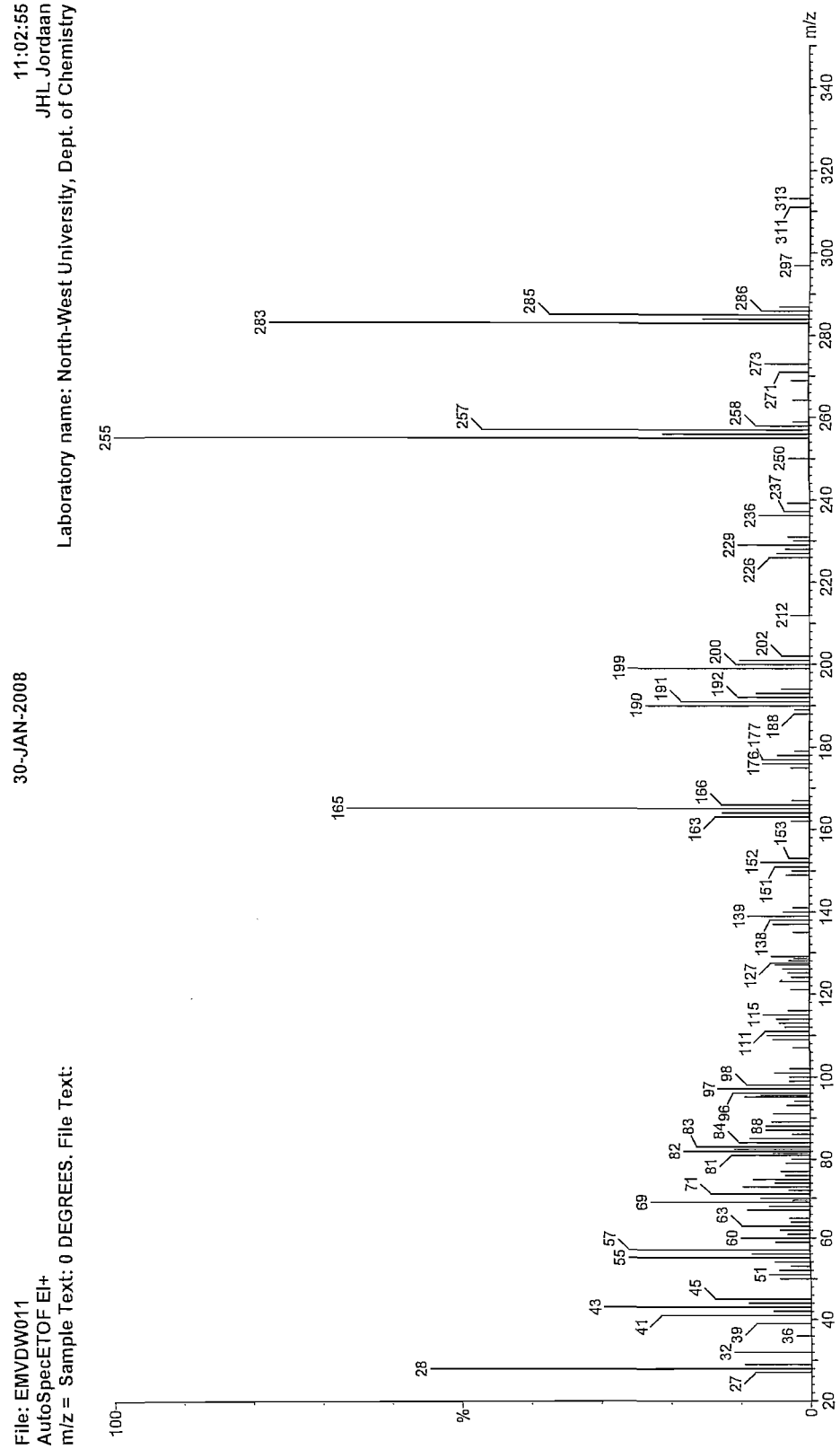

EMVDW011 20.6 mg DMSO 1H
2.90
2.85
2.80
2.75
2.70
2.65
2.60
2.55
2.50
2.45
2.40
ppm
1.00
4.00
1518.433
1500.546
1498.760
1496.968
1495.432
HN
O
O
Cl

EMVDW011 20.6 mg DMSO 1H

4684.858
4683.119
4676.663
4674.951
4665.683
4664.323
4588.876
4515.639
4507.845
4439.429
4431.569
4423.752
4403.626
4394.976
4387.184
4382.641
4381.301
4374.561
4373.408
4365.780
4342.300
4336.949
4325.818
4320.695
4166.998
4158.919

7.80 7.75 7.70 7.65 7.60 7.55 7.50 7.45 7.40 7.35 7.30 7.25 7.20 7.15 7.10 7.05 7.00 6.95 ppm

1.11 1.00 2.01 2.35 2.69 2.74 0.95 4.15 1.61 1.02 2.00

ppm
30
40
50
60
70
80
90
100
110
120
130
140
150
160
170
180
117
EMVDW011 20.6 mg DMSO 13C
5243.61
17911.81
19303.92
19930.37
20231.99
21136.87
22691.39
24176.31
27888.60
5971.16
5992.18
6013.21
6034.21
6055.20
6076.17
6097.07
17045.16
18519.74
18953.13
19057.69
19119.30
19504.51
19765.35
20667.10
O
NH
O
Cl

File: EMVDW012
AutoSpecETOF EI+
m/z = Sample Text: 0 DEGREES. File Text:

30-JAN-2008

11:24:38
JHL Jordaan
Laboratory name: North-West University, Dept. of Chemistry

(8c) (*E*)-5-(3-Fluorostyryl)isatin:

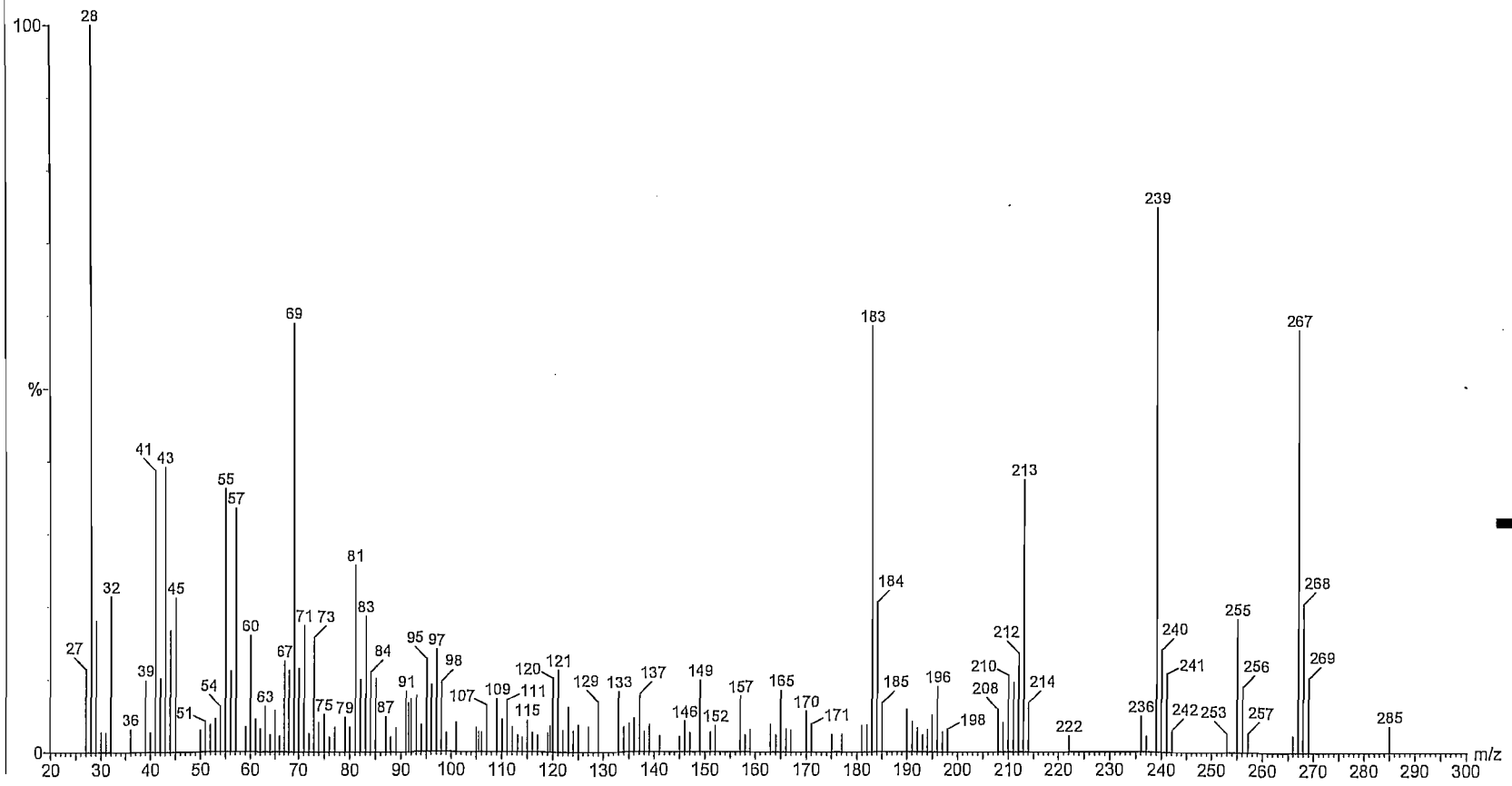

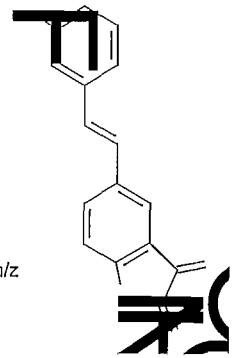

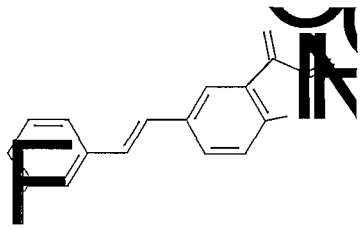

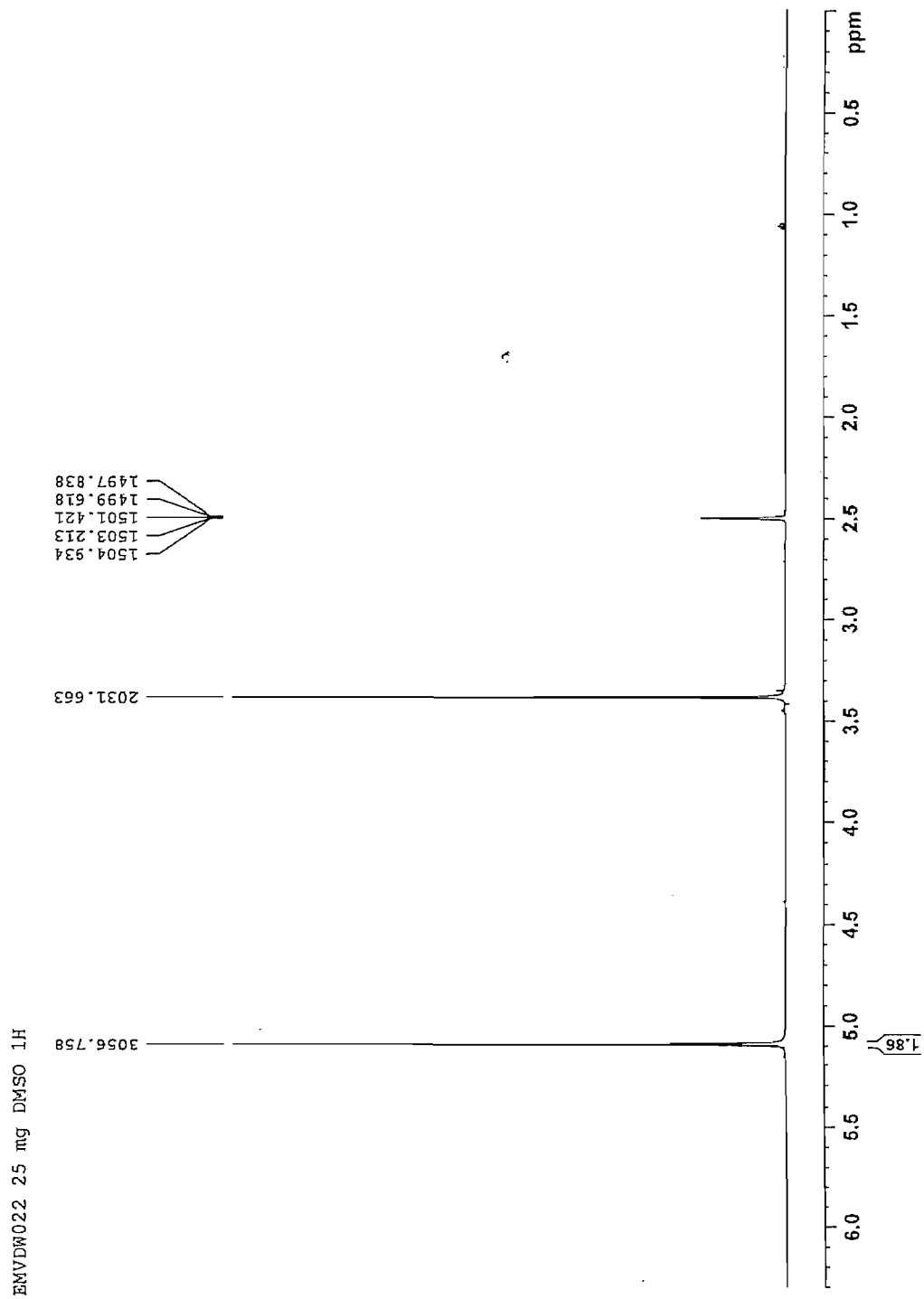
EMVDW022 25 mg DMSO 1H
3056.758
2031.663
1504.934
1503.213
1501.421
1499.618
1497.838
1.86
ppm
6.0
5.5
5.0
4.5
4.0
3.5
3.0
2.5
2.0
1.5
1.0
0.5

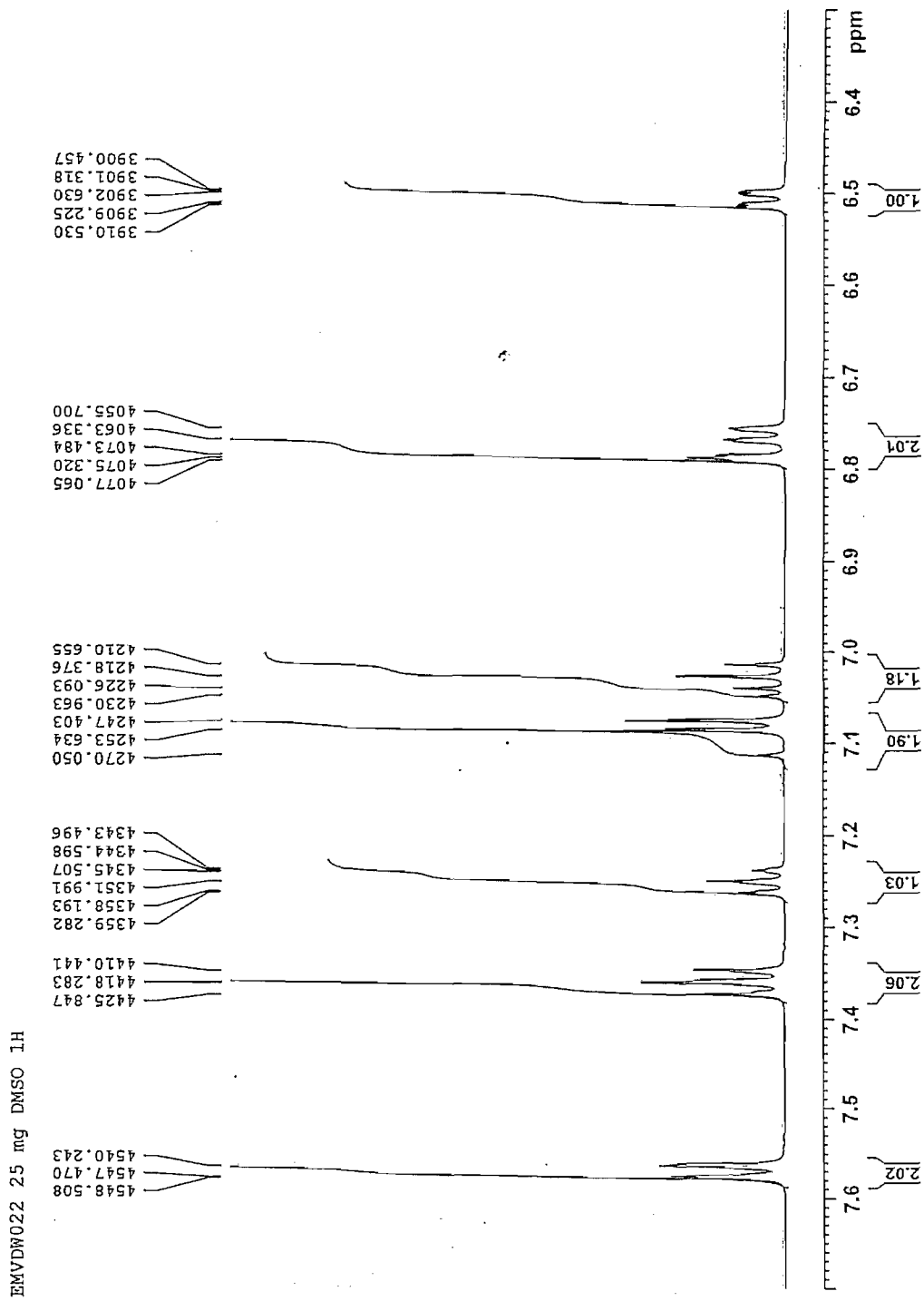
EMVDW022 25 mg DMSO 1H
4548.508
4547.470
4540.243
4425.847
4418.283
4410.441
4359.282
4358.193
4351.991
4345.507
4344.598
4343.496
4270.050
4253.634
4247.403
4230.963
4226.093
4218.376
4210.655
4077.065
4075.320
4073.484
4063.336
4055.700
3910.530
3909.225
3902.630
3901.318
3900.457
7.6
7.5
7.4
7.3
7.2
7.1
7.0
6.9
6.8
6.7
6.6
6.5
6.4
ppm
2.02
2.06
1.03
1.90
1.18
2.01
1.00

EMVDW012 19.7 mg DMSO 1H

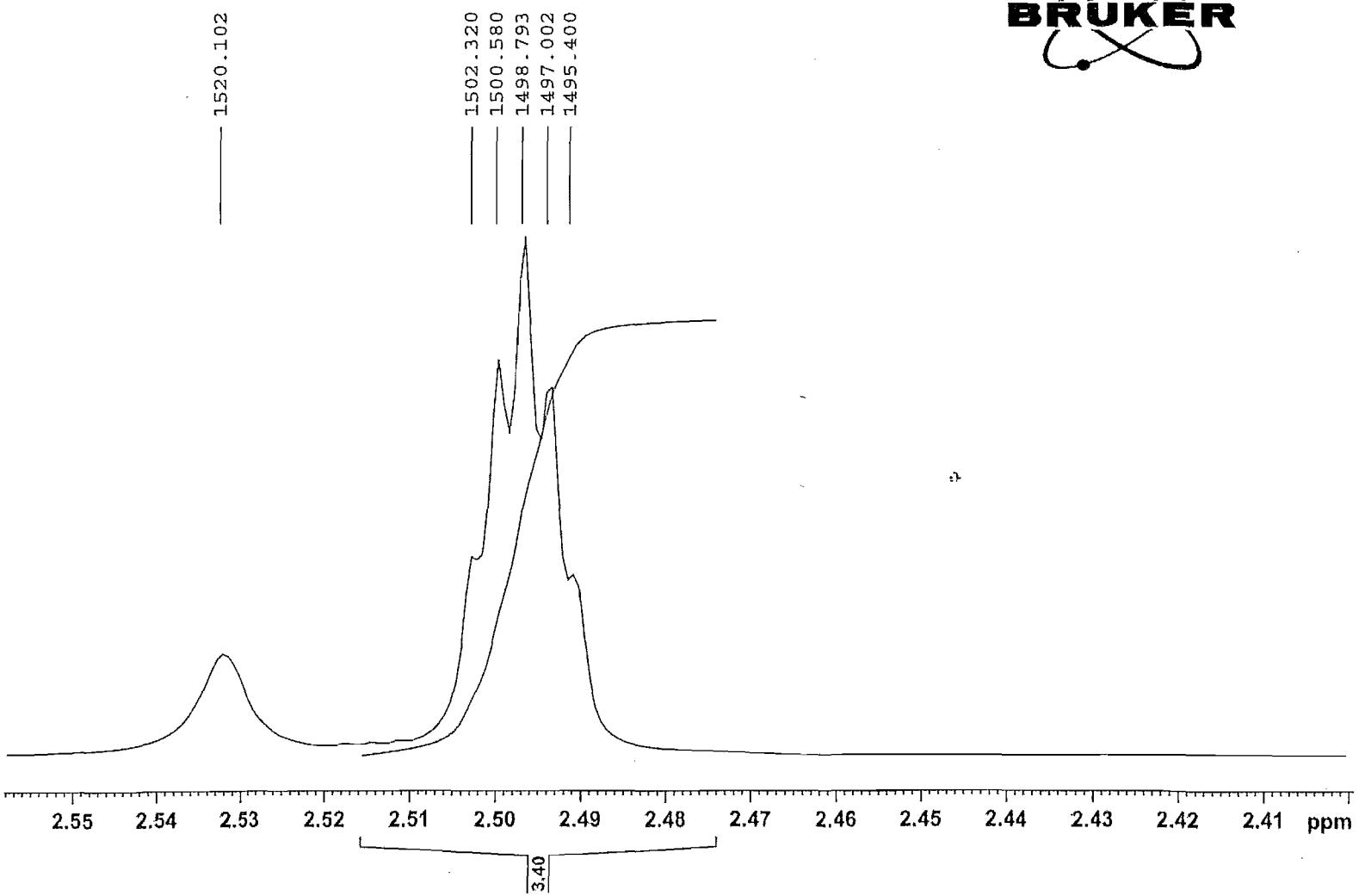

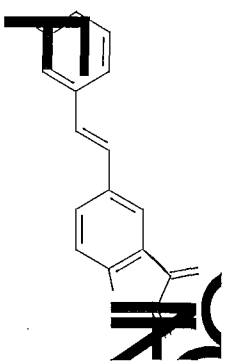

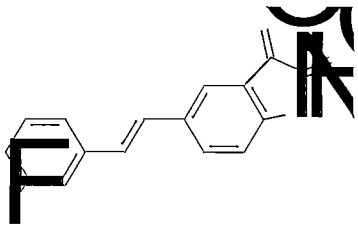

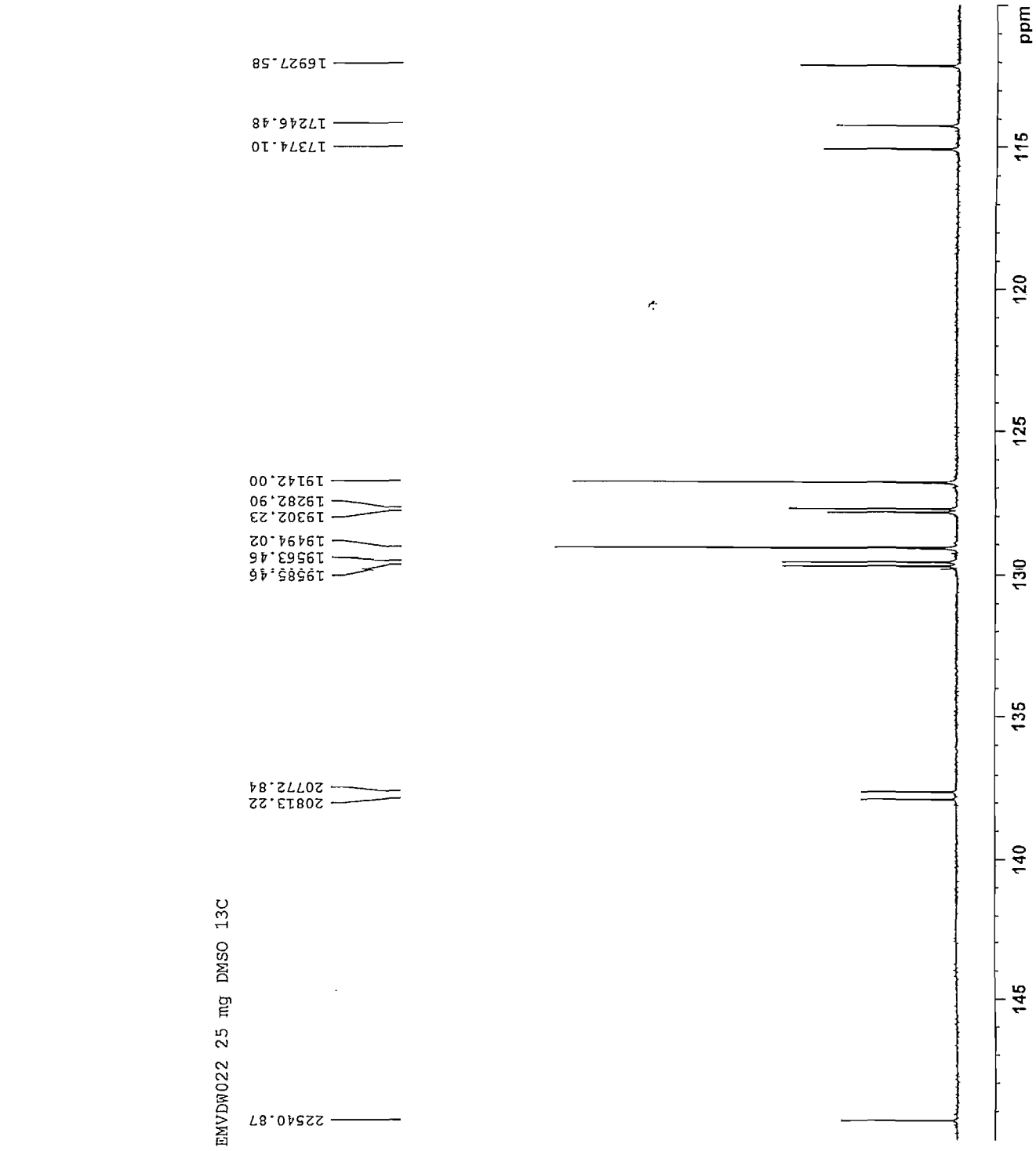
EMVDW022 25 mg DMSO 13C
22540.87
20772.84
20813.22
19585.46
19563.46
19494.02
19302.23
19282.90
19142.00
16927.58
17246.48
17374.10
ppm
115
120
125
130
135
140
145

File:EVDW031A Ident:18_21-10 Win 100PPM Acq:11-JUN-2008 08:46:39 +2:48 Cal:KE11
AutoSpecETOF EI+ Magnet BpM:249 BpI:652128 TIC:4810940 Flags:HALL
Sample Text:0 DEGREES.

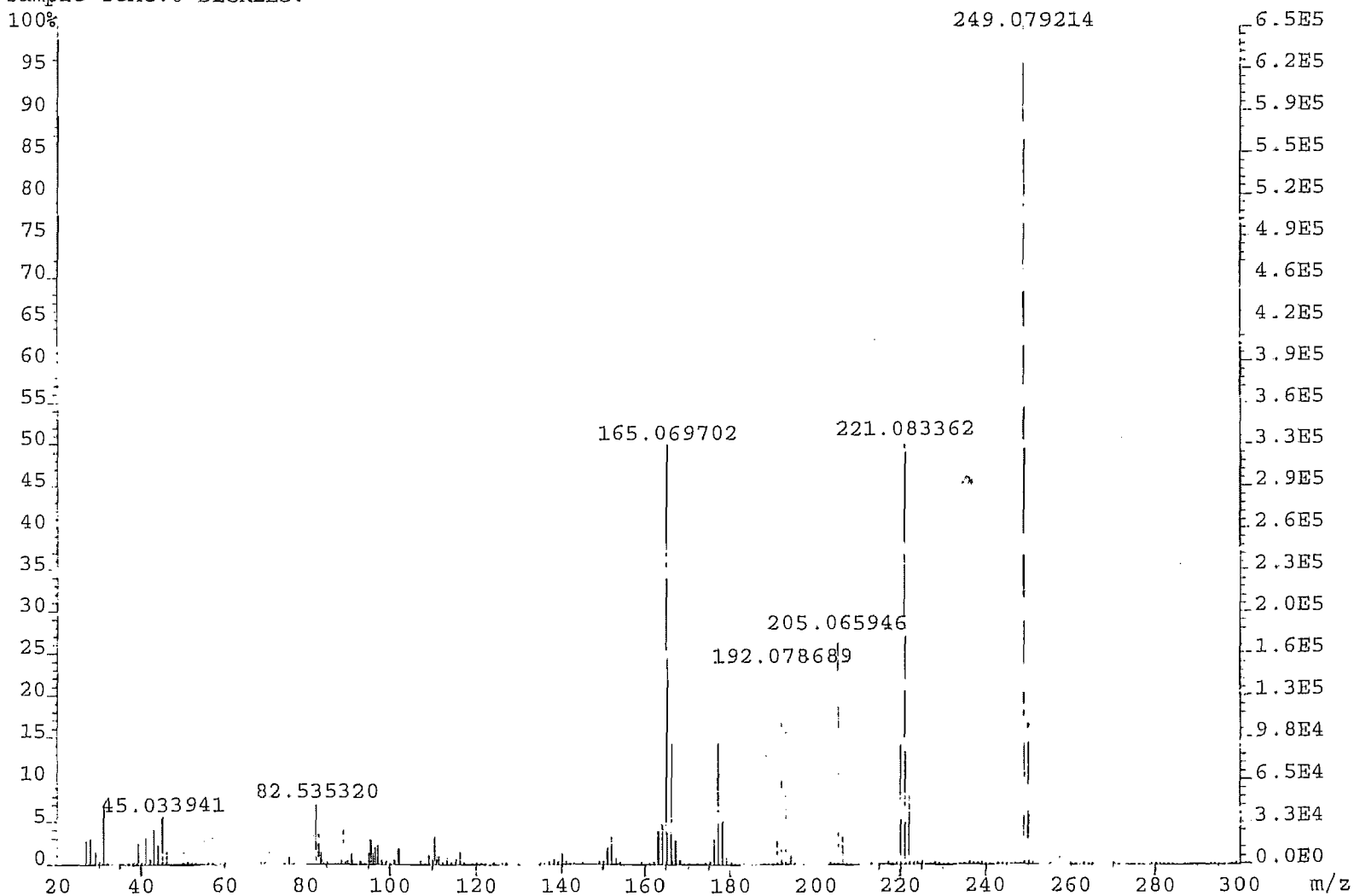

(9a) (*E*)-6-Styrylisatin:

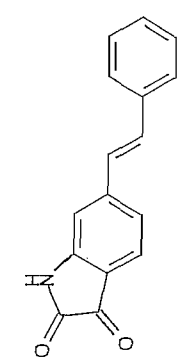

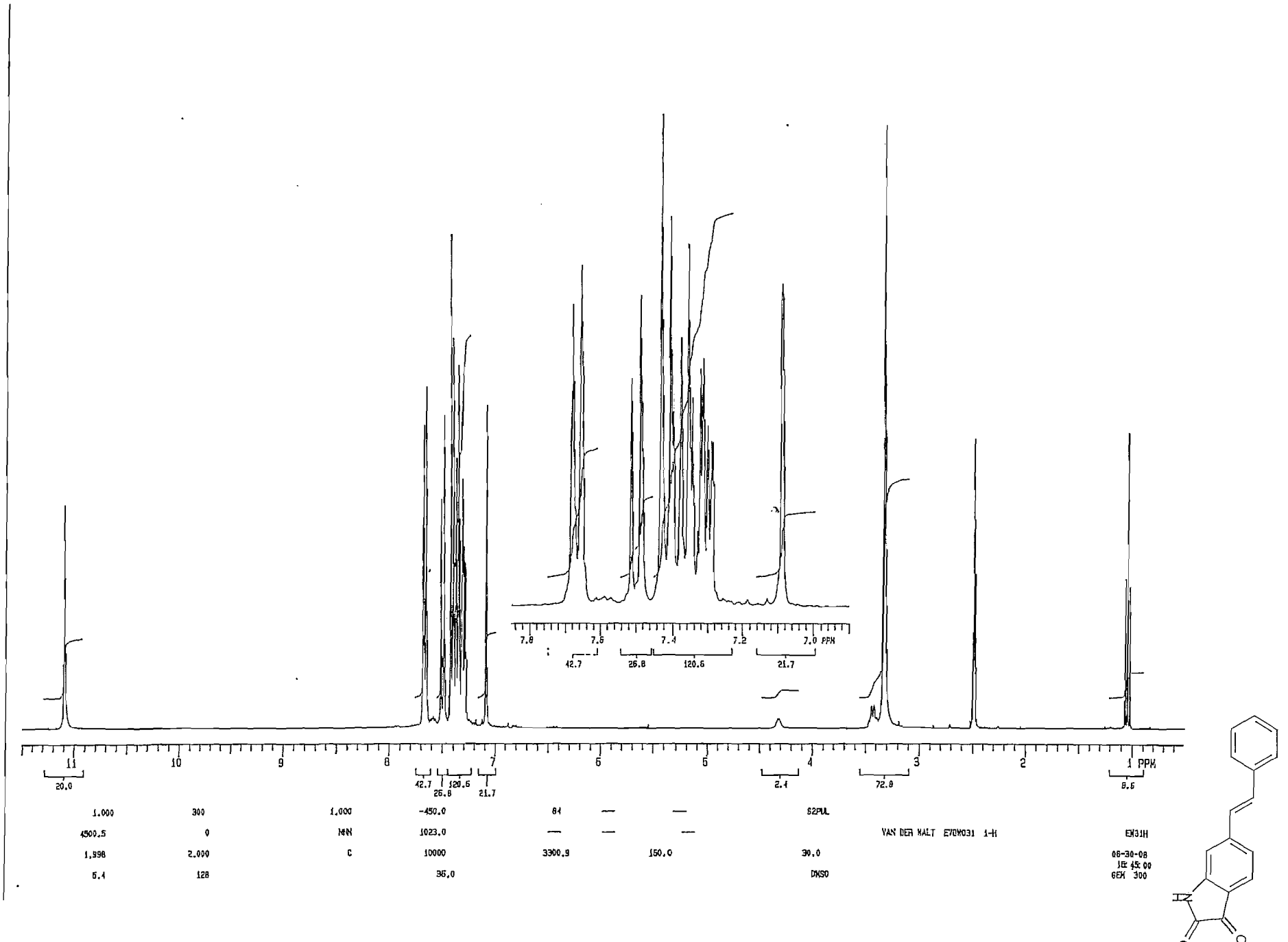
11
10
9
8
7
6
5
4
3
2
1 PPM
20.0
42.7
25.8
120.6
21.7
2.4
72.8
8.6
7.8
7.6
7.4
7.2
7.0 PPM
42.7
25.8
120.6
21.7
1.000 300 1.000 -450.0 64 — — 62PUL
4500.5 0 NON 1023.0 — — — VAN DER MALT EVDM031 1-H EN31H
1.998 2.000 C 10000 3300.9 150.0 30.0 06-30-08
16:45:00
6.4 128 36.0 DMSO GEX 300
O
O

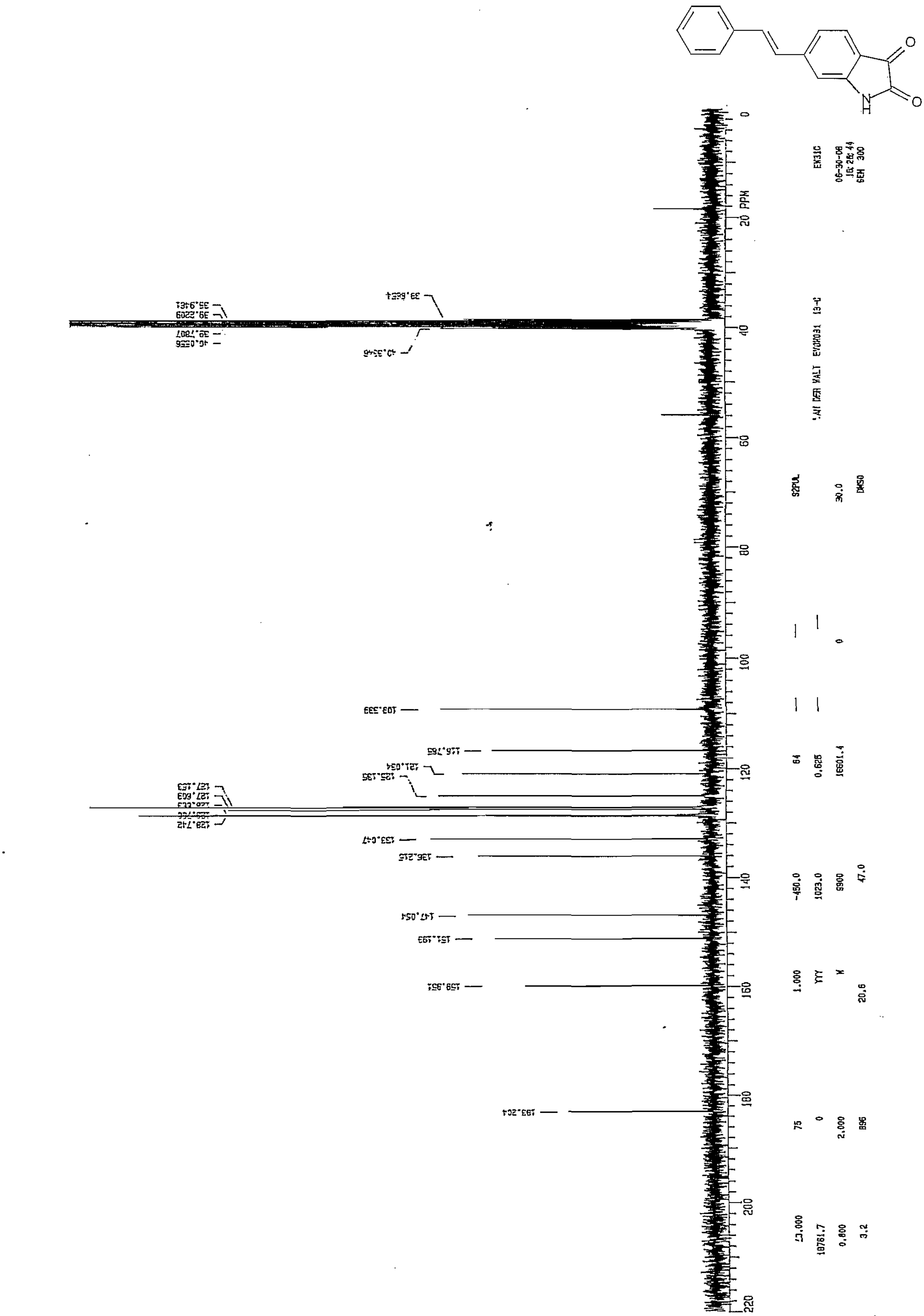
183.204
159.951
151.193
147.054
136.215
133.047
121.034
116.765
108.339
PPM

File:EVDW026A Ident:37-8 Win 100PPM Acq:28-MAY-2008 11:57:21 Cal:KE28
AutoSpecETOF EI+ Magnet BpM:28 BpI:82944 TIC:3437917 Flags:HALL
Sample Text:0 DEGREES.

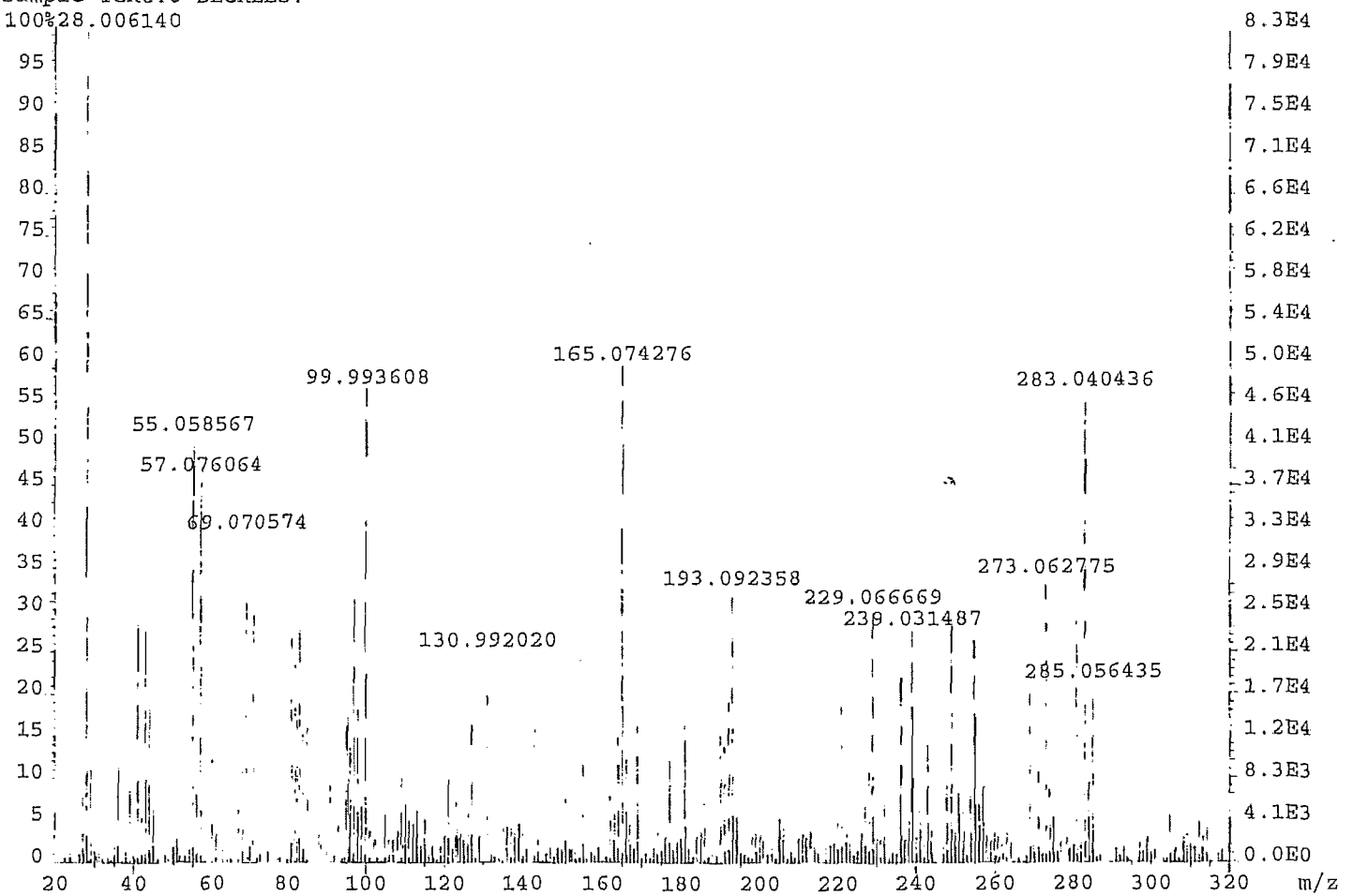

(9b) (*E*)-6-(3-Chlorostyryl)isatin:

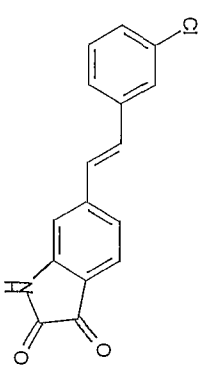

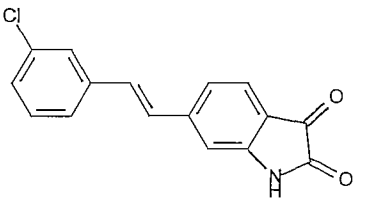
Cl
O
O
N
H

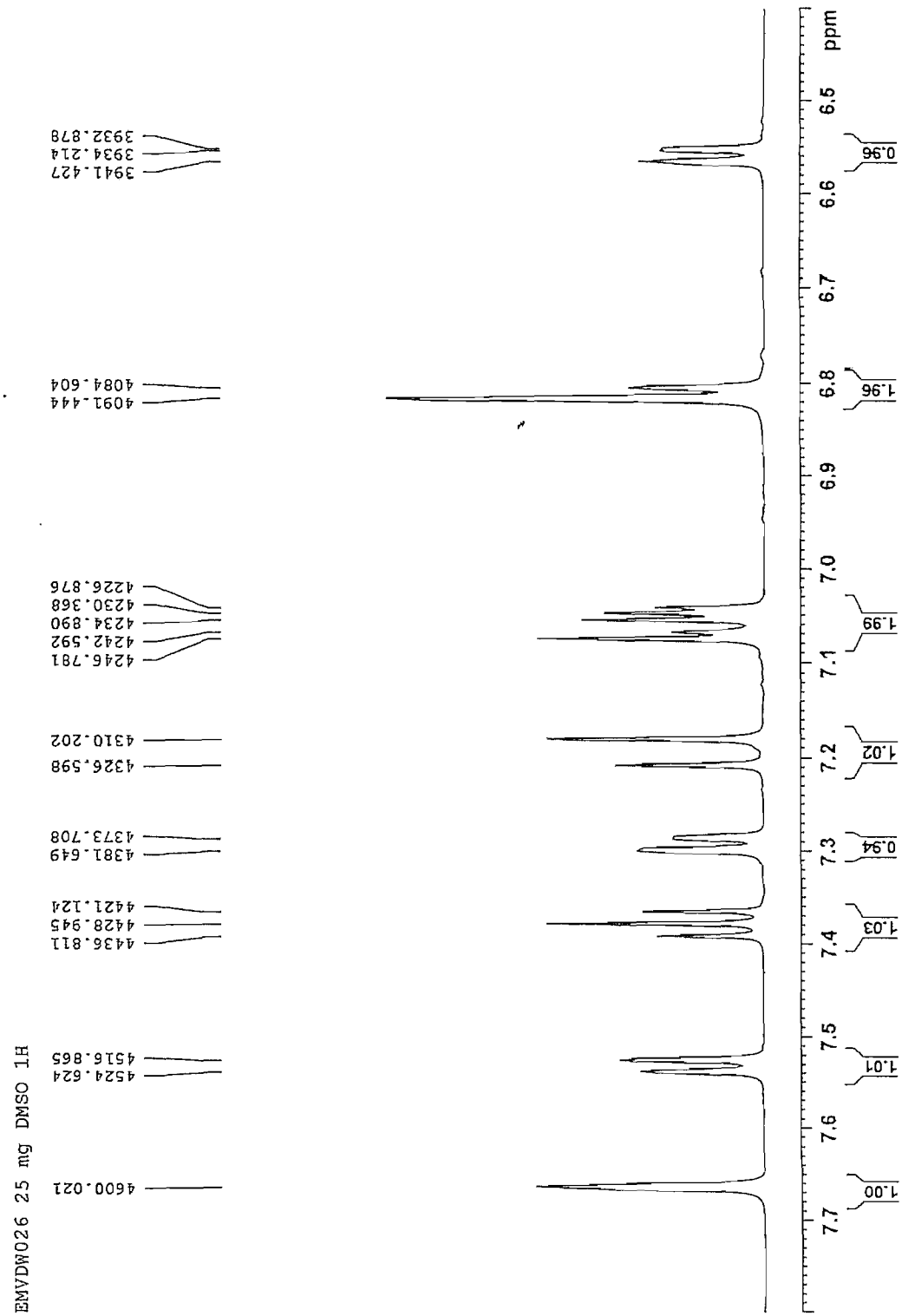
EMVDW026 25 mg DMSO 1H
4600.021
4524.624
4516.865
4436.811
4428.945
4421.124
4381.649
4373.708
4326.598
4310.202
4246.781
4242.592
4234.890
4230.368
4226.876
4091.444
4084.604
3941.427
3934.214
3932.878
ppm
6.5
6.6
6.7
6.8
6.9
7.0
7.1
7.2
7.3
7.4
7.5
7.6
7.7
0.96
1.96
1.99
1.02
0.94
1.03
1.01
1.00

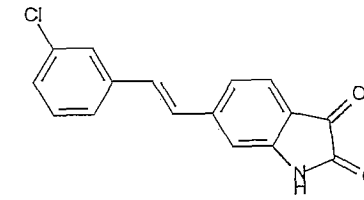
Cl
O
O
N
H

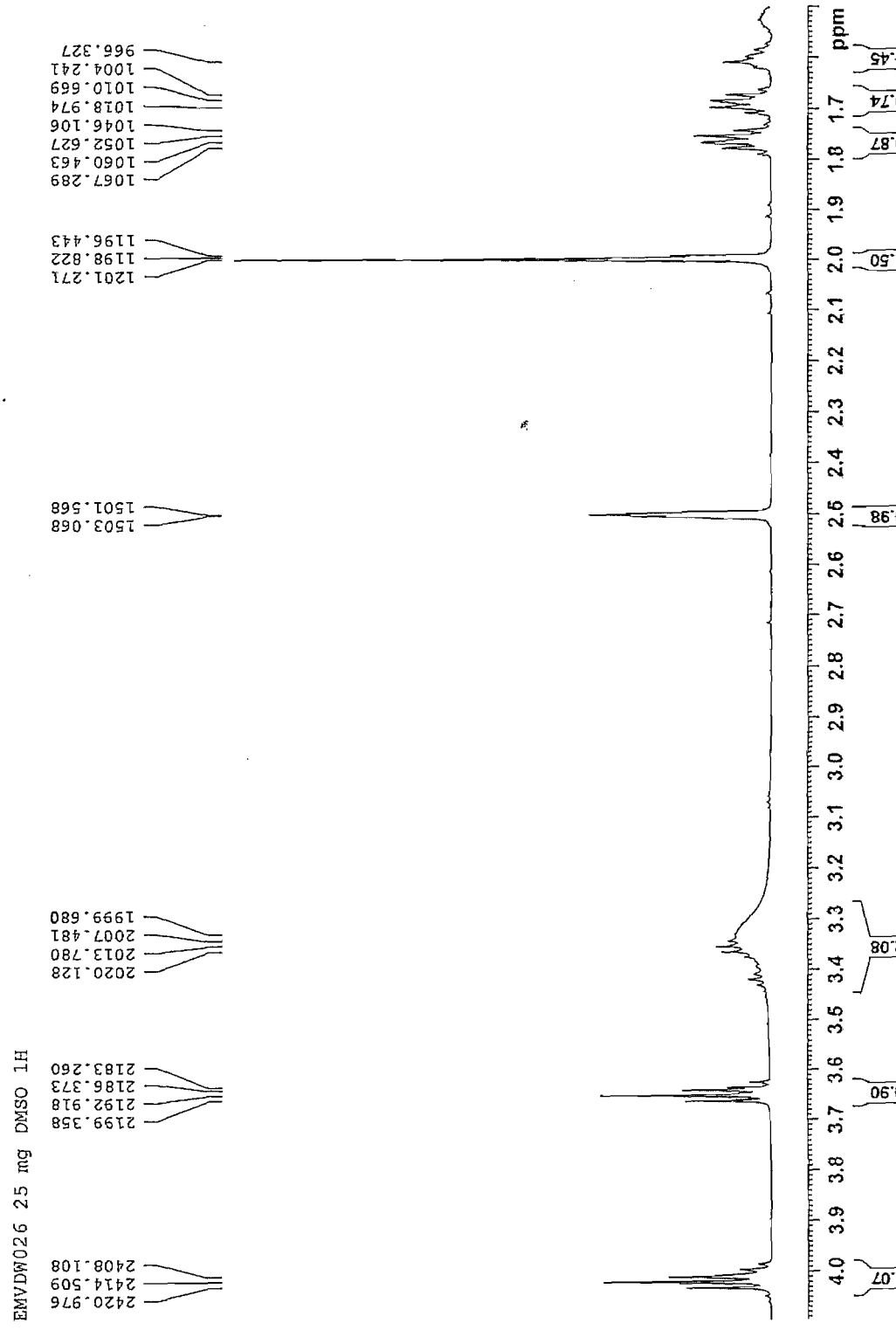
EMVDW026 25 mg DMSO 1H
2420.976
2414.509
2408.108
2199.358
2192.918
2186.373
2183.260
2020.128
2013.780
2007.481
1999.680
1503.068
1501.568
1201.271
1198.822
1196.443
1067.289
1060.463
1052.627
1046.106
1018.974
1010.669
1004.241
966.327
ppm
4.0
3.9
3.8
3.7
3.6
3.5
3.4
3.3
3.2
3.1
3.0
2.9
2.8
2.7
2.6
2.5
2.4
2.3
2.2
2.1
2.0
1.9
1.8
1.7
1.07
0.90
2.08
0.98
1.50
0.87
0.74
0.45

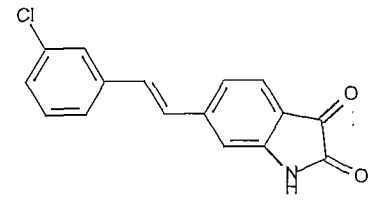
Cl
O
O
N
H

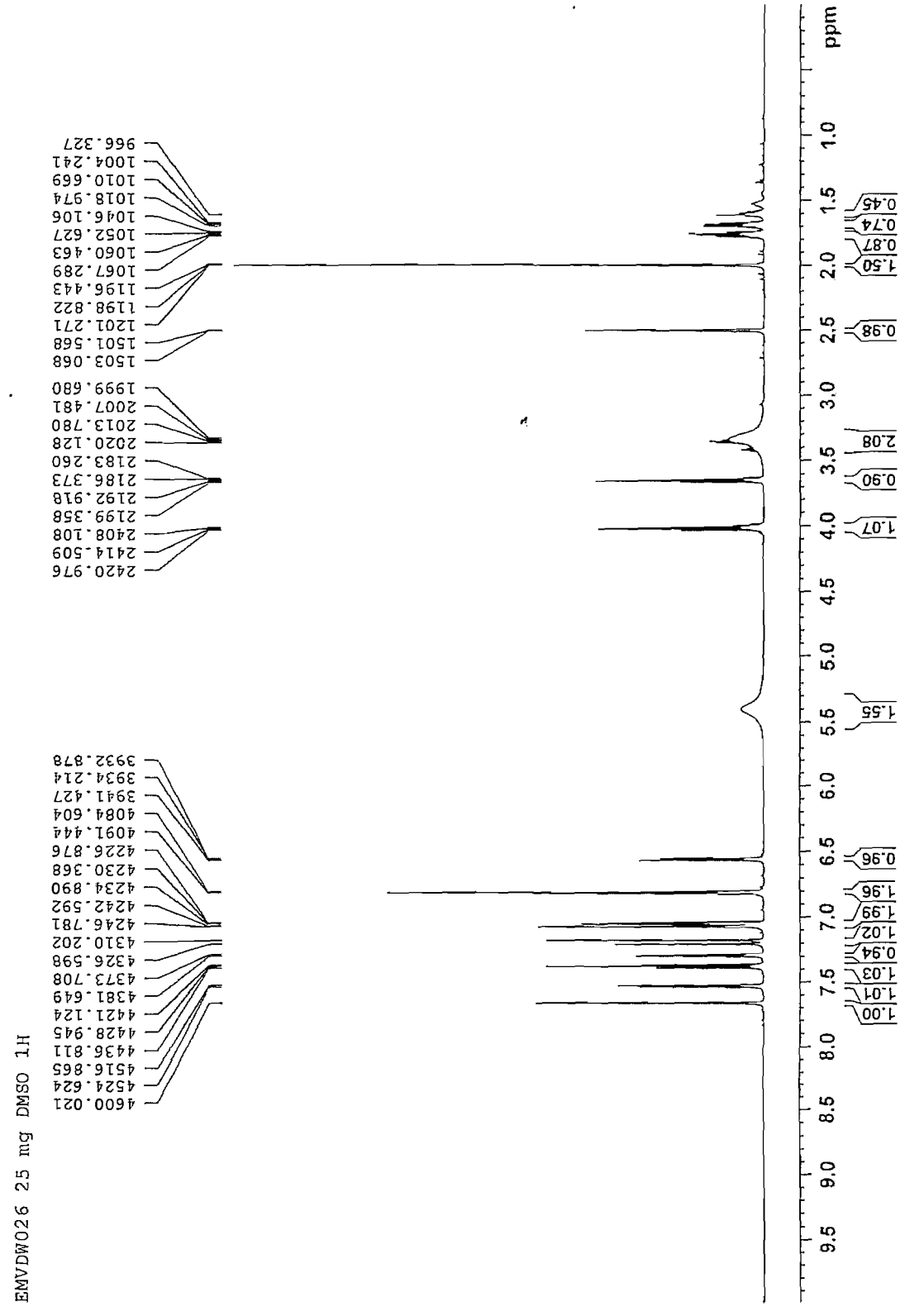
EMVDW026 25 mg DMSO 1H
4600.021
4524.624
4516.865
4436.811
4428.945
4421.124
4381.649
4373.708
4326.598
4310.202
4246.781
4242.592
4234.890
4230.368
4226.876
4091.444
4084.604
3941.427
3934.214
3932.878
2420.976
2414.509
2408.108
2199.358
2192.918
2186.373
2183.260
2020.128
2013.780
2007.481
1999.680
1503.068
1501.568
1201.271
1198.822
1196.443
1067.289
1060.463
1052.627
1046.106
1018.974
1010.669
1004.241
966.327
ppm
9.5
9.0
8.5
8.0
7.5
7.0
6.5
6.0
5.5
5.0
4.5
4.0
3.5
3.0
2.5
2.0
1.5
1.00
1.01
1.03
0.94
1.02
1.99
1.96
0.96
1.55
1.07
0.90
2.08
0.98
1.50
0.87
0.74
0.45

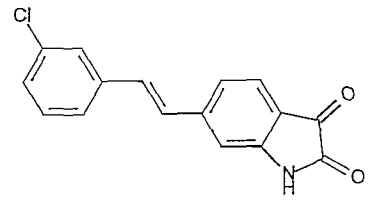
Cl
O
O
N
H

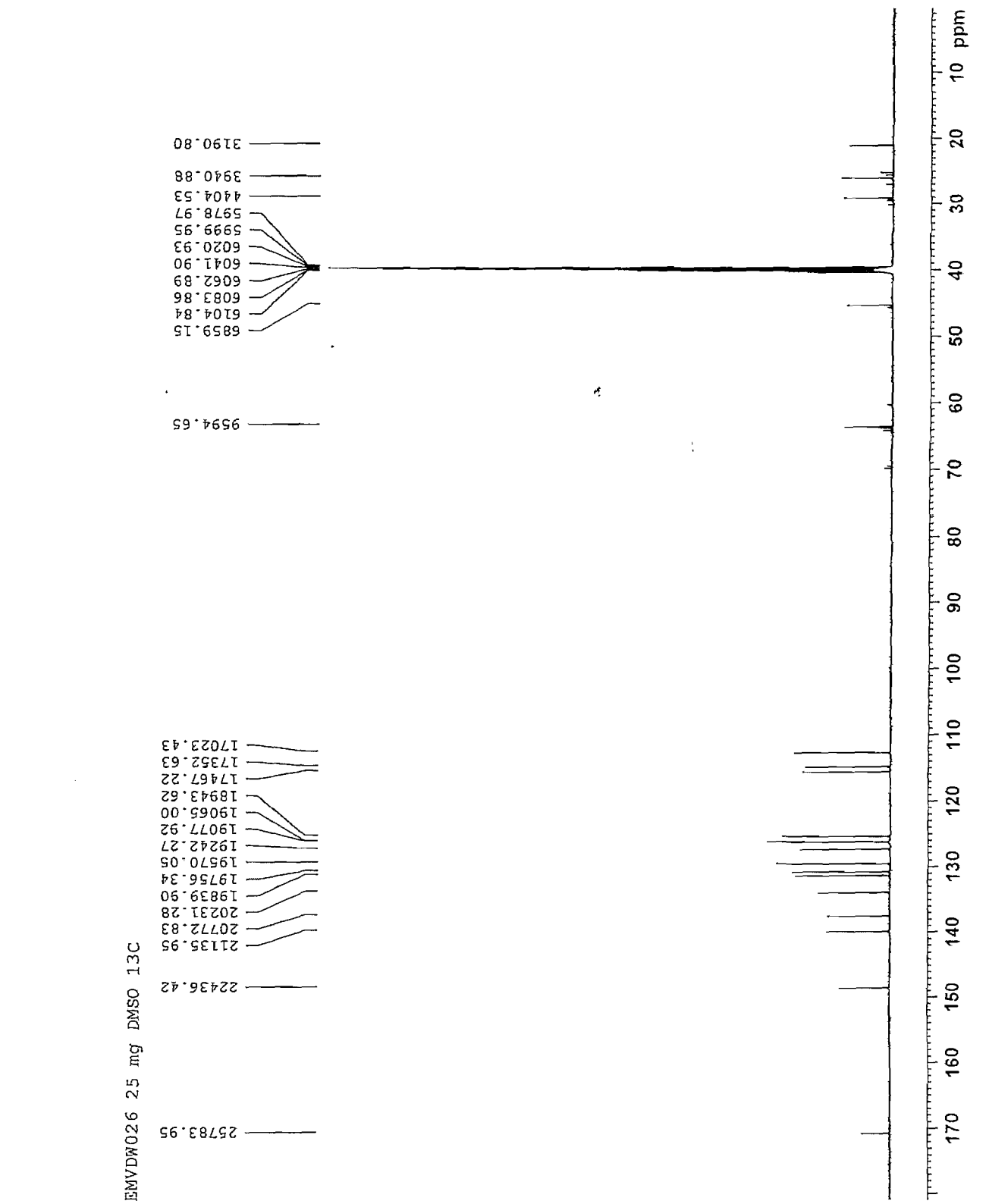
EMVDW026 25 mg DMSO 13C
25783.95
22436.42
21135.95
20772.83
20231.28
19839.90
19756.34
19570.05
19242.27
19077.92
19065.00
18943.62
17467.22
17352.63
17023.43
9594.65
6859.15
6104.84
6083.86
6062.89
6041.90
6020.93
5999.95
5978.97
4404.53
3940.88
3190.80
ppm
10
20
30
40
50
60
70
80
90
100
110
120
130
140
150
160
170

APPENDIX B

Concept article

The synthesis and evaluation of (*E*)-styrylisatin analogues as inhibitors of MAO-B

Elizna M. van der Walt*, Sarel F. Malan, Jacobus J. Bergh and Jacobus P. Petzer

Pharmaceutical Chemistry, School of Pharmacy, North-West University, Potchefstroom, 2520, South Africa.

Abstract— Three (*E*)-5-styrylisatin and two (*E*)-6-styrylisatin analogues were prepared and evaluated as reversible inhibitors of monoamine oxidase B (MAO-B). All the compounds were found to possess enhanced MAO-B inhibitory activity compared to isatin. The most active compound was (*E*)-5-(3-chlorostyryl)isatin with an IC50 value of 20.7 nM.

Monoamine oxidase B (MAO-B) inhibitors are currently clinically used in the symptomatic treatment of Parkinson's disease (PD) and may also possess neuroprotective activity. The irreversible MAO-B inhibitor, (*R*)-deprenyl, is most often used in PD treatment, usually in combination with levodopa as part of dopamine replacement therapy. In contrast with reversible inhibition, enzyme recovery after irreversible inhibition involves *de novo* synthesis of the enzyme, which may require several weeks. This makes reversible MAO-B inhibitors safer and more desirable.

Both isatin (A) and caffeine (B) are small molecules that have been reported to inhibit MAO-B. Isatin is a relatively good endogenous inhibitor (K_i = 3 μM) whereas caffeine is a weak inhibitor (K_i = 650 μM). The inhibitory potency of caffeine has reportedly been improved by substitution at C-8 of the caffeine ring with a styryl side-chain.[1] Addition of an electron withdrawing substituent at C-3 of the phenyl ring produced structures with exceptional reversible MAO-B inhibitory potency, for example (*E*)-8-(3-chlorostyryl)caffeine (C) (K_i = 0.1 μM). In this study we investigated whether styryl substitution of the lead compound, isatin, at C-5 and C-6 will similarly enhance isatin's MAO-B inhibitory potency.

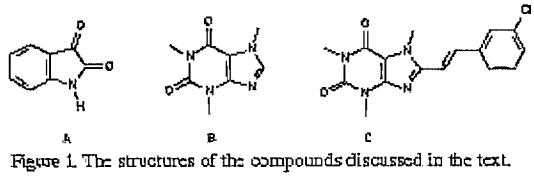

Figure 1. The structures of the compounds discussed in the text.

Two (*E*)-6-Styrylisatin (9a–b) as well as three (*E*)-5-styrylisatin (8a–c) analogues were synthesized according to the same four step synthetic pathway (Scheme 1). Diethyl (4-nitrobenzyl)phosphonate and diethyl (3-nitrobenzyl)phosphonate (3), were prepared from commercially available 4- or 3-nitrobenzyl bromide (1) and triethyl phosphite (2).[1] The intermediate 3 were used in a Wittig condensation reaction with a commercially available benzaldehyde (4) to produce the required 4- or 3-nitrostilbene (5).[2] Subsequent reduction of these nitrostilbenes with hydrochloric acid and tin powder, produced the corresponding 3- or 4-aminostilbenes (6).[3] Following crystallization from a suitable solvent the resulting aminostilbenes were reacted with mesoxalic acid diethyl ester in the presence of an acid and underwent ring closure after oxidative decarboxylation to yield the isatin product.[4,5]

The IC_{50} values of the compounds were estimated by spectrophotometrically measuring the extent by which different concentrations of the analogues slowed the rate of the MAO-B catalyzed oxidation of the substrate MMTP [1-methyl-4-(1-methylpyrrol-2-yl)-1,2,3,6-tetrahydropyridine].[6,7,8] Baboon liver mitochondrial fractions, which are devoid of MAO-A activity, were used as enzyme source.[1]

The inhibitory potencies for all the styrylisatin analogues were expressed in terms of the concentration of the compound necessary for 50% inhibition of the enzyme (IC_{50} value). Reversibility of inhibition was confirmed with a time-dependent inhibition study that documented that the potencies of inhibition of MAO-B by the (*E*)-styrylisatin analogues are independent of the time period for which the analogues were incubated with the enzyme.[11]

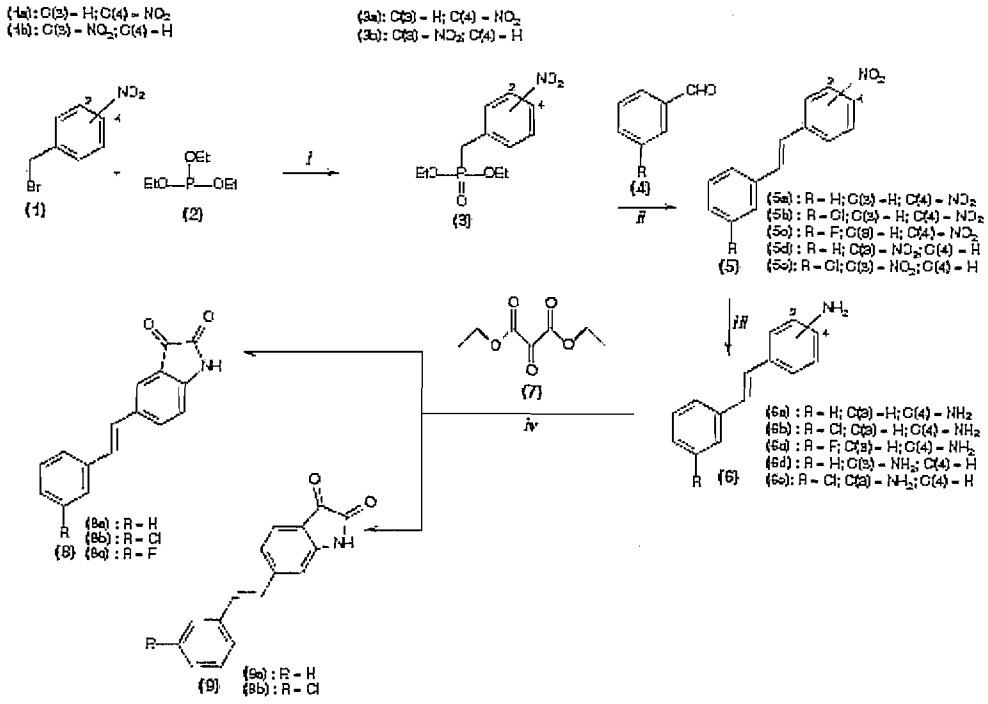

Figure 2. Synthetic pathway to (*E*)-5-styrylisatin- (8a–c) and (*E*)-6-styrylisatin (9a–b) analogues. (i) 130 °C, 3 hrs (ii) NaOEt (iii) $SnCl_2/CH_3COOH$, HCl/H_2O (iv) CH_3COOH, O_2.

The results of these assays are presented in Table 1. The (E)-5-styrylisatin analogues were found to be exceptionally potent inhibitors of MAO-B with IC50 values ranging from 20–42 nM. In comparison, the IC50 value for the lead compound isatin was found to be 8566 nM, approximately 400 times weaker than the most potent (E)-5-styrylisatin inhibitor examined here.

In conclusion, the (*E*)-5-styrylisatin analogues have been identified as promising new reversible inhibitors of MAO-B. This study provides evidence that potent MAO-B inhibitors may be obtained by designing structures that bind to both the entrance and substrate cavities of the enzyme.

Table 1.
IC_{50} values for all compounds tested

Compound	IC_{50} nM[a]
Isatin (A)	8566.6 ± 0.52
(*E*)-5-Styrylisatin (8a)	41.7 ± 1.86
(*E*)-5-(3-Chlorostyryl)isatin (8b)	20.7 ± 0.63
(*E*)-5-(3-Flourostyryl)isatin (8c)	30.1 ± 4.63
(*E*)-6-styrylisatin (9a)	436.8 ± 4.85
(*E*)-6-(3-Chlorostyryl)isatin (9b)	313.2 ± 56.20

[a]Values are means of two experiments

Acknowledgments

The financial support of the National Research Foundation is acknowledged.

References and notes

1. Petzer, J. P.; Steyn, S.; Castagnoli, K. P.; Chen, J. F.; Schwarzschild, M. A. M.; Van der schyf, C. J. *Bioorg. Med. Chem.* 2003, 11, 1299.
2. Kuo, W.; Hsiue, G.; Jeng, R. *J. Med. Chem.* 2002, 12, 868.
3. Hanna, P.E.; Gammans, R.E.; Schon, R.D.; Lee, M. *J. Med. Chem. 1980*, 23, 1038.
4. Da Silva, J.F.M.; Garden, S.J.; Pinto, A.C. *J. Braz. Chem Soc* 2001, 12, 273.
5. *Compound* 8a: Yield 77%; mp (capillary method): 254-255 °C. ^{1}H-NMR (DMSO-d6) δ 6.92 (d, 1H, J = 8.1 Hz), 7.24 (m, 3H), 7.35 (t, 2H, J= 7.2 Hz), 7.56 (d, 2H, J = 7.2 Hz), 7.75 – 7.81 (m, 2H), 11.2 (s, 1H); ^{13}C-NMR (DMSO-d6) δ 112.38, 118.22, 122.03, 126.34, 126.96, 127.51, 127.75, 128.61, 132.12, 136.16, 136.90, 149.69, 159.49, 184.35; EIMS m/z 249 ($M^{+\bullet}$); HR-EIMS m/z calc. 249.078979, found 249.080332. *Compound* 8b: Yield 28%; mp (capillary method): 252 °C. ^{1}H-NMR (DMSO-d6) δ 6.94 (d, 1H, J= 8.1 Hz), 7.22 (1H, 16.5 Hz), 7.29 – 7.34 (m, 3H), 7.39 (t, 1H, J= 7.9 Hz), 7.52 (d, 1H, J= 7.8 Hz), 7.65 (s, 1H), 7.77 – 7.78 (m, 1H), 7.80 (dd, 1H, 8.2 Hz); ^{13}C-NMR (DMSO-d6) δ 113.83, 119.41, 123.46, 126.35, 127.05, 127.46, 128.19, 130.03, 131.77, 132.87, 134.88, 137.78, 140.91, 151.28, 161.18, 185.92; EIMS m/z 283 ($M^{+\bullet}$); HR-EIMS m/z calc. 283.040001, found 283.03829. *Compound* 8c: Yield 5%; mp (capillary

method): 230-235 °C. ^{1}H-NMR (DMSO-d6) δ 6.94 (d, 1H, J= 8.1 Hz), 7.06 – 7.09 (m, 2H), 7.24 (d, 1H, J= 16.5 Hz), 7.31 (d, 1H, J = 16.5 Hz), 7.39 – 7.43 (m, 3H), 7.77 (m, 1H), 7.80 (dd, 1H, J = 1.7, 8.2 Hz); ^{13}C-NMR (DMSO-d6) δ 113.62 (d), 119.55 (d), 123.44, 124.06, 127..79, 129.91, 131.85 (d), 133.05, 137.75, 141.07 (d), 151.39, 161.04, 163.28, 164.90, 185.99; EIMS m/z 267 ($M^{+\cdot}$); HR-EIMS m/z calc. 267.069557, found 267.069991. *Compound* **9a**: Yield 66%; mp (capillary method): 257-258 °C. ^{1}H-NMR (DMSO-d6) δ 7.08 (s, 1H), 7.23-7.45 (m, 6H), 7.46-7.54 (m, 1H), 7.61-7.75 (m, 2H), 11.10 (s, 1H); ^{13}C-NMR (DMSO-d6) δ 109.34, 116.77, 121.03, 125.14, 127.15, 127.61, 128.66, 128.70, 128.74, 133.05, 136.22, 147.05, 151.19, 159.95, 183.20; EIMS m/z 249 ($M^{+\cdot}$); HR-EIMS m/z calc. 249.078979, found 249.082581. *Compound* **9b**: Yield 61%; mp (capillary method): 167-170°C. ^{1}H-NMR (DMSO-d6) δ 6.55-6.57 (m, 1H), 6.81 (d, 2H), 7.04-7.08 (m, 2H), 7.20 (d,1H), 7.20 (d, 1H), 7.38 (t, 1H, J = 7.8 Hz), 7.53 (d, 1H, J = 7.8 Hz), 7.67 (s, 1H); ^{13}C-NMR (DMSO) δ 63.96, 113.49, 115.68, 116.45, 126.29, 127.10, 127.19, 128.28, 130.47, 131.71, 132.27, 134.88, 138.49, 140.91, 149.58, 171.89; EIMS m/z 283 ($M^{+\cdot}$); HR-EIMS m/z calc. 283.040006, found 283.040436.

6. Prof. Neal Castagnoli Jr., Virginia Tech, Blacksburg, USA, generously supplied us with the oxalate salt of MMTP. UV-Vis spectra were recorded on a Shimadzu 2100 UV-Vis spectrophotometer.
7. Inoue, H.; Castagnoli, K.; Van der schyf, C.; Msbic, S.; Igarashi, K.; Castagnoli, N. *J. Pharmacol. Exp. Therapeut.* **1999**, 291, 856.
8. Mitochondrial fractions isolated from baboon liver tissue and stored at -70°C were used.[9] These fractions were suspended in sodium phosphate buffer (100 mM, pH 7.4, containing 30% glycerol, w/v) before determining the protein concentration.[10]

   A typical incubation (500 µl final volume in 100 mM sodium phosphate buffer, pH 7.4) contained MMTP (50 µM) as substrate, the mitochondrial isolate (0.15 mg protein/ml), and various concentrations of the test inhibitors in DMSO. Final incubation mixtures were incubated at 37 ° C for 10 minutes in order to ensure that the initial velocity in the linear phase of metabolite production is measured. The reactions were terminated by adding 10 µl of 70% perchloric acid. The supernatant fractions were removed from the centrifuged (16,000 g for 10 minutes) samples and the concentrations of the product, $MMDP^{+}$, in these fractions were measured spectrophotometrically at a wavelength of 420 nm. The initial velocity (V_i) of MAO-B catalytic oxidation was calculated and plotted as a function of the test inhibitor concentration in order to determine the IC_{50} value. Nonlinear regression analysis was carried out with the Prism software package (GraphPad Software Inc.).
9. Salach, J.I.; Weyler, W. *Methods Enzymol.* **1987**, 142, 627.
10. Bradford, M.M. *Anal. Biochem.* **1976**, 72, 248.
11. Mitochondrial fractions [0.3 mg/ml] were incubated at 37 °C with test inhibitor (40 nM) and these incubation mixtures were added to the substrate MMTP (90 µM) after 0, 15, 30 and 60 minutes respectively to yield an enzyme concentration of 0.15 mg/ml.[9] The resulting incubation mixtures were incubated for a further 15 minutes at 37 °C before terminating the reactions by adding 10 µl of 70% perchloric acid. The supernatant fractions were removed from the centrifuged (16,000 g for 10 minutes) samples and the concentrations of the product, $MMDP^{+}$, in these fractions were measured spectrophotometrically at a wavelength of 420 nm.

ACKNOWLEDGEMENTS

- Firstly, I want to express my gratitude to my family. None of this would have been possible without your love and support.
- Dr. Jacques Petzer, thank you for your patience and dedication. It was truly inspiring and a privilege to have you as a mentor.
- My heartfelt thanks also to all the other lecturers, staff and fellow students at the Department of Pharmaceutical Chemistry for their input and support.
- And last, but not least, I want to dedicate this work to the love of my life...